การสำรวจแผ่นดินไหวบรรพกาลตามแนวรอยเลื่อนคลองมะรุ่ย ภาคใต้ของประเทศไทย

นายศรัณย์ แก้วเมืองมูล

วิทยานิพนธ์นี้เป็นส่วนหนึ่งของการศึกษาตามหลักสูตรปริญญาวิทยาศาสตรมหาบัณฑิต
สาขาวิชาธรณีวิทยา ภาควิชาธรณีวิทยา
คณะวิทยาศาสตร์ จุฬาลงกรณ์มหาวิทยาลัย
ปีการศึกษา 2553

PALEOEARTHQUAKE INVESTIGATIONS ALONG THE KHLONG MARUI FAULT ZONE, SOUHTERN THAILAND

Mr. Sarun Keawmaungmoon

A Thesis Submitted in Partial Fulfillment of the Requirements
for the Degree of Master of Science Program in Geology
Department of Geology
Faculty of Science
Chulalongkorn University
Academic Year 2010

Thesis Title	Paleoearthquake Investigations along The Khlong Marui Fault Zone, southern Thailand
By	Mr. Sarun Keawmaungmoon
Field of Study	Geology
Thesis Advisor	Associate Professor Punya Charusiri, Ph.D.

Accepted by the Faculty of Science, Chulalongkorn University in Partial Fulfillment of the Requirements for the Master's Degree

.... Dean of the Faculty of Science

(Professor Supot Hannongbua, Dr.rer.nat.)

THESIS COMMITTEE

.... Chairman

(Thanop Thitimakorn, Ph.D.)

.... Thesis Advisor

(Associate Professor Punya Charusiri, Ph.D.)

.... Examiner

(Santi Pailoplee, Ph.D.)

.... External Examiner

(Thanu Harnpattanapanich, Ph.D.)

ศรัณย์ แก้วเมืองมูล : การศึกษารอยเลื่อนบรรพกาลตามแนวรอยเลื่อนคลองมะรุ่ย ภาคใต้ของประเทศไทย. (PALEOEARTHQUAKE INVESTIGATION ALONG THE KHLONG MARUI FAULT ZONE, SOUTHERN THAILAND) อ. ที่ปรึกษาวิทยานิพนธ์หลัก : รองศาสตราจารย์ ดร. ปัญญา จารุศิริ, 228 หน้า.

เขตรอยเลื่อนคลองมะรุ่ยในภาคใต้ของประเทศไทยได้ถูกเลือกสรรเพื่อบ่งบอกลักษณะเฉพาะโดยละเอียดและตำแหน่งของรอยเลื่อนมีพลัง ข้อมูลจากโทรสัมผัสและภาคสนามได้ถูกนำมาใช้เพื่อประเมินการเกิดการไหวสะเทือนโบราณในพื้นที่ศึกษา โดยมีวัตถุประสงค์หลักของการศึกษาคือจำนวนเหตุการณ์การเกิดรอยเลื่อนแผ่นดินไหว ขนาดความรุนแรงในอดีต และอัตราการเลื่อนตัวจากการเลื่อน ผลจากการแปลความหมายทางโทรสัมผัสแสดงว่ารอยเลื่อนคลองมะรุ่ยเป็นรอยเลื่อนที่วางตัวในแนวตะวันออกเฉียงเหนือ-ตะวันตกเฉียงใต้และมีความยาว 150 กิโลเมตร เขตรอยเลื่อนนี้เริ่มจากทะเลอันดามันในตอนใต้ผ่านจังหวัดภูเก็ต พังงา กระบี่ และสุราษฎร์ธานี และต่อเลยไปทางเหนือเข้าไปในอ่าวไทย พบรอยเลื่อนย่อยทั้งหมด 16 รอย โดยมีความยาวตั้งแต่ 10 – 55 กิโลเมตร และบางรอยเลื่อนพาดผ่านแอ่งตะกอนมหายุคซีโนโซอิก

ผลจากการแผลความหมายทางโทรสัมผัส การประเมินดัชนีธรณีสัณฐาน ผลงานเดิม และข้อมูลจากสนามแสดงให้เห็นถึงลักษณะภูมิลักษณ์การแปรสัณฐานหลายรูปแบบในตอนกลางของพื้นที่ศึกษา (เขาพนม) โดยเฉพาะรอยเลื่อนย่อยคลองมะรุ่ยซึ่งเป็นรอยเลื่อนย่อยที่ยาวที่สุด

ผลจากการขุดร่องสำรวจหาแผ่นดินไหวโบราณ 2 ร่องและร่องเดิมที่เคยมีสำรวจไว้ก่อนแล้วตามแนวรอยเลื่อนคลองมะรุ่ย พบว่าเคยเกิดแผ่นดินไหวทั้งหมด 4 ครั้ง และที่เกิดอายุน้อยที่สุดเมื่อประมาณ 2,000 ปีมาแล้ว และการเลื่อนตัวตามแนวรอยเลื่อนย่อยคลองมะรุ่ยทำให้เกิดแผ่นดินไหวโบราณขนาดใหญ่ที่สุดประมาณ 7.1 ตามมาตราริกเตอร์ ด้วยอัตราการเลื่อนตัวประมาณ 0.4 – 0.5 มิลลิเมตร/ปี ดังนั้นจึงสรุปได้ว่ารอยเลื่อนคลองมะรุ่ยยังคงมีพลังจนถึงปัจจุบัน โดยที่รอยเลื่อนย่อยเขาพนมและพังงาเคยมีการเลื่อนตัวทางขวาในอดีตและถือว่าเป็นรอยเลื่อนย่อยมีพลังโดยนัยการเลื่อนตัวเป็นแบบซ้ายเข้าในปัจจุบัน

ภาควิชา ....ธรณีวิทยา........... ลายมือชื่อนิสิต...

สาขาวิชา............ธรณีวิทยา............ ลายมือชื่อ อ.ที่ปรึกษาวิทยานิพนธ์หลัก.........................

ปีการศึกษา........2553........................

4972625023 : MAJOR GEOLOGY

KEYWORDS :KHLONG MARUI FAULT ZONE / MORPHOTECTONIC / PAELOEARTHQUAKE / GEOMORPHIC INDICES / LUMINESCENCE DATING

SARUN KEAWMAUNGMOON : PALEOEARTHQUAKE INVESTIGATION ALONG THE KHLONG MARUI FAULT ZONE, SOUTHERN THAILAND. THESIS ADVISOR : ASSOCIATE PROFESSOR PUNYA CHARUSIRI, Ph.D., 228 pp.

The Khlong Marui Fault Zone (KMF) in southern Thailand was selected for identifying its detailed characteristics and locating active faults. The remote-sensing and field data were applied for evaluating the occurrence of paleoseismicity in the study area. The main purposes of this study include events of earthquake faulting, paleoearthquake magnitudes, and slip rates of these fault movements.

Results from the remote-sensing interpretation indicate that the KMF is the northeast-southwest trending oblique-slip fault which the major component is lateral and has a total length of about 150 km. The fault zone can be traced from Andaman Sea in the south through Phuket, Phan Nga, Krabi, and Surat Thani and extends northwards to the Gulf of Thailand. Sixteen fault segments, ranging in length from 10 to 55 km, were recognized, and some of which run and pass through Cenozoic basins. Based on the results of remote-sensing interpretation together with the evaluation of geomorphic indices, earlier geophysical and ground surveys reveal that several morphotectonic features, have been identified in the middle part of the study area (Khao Phanom), especially the Khlong Marui fault segment, which is the longest of KMF. The results from two and earlier excavated paleoseismic trenches along the KMF indicate 4 paleoearthquake events with the lastest movement taking place in 2,000 years ago. It is also estimated that the movement along the segment was triggered by the earthquake with the maximum paleoearthquake magnitude of Mw 7.1. The slip rate of this fault segment is estimated as 0.4 – 0.5 mm/yr. Therefore, it is concluded that the KMF is still active till present, and the Khoa Phanom and Phang Nga segments, which were dextral active, are regarded as the active segments with the present-day sinistral sense of movement.

Department : Geology — Student's Signature ....

Field of Study : Geology — Advisor's Signature ....

Academic Year : 2010

ACKNOWLEDGMENTS

The author wishes to express his profound and sincere appreciation to his advisor, Associate Professor Punya Charusiri, for him enthusiastic support, continuous guidance and invaluable throughout the period of this study.

I would like to thank the Global Land Cover Facility website for the grants and accessibility to the satellites images from the Landsat 7 ETM^{+}, The CGIAR Consortium for Spatial Information (CGIAR-CSI) for SRTM DEM, Royal Irrigation Department for color orthorphoto.

A special thank to the Secretary and staff of Office of Atoms for Peace (OAEP), especially Mr.Pisarn Tungpitayakul for his help in sample analysis with NAA method. I also would like to express my sincerely gratitude to Mr.Arag Vitittheeranon for his help in working in gamma ray issues.

Thanks are also extended to Mr.Suwith Kosuwan, the senior geologist of Environmental Geology Division, Miss Sumalee Thipyopass, the senior geologist of Royal Irrigation Department, for providing permission suggestions in my graduate study.

Special thanks extend to Mr. Preecha Saithong, Mr. Kitti Khaowiset, Mr. Chinda Sutiwanich, Mr. Weerachat Wiwegwin and Mr. Aukkaravit Maneerut for their helping at the fieldwork and manage collectiong all samples. I would like to thank to Associate Professor Montri Chuwong, Dr. Pitsanupong Kanjanapayont, Dr. Santi Pailoplee and staffs of the Department of geology, Chulalongkorn University for all their help and support.

This research was supported by several agency including the 90th Chulalongkorn University Fund from Graduate School Chulalongkorn University.

Finally, a very special thank to my family, my parents for continuous financial and emotional supports throughout the program. No amount of his gratitude of them would be sufficient. Last, but not least, my older sister, Jirattikarn Keawmaungmoon, thank you for your help and being a proofreader. Your responses make my work a better one.

CONTENTS

	PAGE
ABTRACT IN THAI…………	iv
ABTRACT IN ENGLISH…………	v
ACKNOWLEDGMENT…………	vi
CONTENTS…………	vii
LIST OF FIGURES…………	x
LIST OF TABLES…………	xxii
Chapter I Introduction…………	1
1.1 Background…………	1
1.2 Objectives…………	2
1.3 Study area…………	5
1.4 Methodology…………	5
1.5 Research output…………	7
1.6 A Brief Guide to the Thesis…………	7
Chapter II Geological Tectonic Settings…………	10
2.1 Regional Setting…………	10
2.1.1 Structural setting…………	10
2.1.2 Geological setting…………	15
2.2 Neotectonic evolution…………	17
2.3 Active Fault in Thailand…………	21
2.3.1 Previous earthquake studies in Thailand…………	21
2.3.2 Definition of active faults…………	26
2.3.3 Active Faults in Thailand…………	29
2.4 Khlong Marui Fault…………	31
Chapter III Remote-Sensing Investigations…………	39
3.1 Materails…………	39
3.1.1 Landsat 7 ETM^+…………	39
3.1.2 SRTM DEM data…………	40

PAGE

3.1.3 Arial Orthographic image…………………………………………………… 41

3.1.4 Processes in Morphotectonic Investigation………………………………….. 45

3.2 Interpretation……………………………………………………………......................... 53

3.2.1 Sedimentary basins and boundary ………………………………………… 53

3.2.2 Lineament structures………………………………………………………… 53

3.2.3 Geomorphological features ………………………………………………… 54

3.2.3.1 Area A: Amphoe Thap Put, Phang Nga……………………………….. 60

3.2.3.2 Area B: Ban Bang Mai Pao, Surat Thani……………………………… 60

3.2.3.3 Area C: Ban Bang Luek, Surat Thani………………………………….. 61

3.2.3.4 Area D: Ban Bang Riang, Phan Nga…………………………………... 62

3.2.3.5 Area E: Ban Phra Saeng, Surat Thani………………………………… 62

3.2.3.6 Area F: Ban Chao Sai, Surat Thani…………………………………… 62

3.3 Summary………………………………………………………………………………….. 63

Chapter IV Geomorphic Investigations…………………………………………….…. 70

4.1 Geomorphic Indices……………………………………………………………………... 70

4.1.1 Mountain Front Sinuosity Index……………………………………………… 71

4.1.2 Stream Length-Gradient Index………………………………………………. 71

4.1.3 Transverse Topographic Symmetry Factor………………………………… 71

4.1.4 Valley Floor Width to Valley Floor Height Ratio…………………………… 74

4.1.5 Used data and processes…………………………………………………… 74

4.2 Interpretation and Result ……………………………………………………………. 76

4.3 Summary…………………………………………………………………………….…..... 78

4.4 Fault segmentation…………………………………………………………………… 89

4.4.1 Concept of fault segmentation……………………………………………… 89

4.4.2 Results of fault segmentation……………………………………………… 90

Chapter V Field Investigations.. 131

5.1 Previous Investigations.. 131

5.1.1 Sinkholes 131

5.1.2 Natural Hot Spring………………………………………………………… 132

5.1.3 Radon gas survey………………………………………………………….. 133

PAGE

5.1.4 Geophysical survey in study area... 134

5.1.4.1 Electrical resistivity method.. 134

5.1.4.2 Ground Penatrate Radar method.. 134

5.2 Tectonic Geomorphology.. 135

5.3 Paleoseismic Trench 148

5.3.1 Trench 1: Ban Bang Luek... 148

5.3.1.1 Stratigraphic Description.. 148

5.3.1.2 Evidence of faulting.. 150

5.3.1.3 Structural geology.. 151

5.3.2 Trench 2: Ban Thung Sri Ngam 151

5.3.2.1 Stratigraphic Description.. 151

5.3.2.2 Evidence of folding and faulting 152

5.3.2.3 Structural geology 152

Chapter VI Luminescence Dating.. 160

6.1 Basic Concept.. 160

6.2 Laboratory Processes.. 164

6.2.1 Crushing and Sieving... 164

6.2.2 Annual Dose Evaluation.. 166

6.2.3 Paleodose or Equivalent Dose Evaluation.................................... 169

6.2.4 Error Determination... 174

6.3 Dating result from this study.. 176

Chapter VII Discussion.. 181

7.1 Characteristics of the KMF 181

7.2 Geomophic Features and Paleoearthquake Magnitudes 183

7.3 Age, Slip Rates and Recurrence Interval 190

7.4 Neotectonic Evolution of The KMF... 192

CHAPTER VIII CONCLUSIONS 197

REFERENCE 199

Appendix 209

BIOGRAPHY.. 228

LIST OF FIGURES

PAGE

Figure 1.1	Map of Pacific ocean region showing subduction zones on the ring of fire (Modified after http://standeyo.com/Reports/04122.EQ.warning/ West.Coast)..	3
Figure 1.2	Map of mainland Southest Asia showing epicentral distribution from 1912 to 2006 (Data from Nutalaya et al., 1985; Thai Meteorological Department, 2002 and http://neic.usgs.gov/neis/epic/epic_global. html.)..	4
Figure 1.3	Index map of part of southern peninsular Thailand (A) showing the location of accessibility to of the study area………………………………	6
Figure 1.4	Flow chart showing the methodology used in this study………………...	9
Figure 2.1	Regional setting of south and South East Asia showing major tectonic sedimentary basins and main structural (Morley, 2002)…………………	11
Figure 2.2	Location map for tertiary basins in the Gulf of Thailand (modified after Polachan and Sattayarak, 1989)……………………………………………	12
Figure 2.3	Detail of the Thai Peninsula showing the Ranong and Khlong Marui fault (KMF) zones. (a) Fault map, dark grey, metamorphic cores and granite outlines stippled-west of the KMF-belonging to the Western Province and dotted-east of the KMF-belonging to the Eastern Province (modified from Department of Mineral Resources,1982) and basin outlines from Intawong (2006).(b) SRTM (Shuttle Radar Topography Mission) digital elevation model of the same area (Watkinson et al., 2008). Also shown in (b) is the location of the study area (in box)...…………………………………………………………………	13
Figure 2.4	Distirbution of granite belts in Thailand (Charusiri et al., 1993)…………	14
Figure 2.5	Geological map of the study area (A) in the southern peninsular Thailand (B) showing approximate locations of the major faults (modified after Department of Mineral Resources, 2007)………………	18

PAGE

Figure 2.6 (a) Plasticine model of escape tectonics involving a rigid indenter and several laterally moving blocks along the major strike – slip faults. (b) Sketch of the deformation in (a). Note the pull-apart basins along both faults (F1 and F2) (Tapponnier et al., 1982)………………………………. 19

Figure 2.7 Tectonic evolution during 44 Ma (A), 32 Ma (B), 23 Ma (C), 15 Ma (D), and 4 Ma (E), showing the change in the sense of movement of the Ranong and Khlong Marui Faults (RF & KMF), respectively, between 32 and 23 Ma of the Andaman Sea (Curray, 2005)……………………… 22

Figure 2.8 Tectonic map of SE Asia showing major fault systems and the relative movement of the SE Asian crustal blocks in response to India-Asia collision(modified from Polachan, 1989, Charusiri, 2002) (Notes: SMF = Sumatra Fault; SGF = Sagaing Fault; RNF = Ranong Fault; KMF = Khlong Marui Fault; TPF = Three Pagoda Fault; MPF = Mae Ping Fault; SCB = South China Block; STB = Shan Thai Block; LCB = Lamgpang Chaingrai Block; NTB = Nakhon Thai Block; WBB = West Burma Block and ICB = Indo Chian Block (Charusiri el al., 2007)……………... 23

Figure 2.9 Map of Peninsular Thailand and nearby regions showing major active faults : Ranong Fault (RF) and Khlong Marui fault (KMF) and epicenter distribution (A).(modified after Department of Mineral Resources, 2007). Noted that the study area is located as blue box in (B). the study area with epicentral distribution and KMF is shown in (C)……… 24

Figure 2.10 Map of Thailand showing major active faults and quaternary age dating results along the major active faults, (Charusiri et al., 1998). The study area covers along the fault line No.12………………………… 27

Figure 2.11 Map of the Andaman coastal area of Thailand showing distribution of granite plutons and major structures (Garson et al., 1975, and this study)………………………………………………………………………….. 35

Figure 2.12 Index map of Thailand showing major active faults (Department of Mineral Resources, 2006). Noted that the study area is show as red box……………………………………………………………………….. 36

PAGE

Figure 2.13	Major active faults and their segments in Phang Nga province, as identified by Department of Mineral Resources (2007)………………….	37
Figure 2.14	Currently earthquake intensity maps of the KMF showing (a) mercalli scale I-V of the earthquake with M_L 4.1 on 23 December 2008 in Surat Thani and (b) mercalli scale III-IV of the earthquake with M_L 2.7 on 4 May 2008 in Krabi (Royal Irrigation Department, 2008)……………	38
Figure 3.1	Detail of Landsat 7 space-borne image data with its application (a) EM wavelength spectrum (b) individual Landsat7 band application, (Lillesand and Kiefer, 1994) and (c) simply image showing satellite receive EMR from object directly and reflection from Sun, (www.nr.usu.edu)..	41
Figure 3.2	Digital image data of individual bands of Landsat 7 and details of wavelength transmission (modified after Lillesand and Keifer, 1994)….	43
Figure 3.3	SRTM DEM index map of the world (A) showing location and the data sheet 56-11 that cover the study area (http//strm.csi.cgiar.org)………..	44
Figure 3.4	Arial photograph type-orthograph which was used in this research, (http://www4.oginfo.com)..	44
Figure 3.5	Enhanced Landsat 7 ETM^+ with the false-color composite data of bands 4:5:7(red: green: blue) (A) showing the contrasting geographic features of the study area (red box in B) in southern peninsular Thailand………………………………………………………………………..	47
Figure 3.6	Enhanced Landsat 7 ETM+ with the false-color composite image data of bands 4:3/2:4/5 (red: green: blue) (A) showing various-coloured physiographic features of the study area (red box in B) in southern peninsular Thailand………………………………………………	48
Figure 3.7	Enhanced Landsat 7 ETM+ by using the false-color composite image data of bands PCA1: PCA3: PCA2 (red: green: blue) (A) showing physiographic features of study area (red box in B) in southern peninsular Thailand………………………………………………………...	49

PAGE

Figure 3.8 Shade relief image from SRTM DEM data (A) showing structures and fractures in the study area (red box in B) of the southern peninsular Thailand (also see interpretation in figure 3.11)………………………….. 50

Figure 3.9 Assemblage of landforms associated with active tectonic strike – slip faulting (modified after Keller and Pinter, 1996)………………………….. 52

Figure 3.10 Lineament map of study area showing two major lineaments-one in the NE to NNE trend (blue) and the other in the NW to NWW trend (red)……………………………………………………………………… 55

Figure 3.11 Map of the study area showing distribution of lineaments and Cenozoic sedimentary basins interpreted by using the enhanced Landsat 7 ETM^{+} images and SRTM DEM data. Noted that several faults cut across the basins……………………………………………………………………… 56

Figure 3.12 Lineament maps around the study area showing (a) the prominent and major northeast –southwest trending lineaments (211 lineaments), (b) the northwest – southeast trending lineaments (69 lineaments) and (c) Rose diagram base on 290 lineaments of both major trends in study area. Noted that and insert map in (a) showing the study area in southern peninsular Thailand……………………………………………… 57

Figure 3.13 Topographic map of the study area (A) showing location of Khao Phanom area, and aerial photographic images for detailed tectonic landform interpretation in area a to f, in southern peninsular Thailand (B)…………………………………………………………………………... 58

Figure 3.14 Model of geomorphological evidence showing essentail tectonic landforms by (A) normal fault and (B) thrust fault, (Ramsay et al.,1987). 59

Figure 3.15 Arial photograph (left) and interpreted morphotectonic landforms (right) along the fault trace in Area A……………………………………… 64

Figure 3.16 Arial photograph (left) and interpreted morphotectonic landforms (right) along the fault trace in Area B……………………………………… 65

Figure 3.17 Arial photograph (left) and interpreted morphotectonic landforms (right) along the fault trace in Area C. …………………………………….. 66

PAGE

Figure 3.18	Arial photograph (left) and interpreted morphotectonic landforms (right) along the fault trace in Area D…………………………………………	67
Figure 3.19	Arial photograph (left) and interpreted morphotectonic landforms (right) along the fault trace in Area E…………………………………………	68
Figure 3.20	Arial photograph (left) and interpreted morphotectonic landforms (right) along the fault trace in Area F…………………………………………	69
Figure 4.1	Idealized model showing how the mountain front sinuosity (Smf) is calculated, (modified after Keawmaungmoon et al., 2009)……………..	72
Figure 4.2	Idealized model showing how stream length-gradient index (SL) is calculated, (modified after Keawmaungmoon et al., 2009)……………..	73
Figure 4.3	Diagram of a portion of a drainage basin showing how the transverse topographic symmetry factor (TTS) is calculated, (modified After Cox,1994)………………………………………………………………..	75
Figure 4.4	Idealized diagram illustrating how the ratio of valley-floor width to valley height (Vf) is calculated. Note:Left and right is determined by looking Downstream, (Keller and Pinter, 1996)…………………………...	75
Figure 4.5	Index hillshade map of SRTM DEM showing subdivision of the study area into 3 zones (Zone 1, Zone 2, and Zone 3). ………………………..	79
Figure 4.6	Index Landsat 7 ETM+ band 4:5:7 (red:green:blue) map showing locations of mountain front range and valley floor width to valley height ratio in the study area………………………………………………..	80
Figure 4.7	Index map showing locations of selected streams and stream length-gradient of zone 1,2 and 3 in the study area of the southern peninsular Thailand………………………………………………………..	81
Figure 4.8	Sub basins for calculating transverse topography symmetry factor (TTS) of the study area (a) which belongs to Tapee Basin and situated between the West peninsular and East peninsular Basins, southern peninsular Thailand (b), (Royal Irrigation Department, 2007). …………	82
Figure 4.9	Index map showing transverse topography symmetry factor (TTS) range values used for individual subbasin in the study area. …………	83

PAGE

Figure 4.10	A hill shade DEM topographic map with 20m intervals showing different geomorphic indices of Zone 1 in the study area. ……………..	85
Figure 4.11	A hill shade DEM topographic map with 20m intervals showing different geomorphic indices of Zone 2 in the study area. ……………..	86
Figure 4.12	A hill shade DEM topographic map with 20m intervals showing different geomorphic indices of Zone 3 in the study area. ……………..	87
Figure 4.13	Map showing detailed stream length-gradient index around Khao Phanom in zone2 of the study area. Also show is the basin divide and longitudinal stream profile for few selective rivers. Knickpoint of corresponding faults are marked by arrows………………………………	88
Figure 4.14	Topographic (a) and 20-m contour interval DEM (b) map showing Khlong Hiang fault segment (no.1)…………………………………………	98
Figure 4.14 (cont.)c	Active fault evidence enlarged from topographic map (1) and color-orthographic image (2) of Figure 4.14b (Khlong Haing fault segment) showing offset stream (os) with the right displacement of about 560 m.	99
Figure 4.15	Topographic (a) and 20-m contour interval DEM (b) map showing Tha Chang fault segment (no.2)………………………………………………	100
Figure 4.15 (cont.)c	Active fault evidence enlarged from topographic map (1) and color-orthographic image (2) of Figure 4.15b (Tha Chang fault segment) showing offset stream (os) with the left displacement of about 280 m..	101
Figure 4.16	Topographic (a) and 20-m contour interval DEM (b) map showing Vibhavadi fault segment (no.3). ……………………………………………	102
Figure 4.16 (cont.)c	Active fault evidence enlarged from topographic map (1) and color-orthographic image (2) of Figure 4.16b (Vibhavadi fault segment) showing a set of offset stream (os)…………………………………………	103
Figure 4.17	Topographic (a) and 20-m contour interval DEM (b) map showing Khlong Sok fault segment (no.4)……………………………………………	104
Figure 4.17 (cont.)c	Active fault evidence enlarged from Figure 4.17b showing (1) pressure ridges (2) shutter ridges and (3) triangular facets…………….	105

PAGE

Figure 4.18	Topographic (a) and 20-m contour interval DEM (b) map showing Khao Na Dang fault segment (no.5)………………………………………..	106
Figure 4.18 (cont.)c	Active fault evidence enlarged from topographic map (1) and color-orthographic image (2) of Figure 4.18b (Khao Na Dang fault segment) showing linear valley………………………………………………………	107
Figure 4.19	Topographic (a) and 20-m contour interval DEM (b) map showing Khao Wong fault segment (no.6)…………………………………………...	108
Figure 4.19 (cont.)c	Active fault evidence enlarged from topographic map (1) and color-orthographic image (2) of Figure 4.19b (Khao Wong fault segment) showing a set of parallel ridges and a facet spur………………………...	109
Figure 4.20	Topographic (a) and 20-m contour interval DEM (b) map showing Khao Hin Paeng fault segment (no.7)……………………………………...	110
Figure 4.20 (cont.)c	Active fault evidence enlarged from topographic map (1) and color-orthographic image (2) of Figure 4.20b (Khoa Hin Paeng fault segment) showing triangular facets and shutter ridges........................	111
Figure 4.21	Topographic (a) and 20-m contour interval DEM (b) map showing Khao Hua Sing fault segment (no.8)……………………………………	112
Figure 4.22	Topographic (a) and 20-m contour interval DEM (b) map showing Ao Luek fault segment (no.9)…………………………………………………	113
Figure 4.22 (cont.)c	Active fault evidence enlarged from topographic map (1) and color-orthographic image (2) of Figure 4.22b (Ao Luek fault segment) showing a set of linear ridge and fault scarp……………………………	114
Figure 4.23	Topographic (a) and 20-m contour interval DEM (b) map showing Khao Phanom and Khlong Haek fault segment (no.10 and no.11)…….	115
Figure 4.23 (cont.)c	Active fault evidence enlarged from topographic map (1) and color-orthographic image (2) of Figure 4.23b (Khoa Phanom fault segment) showing facet spurs and parallel ridges…………………………………..	116
Figure 4.23 (cont.)d	Active fault evidence enlarged from topographic map (1) and color-orthographic image (2) of Figure 4.22b (Khao Phanom fault segment) showing triangular facets, shutter ridges and sag ponds. ………………	117

PAGE

Figure 4.23 (cont.)e	Active fault evidence enlarged from topographic map (1) and color-orthographic image (2) of Figure 4.22b (Khlong Haek fault segment) showing triangular facets and a shutter ridge……………………………	118
Figure 4.24	Topographic (a) and 20-m contour interval DEM (b) map showing Khlong Marui fault segment (no.12)……………………………………..	119
Figure 4.24 (cont.)c	Active fault evidence enlarged from topographic map (1) and 20-m contour interval DEM (2) of Figure 4.24b (Khlong Marui fault segment) showing triangular facets, shutter ridges and linear valley……………..	120
Figure 4.24 (cont.)d	Enlarged from Figure 4.24c(2) showing offset stream from detailed geodetic survey (1) and color-orthographic image in same area (2)......	121
Figure 4.24 (cont.)e	Enlarged from Figure 4.24c(2) showing offset stream from detailed geodetic survey (1) and color-orthographic image in same area (2).....	122
Figure 4.24 (cont.)f	Enlarged from Figure 4.24c(2) showing offset stream from detailed geodetic survey (1) and color-orthographic image in same area (2)….	123
Figure 4.25	Topographic (a) and 20-m contour interval DEM (b) map showing Plai Phanom fault segment (no.13)…………………………………………...	124
Figure 4.26	Topographic (a) and 20-m contour interval DEM (b) map showing Phnag Nga fault segment (no.14)………………………………………..	125
Figure 4.27	Topographic (a) and 20-m contour interval DEM (b) map showing Tai Maung fault segment (no.15)……………………………………………	126
Figure 4.28	Topographic (a) and 20-m contour interval DEM (b) map showing Pakong fault segment (no.16)……………………………………………	127
Figure 4.28 (cont.)c	Active fault evidence enlarged from topographic map (1) and color-orthographic image (2) of Figure 4.28b (Pakong fault segment) showing shutter ridges, triangular facet, sag ponds and an offset stream with the left displacement of about 200 m………………………..	128

PAGE

Figure 4.29	Sixteen active-faults segments (a) base on result on Remote sensing interpretation and geomorphic indices evaluation of the study area in southern peninsular Thailand (b). The inferred fault segments and epicenters of the study area is shown in (c). Noted that dashed lines are fault segments which are less important but still obvious…………	129
Figure 4.29 (cont.) c	DEM map showing epicentral distribution with small magnitude in study area (Data from Thai Meteorological Department, 2007)………..	130
Figure 5.1	Sink hole map of Thailand showing (A) carbonate rocks (black) and sink hole locations and (B) relationship between sinkholes and active faults in the study are (modified after Department of Mineral,2005)……	136
Figure 5.2	Map of southern Thailand showing relationship between hotspring locations and active fault trace (data from Department of Mineral Resources, 2004)……………………………………………….	137
Figure 5.3	Previous radon survey in Ban Bang Luek, Surat Thani (a) detailed topographic map of Ban Bang Luek trench showing location of radon survey lines, (Department of Mineral Resources, 2006) and (b) graph of gas radon concentration and distance in radon survey lines, (Artyotha, 2007)…………………………………………………………………	138
Figure 5.4	Result of Resistivity survey in Ban Bang Luek (line survey was showed in Figure 5.3a) (a) interpreted of survey line1 (b) interpreted of survey line 3, (modified after Department of Mineral Resources, 2006)……….	139
Figure 5.5	Line of Ground Penetrated Radar survey at Ban Thung Sri Ngam school showing (a) 0-100 distance of line 2 and (b) result of GPR interpretation of line 2, (Royal Irrigation Department, 2008)……………	140
Figure 5.6	Topography view of Khao Phanom where the most sign seeing in remote-sensing visible and triangular-facet (looking southeast)……….	142
Figure 5.7	Color-orthographic image showing triangular facet at Khlong Sok segment, northwestern study area………………………………………	143
Figure 5.8	Hill shade DEM map showing some shutter ridges parallel Khlong Sok segment in west of Surat Thani…………………………………………..	144

PAGE

Figure 5.9	Color-orthographic image showing triangular facet and scarp at west of Khao Phanom in middle of study area…………………………………	145
Figure 5.10	Arial photograph and DEM from topographic map showing line of fault scarp parallel west of Khao Phanom along Phanom segment…………	
Figure 5.11	Orthographic image showing sinistral movement of offset stream nearby Ban Bang Luek and their offset distance…………………………	146
Figure 5.12	Color-orthographic image showing linear ridges along the eastern side of Khao Phanom……………………………………………………...	147
Figure 5.13	Location of paleoseismic trenchings in The Khlong Marui segment, west of Khoa Phanom. ……………………………………………………	149
Figure 5.14	View of paleoseismic trench section on the north-east wall, Ban Bang Luek, Surat Thani showing sediment stratigraphy and faults orientation.	154
Figure 5.15	View of paleoseismic trench section on the south-west wall, Ban Bang Luek, Surat Thani showing sediment stratigraphy and faults orientation.	155
Figure 5.16	Trench log section of the north-west wall, Ban Bang Luek, Surat Thani showing preliminary sediment stratigraphy, major faults orientation…..	156
Figure 5.17	Trench log section of the south-east wall, Ban Bang Luek, Surat Thani showing preliminary sediment stratigraphy, major faults orientation and sample location for dating. ……………………………………………	157
Figure 5.18	View of paleoseismic trench section on the north-west open wall, Ban Thong Sri Ngam school, Phang Nga showing sediment stratigraphy, compress stress orientation and faults. …………………………………...	158
Figure 5.19	Wall log section of north-west open wall, Ban Thong Sri Ngam school, Phang Nga showing preliminary sediment stratigraphy, major faults orientation and sample location for dating. ………………………………	159
Figure 6.1	Generalized processes that produce the luminescence signal (steps 1 and 2), and the sampling and analytical procedure to determine the age of deposition (steps 3 through 6), (Mallinson, 2008). ………………	161

PAGE

Figure 6.2	Applied thermoluminescence method for dating by showing relationship between amount electron in electron trap and time, (modified after Won-in, 2002). …………………………………………..	162
Figure 6.3	Simplified diagram of lattice structure and ionic crystal showing (a) ideal model of completely lattice (b) negative-ion vacancy occurred in ionic crystal cause negative-ion interstitial and substitution impurity center (c) electron capture by electron trap in negative ion vacancy and (d) electron escape from electron trap by heat or Light, (http://www.rses.anu.edu.au). …………………………………………..	163
Figure 6.4	Simplified model showing energy states in Thermoluminescense processes, (Aitken, 1985). ………………………………………………	163
Figure 6.5	Chart of calculate annual dose and equivalent dose for TL and OSL dating, (modified after Takashima and Honda, 1989)……………………	168
Figure 6.6	Summary of neutron activation analysis (NAA) procedures with sample preparation and annual dose determination. ……………………………..	168
Figure 6.7	TL and OSL equipment component.(a) Thermoluminescence Detector (TLD) at geology department, facuty of science, chulalongkorn university (b) Main equipment that comprises the “reader”, which is necessary for measuring the paleodose, irradiating the sample, heating the sample, and deriving a “growth” curve, (Lian, 2007). …….	171
Figure 6.8	Example result of BL1 after run with Thermoluminescence Detector for calculated equivalent dose (a) growth curve (b) grow curve. …………	172
Figure 6.9(a)	Schematic charts of regeneration technique (Takashima et. al., 1989). Note that several portions are used for measurement of the TL intensity; N is natural sample; Io is residual intensity from sample; H is 350°C heated sample; and γ is known dosage that irradiated sample..	175
Figure 6.9 (b)	Thermoluminescence remaining after bleaching by exposes to sunlight For various time (Aitken, 1985). …………………………………	175
Figure 6.10	Trench-log stratigraphy showing faults orientation ,TL and OSL ages of sedimentary layers, on southwest wall, Ban Bang Luek trench. …….	179

PAGE

Figure 6.11	Trench-log stratigraphy showing faults orientation ,TL and OSL ages of sedimentary layers, on northeast wall, Ban Thung Sri Ngam trench…	180
Figure 7.1	Hill shade map of study area and adjacent area showing epicentral distribution from 1912 to 2007, (Data from Thai Meteorological Department, 2007 and http//neic.usgs.gov/neis/epic/epic_global. -html, 2007). ………………………………………………………………..	182
Figure 7.2	Map showing active fault segments, their length and estimated maximum cridible earthquakes of paleomagnitudes of The Khlong Marui Fault Zone. …………………………………………………………..	186
Figure 7.3	Trench log section at the (a) northeast and (b) southwest wall of Ban Bang Luek, Surat Thani showing principle stratigraphy and TL & OSL ages of this study, TL ages of Department of Mineral Resource (2007) and ESR ages of Chansaward (2007). ……………………………………	188
Figure 7.4	Trench log section at the northeast wall of Ban Bang Luek showing structure of reverse-fault and clearly offset of Unit b which displacement approximately 45 cm. ………………………………………	189
Figure 7.5	Acitve fault map of the KMF showing the major period of paleoearth - quakes and the slip rate of Khlong Marui fault segment. Noted that the red line indicates the segments with trenching data support. ………….	194
Figure 7.6	Geometry and anatomy of strike-slip fault showing releasing bend and restraining bend, which help in explaining evolution of Sinistral movement of the Khlong Marui Fault Zone (Crowell, 1974). …………..	195
Figure 7.7	Hypothetical structure showing (a) schematic positive flower structure of Klong Marui shear zone in between Permo-Carboniferous and Mesozoic sedimentary units.(Kanyanapayon et al., 2008) and (b) 3D model of DEM from topographic map in same area. ………………..	196

LIST OF TABLES

		PAGE
Table 2.1	Active fault rank, criteria, and examples in Thailand (modified after Charusiri et al., 2001)…………………………………………………………..	33
Table 2.2	Activity of faults in Thailand based upon age-dating data (modified after Charusiri et al., 2001). ………………………………………………..	34
Table 3.1	Bands spectrum and wavelength interval of Landsat 7ETM+ used by Department of Mineral Resources (2007)………………………………..	40
Table 3.2	Image information from satellite, Landsat 7 ETM+ in this research…….	40
Table 3.3	Image information from STRM DEM used in this research……………..	41
Table 4.1	Results of geomorphic indices in this study area (see locations in Figure 4.10 – 4.12). …………………………………………………………	84
Table 4.2	Types of fault segments and criteria used for active fault in this study (McCalpin, 1996)……………………………………………………………	96
Table 4.3	Fault segment lengths proposed for active fault by various authors (modified after McCalpin, 1996)………………………………………..	97
Table 6.1	TL dating results of quartz concentrates sediments for sample collected from the study area, Surat Thani and Phang Nga, Southern Thailand. ………………………………………………………………..	177
Table 6.2	OSL dating results of quartz concentrates sediments for sample collected from the study area, Surat Thani, Southern Thailand.	178
Table 7.1	Paleoearthquake magnitudes of the KMF in southern Thailand, estimation from Well & Coppersmith (1994)…………………………...	187
Table7.2	Earthquake Events in study area. ………………………………………	193

Chapter I

Introduction

1.1 Background

An earthquake is one of the natural hazards which is natural phenomenon and unable to control or predict. The earthquake is the result of a sudden release of energy in the Earth's crust that creates seismic waves. The seismicity or seismic activity of an area refers to the frequency, types and sizes of earthquakes experienced over a period of times. As commonly known, the earthquakes can occur along subduction zones on the ring of fire (Figure 1.1) and can cause large damages in many parts of the world.

There are two main theories on earthquakes, viz. the elastic rebound model and the dilation source theory. The elastic rebound model states that at a geological fault between two moving plates, stress occurs and deforms the rocks. This theory supports the idea that earthquake mechanisms are directly related to tectonic especially, active tectonic. In Thailand, the major tectonic evolution can be divided into four episodes, including, archeotectonic, paleotectonic, mesotectonic and neotectonic episodes (Charusiri et al., 2002). The archeotectonic episode is a tectonic event that occurred during pre-Paleozoic era, whereas paleotectonic, mesotectonic and neotectonic episodes are limited in Paleozoic, Mesozoic and Ceozoic era, respectively. The neotectonic episode is essential in this study because it can happen to present.

Although Thailand has not been considered to be a seismically active country due to the disappearance of the large earthquakes in the past. Thailand was not absolutely to be save from earthquakes because annals and stone inscriptions indicated that large earthquakes have been recorded many times in several parts of Thailand, especially in the northern and western regions. The important earthquakes with the magnitude greater than ML 5 (Richter scale) have been recorded in northern and western Thailand, such as the event on 22 December 1925 at Nan province. In addition, the present-day earthquake epicenters can be recorded throughout Thailand by using seismographs.

According to the historical and instrumental records, Thailand has been experienced with earthquakes and may have a high chance for future medium to large magnitude earthquakes. Thailand Meteorology Department shows that the distribution of most epicenters place in boundary of Thai-Burma, Thai-Loas, Burma-Chaina and Andaman sea, those reveal that earthquake concern with major faults in this region (Figure 1.2). At present many geologists believe that the SE Asian region is the consequence of the collision between Indian and Eurasian plates since middle Tertiary time (Fenton et al., 1997; Charusiri et al.,2002; Bunopas, 1994 and Hintong, 1991).

The knowledge of earthquakes has continously increased in Thailand. Consequently, two major faults in the south, including the Ranong and the Khlong Marui Fault (KMF of this study). KMF was first classified as the potentially active fault fault by Hinthong (1997) based on preliminary TL dating results. Earlier than that, Chauviroj (1993) only mentioned that the Ranong Fault and KMF were the major northeast-southwest trending faults but he did not defined clearly if or not they are active.

Recently, the Sumatra earthquake on 26 December 2004 with magnitude 9.3 (Richter scale) effected around the Andaman Sea and nearby regions. Such movement caused Phuket Island moved northeastward about 27 cm along the KMF (Lobbonlert, 2007). This result leads Department of Mineral Resource (2007) to investigate the Ranong Fault and KMF using remote-sensing, geological, and geochronological approaches.

In this study, special emphasis is placed on the application of geomorphological index, TL and OSL datings to delineate the fault and to classify fault segments.

1.2 Objectives

The main purposes of this research are to characterize of the Khlong Marui Fault (KMF) zone, in detail and to clarify the paleoearthquakes along the studied fault zone. The main knowledge and techniques used for paleoearthquake investigation in this study include remote-sensing interpretation in addition to investigations on morphotectonic analyses, geomorphic indices, and luminescence-dating results. The prime goal of the output is to help design of building or large construction and planning in order of preventing damages from earthquakes in the future. Consequnly, the results of this research are fulfil the following four fold:

1. Identifying characteristics of the Khlong Marui Fault zone;
2. Delineating active fault traces of the Khlong Mauri Fault zone;
3. Determining the ages of the Khlong Marui fault zone movement; and
4. Estimating the paleoearthquake magnitudes and slip-rates of these fault movement.

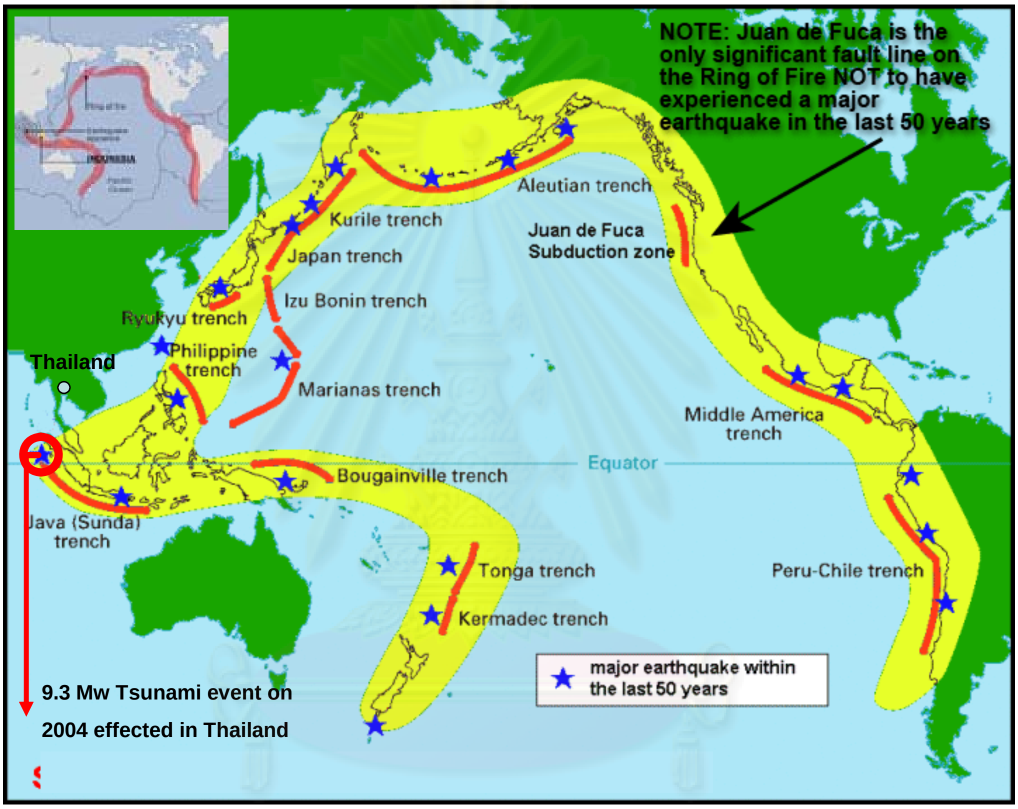

Figure 1.1 Map of Pacific ocean region showing subduction zones on the ring of fire (Modified after http://standeyo.com/Reports/04122. EQ.warning/West.Coast).

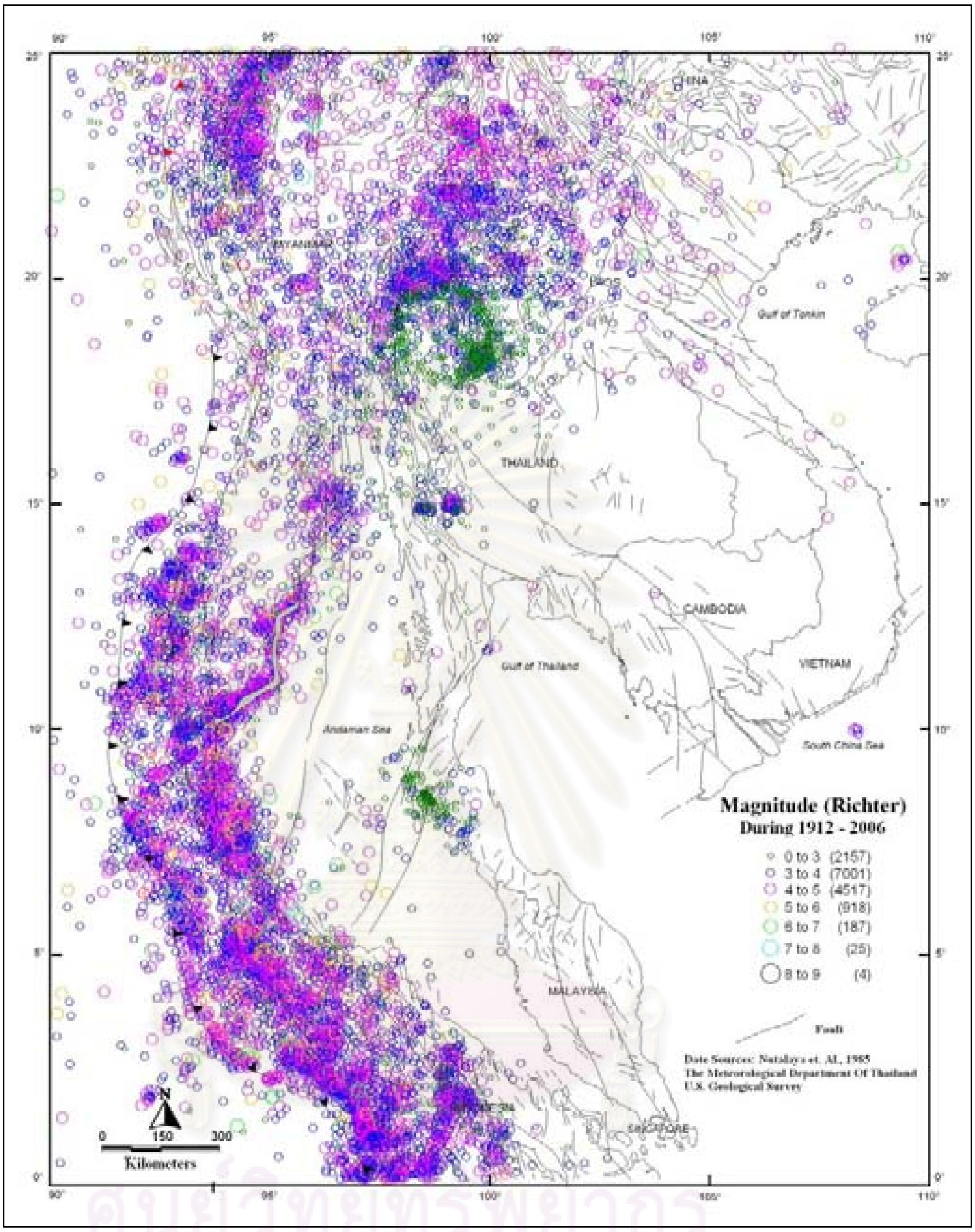

Figure 1.2 Map of mainland Southest Asia showing epicentral distribution from 1912 to 2006 (Data from Nutalaya et al., 1985; Thai Meteorological Department, 2002 and http://neic.usgs.gov/neis/epic/epic_global.html.)

1.3 Study area

The study area selected for the present research is located within the KMF zone. The area under investigation is bounded by latitudes 8° 10’N to 9° 35’ N and longitudes 98° 10’E to 99° 25’E to cover most Surat Thani, Phang-Nga and north Krabi (Figure 1.3). The total study area is about 20,255 km^2, and the study area is approximately 500 km far from Bangkok, the capital city of Thailand.

1.4 Methodology

The study methodology is divided into six steps (Figure 1.4) including:

1.4.1 To collect the report data

The first step involves collecting data for supporting further steps of study. This data is composed of reviewing literatures for pervious work, selecting topographic maps, analyzing geological maps, screening earthquake epicenters, acquiring remote-sensing images and aerial photograph, and other related technical and nontechnical documents.

1.4.2 To interpret remote-sensing images

The second step involves remote-sensing interpretation. Commencement of the stage is to study the small scale using digitally enhanced satellite imageries and interpretation on a large scale with aerial photographs. Basic data for the interpretation is enhanced Landsat 7 and SRTM DEM for determining lineaments, their attitudes and orientations as well as delineating Cenozoic basins. Interpretation was also performed along with the aerial photographs (1:50,000) and color-orthographs (1:15,000) for geomorphology evidence of active tectonic landforms.

1.4.3 To determine geomorphic indices

The third step of this study deals with basic geomorphic indices interpretation. Four geomorphic indices was used in this study, namely mountain front sinuosity, stream length-gradient index, transverse topographic symmetry, and valley-floor width valley-floor height ratio.

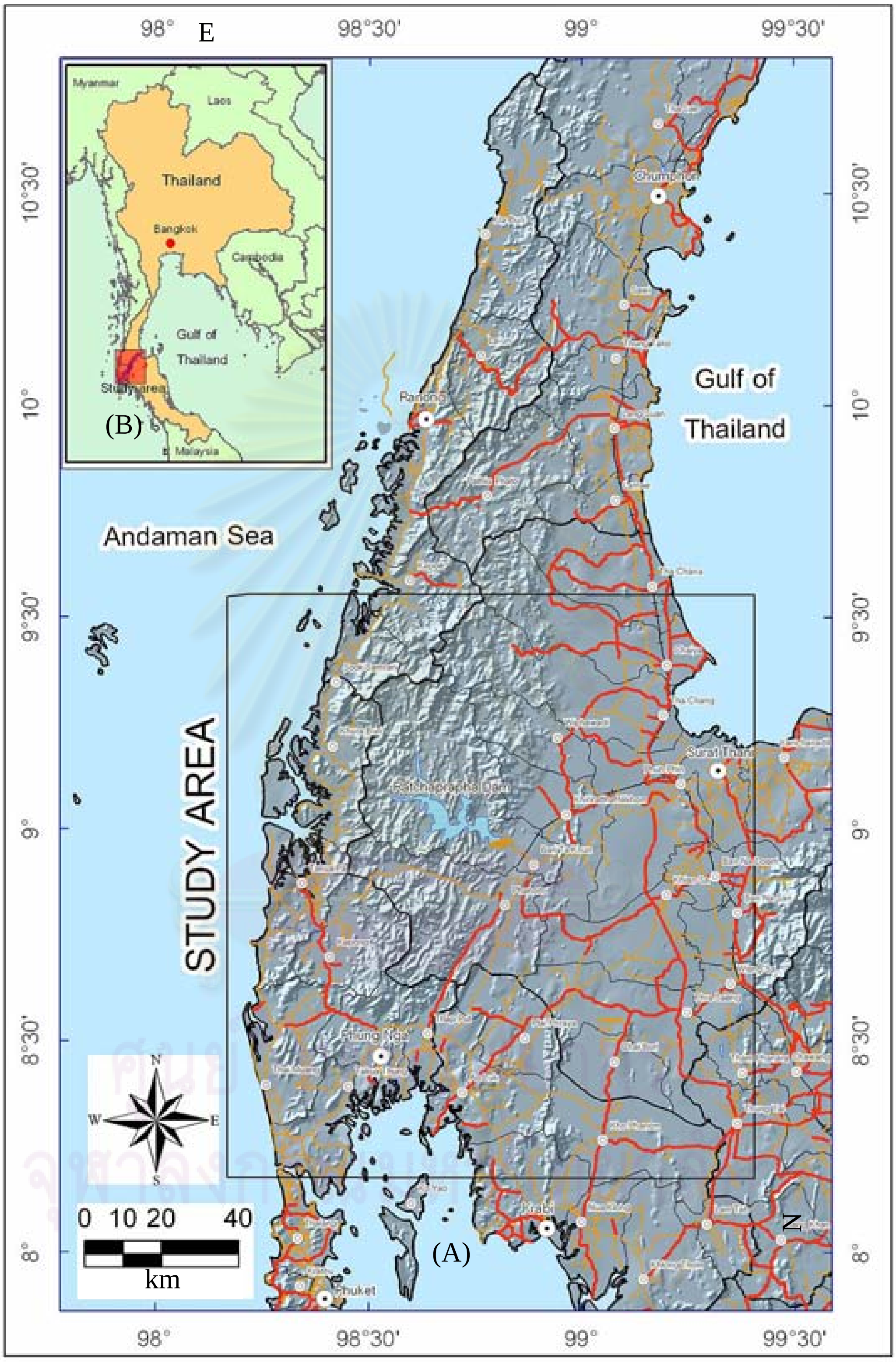

Figure 1.3 Index map of part of southern peninsular Thailand (A) showing the location of accessibility to of the study area.

1.4.4 To do field investigation

This step starts with compilation of previous field data related to fault evidence. Sub sequently identifying sequences of faulting in the selected area with exploratory trenching. Then geological data and sample collection.

1.4.5 To do age-dating

Dating is the fifth step with the main purpose of collecting samples for dating by Thermoluminescence (TL) and Optical Stimulated Luminescence (OSL) method. The dating method follows that of Takashima & Watanabe (1994), commencing at collecting suitable geological samples related to active faults, treatment of quartz-enriched samples for dating, and analyzing both of equivatent and annual doses of quartz concentrates.

1.4.6 To discuss the result and make a conclusions

The last step includes intergration of all the available investigated and surveyed results for discussion on fault characteristic, geomorphic features and paleoearthquake magnitudes, recurrence intervals, slip rates, and neotectonic evolution of the KMF.

1.5 Research output

The clearly-defined segments of KMF and the active fault map at a scale1:50,000 form the main output of this study.

1.6 A Brief Guide to the Thesis

This thesis provides an emphasis on tectonic geomorphology and geochronology of the Khlong Marui fault zone in succession of Chapters as following :

<u>Chapter I</u> mentions about an introduction, objective, study area, methodology and research output to the study project research.

<u>Chapter II</u> notifies the regional setting, neotectonic evolution of tectonic plate in southern Thailand. Active faults studies in Thailand and some investigations on The KMF zone area are included.

Chapter III is the part of detailed remote-sensing investigation including the process of enhancement and interpretation of Landsat 7 images, DEM data and aerial photographs to determine the tectonic landform evidence.

Chapter IV provides the usefulness of physiography and topography is important to analyst together with remote-sensing result for indicate fault segment. 4 geomorphic indices was use in this study.

Chapter V provides the previous investigation related to active fault evidence. Tectonic geomorphology was applied to indicate the active-fault evidences and show the sedimentary layers in trenches with collecting sample location.

Chapter VI mentions the uses of the dated sedimentary ages to approximate the fault ages.

Chapter VII compares the dating and the summary of earlier investigations to discuss on characteristics of the KMF and neotectonic evolution.

Chapter VIII is the conclusion deduced from the result of study project research.

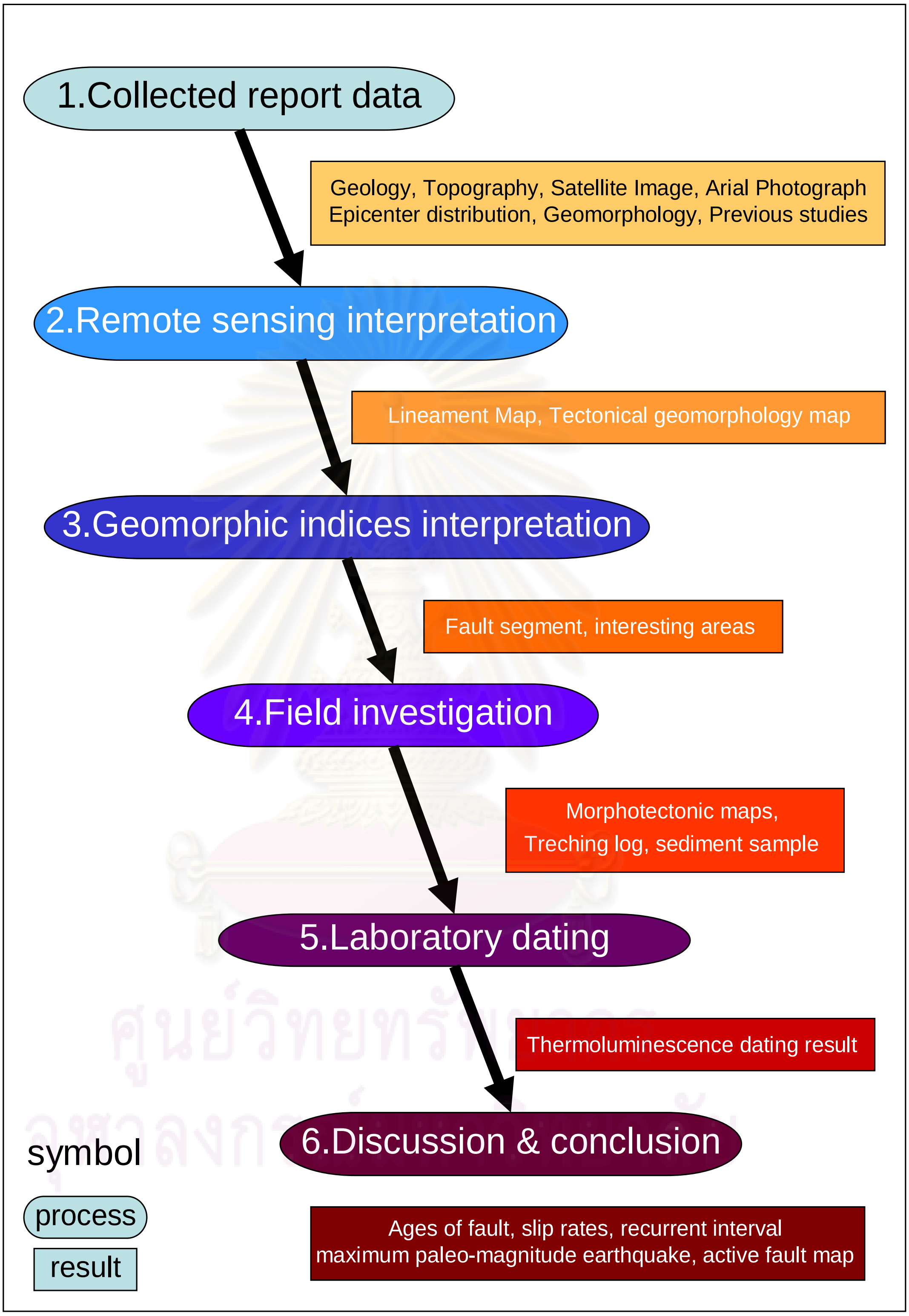

Figure 1.4 Flow chart showing the methodology used in this study.

Chapter II

Geological Tectonic Settings

2.1 Regional Setting

After the great convergent interactions between Indian plate and Urasian plate, the Urasian plate seems to stop its movement, while the Indian plate was still moved northwards. This gave rise to the Southeast Asian region moved with clockwise rotation. Consequently, Cenozoic basins were formed in response to this tectonic process (Figure 2.1). South-East Asia consists of the continent assembles, which called “Sundaland Block” and link up with the China Block in the north and with the subduction zone of Indian plate in the west and connected with the Chinese Sea in the east.

2.1.1 Structural Setting

The Southern Thailand or the Thai Peninsula has the large-scale fold structures with the major fold axis in the north-south trend and some areas have been related to the magmatism and metamorphism. This scenario may have created the mountainous area, which extends from Phetchaburi in the north to Satun in the south. In the Western Thailand and the upper Southern Thailand, there exist several important fault traces collectively called “ Three Pagoda Fault ” (Figure 2.2) lying in the northwest - southeast trend. In the middle of southern Thailand, the structural geology is dominated by the Ranong fault (RF) and the lower almost parallel fault, the Khlong Marui fault (KMF), both of them lying in the NNE-SSW trend. Their fault types are the strike-slip fault zones with ductile deformation in Tertiary (Figure 2.3). According to Watkinson et al. (2008), These faults are bounded and overprinted by brittle strands, which are part of a population of parallel and branching sinistral faults, and they are localised into the two similar, but discrete, fault zones. Rocks in and around the KMF zone are dominantly Late Palaeozoic marine sediments deposited at mid-southern latitudes (Metcalfe, 2002, Ampaiwan et al., 2008). Pebbly mudstones, interpreted as diamictites (Bunopas et al., 1991, Ampaiwan et al., 2008), are ubiquitous to the north of the KMF, and can be recognised even where they have been strongly deformed in the ductile shear zones.

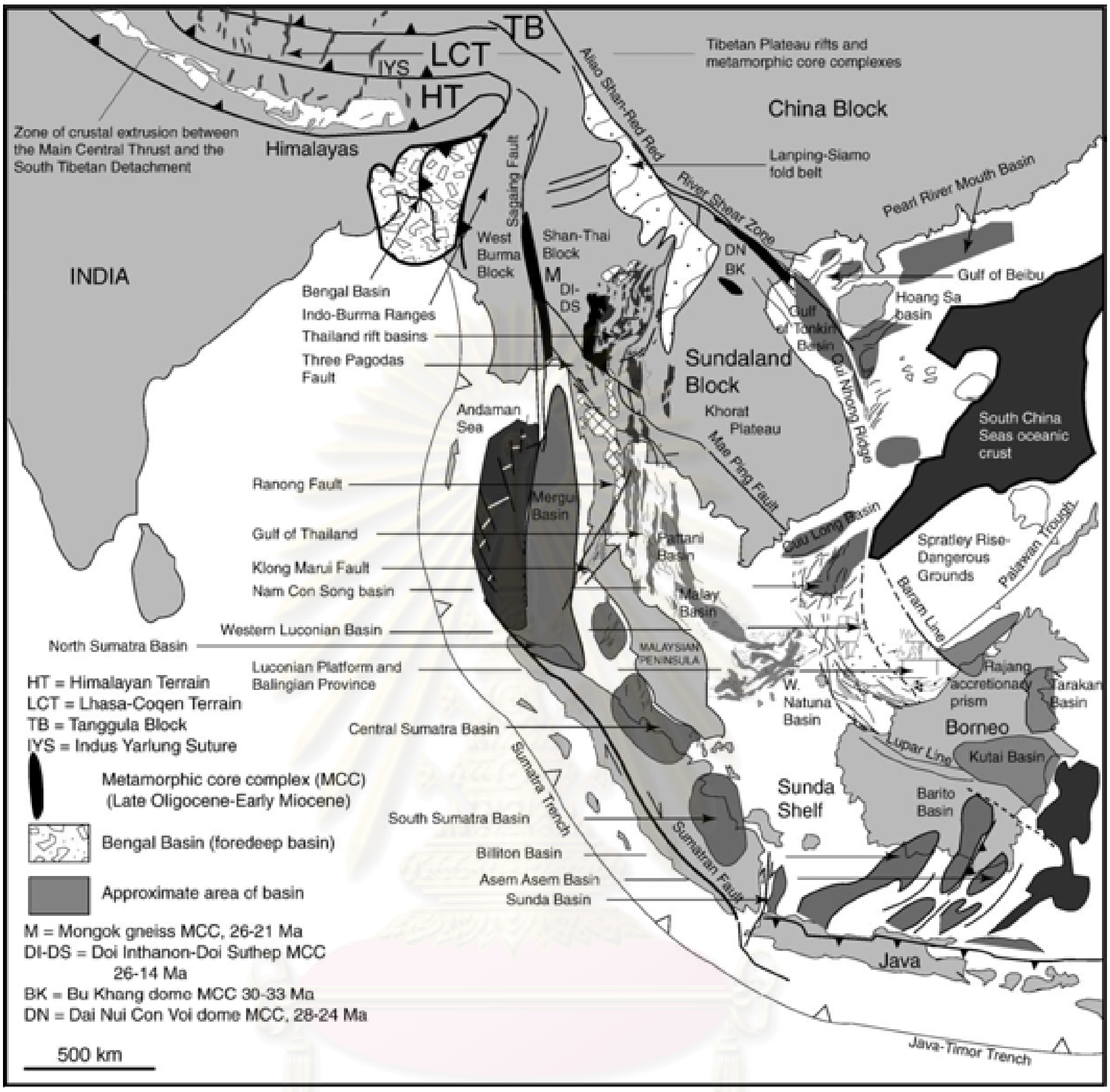

Figure 2.1 Regional setting of South and South East Asia showing major tectonic sedimentary basins and main structural features (Morley, 2002).

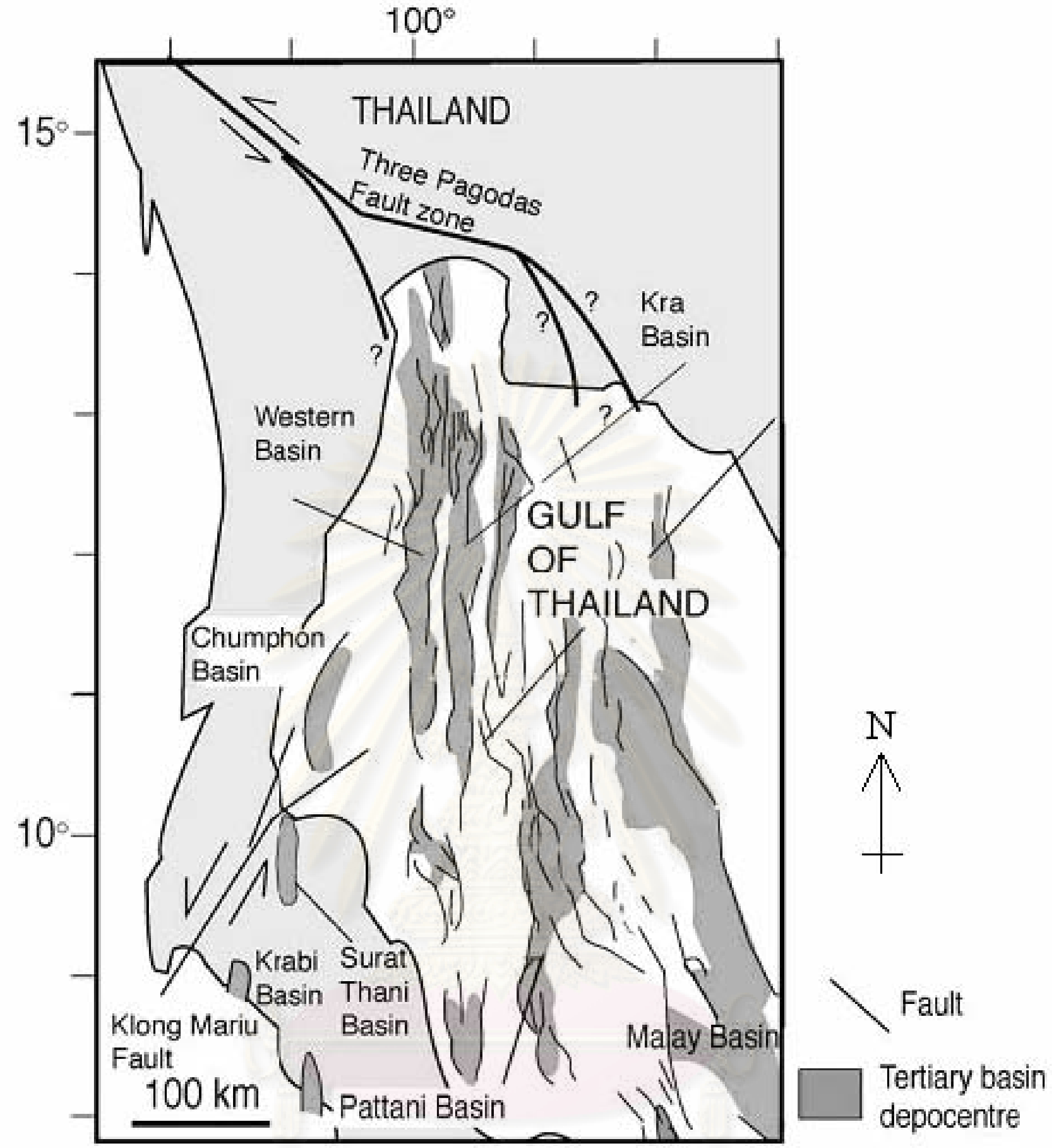

Figure 2.2 Location map for tertiary basins in the Gulf of Thailand (modified after Polachan and Sattayarak, 1989).

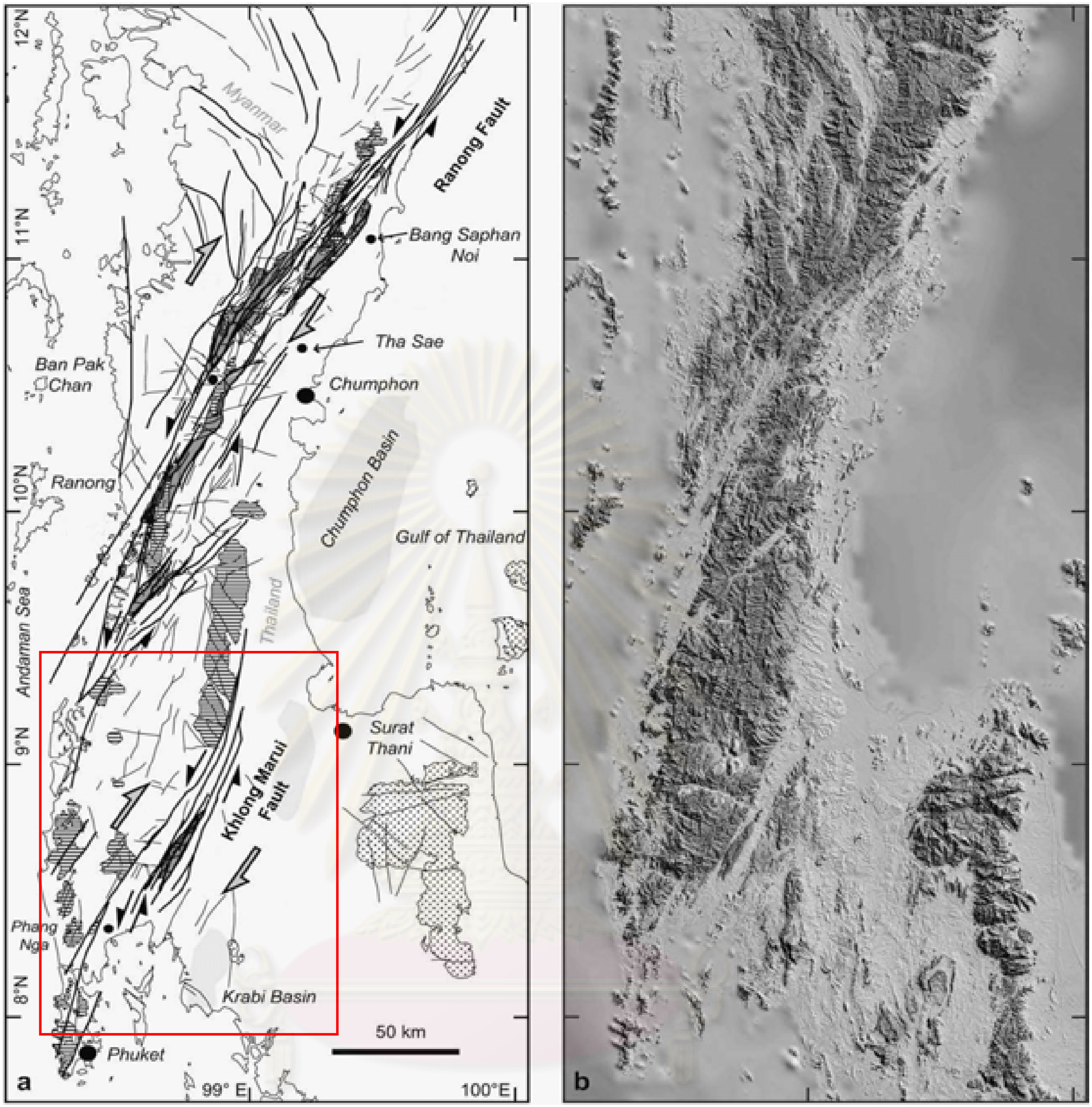

Figure 2.3 Detail of the Thai Peninsula showing the Ranong and Khlong Marui fault (KMF) zones. (a) Fault map, dark grey, metamorphic cores and granite outlines stippled-west of the KMF-belonging to the Western Province and dotted-east of the KMF-belonging to the Eastern Province (modified from Department of Mineral Resources,1982) and basin outlines from Intawong (2006).(b) SRTM (Shuttle Radar Topography Mission) digital elevation model of the same area (Watkinson et al., 2008). Also shown in (b) is the location of the study area (in box).

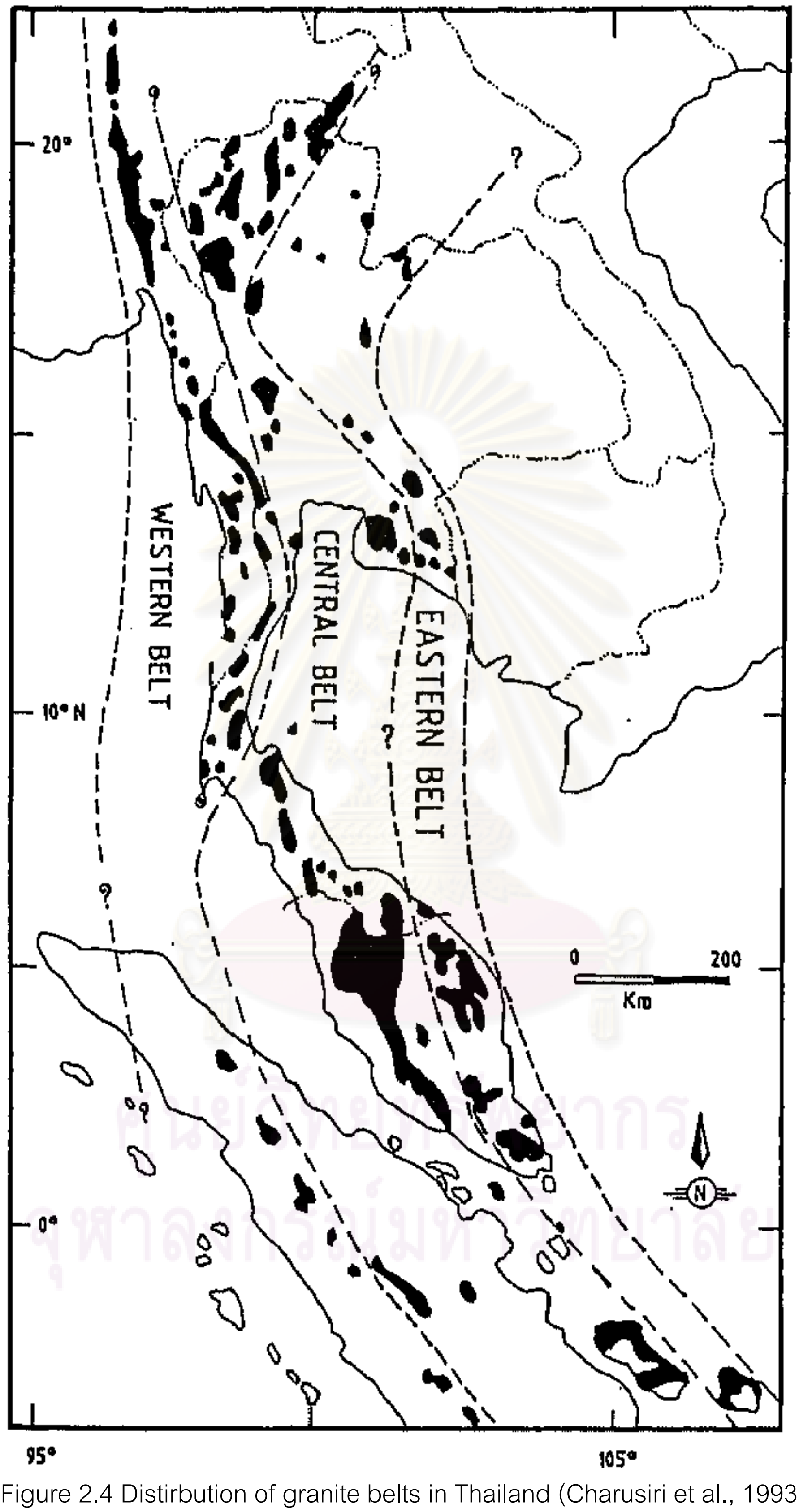

Figure 2.4 Distirbution of granite belts in Thailand (Charusiri et al., 1993).

The Thai Peninsula (Figure.2.1), where the study area is located, lies near the western edge of Sundaland, the southeasttern promontory of the Eurasia plate which is bounded by active oceanic spreading centres, strike-slip faults, and pre-Cenozoic sutures (Hall and Morley, 2004). Four major terranes make up mainland Southeast Asia, including South China, Indochina, East Malaya, and Sibumasu (Metcalfe, 1991). Magmatism attributed to the prolonged phase of subduction, collision and crustal thickening occurred across eastern Myanmar, western Thailand, peninsular Malaysia and Sumatra.

Granitoids rich in ore deposits occur as stocks and N–S trending elongate batholiths, arranged into three geochronologically and petrologically distinct N–S trending bands: the Western, Main Range (or Central), and Eastern Granite Provinces. The granites range from small I-type Triassic intrusions in the east to larger S-type Palaeogene bodies in the west (Charusiri, 1989). Granites of the Western Province lie within and around the KMF and Ranong Fault, while Main Range (or the Central Province) granites crop out immediately SE of the KMF (Figure 2.4). It is noted that the boundary of the Western and Central (or Main Range) Granite Belts is located along the KMF (see Fig. 2.3 and 2.4).

2.1.2 Geological setting

Geology of the region is depicted as a geologic map with scale 1:1,000,000 and modified geologic map scale 1:50,000 of changwat Surat Thani and it consists of severalunits of metasediments and sedimentary rocks and few granite intrusive rocks. Ages of the rocks vary from Carboniferous to Quaternary. Almost all rock units were cut by the KMF. In this thesis, the geology is explained only along and within the KMF (Figure 2.5), based on the work of DMR (2005).

2.1.2.1 Kaeng Krachan Group (CP) covers most of the study area and composed of gray pebble mudstone, shale, siltstone and sandstone of Carboniferous – Permian period behaves continuously sequence and overlain by the limestone of Ratburi group, which in Permian period. This group is subdivided based on textures, structures, and occurrences, into four formations from bottom upward, namely Khao Wang Kradat formation, spillway formation, Khoa Hea formation and Khoa Pra formation, respectively.

I Khao Wang Kadat Formation composed of graywake sandstone and mudstone

II Spillway formation composed of well- sorted siltstone with abundant worm burrow and bioturbation. The structure resembles dropstones and generally often has the quartzitic sandstone interbeded with hummocky cross bedding type, interpreted to be accumulated beneath the influence of wind storm condition.

III Ko He formation consisting of gravelly mudstone, sandstone, and collectively called diamictic mudstone with channel-filled structure.

IV Khao Phra formation comprises mudstone, siltstone, quartzitic and arkose sandstones with limestone lens but accept to key bed with abundant fossils including corals and bryozoa.

2.1.2.2 Ratchaburi Group (P) is sedimentary sequence which is dominated by thick-bedded to massive the Permian limestone. It is pale gray to dark grey, with chert nodules in lower beds. Generality a lot of fossils particularly fusulinid, brachiopod, bryozoa, coral and foraminifera were found.

2.1.2.3 Triassic-Jurassic Sedimentary Rocks is distributed along the shore line in the eastern side of the KMF. Rocks are marine siltstone interbeded sandstone and with limestone lenses in some area.

2.1.2.4 Triassic-Cretaceous Sedimentary Rocks expose around the eastern side of the KMF. The rocks are non-marine shale, siltstone, and sandstone from reddish brown to red colors. In some area, cross beddings and ripple marks are discovered.

2.1.2.5 Cenozoic sedimentary rocks are young and semi-consolidated deposits. Shoreline sediment (Q) is composed of unconsolidated near-shore sediment, such as sand and fine sand with shell leavings and corals. Alluvial sediment (Qa) is deposited from active rivers covering some coast and tidal flat plain. Terrace deposits consist of pebble, sand, clay, and mud. Colluvial sediment (Qt) includes of gravel, sand, laterite and alluvial terrace this sediment often appear to follow the foothills and short hill.

2.1.2.6 Igneous Rocks are mainly granites of Triassic & Jurassic ages (Trgr & Jgr), distributed within the narrow area on the western part of the KMF with the large-sized massive (batholiths and plutons) intrusives. (Department of Mineral Resources, 2005). Granite is mainly characterized by large-sized sediment xenoliths and composed largely of feldspar, quartz, biotite and muscovite. In some small stockes, granites contain hornblende and magnetite. Most granites, particularly in the study area, are of Cretaceous age (Kgr).

2.2 Neotectonic Evolution

Deformation of Thailand throughout Cenozoic Period is a result of the collision between the Shan Thai block and Indochina block in the first collision (Paleotectonic) and between Indian plate and urasian plate in the second collision (neotectonic). The interaction of Shan Thai and Indochina blocks at late Paleozoic age is the reason of main conjugate fractures system in northeast line and the northwest line in Thailand (Bunopas & Vella, 1983, Charisiri, 1989). The major northeast fractures and faults are Nam Pat, and Thoen-Long-Phrae Faults in northern Thailand and Ranong and Khlong Marui Faults in southern Thailand.

The experiments with plasticine of Tapponnieir et al. (1982) are shown in Figure 2.6. They indicated many similarities between the results of their experiments and those of the geology of the Southeast Asia. For instance, they proposed that the F2 fault in the experiment corresponds to the Altyn Tagh Fault, and the F1 corresponds to the Red River Fault. The tectonics of eastern of eastern Asia would thus reflect the succession in time of two major phases of the continental extrusion. The gap between block 2 and block 1, which are compared to the southern China and the Indonesia, respectively (Figure 2.6); would be analogous to the South China Sea, whereas the gap A, between the rigid block and block 1, corresponds to the Andaman Sea.

Focus on the neotectonic crash, the soft collision (early collision) between Indian and Eurasian plates commenced during Late Paleocene to Middle Eocene (58-44 Ma), whist the hard collision began in the Middle Eocene (44 Ma) (Curray, 2005). The Ceozoic tectonic evolution of this region can be separated into four stages, related to the northward movement of the Indo-Ausralian plate relative to the Eurasian plate. It is postulated by Srisuwan (2002) that the Cenozoic tectonic evolution of this region can be

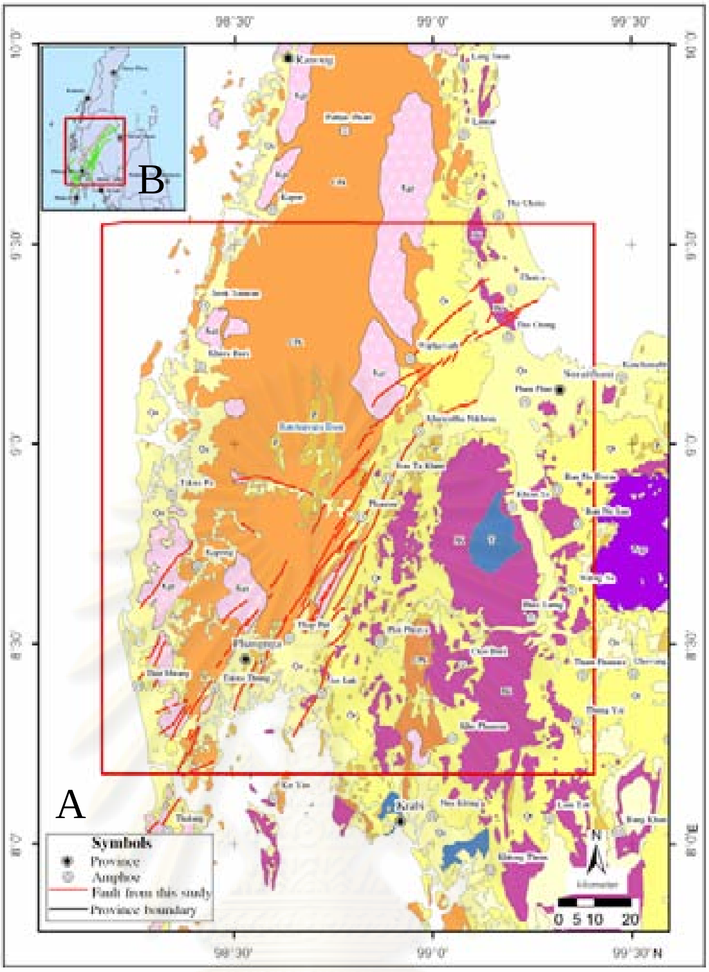

explanation

Sedimentary and Metamorphic rocks

Qa	Alluvial deposits : Gravel, sand, silt and clay
Qt	Terrace and colluvial deposit : Pebbles, gravel, sand, silt and clay
JK	Sandstone and siltstone,interbeded, reddish-brown,purlish-red, and whiish-gray frequently with gray to dark limestone and algal limesone, lens and limestone lens and locally interminable bivalves
T	Sandstone, siltstone, interbebed, reddish brown to brown : conglomeratic sandstone, conglomerate and dolomitic limestone with cross bedding, ripple mark and basal conglomerate
P	Limestone, light gray to dark gray, massive to bedded, coarse to fine crystalline, locally chert modules and labers : interbedded with sandstone shale, with fusulinids, brachiopods, corals, ammonoids, pelecypods and crinoids
CPk	Pebby mudstone, gray to brownish-gray, with pebbles of quartzite, granite and limestone :alternated shale and sandstone, shale and sandstone, white, medium=grained, well-beded

Igeous rocks

Kgr	Granite : Porphyritic granite, biotite-bornblende-muscovite granite and fine tourmaline granite
Trgr	Biotite granite, biotite-hornblende granite, porphyritic granite and biotite-muscovite-tourmaline granite

Figure 2.5 Geological map of the study area (A) in the southern peninsular Thailand (B) showing approximate locations of the major faults (modified after Department of Mineral Resources, 2007).

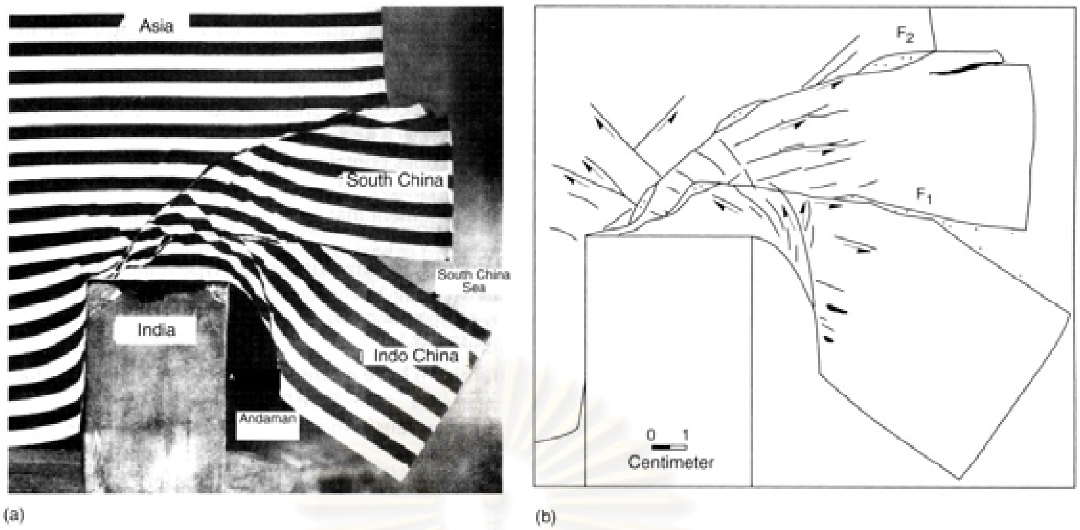

Figure 2.6 (a) Plasticine model of escape tectonics involving a rigid indenter and several laterally moving blocks along the major strike – slip faults. (b) Sketch of the deformation in (a). Note the pull-apart basins along both faults (F1 and F2) (Tapponnier et al., 1982).

discussed in four stages as follows.

Stage I: Early Eocene to Early Oligocence (50 to 32 Ma): the South China Sea margin extension commenced earlier than the collision of Indo-Australian with Eurasian and the supposed time of initiation of the Red River Fault. The more extensive rifting in the South China Sea is noted and the first time rifting in the West Natuna Basin area is also mentioned to commence at this stage. The Malay, Mekong Delta and parts of Gulf of Thailand had been openning at 40-35 Ma.

Stage II: Early Oligocence to Early Miocence (32 to 23 Ma): end of the lateral Mea Ping Fault was approximately 30 Ma. Simultaneously, the onset of widespread extension in the Gulf of Thailand, Malay and West Natuna Sea Basins began during Late Oligocence, and continued to Early Miocence. The northern Thailand basins probably developed at this stage. The Mea Ping and Three Pagodas Faults changed to dextral sense of movement whereas the Mea Chan, Uttaradit, and Phrae-Thoen Faults became sinistral.

Stage III: Early to Middle Miocence (23 to 15 Ma): clockwise rotation of the entire Greater Sunda Block and increasing in the convergence rate along the Sunda Arc. North Sumatra Basin and Central Thailand Basins were still undergoing extension. During 20-15 Ma, clockwise rotation of Southern Thailand and counter-clockwise rotation of Malay Peninsular and Sumatra were reported. Inversion in the Malay and West Natuna Basin, most Cenozoic basins in the Gulf of Thailand and onshore Thailand experienced uplift and erosion that corresponded to a pervasive Middle-Miocence unconformity.

Stage IV: Middle Miocence to Recent (<15 Ma): the counter-clockwise rotation of Borneo still continued while rotation of the Thai-Malay Peninsular and Sumatra ceased, and continued northward moving of Australia. North Sumatra had rotated counter-clockwise with south Malaya and the rotation proceeded the orientation of the Sumatran margin became less oblique to the Indian plate motion vector. This caused the dextral Sumatran strike-slip system, and extension in the Andaman Sea region.

Extension occurred in the Gulf of Thailand and inversion in the Malay and West Natuna Basins, whereas the Andaman Sea continued opening toward its present extent. All NW trending strike-slip fault zones in the Sunda region were dextral. The inversion and uplift episode, the structural activity in the Cenozoic basins of the Sunda region slowed down toward quiescence around 10 Ma to 5 Ma, during which period regional subsidence occurred and was probably induced by post-rift thermal re-equilibrium. This late-stage subsidence has continued to the recent time (Figure 2.7).

According to the convergent of Indian plate and Urasian plate in late Ceozoic, there were development of the South China Sea, and Cenozoic basins of offshore Vietnam, Cambodia and in Northern Thailand, have also been attributed to movement on the NW-trending strike-slip faults (Tapponnier et al., 1986), and offshore extensions of the KMF and RF have been linked to extension in the Andaman Sea and the Gulf of Thailand. However, Pacific plate still move to go to the northwest but Urasian plate almost still motionless while Indian and Indonesia-Australian plate moves to upward in the north in the character clockwise, all about these were cause of continuously evolution of structure in the South-east Asia (Watkinson et al, 2008) (Figure 2.8).

2.3 Active Faults in Thailand

2.3.1 Previous earthquake studies in Thailand

In Thailand, the first explanation on the earthquakes has been recorded directly from annals or stone inscription and astronomy. At present, there are many earthquake have been reported in Thailand, especially western and northern part of Thailand. However, a few researches have been reported, they have been more or less conce 25 with structural geology and tectonic geomorphology of southern Thailand.

Nutalaya et al. (1985) first studied characteristic earthquakes and described seismic source zones in the Myanmar, Thailand and Indochina areas. Twelve seismotectonic zones were identified. They located Thailand within zone F and zone G on the west and the north, respectively. However, from their report, southern Thailand and parts of northeastern Thailand were identified in the area without seismic source zones.

Siribhakdi (1986) studied seismogenic areas in Thailand and periphery and reported that earthquakes in Thailand throughout her past 1,500 year’s history. The foci and epicenters of the seismicity have been located both in Thailand and neighboring

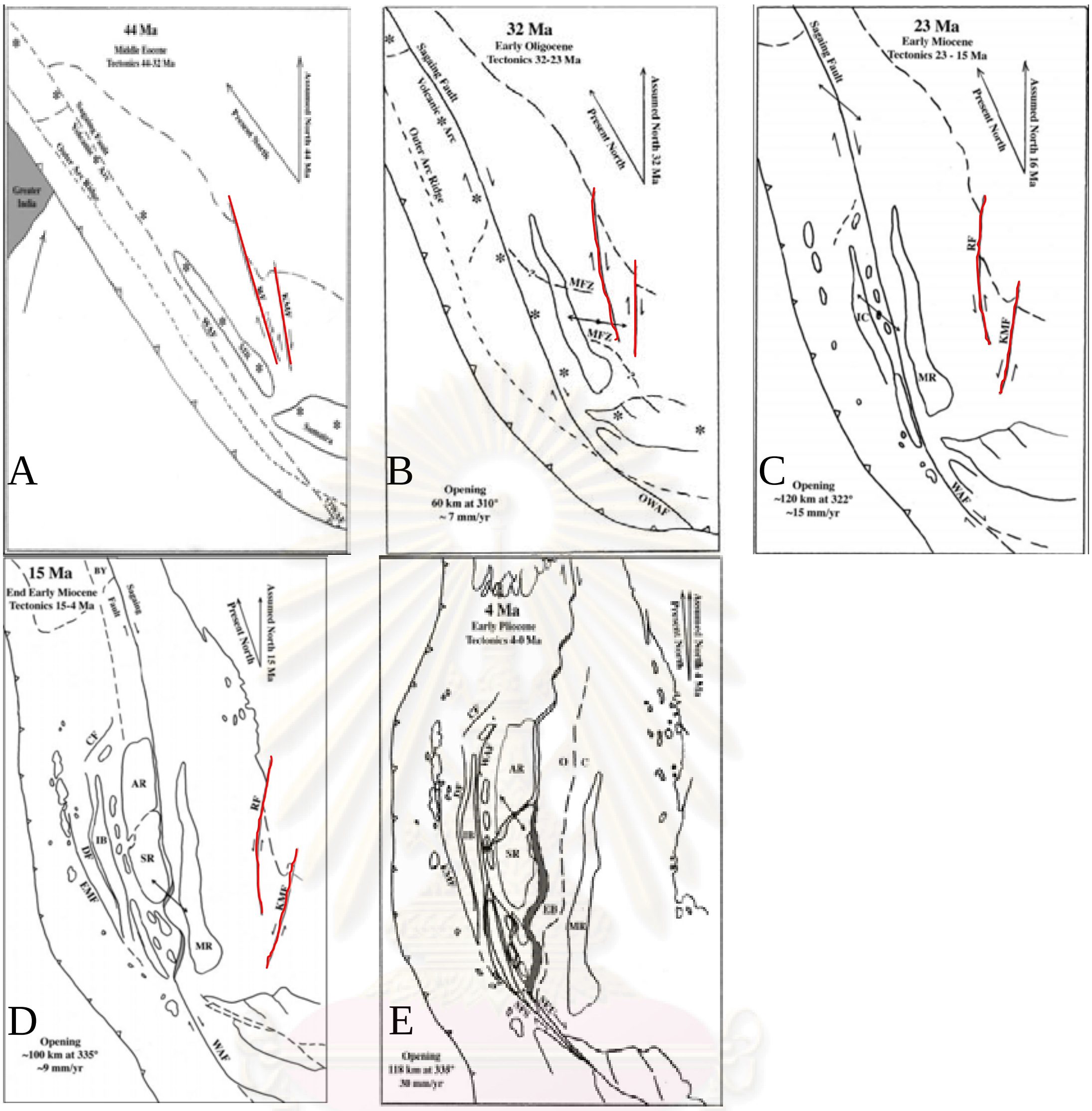

Figure 2.7 Tectonic evolution during 44 Ma (A), 32 Ma (B), 23 Ma (C), 15 Ma (D), and 4 Ma (E), showing the change in the sense of movement of the Ranong and Khlong Marui Faults (RF & KMF), respectively, between 32 and 23 Ma of the Andaman Sea (Curray, 2005).

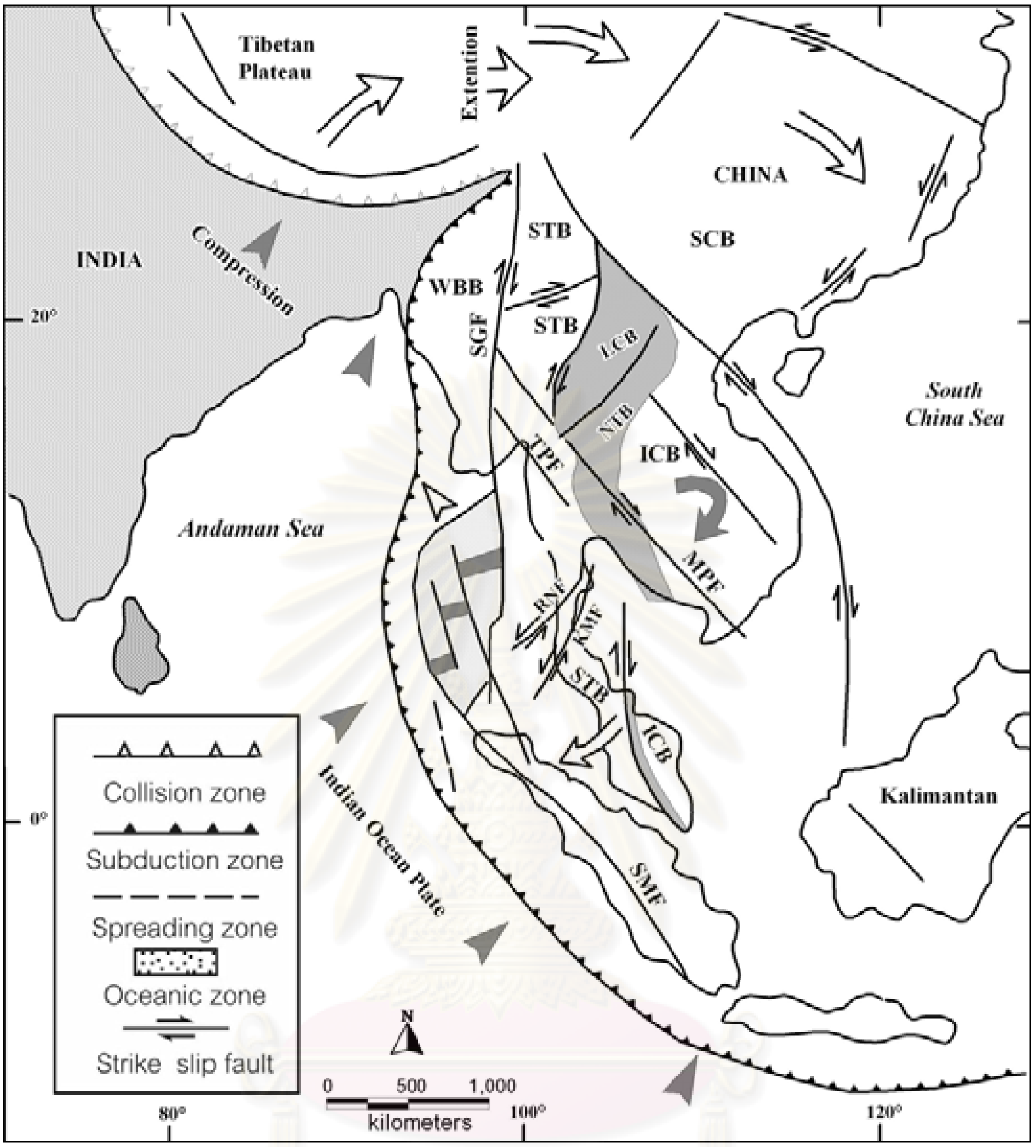

Figure 2.8 Tectonic map of SE Asia showing major fault systems and the relative movement of the SE Asian crustal blocks in response to India-Asia collision(modified from Polachan, 1989, Charusiri, 2002) (Notes: SMF = Sumatra Fault; SGF = Sagaing Fault; RNF = Ranong Fault; KMF = Khlong Marui Fault; TPF = Three Pagoda Fault; MPF = Mae Ping Fault; SCB = South China Block; STB = Shan Thai Block; LCB = Lamgpang Chaingrai Block; NTB = Nakhon Thai Block; WBB = West Burma Block and ICB = Indo Chian Block (Charusiri el al., 2007).

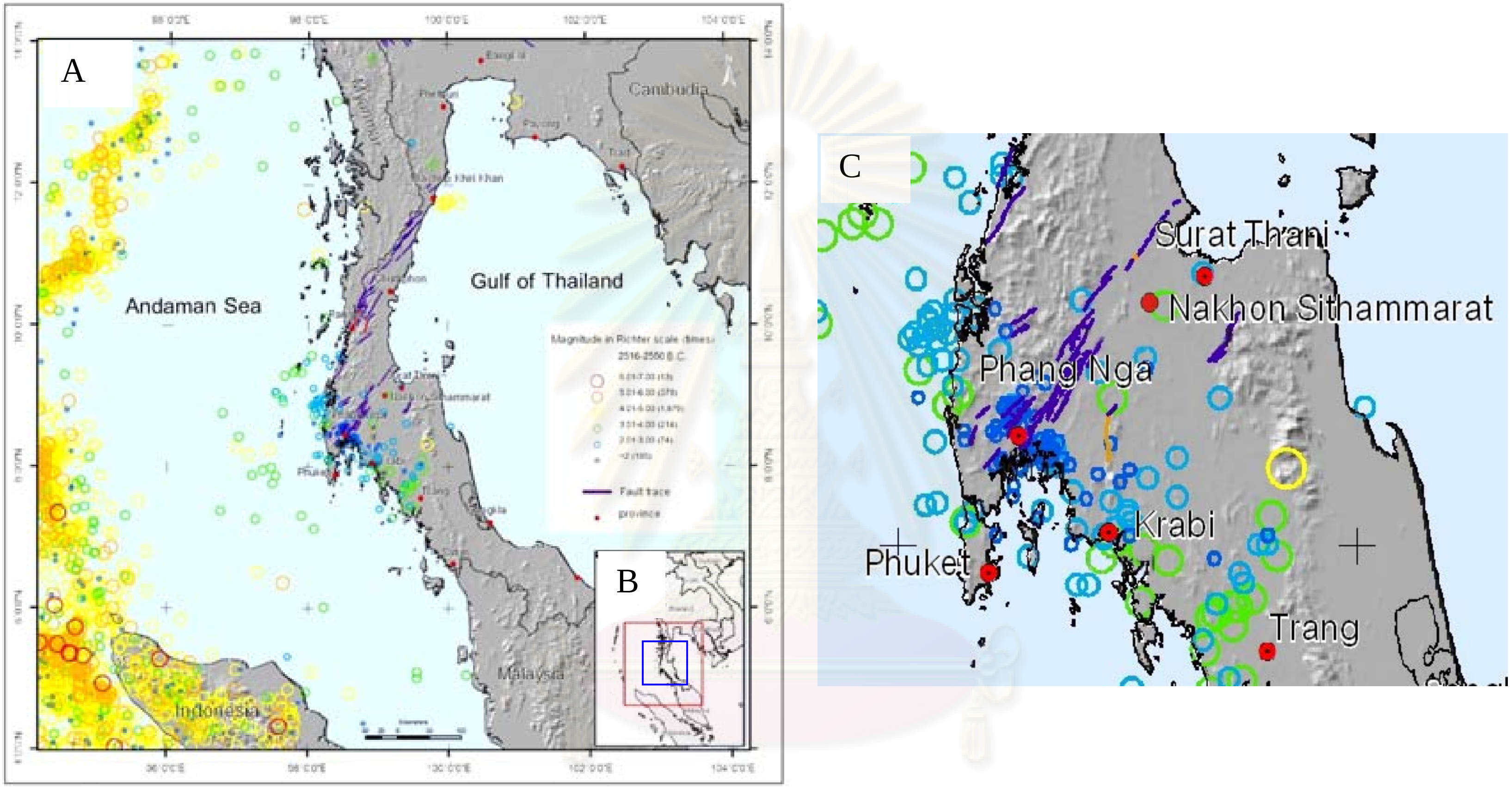

Figure 2.9 Map of Peninsular Thailand and nearby regions showing major active faults : Ranong Fault(RF) and Khlong Marui fault (KMF) and epicenter distribution (A).(modified after Department of Mineral Resources, 2007). Noted that the study area is located as blue box in (B). the study area with epicentral distribution and KMF is shown in (C).

24

countries. Many of the earthquakes in Thailand have close relation with four major faults including the Three pagoda, the Si Sawat, the Moei-Uthai-Thani and the Mea Hong Son-Mea Sariang Faults. He also mentioned that earthquakes in Thailand are associated with Tectonism, which is believed to be related to the subduction zone and spreading ridge in Andaman Sea (Figure 2.9).

Chuavirote (1991) studied major faults in Thailand and identified 13 faults including Ranong and Khlong Marui faults. He said that Ranong and Khlong Marui Faults were strike-slip faults and mainly trend in the northeast-southwest direction.

Garson and Michell (1970, 1975) studied transform faulting in Thai peninsular. They showed that the Keang Krachan Group, along the KMF was displacement at least 20 km in Tertiary time. The results of this study revealed that the KMF showed approximately 150 km slip from late Jurassic to early Cretaceous, due to subduction zone between Indian and Urasian plates.

Tapponnier et al (1986) investigated the mechanics of the collision between India and Asia, and suggested that the Ranong Fault was sinistral movement, and at the same time the KMF was dextral. However, in the middle Cretaceous, they commended that the KMF was sinistral as the Ranong Fault.

Charusiri et al (1996) applied several remote sensing techniques to study geological structures related to earthquakes in Thailand and neighboring countries. The results are useful in determining the seismic source zones to indicate the earthquake-prone areas. A new seismotectonic (or seismic-source) map is also proposed. According to this study, the Ranong and the KMF were located in zone G of their seismic-source map.

Hintong (1997) reported “Study of Active Faults in Thailand” and first produced the active fault map of Thailand. Based upon geologic and geochronological available data, and with exclusion of the tentatively inactive and inactive classification, fault activity can be classified as three classes namely, active, potentially active and tentatively active. Basically, there are three major criteria for recognition of active faults, namely, geologic, historic and seismologic criteria. Four classes have been proposed of active faults in Thailand including, potentially active, historically and seismologically active, neotectonically active, and tentatively active, respectively.

Charusiri et al. (1998) reclassed the active faults in Thailand into three classes, namely active, potentially active, and tentatively acitve based on results of morphotectonic and TL dating results. The KMF have been classed as potentially active fault (Figure 2.10).

Royal Irrigation Department (2006) studied seismotectonic investigation in the project “Rabrho Reservoir” in Chumphon provinece for consideration of suitability and environment effect of Thasae Reservoir. The results revealed that the Ranong, the Khlog Marui and Chumphorn Faults show no movement during Holocence and these faults are not active.

After an accident earthquake event on 27-28 September 2006 and 8 October 2006, Department of Mineral Resources (2006) and Royal Irrigation Department (2006) reported the macroseismic investigation and produce intensity maps from earthquake. The maps indicated that the most probable location of those epicenters are in the Gulf of Thailand rather than the Kungyangale Fault in southern Myanmar.

Department of Mineral Resources (2007) investigated the Ranong and Khlong Marui Faults with integration of data from remote-sensing, field work, and TL dating data. The result shows that both faults were sinistral strike-slip faults and have the latest movement at about 40,000 and 1,200 years ago, respectively.

Watkinson et al. (2008) studied the kinemetic history of the Khlong Marui and Ranong Faults, southern Thailand. They suggested that the Khlong Marui Fault was the zone of strike-slip faulting with 4 stress phases. They are, D1: low grade ductile dextral strike-slip shear complete before 87 Ma ; D2: medium to high grade ductile dextral strike-slip shear after 72 Ma and before 56 Ma; D3: brittle sinistral and sinistral reverse oblique strike-slip shear after 52 Ma; and D4: brittle dextral strike-slip shear at about 23 Ma.

2.3.2 Definition of active faults

The definition of active faults varies widely. Willis (1923) defined an active fault as the one on which a slip is likely to occur in the future, and a dead fault as the one on which no movement may be expected.

Albee and Smith (1996) proposed a definition of an active fault in a geologic sense as a fault which has moved in the past and will eventually break again in the

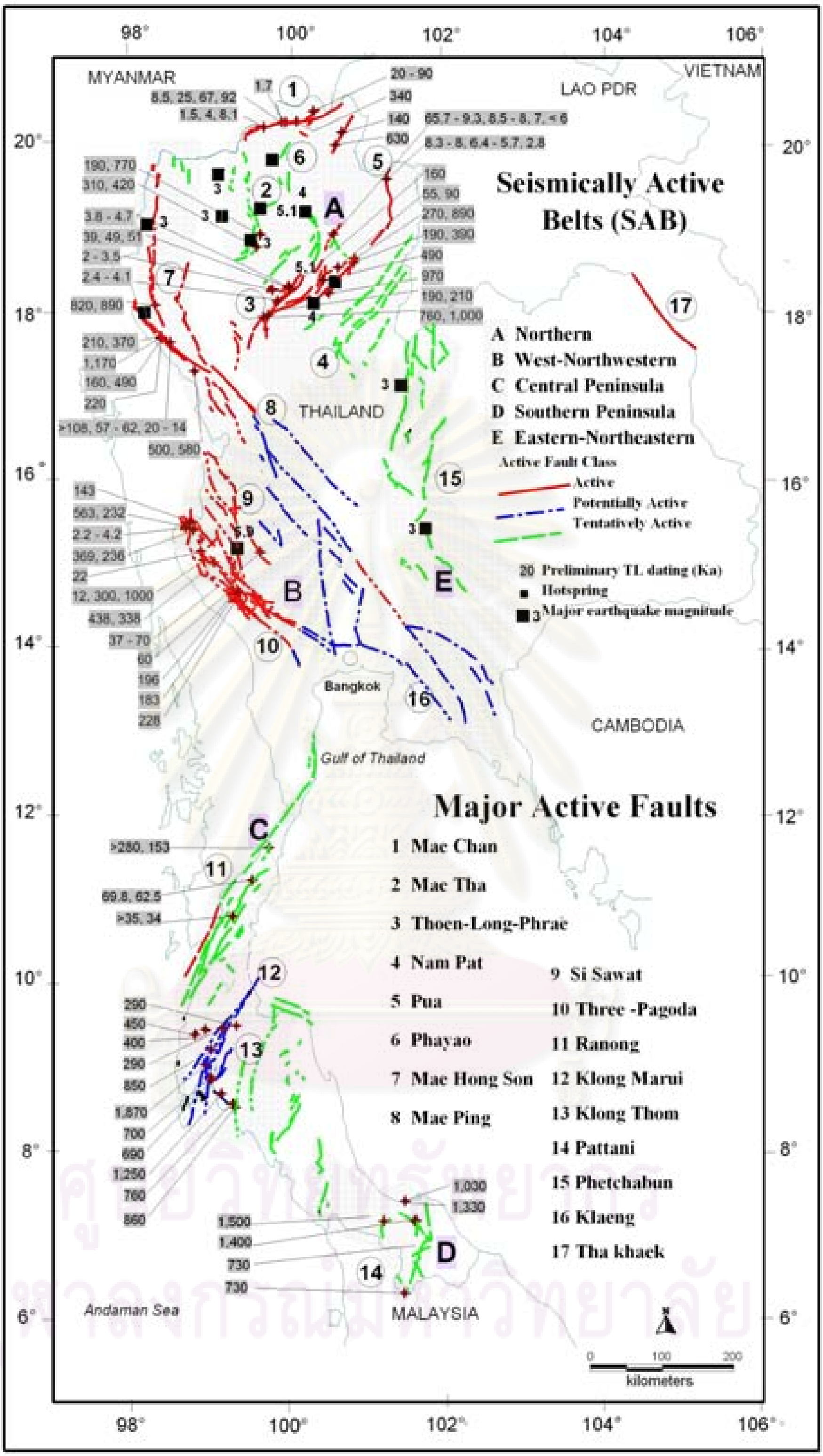

Figure 2.10 Map of Thailand showing major active faults and quaternary age dating results along the major active faults, (Charusiri et al., 1998). The study area covers along the fault line No.12.

future. The activeness of a fault is not just a single state that depends on the degree of activity.

An active fault in the definition of Wood (1915) refers to the historic movement that shows evidence of recent surface movement known as the trace phenomena.

Cluff and Bolt (1969) said that a fault should be considered active if it has displaced recent alluvium or other recently formed deposits, whose surface effects have not been modified to an appreciable extent by erosion.

Allen et al. (1965) stated that faults, which have had sufficiently recent movement to displace the ground surface are usually considered active by geologists simply because the ground surface is a very young and ephemeral feature. If stream offsets and scarps in alluvium are to be the criteria for activity of faults, then the term “active” must be applied to events dating back into the Pleistocence Epoch, perhaps as mush as 100,000 years.

In engineering design, fault activity is restricted to fault movement during the last 10,000 years, to the Holocence Epoch. This study adopted the definition proposed by the United States Bureau of Reclamation that an active fault is the fault that has a relative displacement within the past 100,000 years.

At present, methods for estimating future hazards of faults are deficient. The designation of a fault merely as active provides an inadequate indication of the attendant hazard. Restricting of the definition of active faults to those having had displacement within a defined past period of time, such as 10,000 or 100,000 years, provides little assessment of the hazard. In addition, the adoption of different restricted definitions by different agencies has caused confusion. An accurate expression of the probability of occurrence of future displacement, of earthquakes generated, and of the size of such events is needed in evaluating the hazards of active faults (Wallace, 1980).

The active fault, as used by United State Geological Survey (USGS), is a fault that is likely to have another earthquake some times in the future. Faults are commonly considered to be active if they have moved one or more times in the last 10,000 years.

The active fault based on International Commettee on Large Dam (ICOLD, 1989), is a fault reasonably identified and located, known to have produced historical fault movements or showing geologic evidence of Holocence, around 11,000 years, displacements and which, because of its present tectonic setting, can undergo movement during the anticipated life of man-made structures.

The Western States Seismic Policy Council (WSSPC, 1997) recommends that the following guidelines be used in defining active faults in the Basin and Range physiographic province. Active faults can be categorized into three types, recognizing that all degrees of fault activity exist and that it is the prerogative of the user to decide the degree of anticipated risk and what degree of fault activity is considered “dangerous”. They are: “Holocence Active Fault” – a fault that has moved within the last 10,000 years; “Late Quaternary Active Fault” – a fault that has moved within the last 130,000 years; and “Quaternary Active Fault” - a fault that has moved within the last 1,600,000 years. It should be emphasized in this thesis that half of the historic magnitude 6.5 or greater earthquakes in the Basin and Range province have occurred on faults that did not have Holocence activity, furthermore, earthquakes in the province will occur on faults in all three categories.

Site investigations for foundations of muclear power plants and research reactors (IAEA, 1988 and 1992; U.S. Nuclear Regulatory Commission, 1982.) states that a “capable fault” is a fault which has exhibited one or more of the following characteristics: Movement at or near the ground surface at least once within the past 35,000 years or movement of a recurring nature within the past 500,000 years; Macro-seismicity instrumentally was determined with records of sufficient precision to demonstrate a direct relationship with the fault; and a structural relationship to a capable fault according to characteristic 1) or 2) such that movement on one could be reasonably expected to be accompanied by movement on the other.

2.3.3 Active Faults in Thailand

Hintong (1995, 1997) reviewed the present status of the study of active faults program in Thailand. Apart from the knowledge of the importance of understaning of active faults, the various basic concepts, principles or even the implications have been laid out for refining. Approaches towards refining their definitions and classifications, as well as their criteria for recognition of active faults have been complied form various sources. The importance of active fault evaluation to society is that it provides the basis for design, sitting, zoning, communication, and response to earthquake hazards. It is necessary for all types of major engineering structures in order to reduce potential loss of life, injury or damage.

According to various authors and researchers, three approaches to define active faults can be distinguished and applied. These three definitions are characterized as general technical definition, engineering definition, and regulatory definition. Those three applications of definitions were discussed, based primarily on its original definition which was proposed in the context of a two-fold classification of dead and alive or active faults, and with respect to their potential for future renewal or recurrence of displacement or offset.

In consideration that based upon available data, and with the exclusion of the tentatively inactive and inactive classifications, fault activity can be classified as three classes, namely active, potentially, and tentatively, active. Basically, there are three major criteria for recognition of active faults: geologic, historic, and seismologic criteria.

In order to scope with the problems of the study of active faults in Thailand, the adoption of active fault classifications, specifically for the benefit of the utilization only in Thailand, four classes have been proposed, namely, potentially active, historically and seismologically active, neotectonically active, and tentatively active faults.

Consequently, with the restriction, deficiency of necessary data, and the lack of various seismologic, geodetic, geophysical, and other subsurface methods of analysis, not only supported by some thermoluminescence dating, the inventory of twenty-two preliminary active faults in Thailand have been outlined. The related purpose was to lay out major faults and fault zones for the preparation of preliminary active faults map of Thailand, scale 1:1,000,000.

Consequently, Charusiri et al, (2001), ranked the active faults, based upon historic, geologic, and seismologic data (Table 2.1). Since Thailand is not the main site for present-day large earthquakes as compared with those of the nearby countries, the best definition used herein is from the combination and modification of those above-mentioned definitions. Additionally, the age of the fault is also essential in their justification, it is proposed that the fault becomes “active” if it displays a slip movement in the ground at least once in the past 35,000 years ago or a series of quakes within 100,000 years. If the fault shows only one movement within 100,000 years, it would be defined as “potentially active”. Furthermore, if only once in the past 500,000 years, it would be become “tentatively active”. All of these faults are expected to occur within a future time span of concern to society. The fault becomes “neotectonic” if it occurred in Pliocene or Late Tertiary, and it is regarded as “paleotectonic” or “inactive” if it occurred before Pliocence (Table 2.2).

2.4 Khlong Marui Fault

Garson et al. (1975) were the first to create the name of Khlong Marui Fault in Phang Nga due to the fact that the fault runs parallel to Khlong Mauri stream. In their study there are many faults that were identified as the Khlong Marui Fault and they were shown in their structural map of Phuket – Phang Nga – Tai Maung. (Figure2.12)

The Khlong Marui Fault (KMF) has been suggested as one of thirteen active faults in Thailand (Figure 2.13) base on the report by Department of Mineral Resources (2000). The Khlong Marui Fault (KMF) and Ranong Fault (RF) are the major NNE-trending strike-slip faults which dissect peninsular Thailand. They have been assumed to be conjugate to the NW-trending Three Pagodas Fault (TPF) and Mae Ping Fault (MPF) in Northern Thailand, which experienced a diachronous reversal in shear sense during India–Eurasia collision (Watkinson et al., 2008).

Department of Mineral Resources (2007) investigated the paleosiesmicities in southern Thailand using the remote-sensing interpretation and dating in some selected areas. Base on their study in Phang Nga and Surat Thani provinces, both Ranong and Khlong Marui Faults are defined as the lateral faults that are almost parallel to one another. These two faults trend in the northeast-southwest direction. The KMF has the length of about 180 km and consist of 10 segments (Figure 2.13). The maximum paleoearthquake magnitude can be estimated from the length of fault segment (Well and Coppersmith, 1994) deduced from remote-sensing interpretation. The result revealed that the Khlong Marui fault also generated several paleoearthquakes with magnitudes of about 6.3 -7.2.

Royal Irrigation Department (RID, 2009), studied “Active fault investigation of Khlong Lum Rhoe Yai Dam Project”, Tai Maung, Phang Nga, RID (op.cit.) stated that Lum Loo and Khlong Suk segment of the KMF can generate large earthquakes with magnitudes of about 5.75 and 6.74 at areas of Vibhavadi to Ban Tha Khun and Ban Tha Khun to Phang Nga, respectively. The return period is estimated to be 2,000 years. Additionally, RID shows that the earthquakes with magnitudes 2.7 and 4.1 triggered at the scales of I to V on the Mercalli intensity. (see Figure 2.14). Intensity map of east Khao Phanom by earthquake on 23 December 2008 event in Surat Thani and on 4 May 2008 in Krabi (Figure 2.14) were also constructed.

Table 2.1 Active fault rank, criteria, and examples in Thailand (modified after Charusiri et al., 2001).

Rank	Historic	***Geologic***	Seismologic	*Examples*
Active (AF): ***Tectonic fault which displays a history of strong earthquake or surface faulting in the past 35,000 yrs, or a series of quakes during 100,000 yrs, and is expected to occur within a future time span of concern to human society.***				
	Surface faulting and assoc. strong quakes, also with geodetic evidence.	***Young Quaternary deposits cut by fault, distinct youthful geomorphic features.***	Epicenters along that fault.	*MaeChan,Phrae,Thoen,Pua.*
Potentially Active (PAF): ***A tectonic fault without historic surface offset, but with a recurrence interval sufficient to human concern, and with an earthquake within 100,000 yrs.***				
	Surface faulting unclear.	***Subdued & eroded geomorphic features, faults not known to cut young alluviums, but offset older Quaternary deposits.***	Alignment of epicenters but with low confidence of assigned locations.	*Mae Tha, Mae Hong Son, Srisawat, Three - Pagoda.*
Tentatively Active (TAF): ***A fault with insufficient data to define past activity and its recurrence interval is relatively very long or poorly defined, or displaying an earthquake within 500,000 yrs.***				
	Data indicate fault evidences, but evidences may not be definitive.	***Traced clearly by remote-sensing data with some hot springs.***	Scarce and low seismicity.	*Payao, Nam Pat, Ranong, Klong Marui, Klong Thom, Southern Peninsula.*

Table 2.2 Activity of faults in Thailand based upon age-dating data (modified after Charusiri et al., 2001).

Era	Period	Epoch	Yrs before	Fault activity
			0	
C E N O Z O I C	Quaternary	Holocene	11,000	**Active fault** is categorized within one of these events: 1) ***Active***- if one quake within 35,000 yrs, or several within 100,000 yrs. 2) ***Potentially active***- if one quake within 100,000 yrs 3) ***Tentatively active*** – if one quake within 500,000 yrs Neotectonic fault (difficult to determine-active or inactive)
		Pleistocene	160,000	
	Tertiary	Pliocene	350,000	
		Pre-Pleiocene	650,000,00	(Paleo-)Tectonic fault (or inactive)
Pre-Cenozoic				

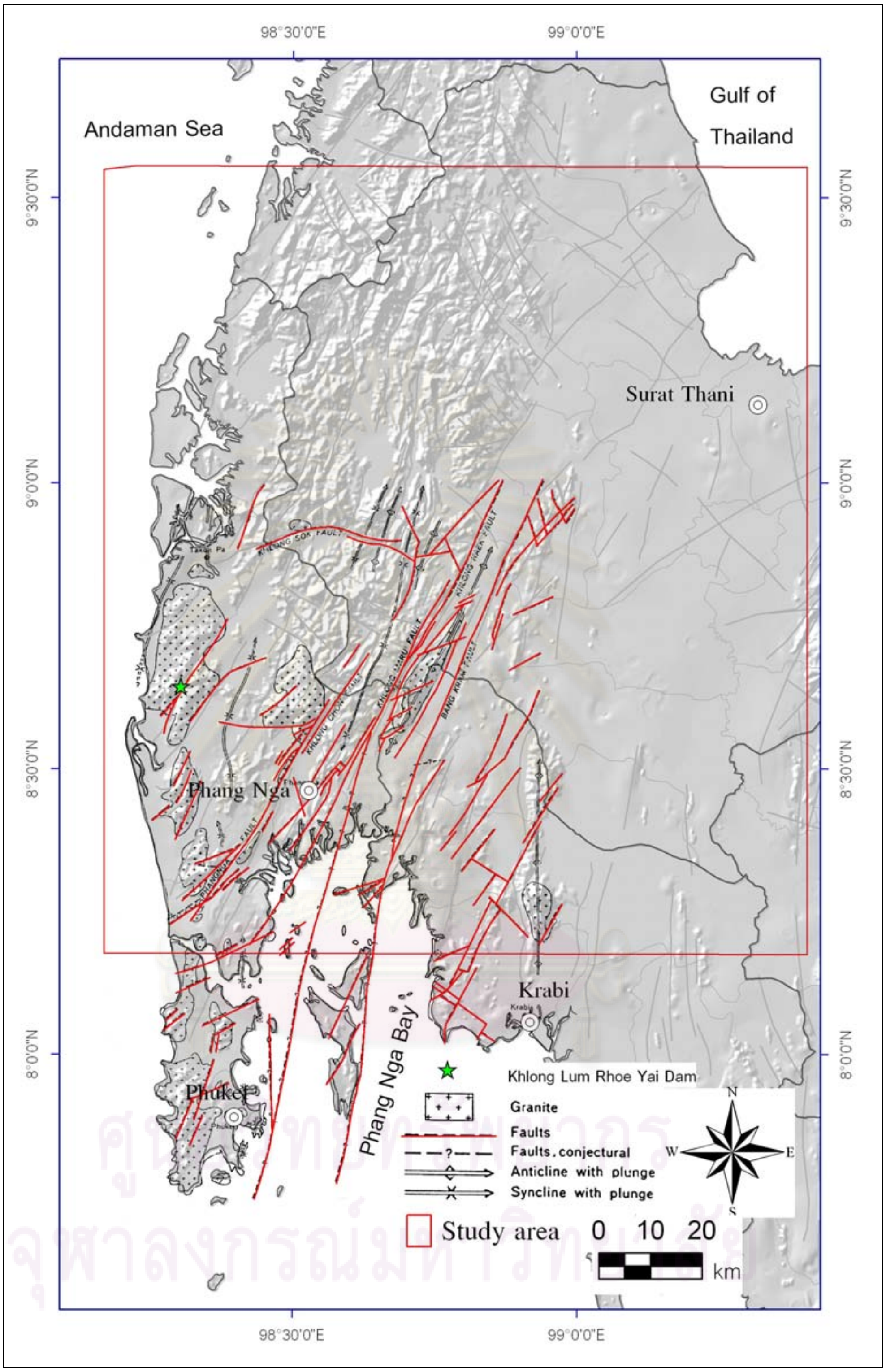

Figure 2.11 Map of the Andaman coastal area of Thailand showing distribution of granite plutons and major structures (Garson et al., 1975, and this study).

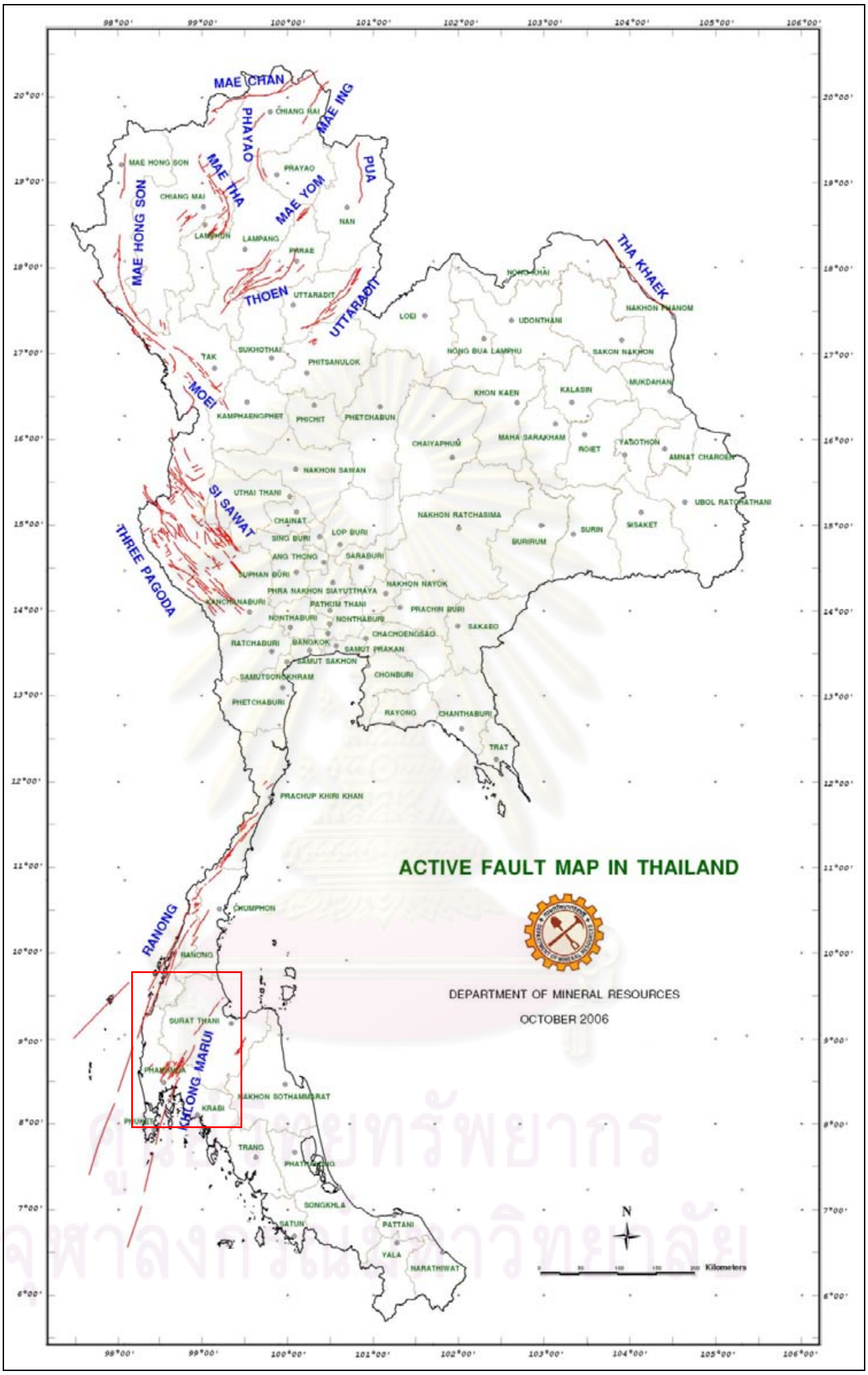

Figure 2.12 Index map of Thailand showing major active faults (Department of Mineral Resources, 2006). Noted that the study area is show as red box.

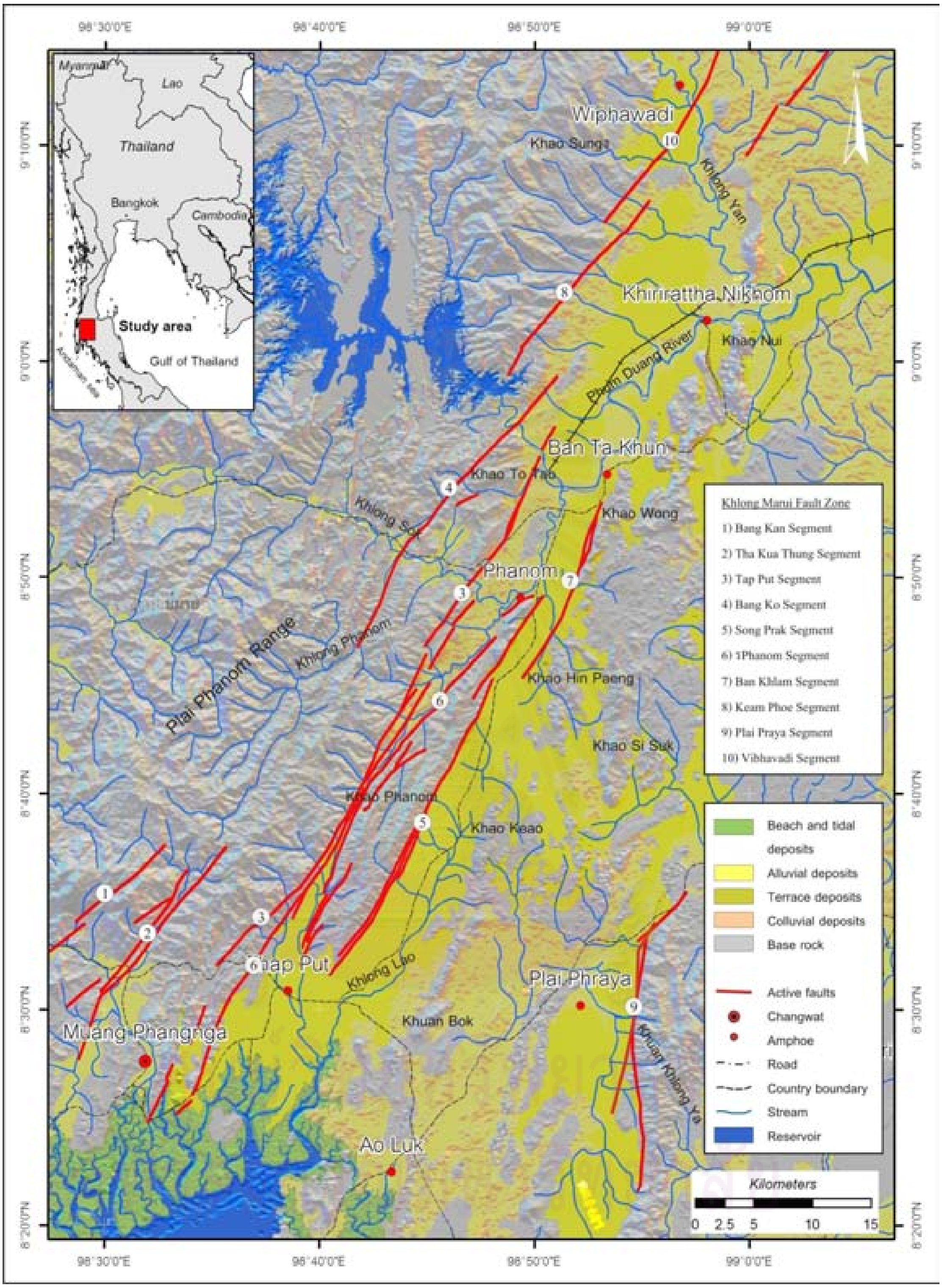

Figure 2.13 Major active faults and their segments in Phang Nga province, as identified by Department of Mineral Resources (2007).

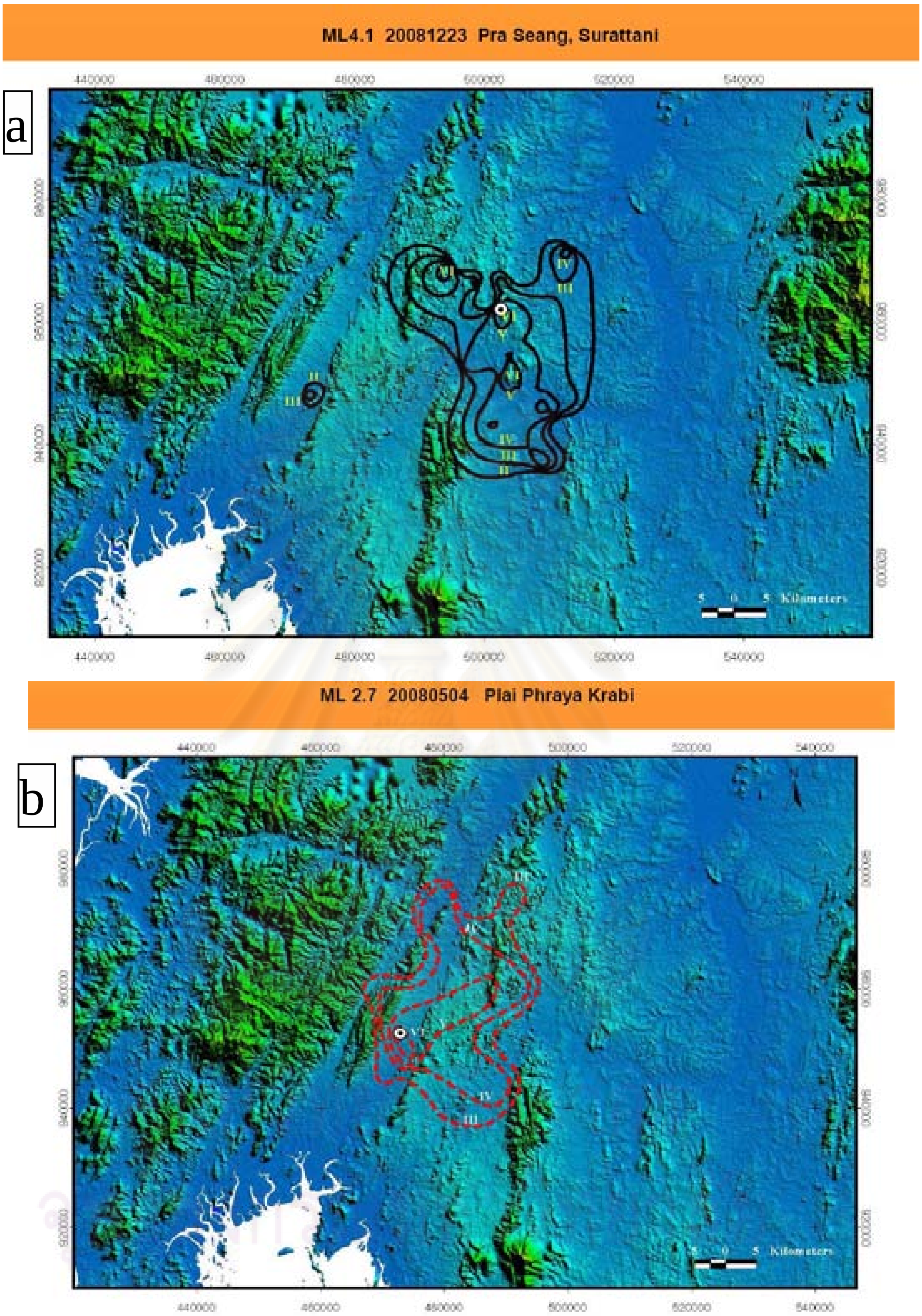

Figure 2.14 Currently earthquake intensity maps of the KMF showing (a) mercalli scale I-V of the earthquake with M_L 4.1 on 23 December 2008 in Surat Thani and (b) mercalli scale III-IV of the earthquake with M_L 2.7 on 4 May 2008 in Krabi (Royal Irrigation Department, 2008).

Chapter III

Remote-Sensing Investigations

In this paleoearthquake research the remote-sensing data have been used to interpret geology and structure geology. Remote-sensing data for this study comprises of satellite images, digital elevation model (DEM) data and aerial photographs satellite image were applied to cover the overall study area between latitudes of 7° 50’ to 11° 40’ and longitudes of 98° 10 to 99° 40’. The result from the remote sensing interpretation can be helpful in the study of geomorphic indices investigation and field investigation.

3.1 Materials

The image data from Landsat 7 ETM^{+} (enhanced thematic mapping), shuttle radar topography mission digital elevation model (SRTM DEM) and aerial photographs were applied in this investigation.

3.1.1 Landsat 7 ETM^{+}

The pictorial information was obtained from the satellite Landsat 7 ETM^{+}, which liberated to the space since April year 1999. This satellite takes electromagnetic wave signal that release out from earth surface (Figure 3.1) there are 2 types of EM-waves – one release from the sun to earth’s surface and refract out to the space and the other one is the electromagnetic waves that liberate to come out from world surface directly. Each kind on the Earth's surface has the ability in reflecting definite frequency waves spectrum (Figure 3.2). Because the pictures have the difference of contrast following each kind of signal electromagnetic wave. Satellite Landsat 7 ETM^{+} receive 7 wave bands, of which bands 1-3 are visible wavelength, bands 4, 5 and 7 are infrared wavelength, and wave band 6 is thermal infrared.

While the satellite orbited around the world, it toke a photograph, which covers 186 x 186 square kilometer areas. Each Landsat7 ETM^{+} image had the control’s number to keep running rounded orbit line, such as path 130/row 47 of Landsat 7 ETM^{+} image in this study, which were received from The Global Land Cover Facility.

Table 3.1 Band spectrum and wavelength interval of Landsat 7 ETM$^+$ used by Department of Mineral Resources (2007).

Band No.	Wavelength Interval (μm)	Spectral Response	Resolution (m)	Signal Quantization Levels
1	0.45 - 0.52	Blue-Green	30	8 bits
2	0.52 - 0.60	Green	30	8 bits
3	0.63 - 0.69	Red	30	8 bits
4	0.76 - 0.90	Near IR	30	8 bits
5	1.55 - 1.75	Mid-IR	30	8 bits
6	10.40 - 12.50	Thermal IR	120	8 bits
7	2.08 - 2.35	Mid-IR	30	8 bits

In this research 2 images data from the satellite Landsat 7 ETM$^+$ were used for interpreting structural geomorphology in the study area. The informative image detail is shown in tables 3.2.

Table 3.2 Image information from satellite, Landsat 7 ETM$^+$ applied in this research

No.	Path/Row	Data of Acquisition	Spectral Bands (no.)	Spatial Resolution (m)
1	129/54	22-02-2001	7	30 m (MX), 60 m (TI)
2	130/54	15-01-2002	7	30 m (MX), 60 m (TI)

3.1.2 SRTM DEM data

Shuttle Radar Topography Mission Digital Elevation Model or SRTM DEM, which is a kind of data from the satellite was used in this research. It was digital format that altitudes of world surface. The image data is the mathematic model for dilineating real topography and can be expressed in truthfully topographic map (or 3 dimension model). DEM pictures had applied the advantage for many research that related to topography work. DEM data was very useful to use in geology, especially study geomorphology for separate stone types and geological structure. SRTM DEM in this research received data assistance from CGIAR-CSI by the area researches cover lower southern Thailand (Figure3.3).

Table 3.3 Image information from STRM DEM used in this research

No.	Path/Row	Data of Acquisition	Spatial Resolution (m)
1.	STRM 56-11	29-06-2006	90x90

3.1.3 Arial Orthographic image

Aerial photography is the taking of photographs of the ground from an elevated position. The term usually refers to images in which the camera is not supported by a ground-based structure. Cameras may be hand held or mounted, and photographs may be taken by a photographer, triggered remotely or triggered automatically. Platforms for aerial photography include fixed-wing aircraft, helicopters, balloons, blimps and dirigibles, rockets, kites, poles and parachutes (Figure 3.4). Aerial photography should not be confused with Air-to-Air Photography, when aircraft serve both as a photo platform and subject (http://en.wikipedia.org/wiki/Aerial_photography).

As opposed to a bird's-eye view, photographs can be directed vertically. These are often used to create orthophoto – photographs which have been "corrected" so as to be usable as a map. In other words, an orthophoto is a simulation of a photograph taken from an infinite distance, looking straight down from nadir. Perspective must obviously be removed, but variations in terrain should also be corrected. Orthophotos are commonly used in geographic information systems, such as are used to create maps. Once the images have been aligned, or 'registered', with known real-world coordinates, they can be widely deployed. Orthophotos at a scale of 1:50,000 in this research were obtained from Department of Public Works and Town & Country Planning, and color-orthophoto at a scale of 1:15,000 were obtained from Royal Irrigation Department, covering Khao Phanom area, Surat Thani in southern Thailand, both of them were registered wgs-1984 zone 47N coordinates.

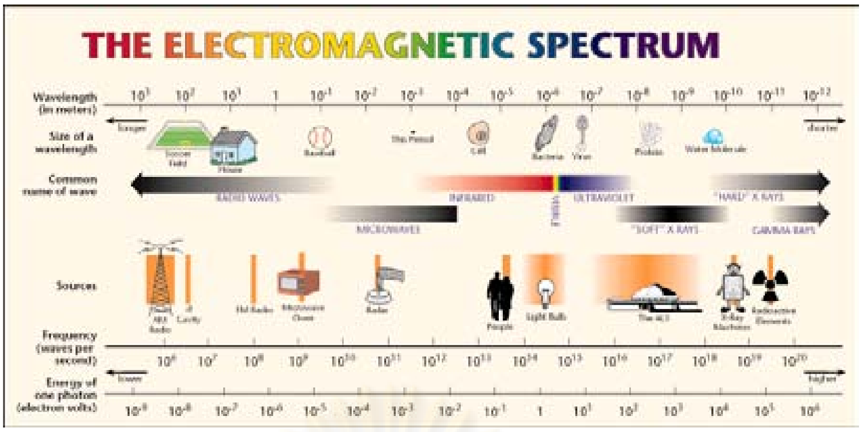

Landsat 7 Band Number	Applications
1	coastal water mapping, soil/vegetation discrimination, forest classification, man-made feature identification
2	vegetation discrimination and health monitoring, man-made feature identification
3	plant species identification, man-made feature identification
4	soil moisture monitoring, vegetation monitoring, water body discrimination
5	vegetation moisture content monitoring
6	surface temperature, vegetation stress monitoring, soil moisture monitoring, cloud differentiation, volcanic monitoring
7	mineral and rock discrimination, vegetation moisture content
	For more details see: Lillesand, T. and Kiefer, R., 1994. *Remote Sensing and Image Interpretation*. John Wiley and Sons, Inc., New York, p. 468.

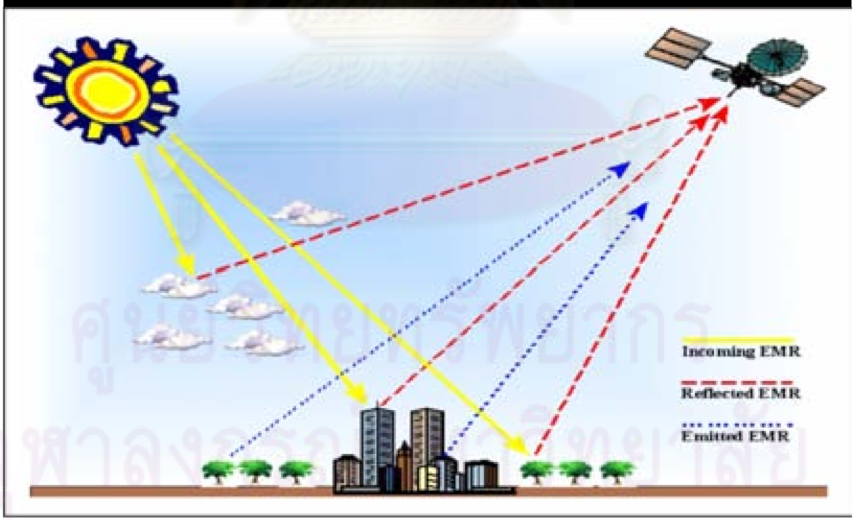

Figure 3.1 Detail of Landsat 7 space-borne image data with its application (a) EM wavelength spectrum, (b) individual Landsat7 band application, (Lillesand and Kiefer, 1994), and (c) simply image showing satellite receive EMR from object directly and reflection from the sun (www.nr.usu.edu).

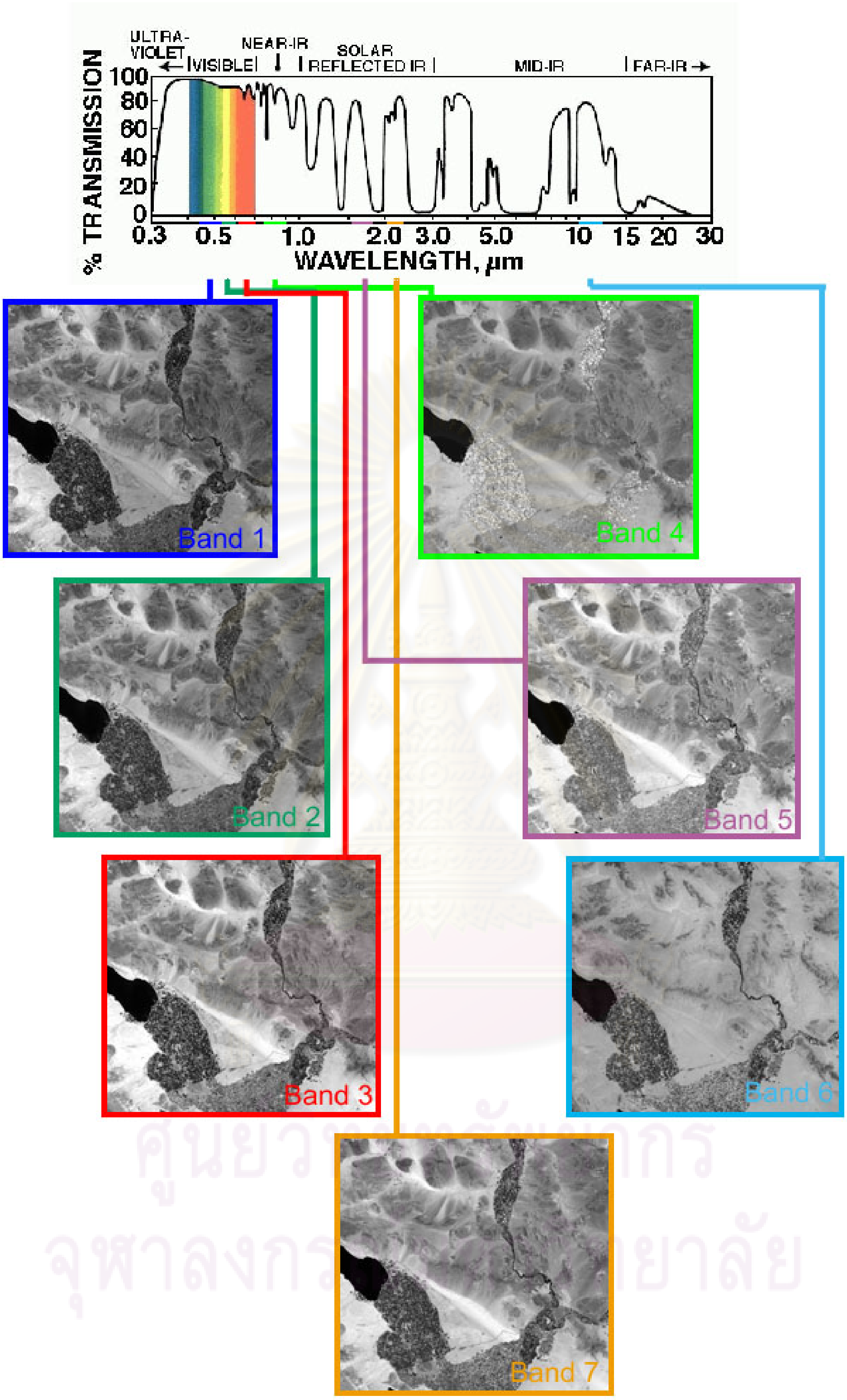

Electromagnetic Spectrum Image from Virtual Hawaii.

Figure 3.2 Digital image data of individual bands 1 to 7 of Landsat 7 and details of wavelength transmission (Lillesand and Keifer, 1994).

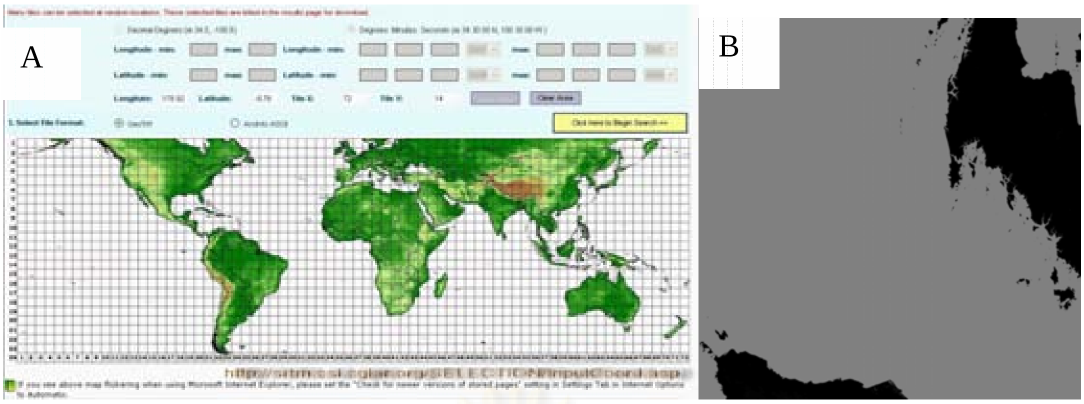

Figure 3.3 SRTM DEM index map of the world (A) showing location and the data sheet 56-11 that cover the study area (http//strm.csi.cgiar.org).

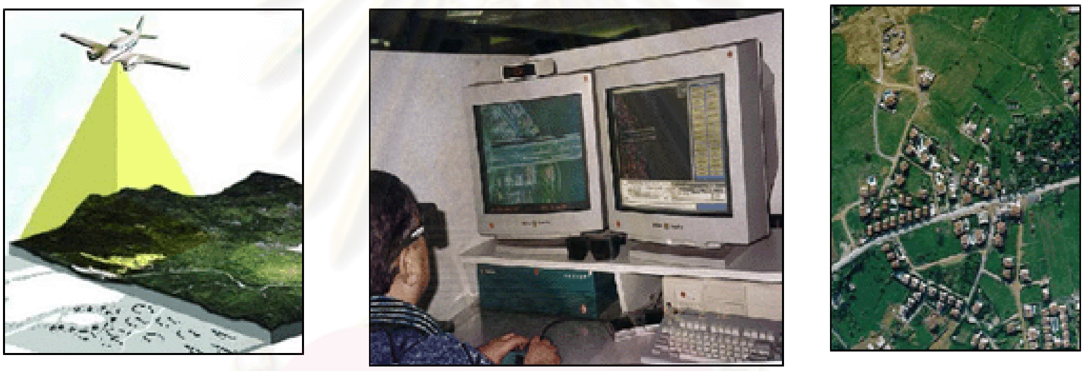

Figure 3.4 Arial photograph type-orthograph which was used in this research, (http://www4.oginfo.com).

3.1.4 Processes in Morphotectonic Investigation

In this study has used a program ENVI 4.0 was applied for data processing and adjust pictorial information quality from the satellite Landsat 7 ETM^{+} images and SRTM DEM data. Then the program ArcGis 9.3 was used in order to translate data in GIS format (Geographic Information System), one type of the digital data, which geographical coordinate system WGS 84 zone 47N was correctly adjusted in order to use easily and fast convenient. Based on geomorphology, color tone and stream pattern, the interpretation was divided into 2 parts-one is boundary limit of basins, which separated rock basements and currently young sediments, and other part was lineament structure interpretation from SRTM DEM data with topographic modeling or map topography shade (shade relief) by emphasized the fractures which sharp and continuous lines. The results of above-mentioned processes can be indicated that the structures happen not long ago and if those structure leaned across sediment basin area, which Quaternary sediment deposited with age of about 10,000 years to present-day, the traces line can be potentially active faults.

In this research Landsat 7 ETM^{+} images were adjust better quality with the PCA method and mixing false-colored composite image with the use of band 4 (red): 5 (green) : 7 (blue) shown in Figure 3.5, band 4 (red): 5 (green) : PCA7 (blue) in Figure 3.6, and PCA1 (red) : PCA3 (green) : PCA2 (blue) to interpret together with shaded relief map from the SRTM DEM data (Figure 3.7) with sunlight elevation 15° from ground surface and used sunlight direction in azimuth system 45° and 315°, in this case study for separated the different materials properties on surface.

Principle Component Analysis (PCA) was the method that is usually used in enhancing quality pictorial information satellite adaptation. The PCA was the procedure of reducing the non-relation data (uncorrelated output band) of DN value (digital number) from many satellite images in many wave bands to manage renewal data by statistics of calculating the average of the DN value for better more quality data (http://www.fas.org/irp/imint/docs/rst/Sect1/Sec1_14.html). In this study the PCA technique was applied to in enhance quality pictorial information satellite adaptation of Landsat 7ETM^{+} by choosing data during visible waves to mid-infrared waves including band 1-5 and band 7 (excepted band 6 because of it was thermal-infrared band). After post-processed PCA method, the results suggested that images from mixing false-colored composite band PCA1 (red) : PCA3 (green) : PCA2 (blue) was suitable for distinguishing young sediments from rock basement.

Contrast stretching, one of the adjusted data quality methods, was used because sometimes pictures from original satellite or pictures, which the quality had been adjusted with other way, show less sharpness pictures. The reflecting light from the materials had not enough that outcome picture have not different contrast too. From contrast stretching processed, the pictures had matched up color tone characters, more different contrast and more clearly sharpness. Topographic modeling was constructed from DEM data to bring out character topography models, which can be shown in various kinds such as contour line, TIN (Triangulated Irregular Network), Shaded relief, and three-dimension.

In this research pictures were made up the characteristic of shaded relief (Figure 3.8), which pictures had gray tone scale and dark tone level depending on the sunlight direction (azimuth) and the elevation the sunlight (sun angle) and if the sunlight decrease the angle, whereas the intensity level of gray will increase continually darker until black color. Furthermore, gray tone still depends on topography character, such as slope angle, slope direction (Aspect). DEM data was usefulness in geomorphology study, rock classification and structural geology, in this research used a program EVNI 4.0 to building shaded relief from the SRTM DEM data and SPOT DEM data by used sunlight direction azimuth 45^{o} and 315^{o} with sunlight angle 15^{o} and 45^{o}, respectively.

Next process was aerial photograph interpretation, based on the prominent structure, which had the clearness and the most interesting in all northeast-southwest line. The most selected area had suppose to found some evidence of active tectonic landform, especially clearly northeast-southwest line. Consequencely, choose aerial photograph scale 1:50,000 and 1:4,000 of aerial color photograph follow the range of Khao Phanom; the stand for northeast-southwest trend and south part of Ratchaprapa

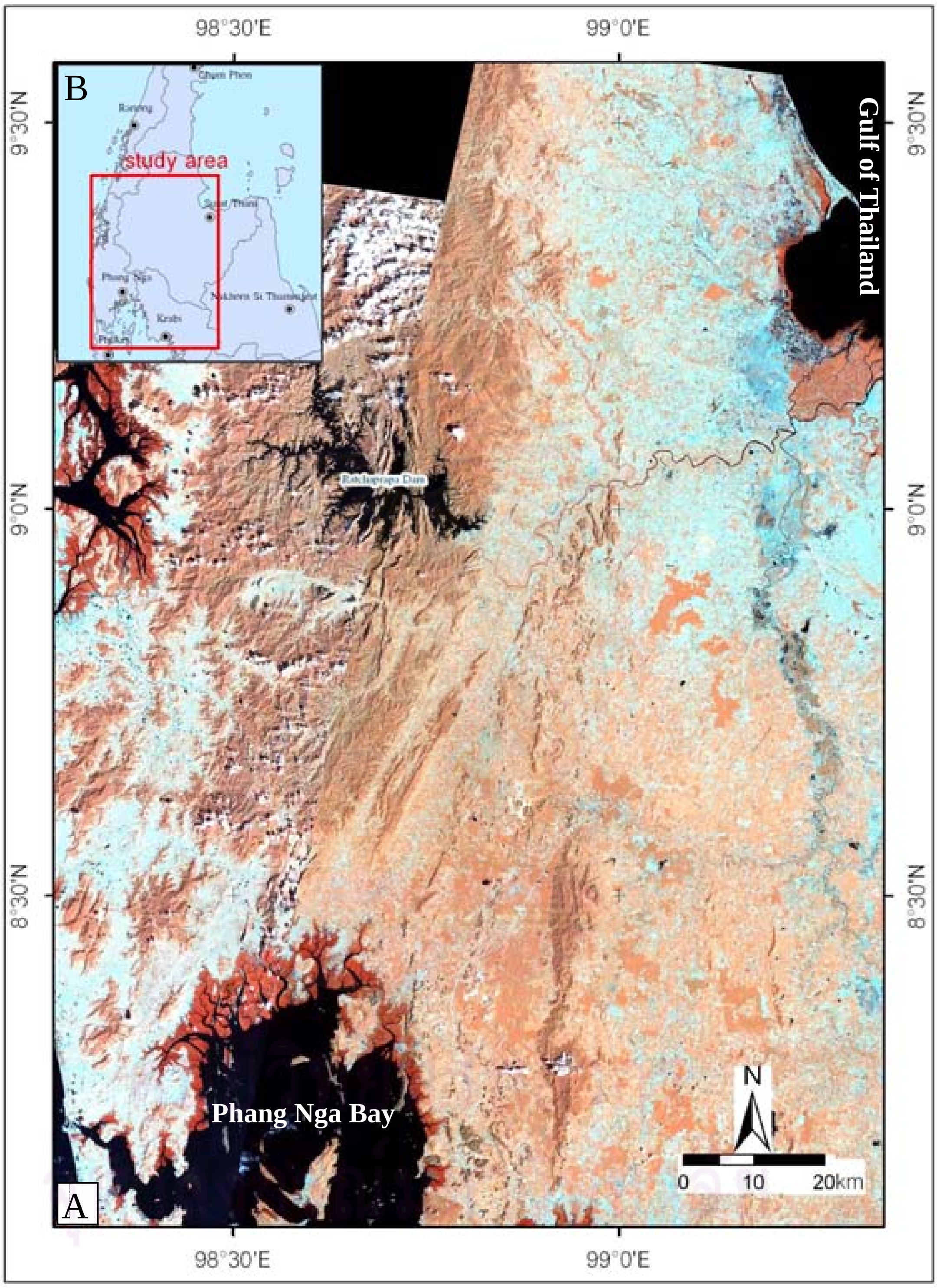

Figure 3.5 Enhanced Landsat 7 ETM+ with the false-color composite data of bands 4:5:7 (red: green: blue) (A) showing the contrasting geographic features of the study area (red box in B) in southern peninsular Thailand.

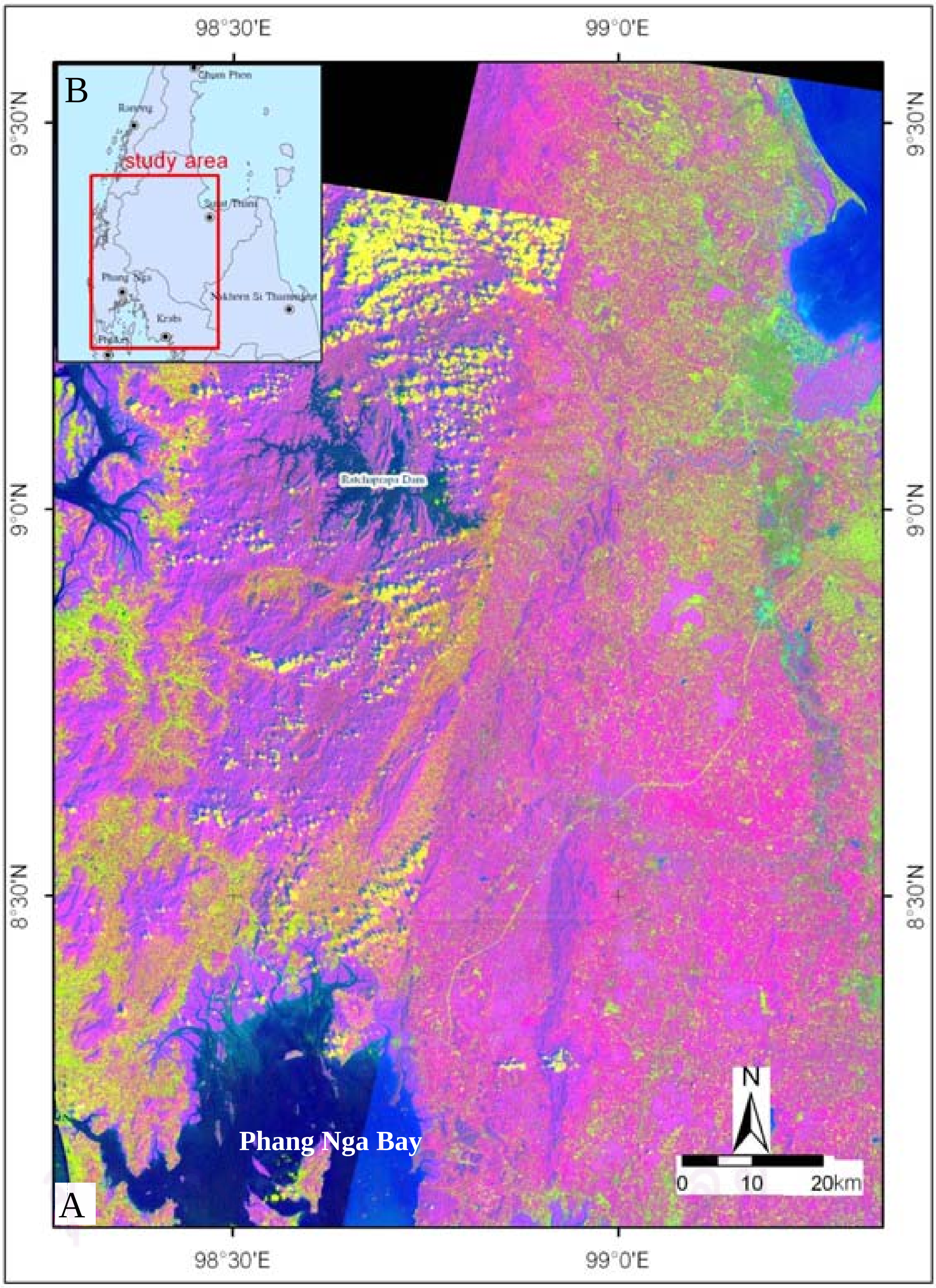

Figure 3.6 Enhanced Landsat 7 ETM+ with the false-color composite image data of bands 4:3/2:4/5 (red: green: blue) (A) showing various-coloured physiographic features of the study area (red box in B) in southern peninsular Thailand.

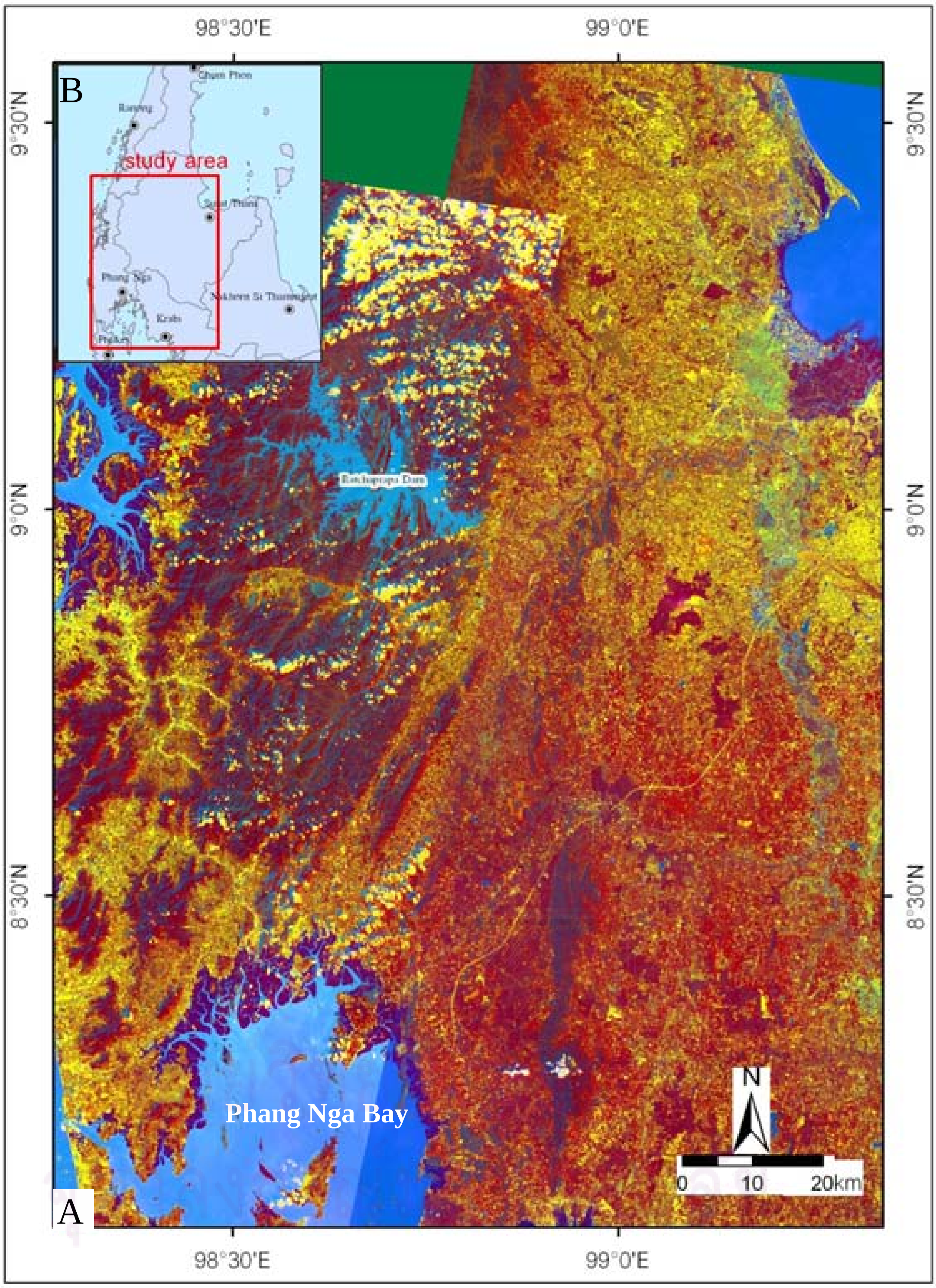

Figure 3.7 Enhanced Landsat 7 ETM+ by using the false-color composite image data of bands PCA1: PCA3: PCA2 (red: green: blue) (A) showing physiographic features of study area (red box in B) in southern peninsular Thailand.

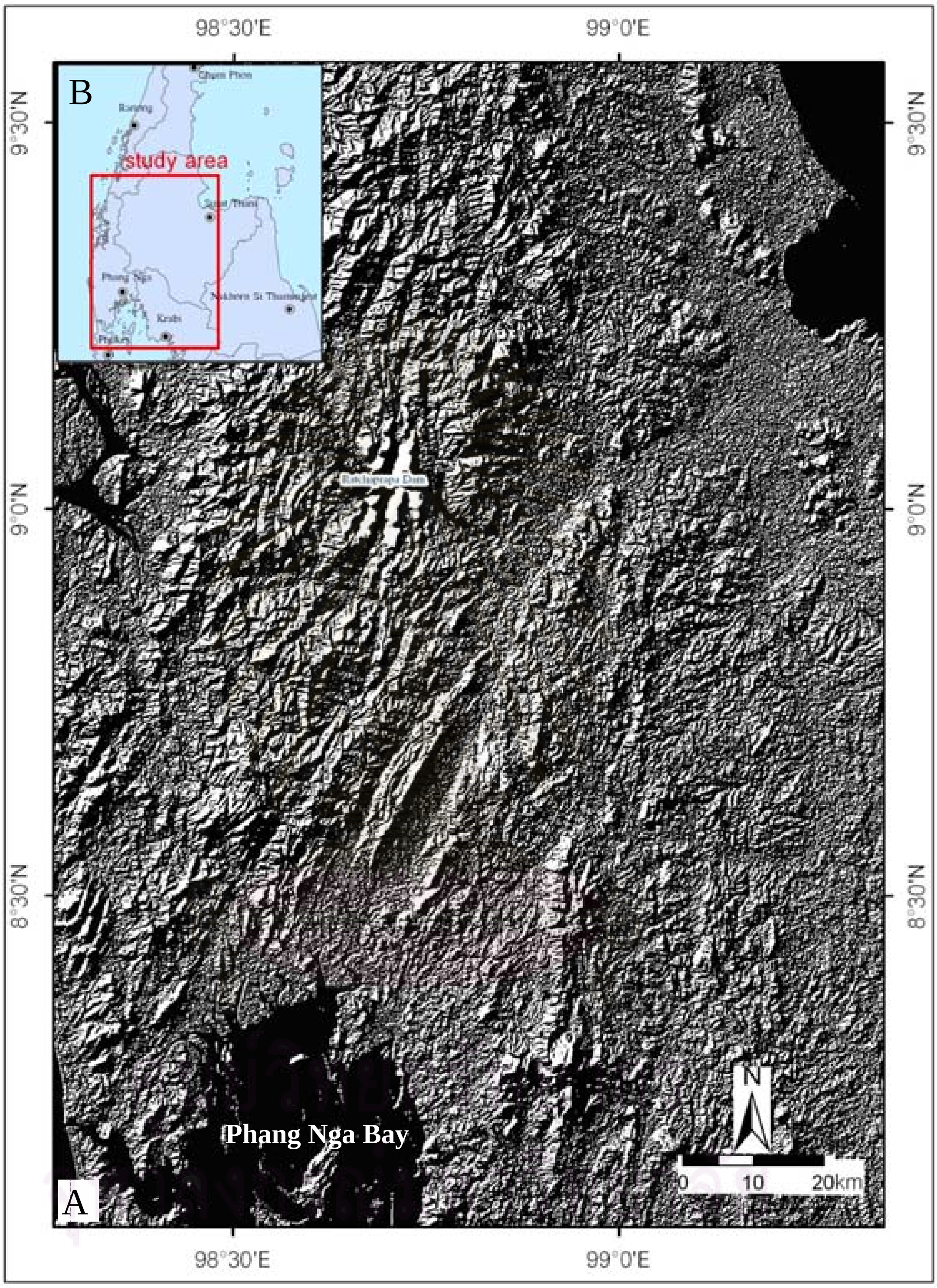

Figure 3.8 Shade relief image from SRTM DEM data (A) showing structures and fractures in the study area (red box in B) of the southern peninsular Thailand (also see interpretation in figure 3.11).

dam, which stand for northwest-southeast trend. The aerial photograph interpretation in the detail geomorphology was used the indicator feathers such as color, tone, texture, format, pattern, size, shape and shadow (Sarapirome, 2002) associated with active tectonic landforms for strike-slip faulting (Keller and Pinter, 1996), there were several explanation of each tectonic landform associated with active fault as explained below (Figure 3.9).

(1) Linear valleys was generated from a transform faulting (strike-slip fault), which controls straight of the stream channels.

(2) Shutter ridge, which is a long and narrow mound that obstructs stream flow. The shutter ridge had effected of fault cutting through the hill ridge and appeared the ridge moved out from the originally mountain line, common evident of strike-slip fault.

(3) Offset stream which was a result of strike-slip fault by cutting through the stream, effect stream, which originally flow straight line was moved out and distance of movement from the originally stream line can be refered to displacement of fault movement.

(4) Beheaded stream, one of the cause of strike-slip fault, was formed by stream, which appear as a straight line and was cut from originally line. A new stream shows no connection with the main stream.

(5) Fault scarp, the characterized slanting cliff, was caused of fault cut through that area, which can be controlled by both of normal fault and strike-slip fault. Common appear in the topography that showed steep cliff next to the basin and saw in rows a trace moves distinctly.

(6) Sag pond, which was effected from strike-slip fault and caused of subsidence of the land in the area, where fault cut through and filled by parallel fault water pond, normal fault and strike-slip fault can be caused of them.

(7) Spring and hot spring, which generated open gap of fracture subsurface consequence the underground water in that area flows out from subsurface. Somewhere was related to hydrothermal in hot spring form.

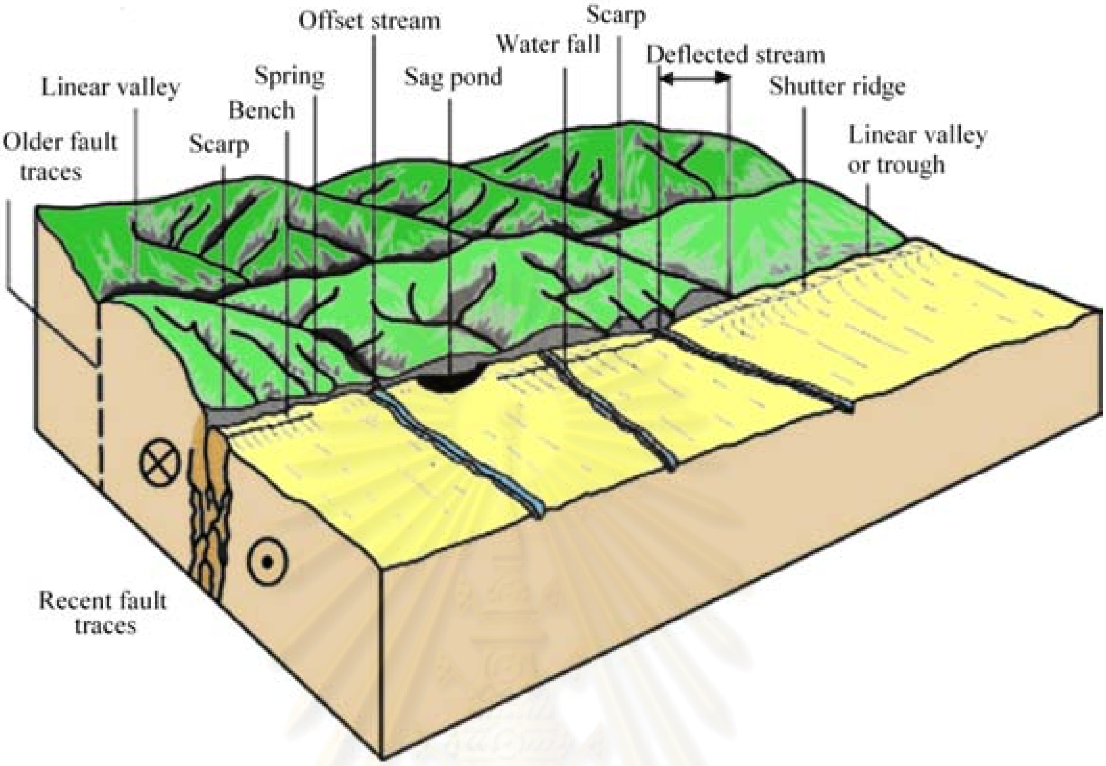

Figure 3.9 Assemblage of landforms associated with active tectonic strike – slip faulting (modified after Keller and Pinter, 1996).

(8) Triangular facet, the result of vertical movement of normal fault, was effected by surface erosion until have the look like triangle cliff character.

(9) Bench, the topography landform, that was developed from later triangular facet landform, where happen from normal fault until cause resemble like steps.

(10) Wine glass canyon; effected from normal fault, which cut through a stream channel and continue developed in erosional surface from horizontal erosion changed to vertical erosion. The result of valley that had resemble in wine glass, that is to say, the top of valley rather wide and below part will narrow and deep.

(11) Parallel ridge, the landform characterized not height hill and there was the wideness more than the length very much. It would be often appearance within 2 parallel fault segments, relative with horizontal fault movement rather than vertical fault movement.

3.2 Result and Interpretation

The interpretation from the remote-sensing founded that majority sediment basins deposited in small-sized sediments between the valley and coastal sediment and structural line which perhaps active faults compose of main northeast – southwest lineament group called Khlong Marui fault zone which began obviously visible on the land acrossed Phuket, the north of Phang Nga, the some area of the Krabi and the middle of the Surat Thani, respectively (figure 3.10). Furthermore, results of aerial photograph was supported of active tectonic from several evident active landforms.

3.2.1 Sedimentary basins and boundary

The characteristic of topography in the study area was majority mountain range in the west and east parts of the study area. The mountains lie in the northeast-southwest trend. From the interpretation it is suggested that sediment layers deposited in basins between mountain ranges both in the east and west were dissected by lineaments (or faults) (Figure 3.11). Besides, the interpretation it is simplified to separate sediment into three kinds, i.e., 1) colluvial sediment; A loose deposit of rock debris accumulated through the action of rainwash or gravity at the base of a gently sloping hill or slope area, found in mountain zone both in the west and the east, including valley basin.

3.2.2 Lineament structures

In an attempt to understand regional characteristics and patterns of geological lineaments in the study area and nearby, Landsat 7 ETM+ imageries and SRTM DEM data were conducted for lineament interpretation approach. The Landsat 7 ETM+ image with scale 1:250,000. In addition SRTM DEM data were used for creating a hill shade image or virtual terrain model as following to the above processes. In this study, lineaments longer than 0.5 km were delineated and shown in the lineament map.

The interpretation result from both enhanced Landsat 7 ETM+ images and SRTM DEM for neotectonic evidence was displayed (Figure 3.11). The false-colored composite (red, green, and blue) are digitally added to the image data. Hill shade image interpretation is used to assist in delineating large scale neotectonic features and to difine orientations and directions of the investigated fault segments (McCalpin, 1996). The results showed the appearance of several neotectonic features including fault scarps, triangular facets, offset streams and shutter ridges. Based upon Landsat 7 and DEM interpretation, there exists two series of faults – one trending in the northeast-southwest direction and the other in northwest-southeast direction (Figure 3.12). The major lineaments of faults lines, which are in the northeast-southwest direction, play a major role in shaping up the coast lines of Thailand Peninsular. Earlier works (such as Polachan, 1988, Charusiri et al., 2009) considered these fault zones was developed in Cenozoic time relative to the opening of basin in the Gulf of Thailand. The minor lineaments, which lie in the northwest-southeast and east-west directions, forming the conjugate sets of the major northeast – southwest – trending lineaments, appeared less numeral densities and shorter length than major trends (usually less than 10 km). As shown in Figure 3.12, most of lineaments which oriented in the northwest-southeast direction situate in the area dominated by basement rocks, whereas the lineament in the northeast-southwest direction situate in the area occupied by both basement rocks and and sedimentary basin. Additionally, those structural lineaments in the northeast – southwest accompanies mountain range lines.

There are about 211 lineaments which align in the northeast – southwest direction (Figure 3.12a) and about 69 lineaments in the northwest – southeast direction. The total of 290 lineaments were used to construct the rose diagram as shown in Figure 3.12c. The result indicates that the northeast – southwest – trending lineaments are much more distinctive.

3.2.3 Geomorphological features

Aerial photographs at the scale of about 1:50,000, which were used in this research, were obtained from Royal Thai Survey Department, and aerial color photographs at the scale of about 1:15,00 were obtained from Royal Irrigation Department, Ministry of Agriculture and Cooperatives. Based on results of lineament analysis by satellite image interpretation, several areas for aerial photographic investigation were selected. Regarding the result of aerial photograph interpretation, at least 6 areas are outstanding and shown in Figure 3.13 including areas A, B, C, D, E

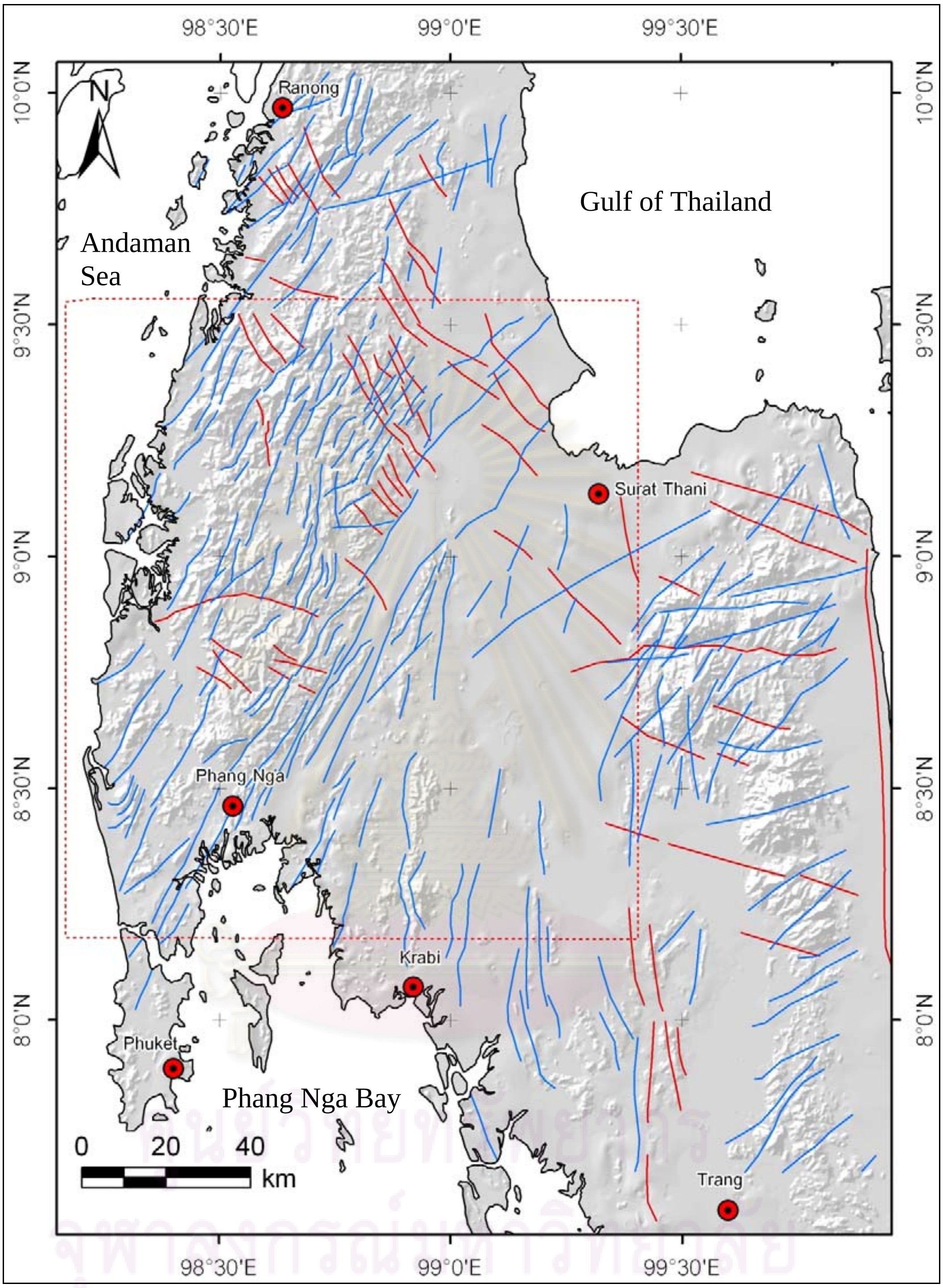

Figure 3.10 Lineament map of study area showing two major lineaments-one in the NE to NNE trend (blue) and the other in the NW to NWW trend (red).

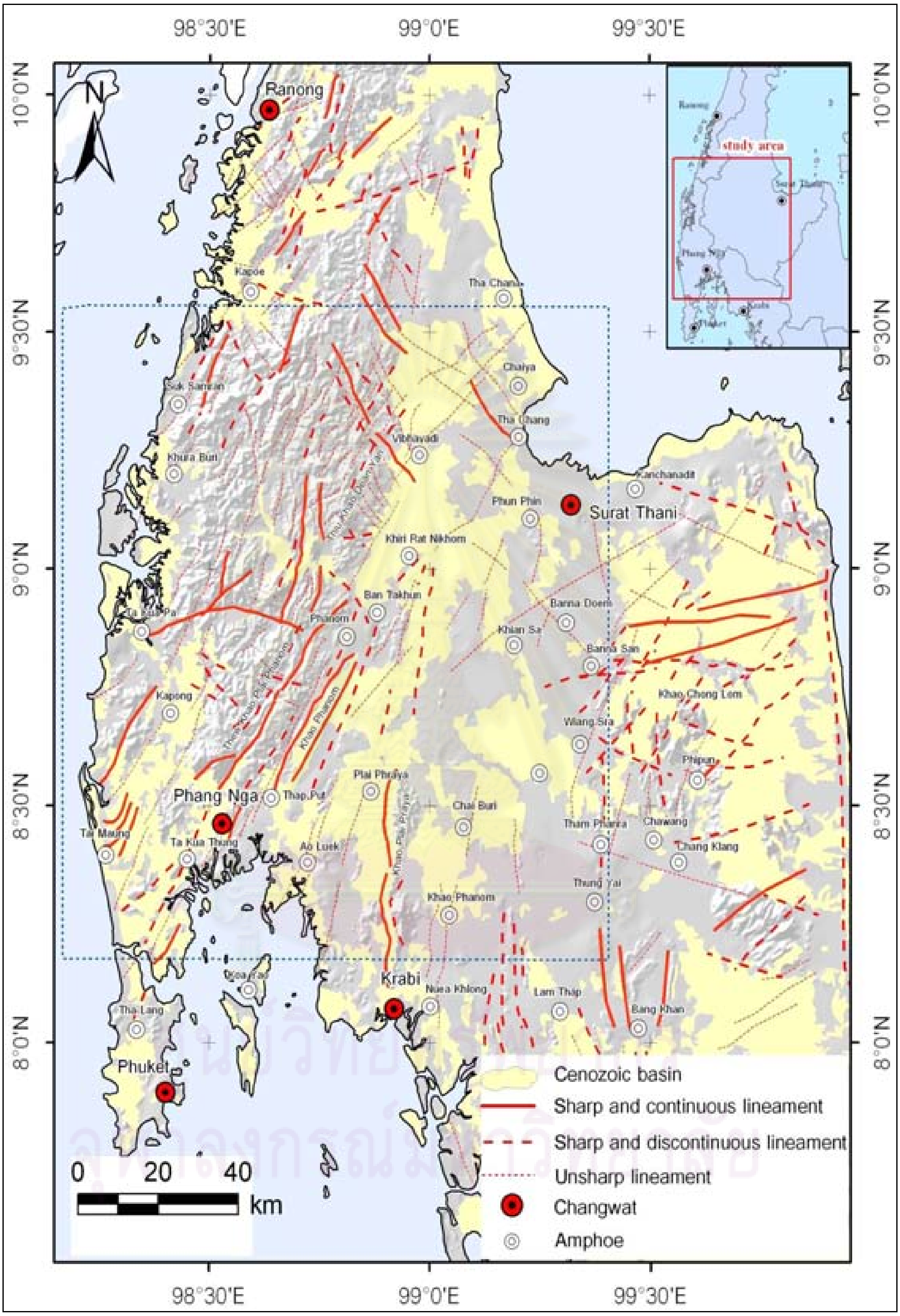

Figure 3.11 Map of the study area showing distribution of lineaments and Cenozoic sedimentary basins interpreted by using the enhanced Landsat 7 ETM$^+$ images and SRTM DEM data. Noted that several faults cut across the basins.

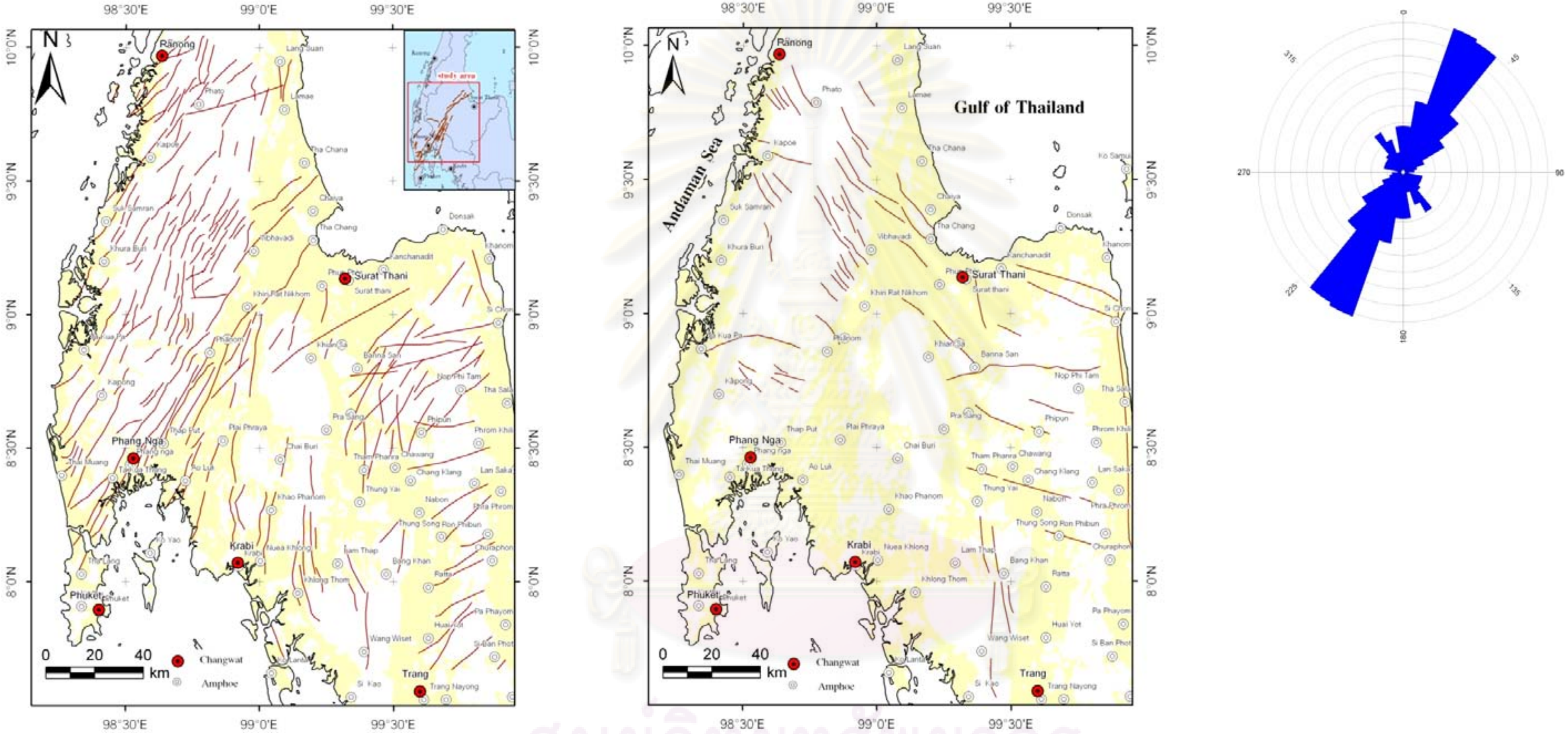

Figure 3.12 Lineament maps around the study area showing (a) the prominent and major northeast – southwest trending lineaments(211 lineaments), (b) the northwest – southeast trending lineaments (69 lineaments) and (c) Rose diagram base on 290 lineaments of both major trends in study area. Noted that and insert map in (a) showing the study area in southern peninsular Thailand.

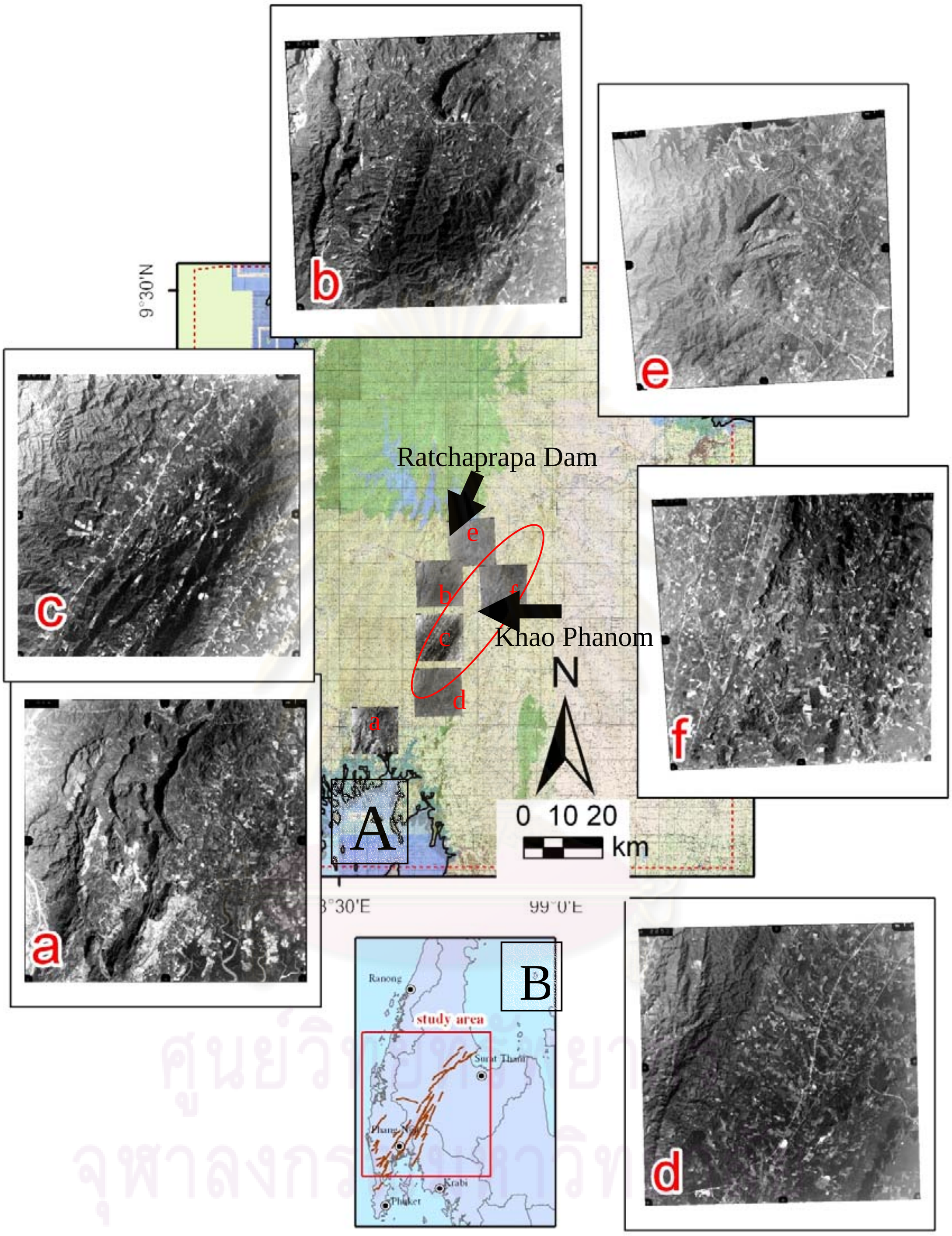

Figure 3.13 Topographic map of the study area (A) showing location of Khao Phanom area, and aerial photographic images for detailed tectonic landform interpretation in area a to f, in southern peninsular Thailand (B).

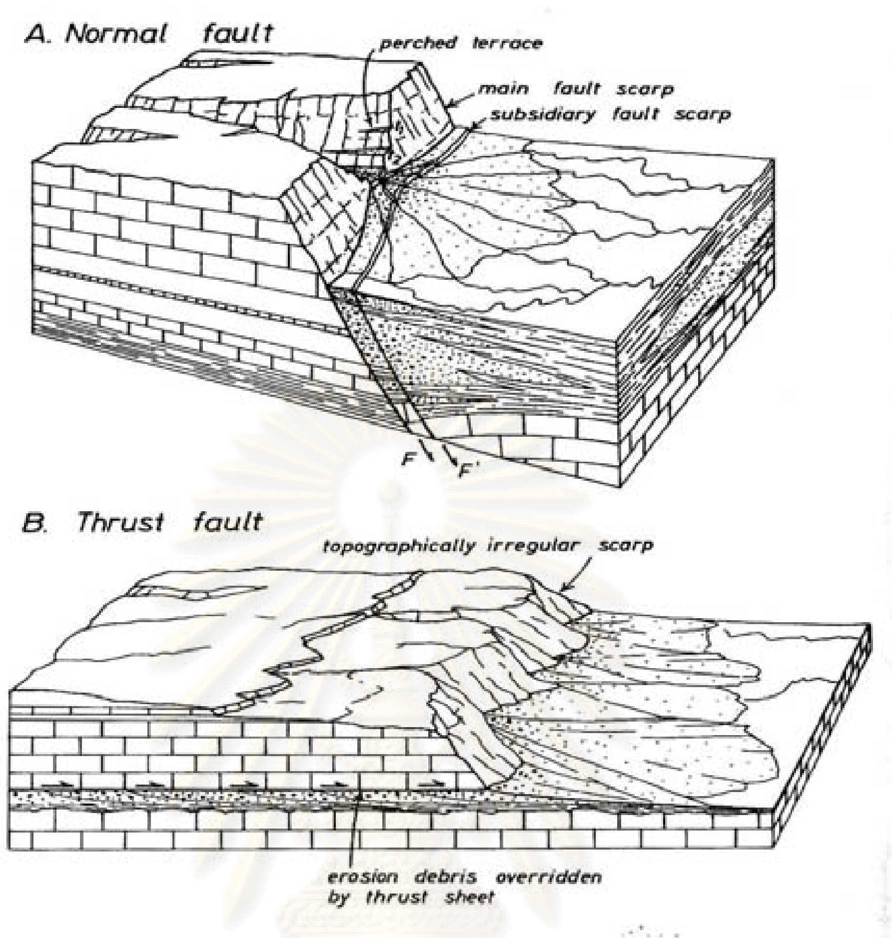

Figure 3.14 Model of geomorphological evidence showing essentail tectonic landforms by (A) normal fault and (B) thrust fault, (Ramsay et al., 1987).

and F. The interpreted maps are shown in Figure 3.9 to 3.14. Khao Phanom, which is located in the middle part of the study area is very interesting because it always shows several obvious morphotectonic features.

3.2.3.1 Area A: Amphoe Thap Put, Phang Nga

The study area (area A) is located in southern part of Khoa Phanom, in Amphoe Thap Put. Its geology is characterized by limestone and unconsolidated sediment from fluvial and mountain systems, where sandstone and clay are the main components. Fluvial deposits occupied on both sides of Khlong Sri Mat and Khlong Marui river. Besides, limestone mountain range is the prominent landform in the west. It lies in the northeast-southwest direction following the regional structural lineament and can be separated from sandstone mountains and hills by its narrow and steep slope.

The result from aerial-photographic interpretation at Thap Put District along the south of Khao phanom is shown in Figure 3.15. Important tectonic geomorphologic features are sets of shutter ridges in the area nearby Ban Khao Tao Nai and Ban Na, which are about 400- 800 meters average base width, and about 60-140 meters of height. In the limestone range, near Khao Pak Dan, some small scarps (perhaps fault scarps) were found with the height of 200-300 meter. These scarps have their slope angles dipping to the east of about 40 – 50^{o}. In the west of Amphoe Thap Put, the small stream is shifted for about 80-150 m to the south, suggesting a left-lateral movement (Figure 3.15).

3.2.3.2 Area B: Ban Bang Mai Pao, Surat Thani

Topography in this area (area B) is denoted by the mountain range in the south, which consists mainly of sandstone, whereas some limestone mountain ranges are minor and shows steep slopes. In the middle part of the study area the narrow flood plain of Khlong Sok River, which is controlled by faulting, flows eastward to the main Phum Duang River.

Morphotectonic evidence indicates that the active tectonic morphology includes triangular facets and a shutter ridge. Along the Khlong Sok, several triangular facets with about 200-500 m base width and about 30-80 m height from the base can be recognized. These facet spurs dip to the southeast with angles of about 40^{o}-60^{o}. Close to this spurs the feature of a few shutter ridges, which are parallel to the main lineament can be identified. Besides linear valleys and offset streams were found in southeast of the concerned area in some small branches of the Khlong Sok river (Figure 3.16).

3.2.3.3 Area C: Ban Bang Luek, Surat Thani

The study area (area C) is located in the western part of Khoa Phanom, south of Ampheo Phanom. The geology is similar to that of the Ratchaprapa Dam area. The mountains are high and steep and show erosion resistant features of sandstone strata with interbeded shale. Some igneous intrusive rocks are found in the south. Fluvial deposits are derived mainly from the Phum Duang River. Besides, Khlong Hak was the main stream in the north, with lie in northeast-southwest trend following the main structural lineament.

The result from aerial-photographic interpretation at Ban Bang Luek along the west of Khao phanom is shown in Figure 3.17. Important tectonic geomorphologic features are sets of triangular facets in the area nearby Ban Bang Luek and Ban Bang Whoe, which consist of 4 triangular facets with the about 150 – 300-meter base width and about 20 -140-meter height and 40-50^{o} slope angle dipping to the east. In western valley basin of Khao Phanom, the stream is shifted at about 80-170 m to the south, suggesting a left-lateral displacement.

Along the west of Khao Panom, a set of 7 triangular-facets was encountered. They have the average base width of about 250 m and of about 60 m average height. These facet spurs dip about 45^{o} to northwest. Additionally, a northeast to northnortheast – trending shutter ridge with the length of about 250 m and the average height of about 250 m was found in the upper part of this study area parallel to the main lineament pattern. Many streams in this study area display the shift to the south with the displacement of about 80-100m.

3.2.3.4 Area D: Ban Bang Riang, Phan Nga

At the area of Bang Riang (area D), the aerial photographic analysis reveals several features of morphotectonic evidence along the south of Khao Phanom (Figure 3.18), such as offset streams, triangular facets, and fault scarps. A set of the northwest – southeast trending triangular facets has an average base width of about 1 km, and an average height of 80 m from the base, with dipping northwestward. The tectonic geomorphology indicates a normal fault with the left-lateral movement. Additionally, the area shows the lineament which extends southeastward to Ban Bang Sai in Krabi, and this lineament pattern shows a set of triangular facet at Khao Hua Sing. The facet spurs dip westward with the average base width of about 400-600 m and the average height of 300 m.

3.2.3.5 Area E: Ban Phra Saeng, Surat Thani

Ban Phra Saeng area (aea E) is located at the south of the Ratchaprapa Dam, Surat Thani, is dominated by the northeast – southwest trending mountain range (Figure 3.19) with the outstanding erosional resistant rocks and dendetric and parallel drainage patterns. The area comprises the sandstone strata with shale and mud stone interbeds. The mountain range in the southeast, show karstic topography, indicative of Permian limestone and carbonates. The main and straight river; Phum Duang River, flows to the southeast, the branch streams which are perpendicular to the main stream are in the northwest - southeast direction and act as the conjugate fault set. Several features of morphotectonic evidences are found along the trace lines such as, at Khao Pang, which are represented by the fault scarps parallel to the fault, some streams which shift to the left side, and the northeast – southwest – trending linear valleys.

3.2.3.6 Area F: Ban Chao Sai, Surat Thani

Aerial photographic analysis of Ban Chao Sai area (area F) reveals several features of morphotectonic evidence along the south of Khao Phanom (Figure 3.20), such as offset streams and fault scarps. The main scarps have the northwest trending feature with the length of about 3-5 km, the average wide of about 50-100 m and an average height of about 80 m. Near Khao Wong, the fault dips prominently to northwestward. The tectonic geomorphology indicated a normal fault with the left-lateral movement.

3.3 Summary

The results from space-borne data interpretation indicates that the major trend of lineaments are in the northeast-southwest direction and the minor are in the northwest-southeast direction. Along the basin boundary, the young faults were discovered and revealed evidence of active tectonic landforms. These landforms are shown both sinistral and dextral movement by their streams offset in the opposite directions. Fault scarps, triangular facets, parallel ridges and linear valleys were also encountered in this region. All of these features were the result of the major strike slip movement together with a minor normal fault displacement along the study KMF.

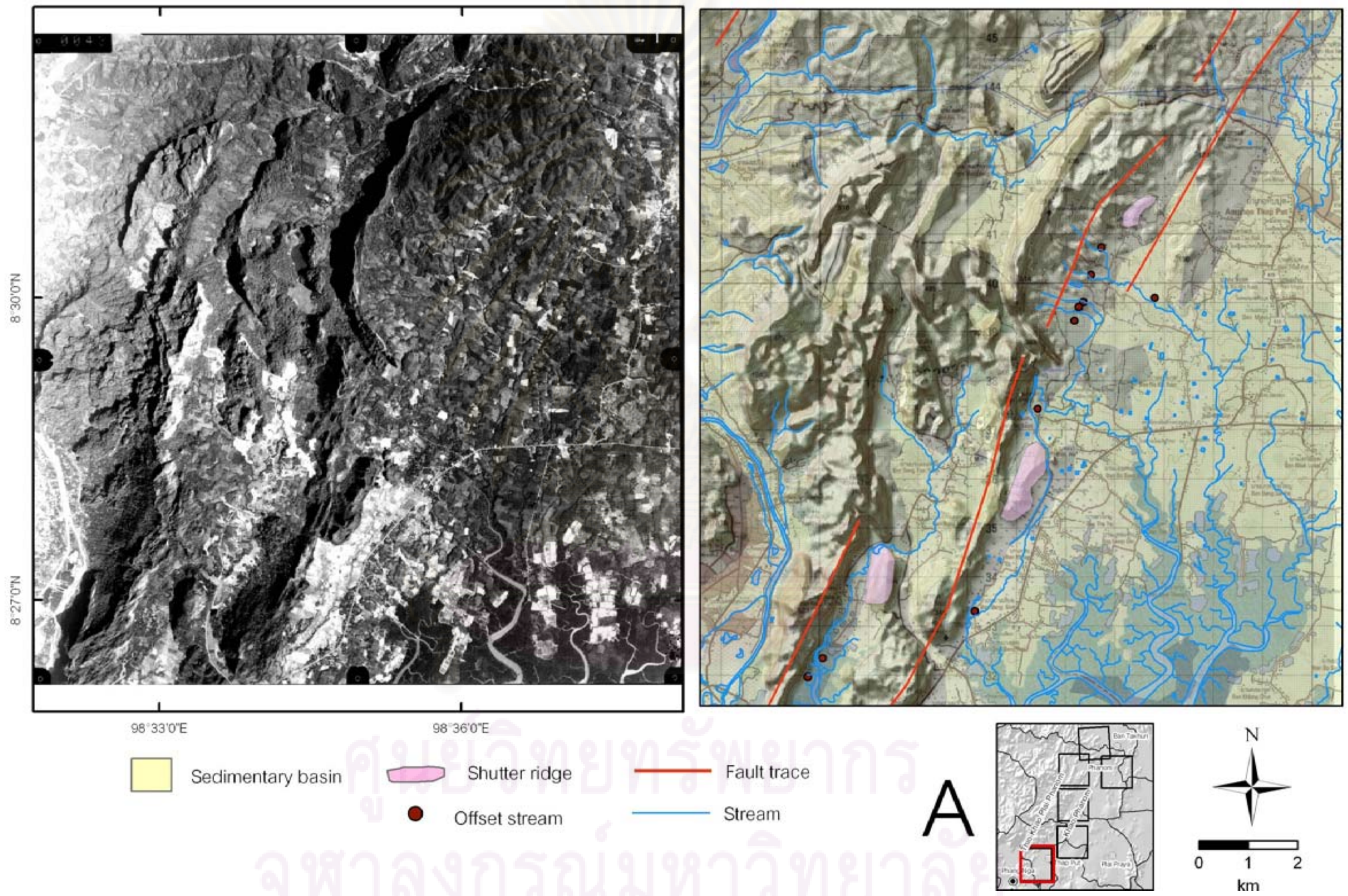

Figure 3.15 Aerial photograph (left) and interpreted morphotectonic landforms (right) along the fault trace in Area A.

64

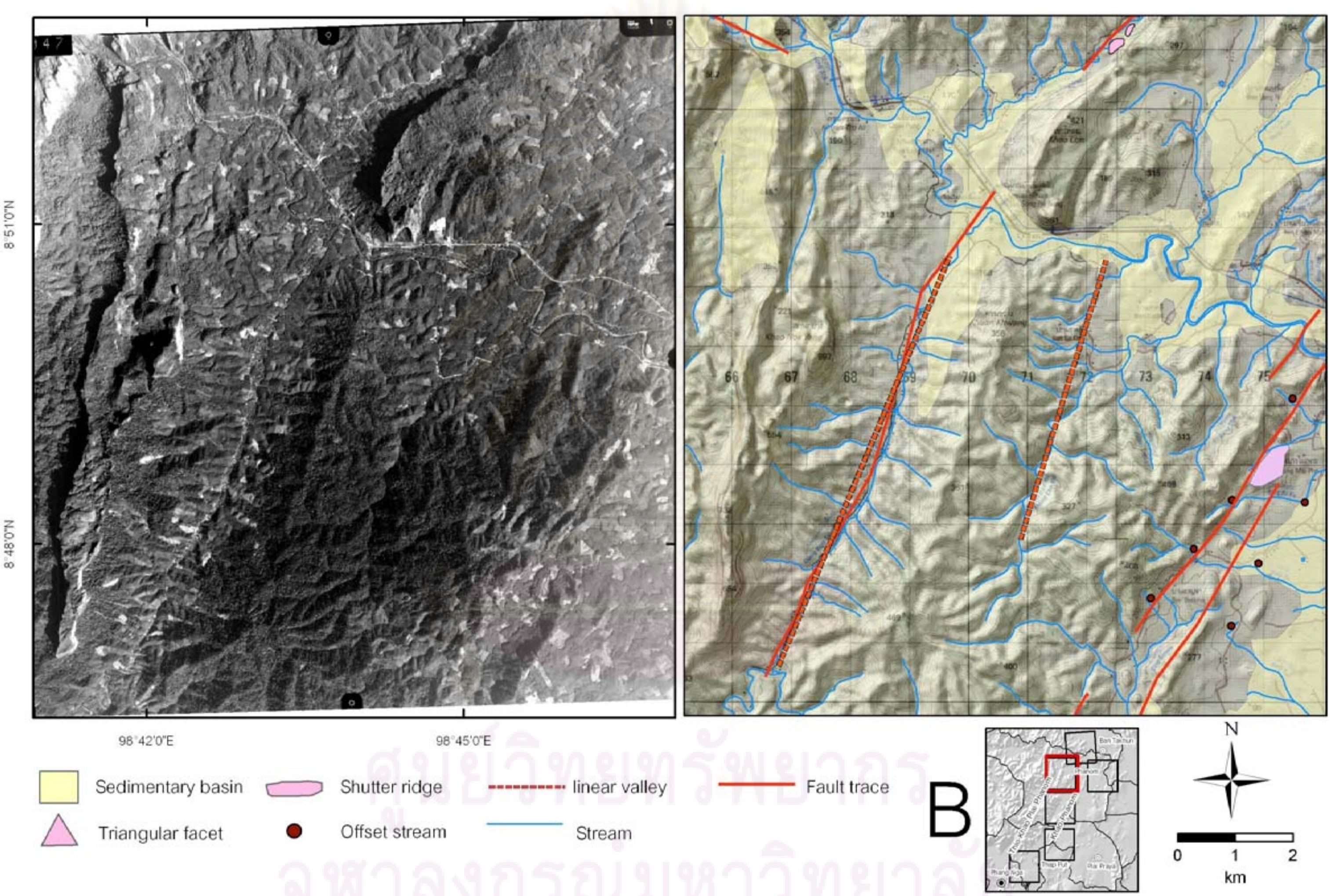

Figure 3.16 Aerial photograph (left) and interpreted morphotectonic landforms (right) along the fault trace in Area B.

65

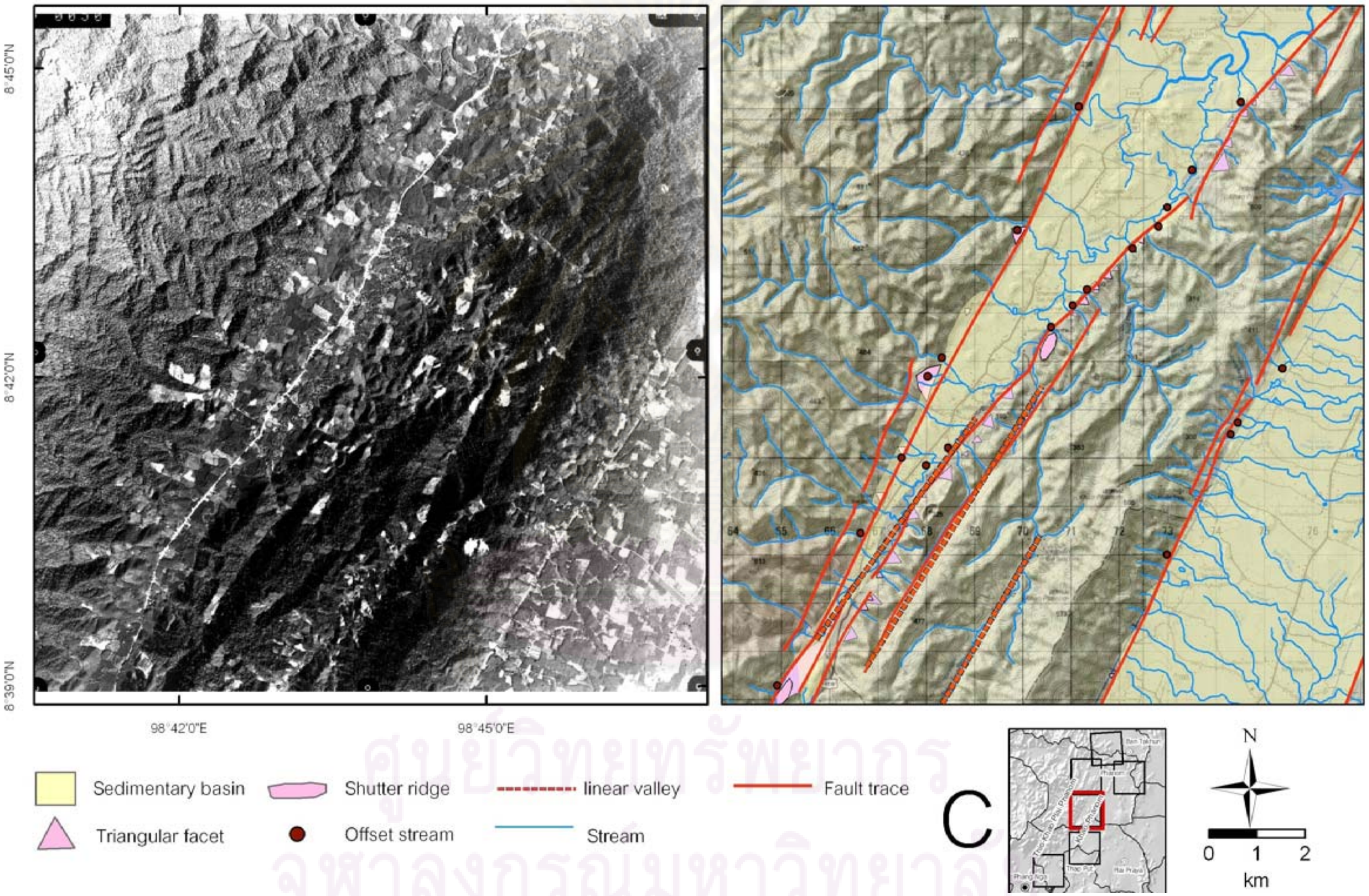

Figure 3.17 Aerial photograph (left) and interpreted morphotectonic landforms (right) along the fault trace in Area C.

66

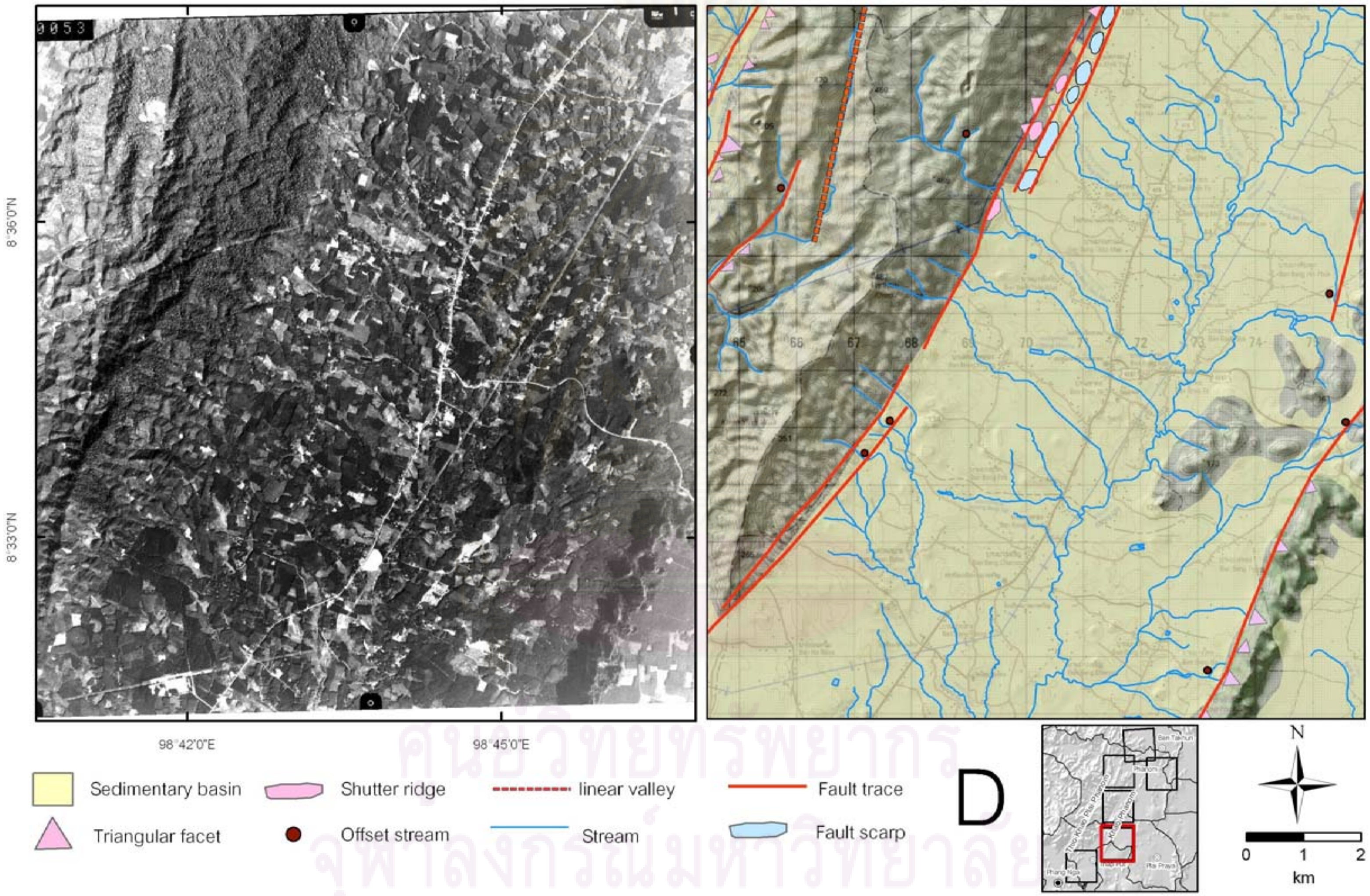

Figure 3.18 Aerial photograph (left) and interpreted morphotectonic landforms (right) along the fault trace in Area D.

67

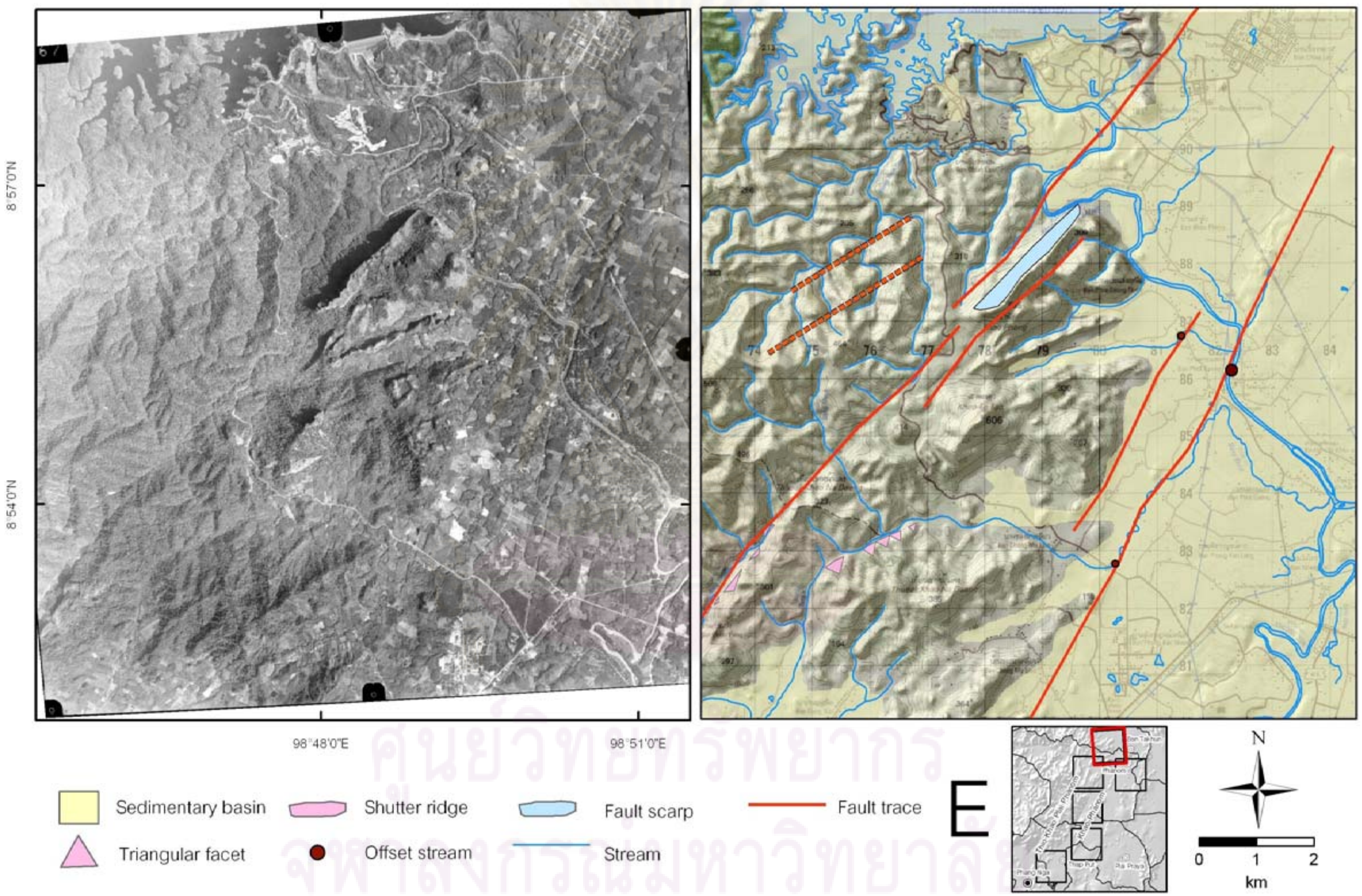

Figure 3.19 Aerial photograph (left) and interpreted morphotectonic landforms (right) along the fault trace in Area E.

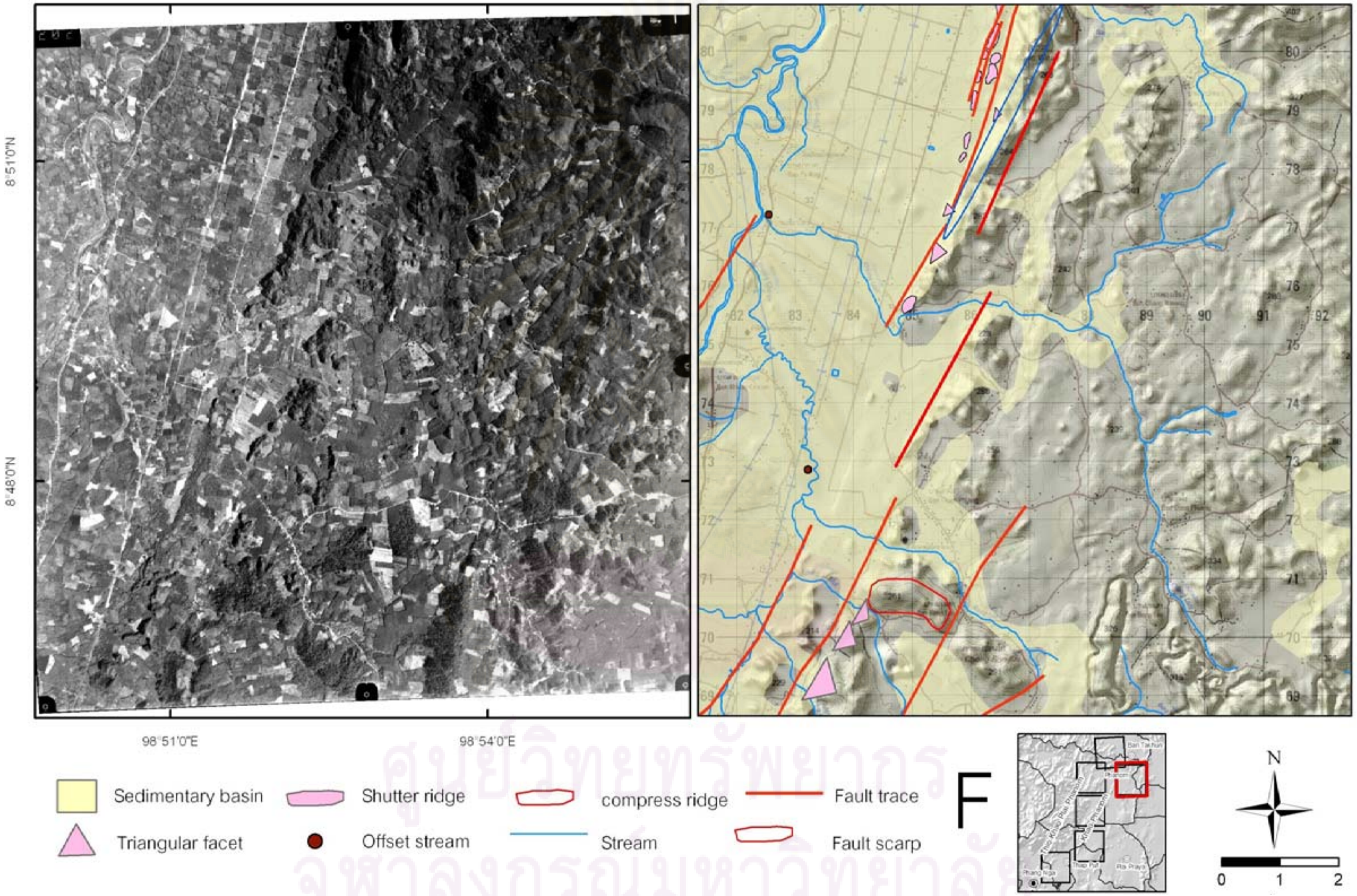

Figure 3.20 Aerial photograph (left) and interpreted morphotectonic landforms (right) along the fault trace in Area F.

69

Chapter IV

Geomorphic investigations

Several present-day tectonic landforms have been used to indicate the activeness of neotectonical geomorphology. These landforms of both primary and secondary features can be clearly seen by the uses of remote-sensing information. From last chapter, there are several tectonic landforms, such as offset streams, shutter ridges, fault scarp, and triangular facets, which are important for investigations of tectonic geomorphology. Recently, with the use of topography maps and, aerial photographs or DEM with the application the ArcGIS can be easily evaluated several morphotectonic features with a very low cost and high quality results. In Thailand the first morphometric analysis on the fault activeness was reported by Charusiri et al. (2004) in Mae Hong Son and Mae Sariang areas of northwestern Thailand. But in the southern Thailand Keawmaungmoon et al. (2008) first applied the geomorphic indices for Khao Phanom area of Surat Thani, with a special emphasis on the Khlong Marui Fault Zone.

In this study 4 morphometric indicators, namely mountain front sinuosity index (Smf), stream length-gradient index (S_L), transverse topography symmetry (T) and valley-floor width to valley-floor height ratio (Vf), were applied to determine the fault activities in and around Khao Phanom area, particularly along the main northeast-southwest trending of Khlong Marui Fault Zone. The available maps including 1:250,000 geologic map, 1:50,000 topographic map and DEM data are used together with aerial-photograph for preliminary morphotectonic analyzed.

4.1 Geomorphic Indices

For this study, we use several geomorphic indices, which are based on the topographic data, were applied in order to evaluate the relative rates at which constructive and destructive processes are operating in the landscape. A comprehensive introduction to these techniques is given in Keller and Pinter (2002).

4.1.1 Mountain Front Sinuosity Index

The mountain front sinuosity index (Smf) is calculated as a ratio of the length of the mountain front measured along the foot of the mountain at the pronounced break of the slope (L) to the straight line length of the mountain front (Ls):

$Smf = L / Ls$ ……………………………………………(equa. 1)

The Smf index reflects the balance between erosional and tectonic forces affecting a mountain front. Values of Smf close to 1 indicate that mountain fronts are associated with high tectonic activity (straight mountain front); values are increasing as the erosional processes dominate, producing more irregular mountain fronts (Bull & McFadden 1977).

4.1.2 Stream Length-Gradient Index

The stream length-gradient index (SL) is correlated to stream power and is defined by

$SL = (\Delta H/\Delta L) \times L$ ……………………………………….. (equa. 2)

where L is the total channel length from the site upstream to the highest point on the channel, ΔH is the change in elevation of the reach and ΔL is the length of the reach (Hack 1973). The SL index is very sensitive to changes in channel slope, to rock resistance, to topography and to the length of the stream, which is related to the ability of a stream to erode its bed and transport sediments. SL index values are in gradient meters. SL values of graded streams are homogeneous, whereas relatively high values indicate steepening of the slope.

4.1.3 Transverse Topographic Symmetry Factor

Transverse Topographic symmetry (T) is a quantitative index to evaluate drainage basin (i.e. the catchment area) asymmetry and is defined as (Cox, 1994):

$T = Da / Dd$ ……………………………………………………..(Equa. 3)

Where Da is the distance from the midline of the drainage basin to the midline of the active meander belt, and Dd is the distance d from the basin midline to the basin divide. This index does not provide direct evidence of ground tilting but is useful as a reconnaissance method for rapidly identifying possible tilt. For a perfectly symmetric

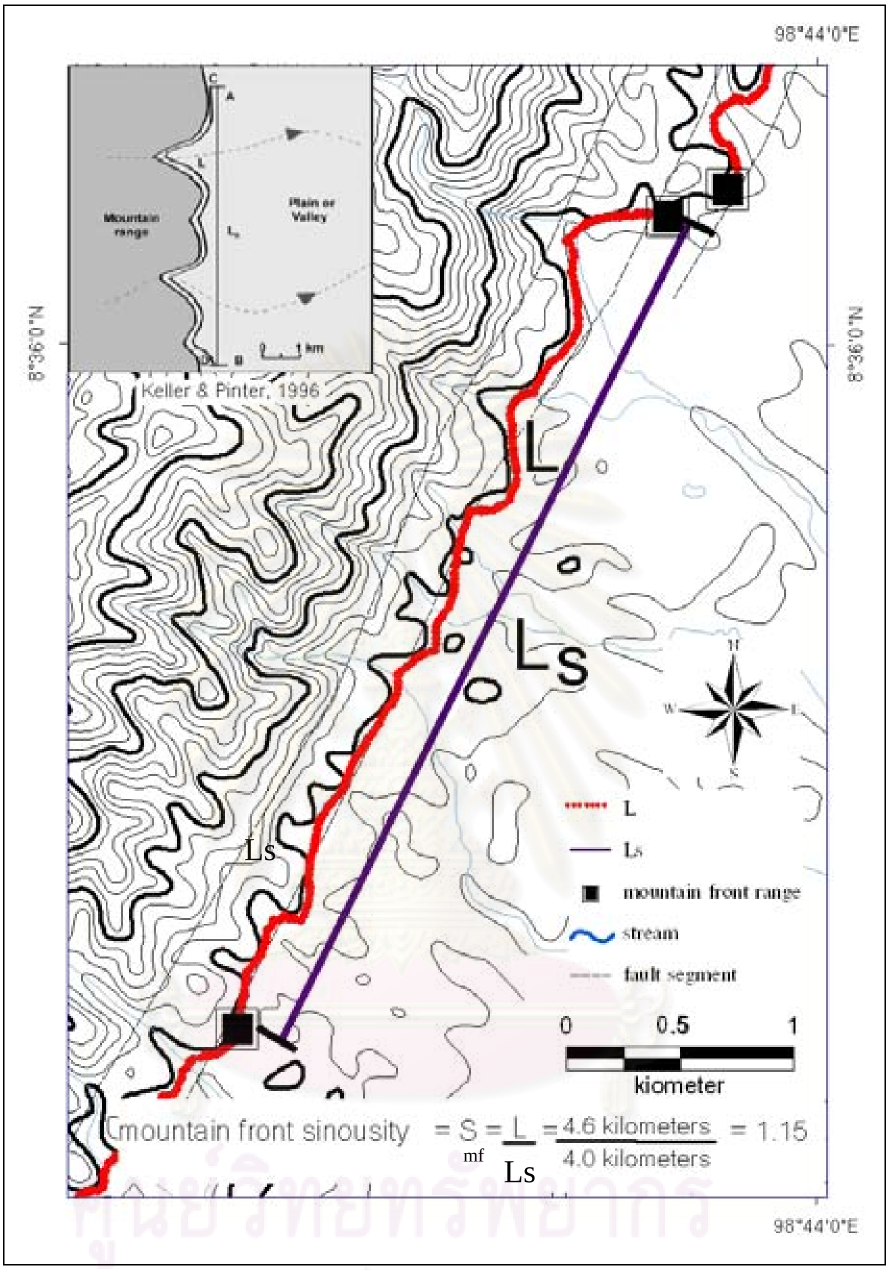

Figure 4.1 Idealized model showing how the mountain front sinuosity (Smf) is calculated, (modified after Keawmaungmoon et al., 2009).

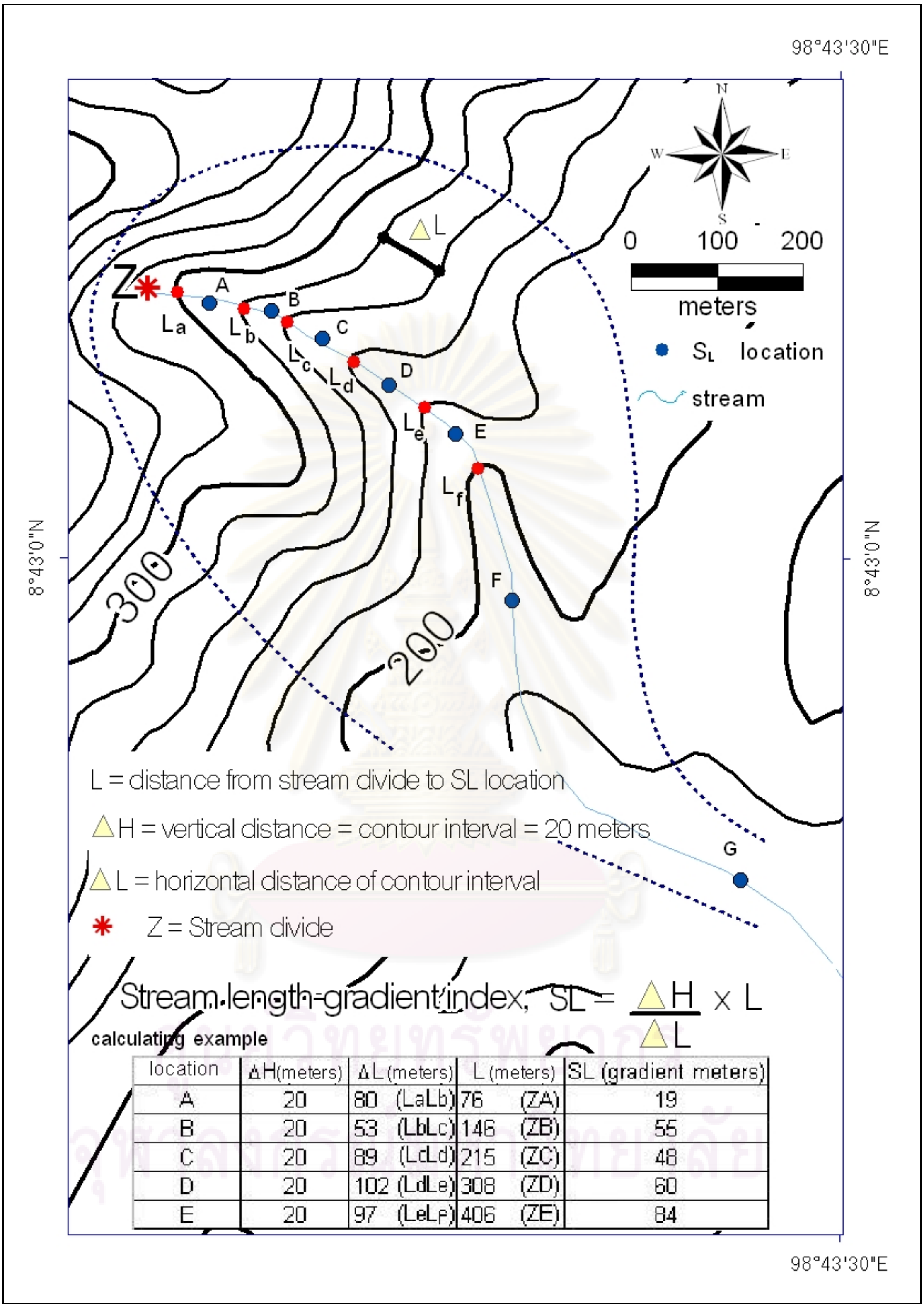

location	ΔH(meters)	ΔL (meters)	L (meters)	SL (gradient meters)
A	20	80 (LaLb)	76 (ZA)	19
B	20	53 (LbLc)	146 (ZB)	55
C	20	89 (LcLd)	215 (ZC)	48
D	20	102 (LdLe)	308 (ZD)	60
E	20	97 (LeLf)	406 (ZE)	84

Figure 4.2 Idealized model showing how the stream length-gradient index (SL) is calculated, (modified after Keawmaungmoon et al., 2009).

basin, T = 0. As the asymmetry increases, T increases towards 1, assuming that the migration of stream channels is an indication of possible ground tilting where the bedrock has negligible influence on stream migration.

4.1.4 Valley Floor Width to Valley Floor Height Ratio

The ratio of valley floor width to height (Vf) is an index based on the observation that incised streams with narrow valley floors and V-shaped valley profiles mark areas undergoing rapid uplift. It is defined by Bull (1977) as:

Vf = 2 Vfw / (Eld – Esc) + (Erd – Esc) …………………………………..(Equa. 4)

Where, Vf is the valley floor width-to-height ratios, Vwf is the width of valley floor, Eld and Erd are elevations of the left and right valley divides (looking downstream), and Esc is the elevation of the valley floor. High values of Vf are usually related to low tectonic activities whereas low values are always associated with active areas of undergoing relatively rapid uplift and valley incision (Azor et al., 2002).

4.1.5 Used data and processes

In this study we subdivided the Khlong Marui Fault zone into three zones based on remote sensing information. Their continuity and orientations form the essential parameters for such subdivision, as shown in the Figure 4.5.

Mountain front sinuosity index (S) was calculated from the SRTM data generated contours. Contours were derived with help of ArcScene Software (ESRI) and were calculated in the GIS environment after careful comparison with the 1: 50,000 topographic map. For the calculation, equal distances of Ls were used. L was measured along the intersection of a horizontal plane that cuts the morphology at the foot of the mountain (Figure 4.6), which have been carried out for the border faults and the scarp.

For the first step in calculation of SL the study area was separated into each water divide, then the streams were selected out for to evaluating SL index. In this study, the calculated spots were between contour intervals along the selected streams map as shows in figure 4.7. Digital topography map with contour 20m Interval was used for ΔH

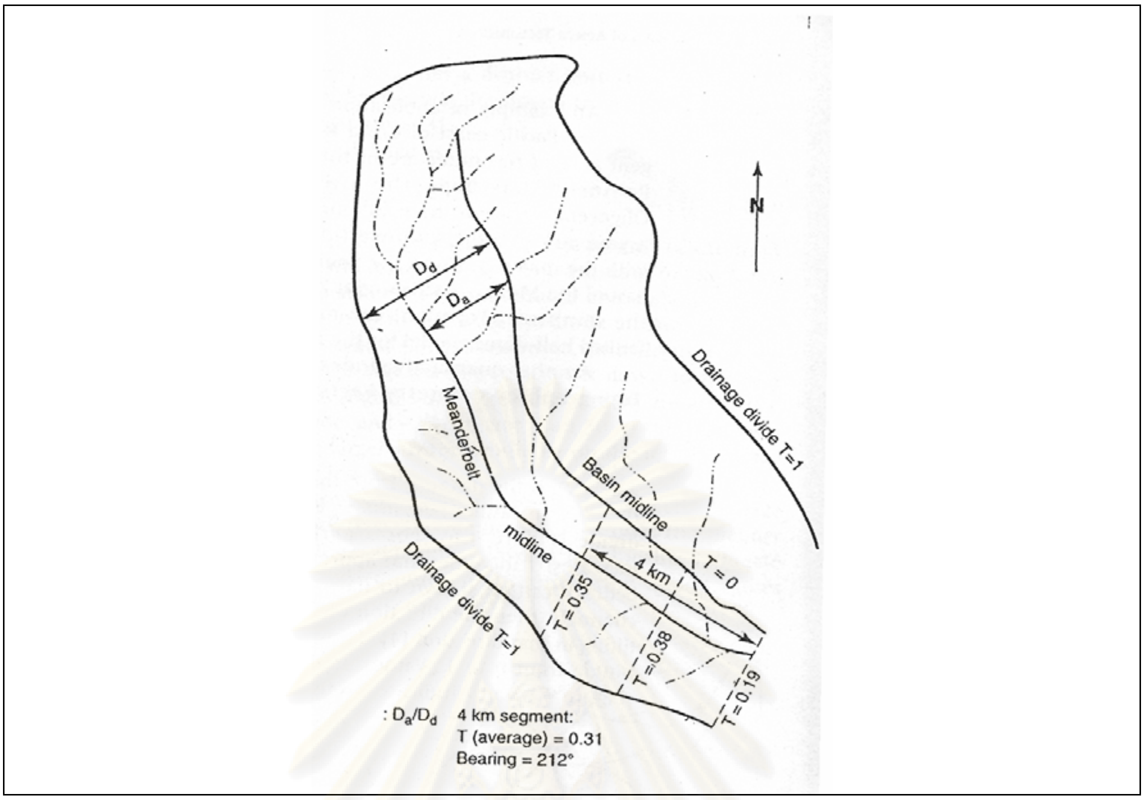

Figure 4.3 Diagram of a portion of a drainage basin showing how the transverse topographic symmetry factor (TTS) is calculated (modified after Cox,1994).

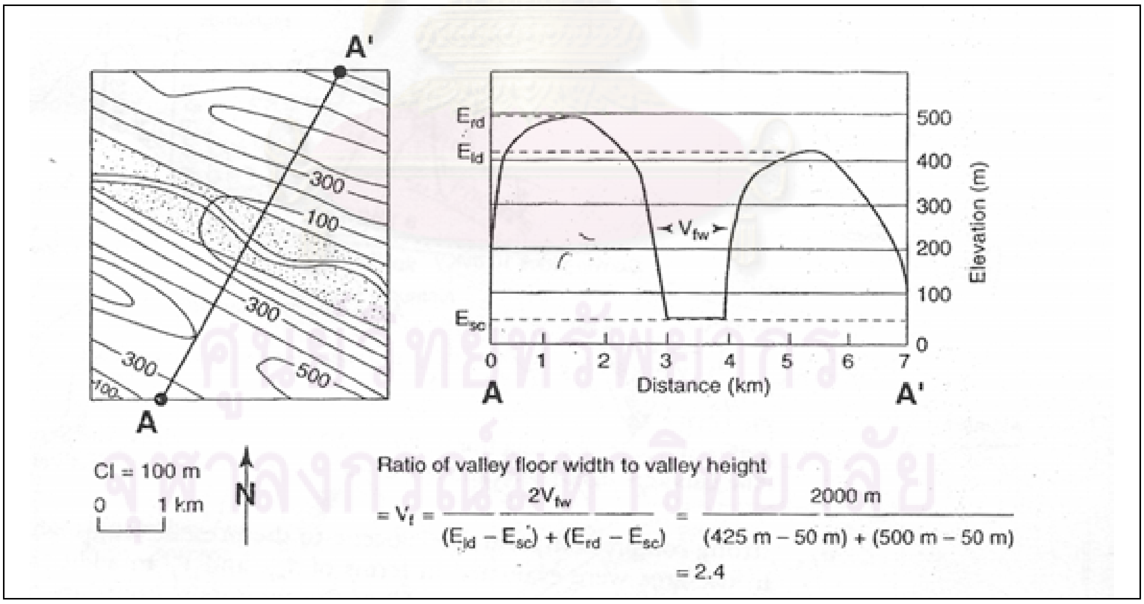

Figure 4.4 Idealized diagram illustrating how the ratio of valley-floor width to valley-floor Height ratio (Vf) is calculated. Note: Left and right is determined by looking downstream (Keller and Pinter, 1996).

and ΔL is the horizontal distance of the same 20m contour interval segment, whereas L is the total upstream channel length from the calculated spot to the highest point of the channel.

Based on the work of Royal Irrigation Department (2007), the study area was divided into 3 basins, namely Eastern Peninsular Basin, Tapee Basin and Western Peninsular Basin for calculating transverse topography symmetry factor, then these 2 basins were separated into 28 subbasins (Figure 4.8). Midline basinsand straight lines fit to the main streams were generated for measuring Da and Dd, where Da is the distance from the stream channel to the midline of basin (measured perpendicular to a straight line segment fit to the channel), and Dd is the distance from the basin margin (divide) to the midline of the basin. In order to calculate the T index along main stream, the straight line was divided into 0.5 km-long segments fit to the channel. The values of T are calculated for each segment and its direction was perpendicular to the segment of the stream. The vector direction indicates movement of the basin.

The last index was the Vf, which measured the valley shape performed close to the border fault or mountain-front fault. An example is shown in Figure 4.6. Quantification of the valley-floor width-to height ratio, Vf index, proved to be a useful tool to evaluate fluvial incision in uplifted areas (Bull and Mcfadden, 1977). In addition to uplift, the shape of valley cross-sections depends on the lithology of the bedrock and the erosive ability of the river.

4.2 Result and Interpretation

With the application of ArcGIS, we are able to calculate values of Smf, SL and Vf for each zone were calculated as shown in Table 4.1 and, Figures 4.10 – 4.12, and the result of T is shown in Figure 4.9.

The result reveals that a few areas have Smf values close to 1 with the average value of 1.14. The minimum S value of about 1.07 was encountered at Ban Song Prak and Ban Ben-Cha whereas the maximum S Value of about 1.27 is estimated at Ban Bang Riang Tai. The mean Smf for the zone1, zone 2 and zone 3 are 1.13, 1.23 and 1.14, respectively.

The Smf values decrease eastwards, usually from 1.68 to 1.32 for both west and east sides of the mountain fronts, so Khoa Phanom is likely to be associated with active uplift as indicated by relatively straight fronts and low values of Smf index. In arid region of the Basin and Range Province, the Smf range between 1.2 -1.6 (Bull and McFadden, 1977). For slightly active and inactive regions, the Smf values tend to be between 1.8 – 3.4 and 2 – 7, respectively (Bull and McFadden, 1977).

For the SL values, approximately 950 elevation spots were selected for the analysis at all 3 zones. Based on SL range value in this study, 5 range values were used following the pioneer work in Thailand by Keawmaungmoon et al. (2008). From this study it has been found that the zone 2 has the minimum SL value of 12 gradient meters as observed at Ban Nong Plong, Ao Luek District of Krabi Province. The maximum SL value of up to 1,400 gradient meters is discovered at Ban Bang Luek, Phanom District of Surat Thani Province. The SL values are less than 175 gradient meters are shown at Ban Hu Nop and Ban Pak Dan, Thup Butr District of Phang Nga Province (Keawmaungmoon et al., 2008). However, for both of zones 1 and 3, the SL minimum and maximum values are beyond the range value of zone 2. The minimum SL value of about 35 and the maximum value of about 2,621 were encountered for zone1, whereas the minimum SL value of about 17 and the maximum value of about 453 were calculated for zone 3.

From the SL results, it has been found that the areas of anomalously high values of SL are primarily located at and near Ban Pak Dan and Bang Luek along the northeast-southwest trend at Khao Phanom. The indices are anomalously high in Zone 2 and for some rivers, such as Huai Vae, in Zone 1.

Transverse Topographic Symmetry factor was calculated and plotted for the subbasins covering zone 2 in order to roughly estimate a possible basin tilt. Different T values were plotted in Figure 4.9. The drainage basin asymmetry can easily be visualized and interpreted using a 3D river networks in Arcscene program. Tributaries to streams that flow down steep regional slopes can be asymmetrical with active tilting, with longer distances between the channel and the drainage divide on the high side of the basin. The asymmetry indicates that Tapee basin is elevated, particularly in its northeastern part towards the east. Most river flows along the eastern side of the basin. Main rivers clearly maintain incision through the interior of the zones and local asymmetry along some river suggests some eastward tilting of the block. It has been believe that the river/stream flow from east to west following trends of major faults. The result indicates that the southern part of Phum Duang subbasin shows the maximum tilting whereas Khlong Takua Pa subbasin shows no tilting.

The Vf values were calculated for the most important canyons (rivers, valleys) along the mountain fronts. Bull and McFadden (1977) showed the Vf values of active tectonic zones in arid areas were characterized by the Vf values of 0.05 to 0.9, while the Vf values of the slightly active tectonic and inactive areas tended to be between 0.5 to 3.6 and 2 to 47, respectively. In this study, transverse valley profiles for determining Vf were located ~500 m upstream from the mountain front and the Vf values was shown in each zone in Figures 4.10, 4.11 and 4.12 with the values varying from 0.29 to 37.1. According to Vf theory, high values of Vf characterize low tectonic activity valleys, while low Vf values characterize actively incising valleys. High values were found at Ban Tham Phueng, and Ban Kraison. On the contrary, low values are redognized at Ban Khok Wua and Ban Fai Tha, suggesting low tectonic activity.

4.3 Summary

Based on 4 geomorphic indices, the result reveals that zone 1 has the Smf values of 1.40-1.53, SL values in the ranges of 35-2,621 gradient-meter and Vf in ranges of 5.56-30.0, whereas the zone 3 has the Smf value of 1.41-2.91, SL vaule of 17-453 and rather low of Vf with values of 1.2-8.0. Zone 2 shows the lowest Smf of 1.33, SL: 11-2,047, and the lowest Vf: 0.29 in west of Khao Phanom. According to above data, it is suggested that zone 2 perhaps indicates more active tectonic region than zone 1 and zone 3 in term of geomorphic investigations.

The results from this study together with results on remote-sensing interpretation and ground-geophysical survey can help us to estimate fault segments of the KMF and to locate paleoseismic trenching.

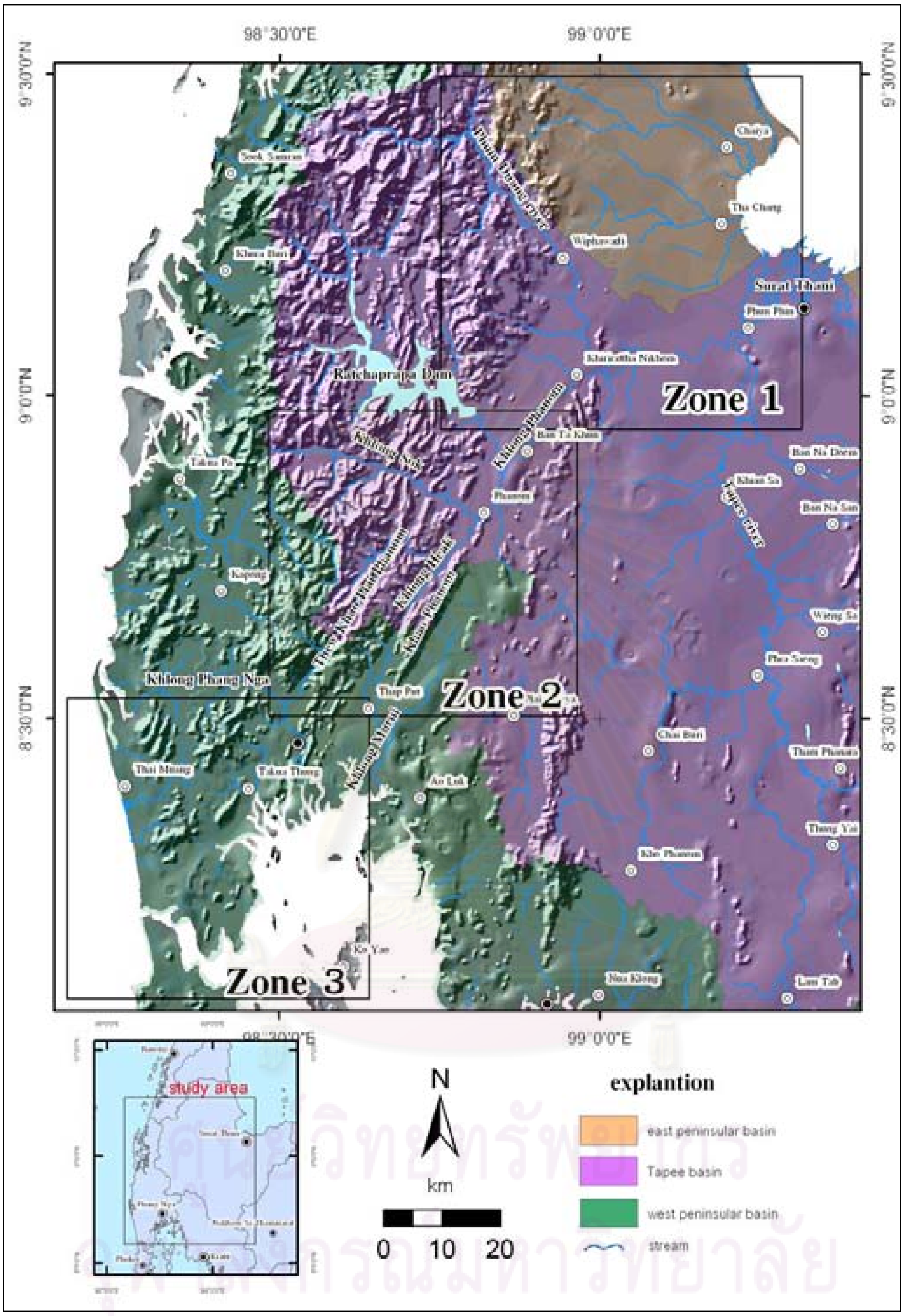

Figure 4.5 Index hillshade map of SRTM DEM showing subdivision of the study area into 3 zones (Zone 1, Zone 2, and Zone 3).

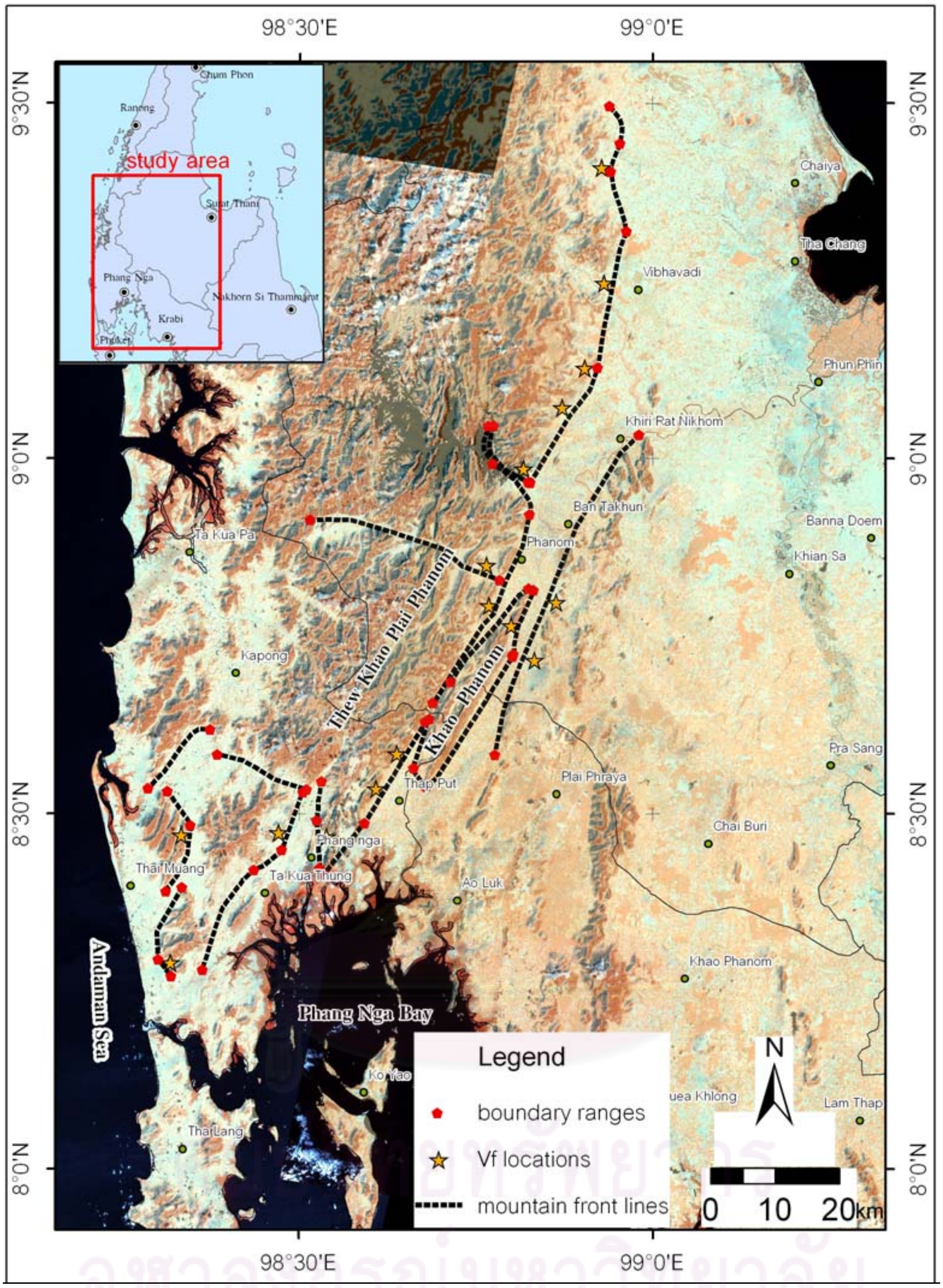

Figure 4.6 Index Landsat 7 ETM+ band 4:5:7 (red:green:blue) map showing locations of mountain front range and valley floor width to valley height ratio in the study area.

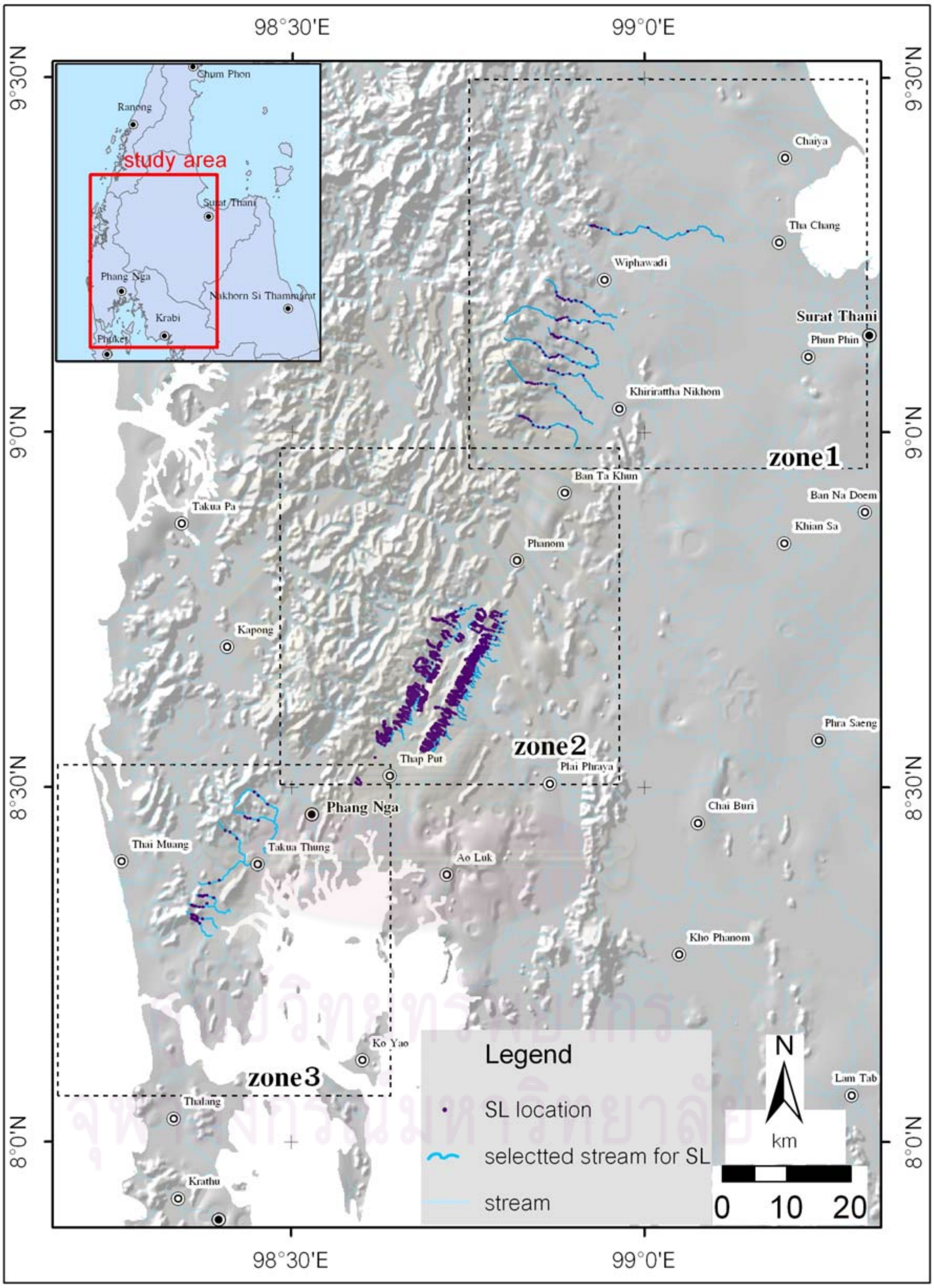

Figure 4.7 Index map showing locations of selected streams and stream length-gradient of zone 1,2 and 3 in the study area of the southern peninsular Thailand.

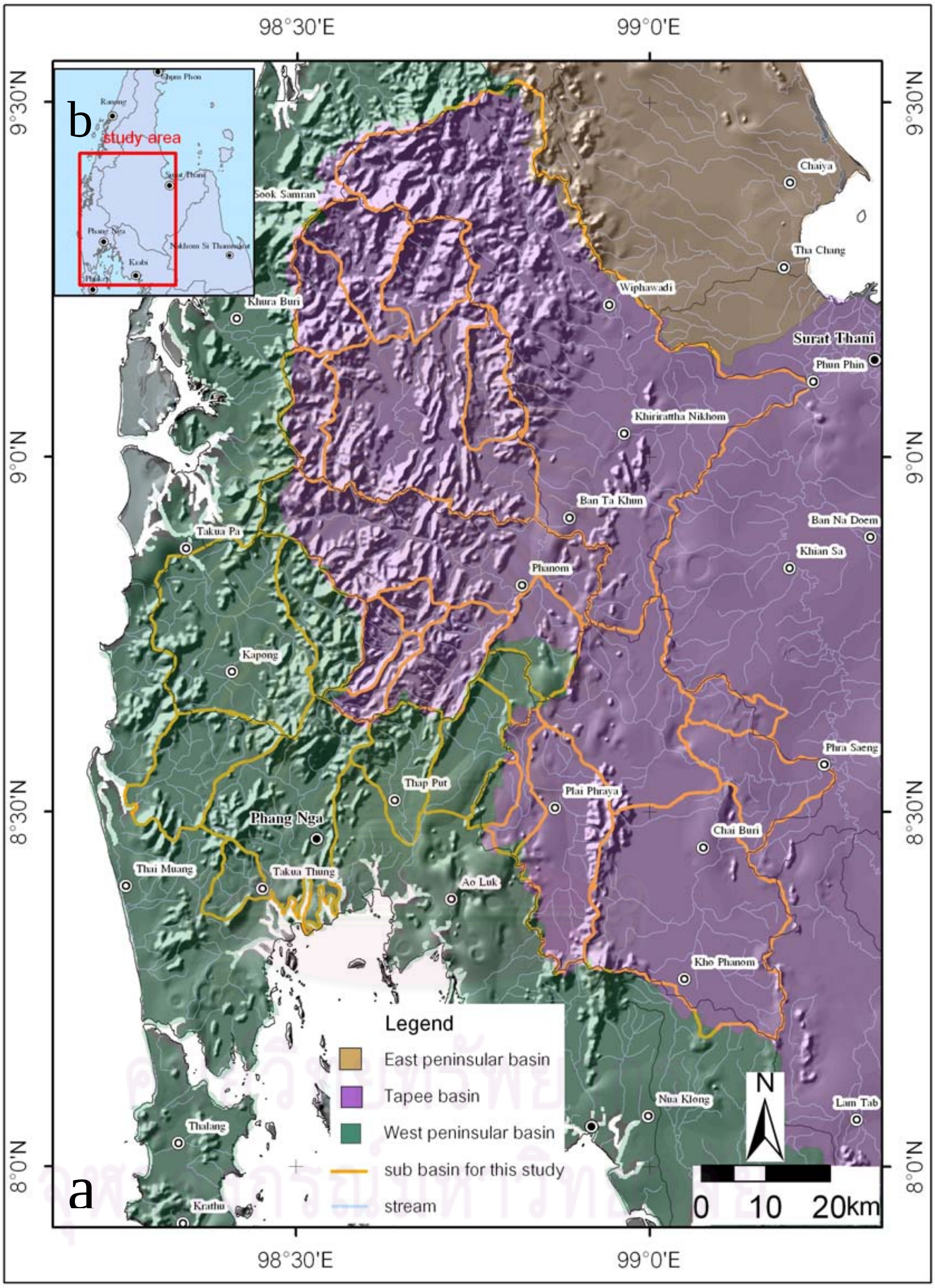

Figure 4.8 Sub basins for calculating transverse topography symmetry factor (TTS) of the study area (a) which belongs to Tapee Basin and situated between the West peninsular and East peninsular Basins, southern peninsular Thailand (b), (Royal Irrigation Department, 2007).

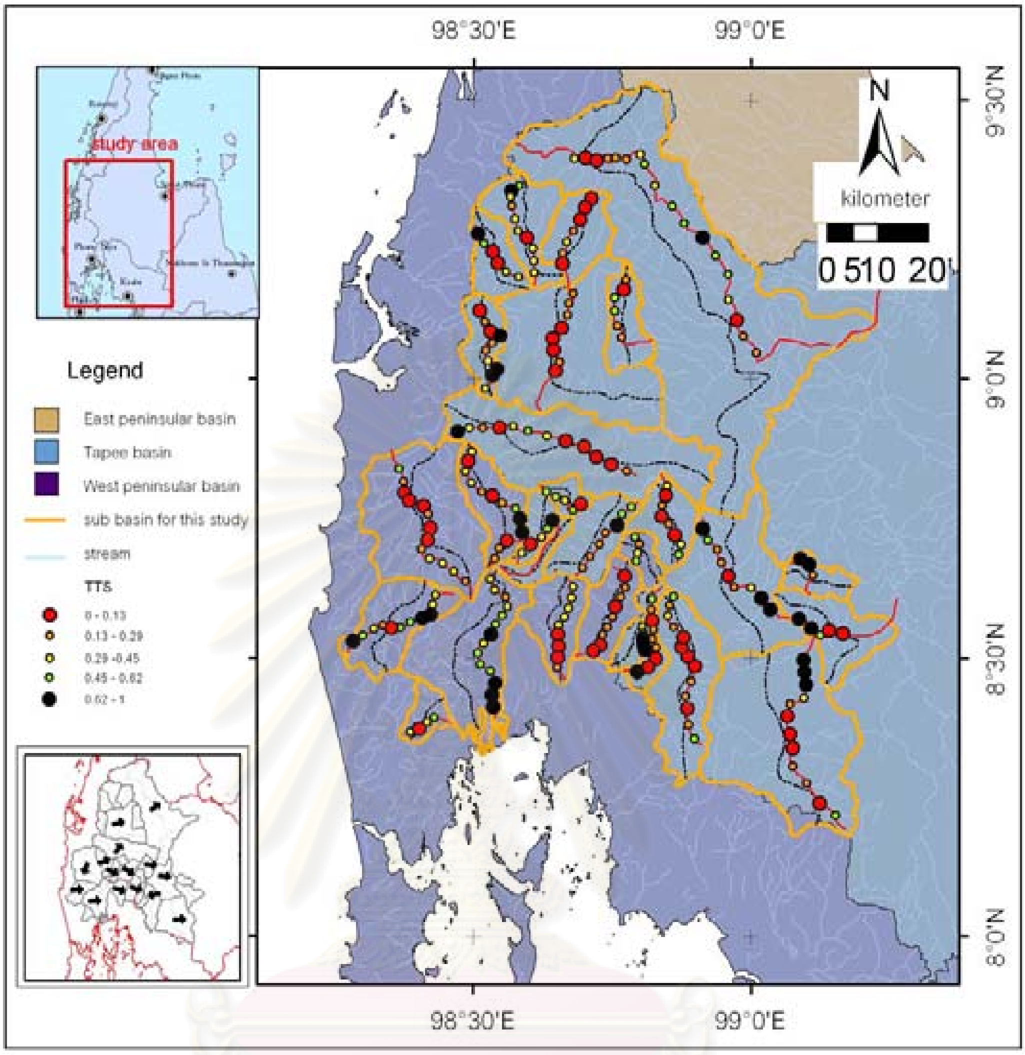

Figure 4.9 Index map showing transverse topography symmetry factor (TTS) range values used for individual subbasin in the study area.

Table 4.1 Results of geomorphic indices in this study area (see locations in Figure 4.10 - 4.12).

Area	Smf (number)	SL gradient-meter (number)	Vf
Zone 1	1.40 – 1.53 1.32 – 1.4 (1) 1.4 – 1.5 (3) 1.5 – 1.68 (2) 1.68 – 2.11 (2) > 2.11 (0)	35-2621 < 175 (58) 176-350 (25) 351-525 (7) 525-700 (5) >700 (10)	5.56 9.47 10.71 12.5 30.0
Zone 2	1.33-2.74 1.32 – 1.4 (4) 1.4 – 1.5 (2) 1.5 – 1.68 (2) 1.68 – 2.11 (1) > 2.11 (3)	11-2047 < 175 (400) 176-350 (280) 351-525 (94) 525-700 (14) >700 (10)	12.5 6.8 6.82 0.29 7.78 37.1 8.18
Zone 3	1.41-2.91 1.32 – 1.4 (0) 1.4 – 1.5 (1) 1.5 – 1.68 (3) 1.68 – 2.11 (3) > 2.11 (3)	17-453 < 175 (33) 176-350 (15) 351-525 (2) 525-700 (0) >700 (0)	2.33 8.0 1.2 3.64

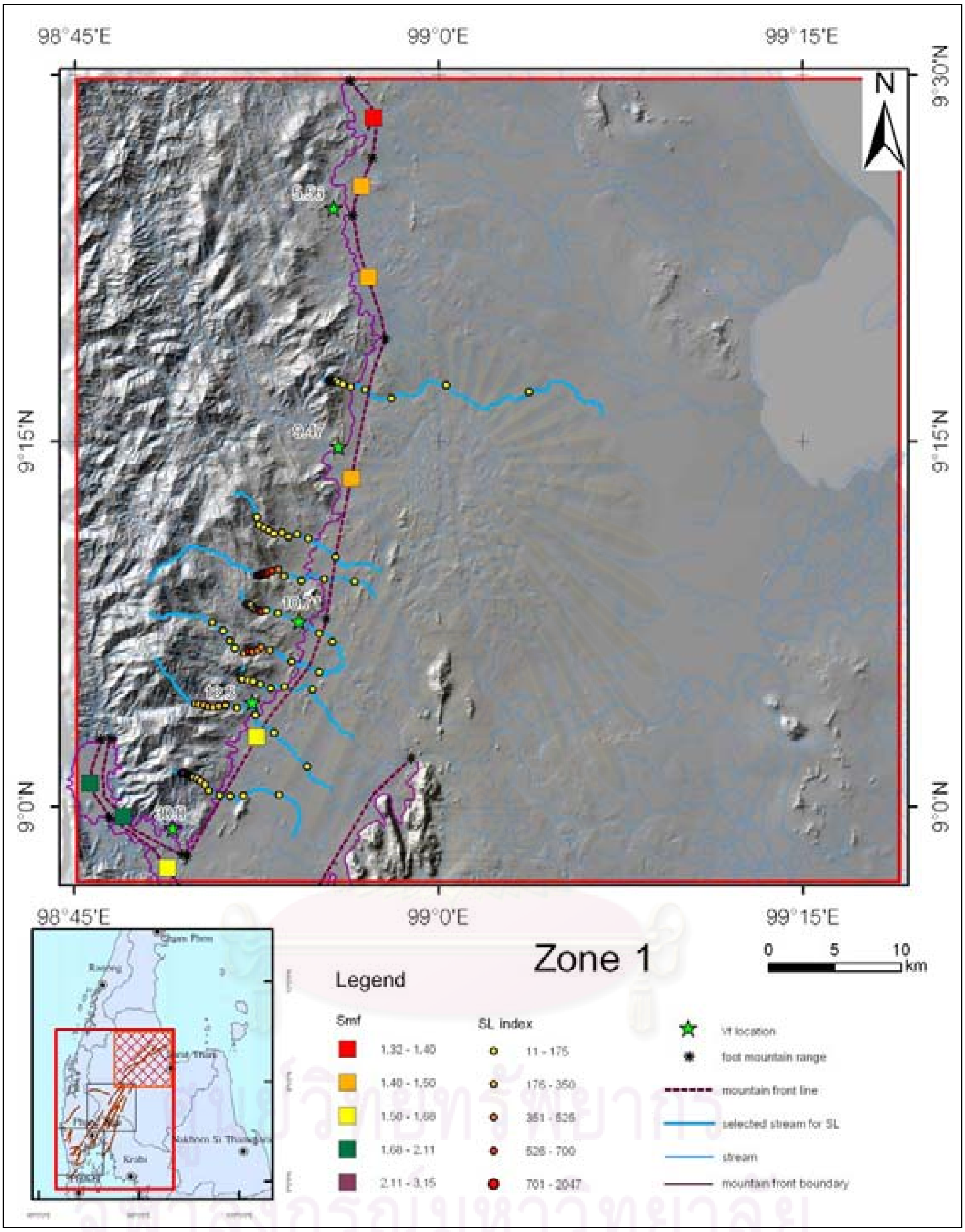

Figure 4.10 A hill shade DEM topographic map with 20m intervals showing different geomorphic indices of Zone 1 in the study area.

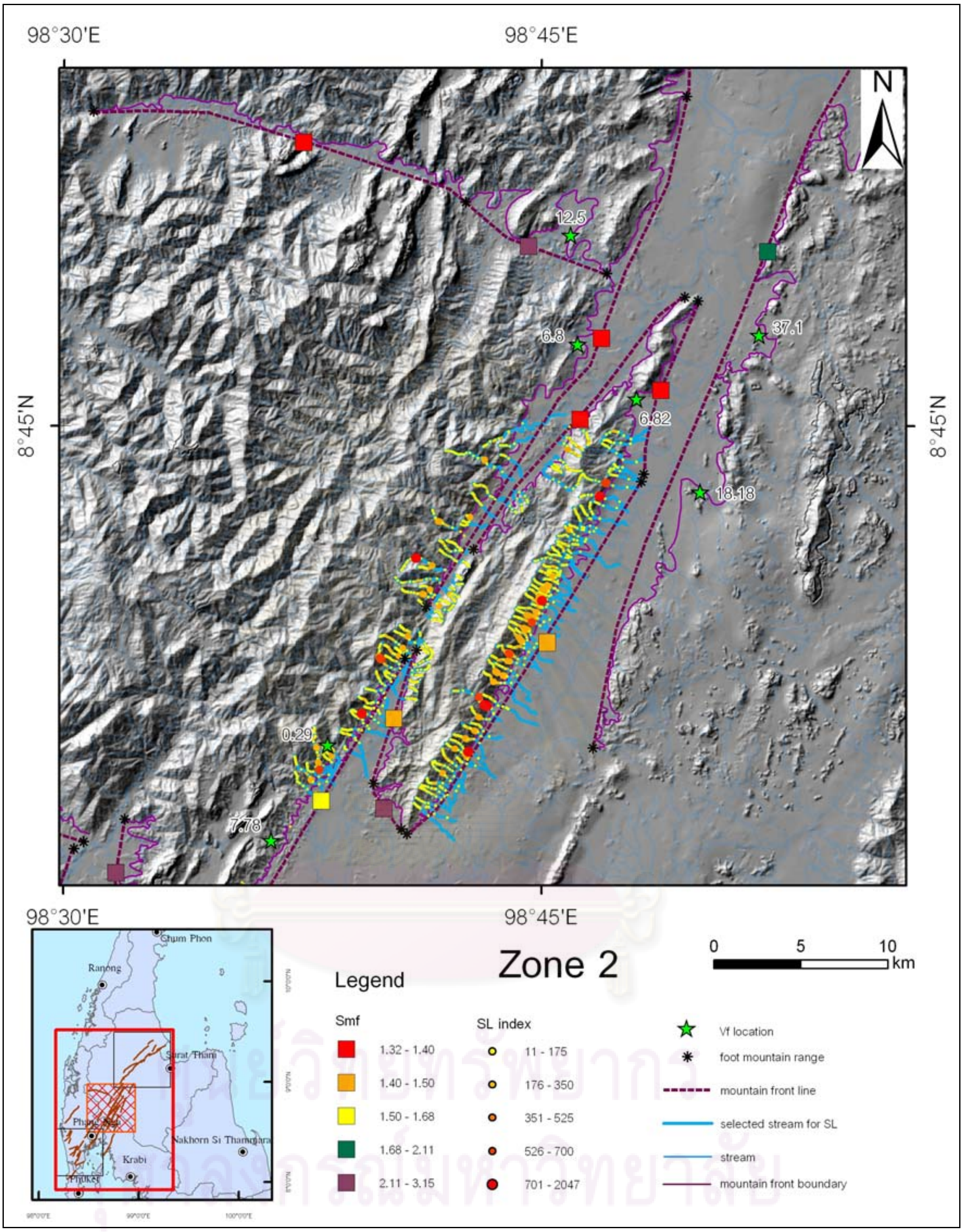

Figure 4.11 A hill shade DEM topographic map with 20m intervals showing different geomorphic indices of Zone 2 in the study area.

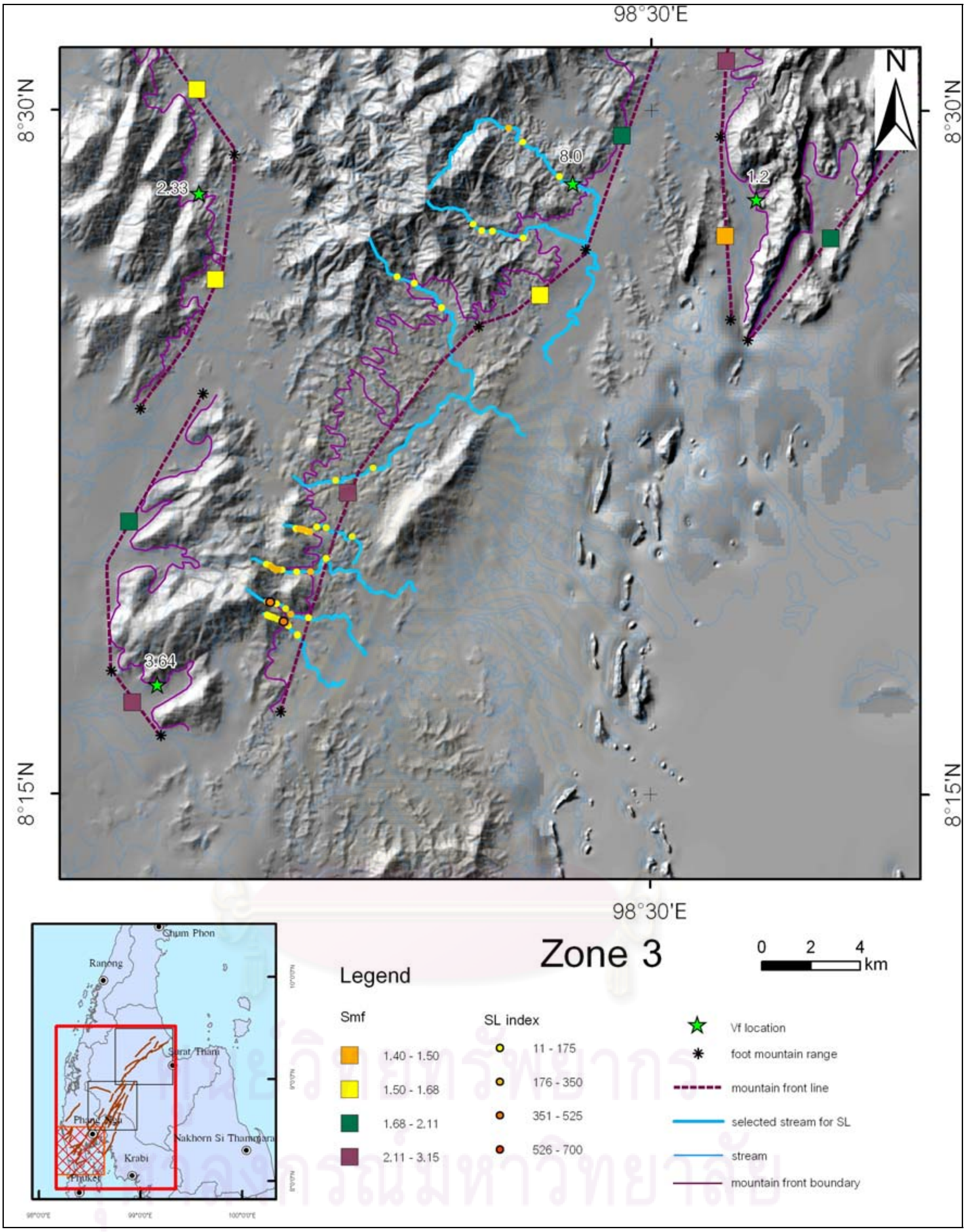

Figure 4.12 A hill shade DEM topographic map with 20m intervals showing different geomorphic indices of Zone 3 in the study area.

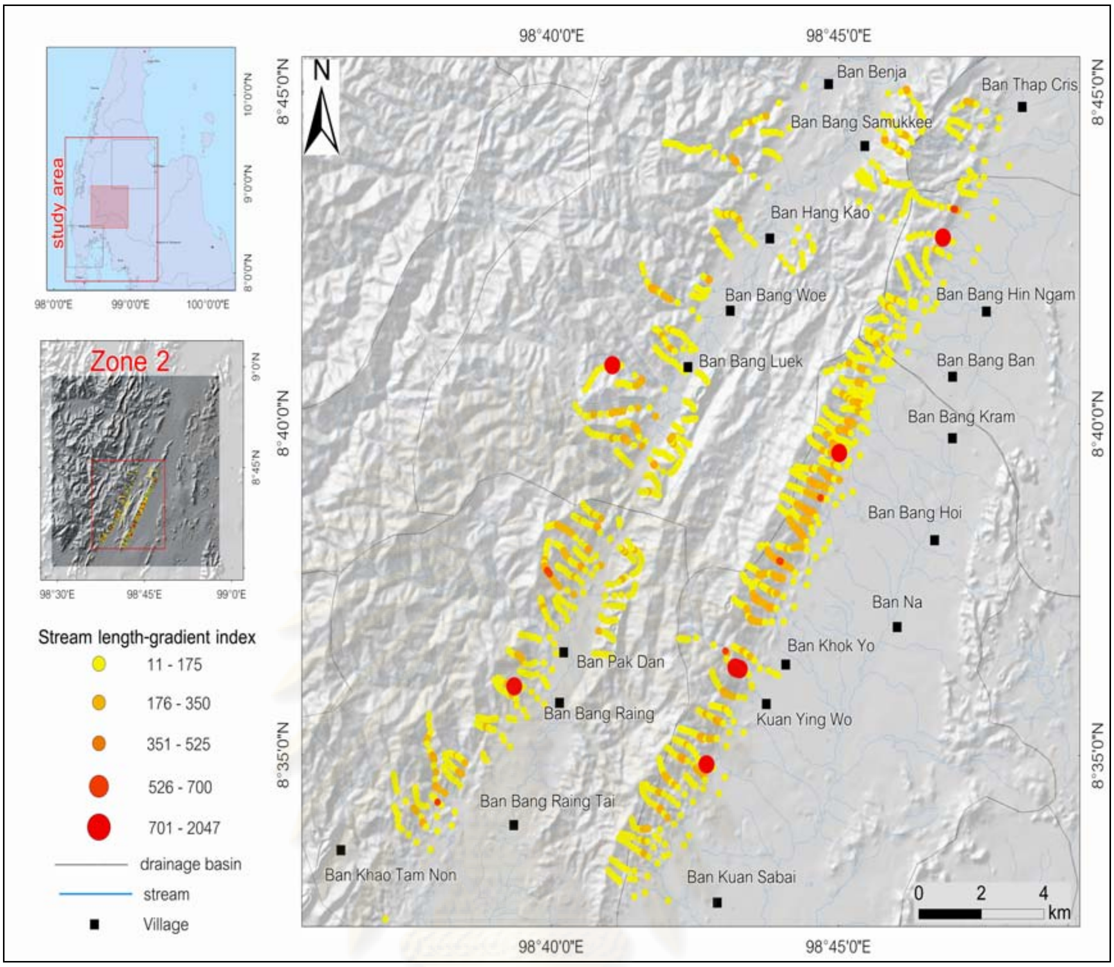

Figure 4.13 Map showing detailed stream length-gradient index around Khao Phanom in zone 2 of the study area. Also show is the basin divide and selective rivers.

4.4 Fault segmentation

4.4.1 Concept of fault segmentation

Concept of fault segmentation is elucidated by the fact that historical surface ruptures triggered by earthquakes along the long faults seldom occurred throughout the entire length, and just only one or two segments became ruptures during large earthquake (McCalpin, 1996). For instance, the San Andreas Fault zone of California was divided into four segments based on difference of historical surface rupture (Allen, 1968). The long fault trace is composed of numerous discrete segments (Segall and Pollard, 1980). The segmentation of fault systems is related to the identification of individual fault segments, based on continuity, character and orientation. It is recommended that a segment can rupture as a unit (Slemmons, 1982). Aki (1984) suggested that the delineation of segments is related to the identification of discontinuities in the fault system. Discontinuity can be divided into two main 75 groups: geometric and inhomogeneous group. Note that this statement has borrowed from seismologists who have used these terms for asperities and barrier. In addition, it is believed that fault may be segmented at a variety of scale that is from a few meters to several tens of kilometers in length (Schwatz, 1989).

All fault segments have their own boundaries. In this study, the segment boundary is a portion of a fault where at least two preferable successive rupture zones have ends (Wheeler, 1989). There are several geomorphic features related to fault boundary or termination. For example, releasing bends and steps, restraining bends, branch and cross-cutting structures, and change in sense of slips are commonly observed at segment termination of strike-slip fault (Knuepfer, 1989). For normal and reverse faults, geomorphic features for definition segment endpoints are not clear (McCalpin, 1996).

Since late 1970s, many workers have found that not all faults have historical rupture records along their fault zone. Thus numbers of criteria have been conducted in order to work on fault segmentation approach such as geometric, structural, geophysical, and geological criteria. McCalpin (1996) had summarized criteria for fault segmentation into five types (Table 3.1). According to new criteria of fault segmentation have arisen, one fault has been segmented by various authors depending upon different criteria. For example, the San Andreas Fault was divided into segments by at least four authors (Table 4.3).

In Thailand, the term “fault segmentation” was first introduced by Fenton et al. (1997) and at least two geologists who show the supporting evidence for fault segmentation, namely Won-in (1999) and Kosuwan et al. (1999). According to Fenton et al. (1997), two active faults in basin and range provinces of northern Thailand are recognized by fault segmentation, including the Thoen Fault in Changwat Lampang and the Pua Fault in Changwat Nan. In their work, criteria used for segmentation comprise geomorphic features, structural styles, and senses of offsets.

4.4.2 Results of fault segmentation

In this study we use three criteria for fault segmentation which are structural, geological and geometric applied following those purposed by McCalpin (1996). Previous sections play an important role not only for locating and delineating the fault but also for segmenting fault. Based on the results of fault segmentation integrated with the previous study (Department of Mineral Resource, 2007), the KMF can be divided into 16 fault segments see Figures 4.14 a – p, and Figure 4.15 shows the overall fault segments. Individual segments are Khlong Hiang (22.5 km), Tha Chang (23.0km), Vibhavadi (27.5 km), Khlong Sok (23.3 km), Khao Na Dang (15.8 km), Khao Wong (14.4 km), Khao Hin Paeng (10.1 km), Khao Kua Sing (18.2 km), Ao Luek (26.2 km), Khao Phanom (28.1 km), Khlong Haek (35.2 km), Khlong Marui (54.8 km), Plai Phanom (15.1 km) (Phang Nga 31.8 km), Tai Maung fault (13.4 km), and Pakong fault (24 km). In this study, the Khlong Marui segment is the longest segment, which is located on the western side of Khao Phanom. Followings are the detail of individual segments.

Khlong Hiang segment is the northernmost segment and consists of only 1 segment. The segment commences from Ban Neur Tha and terminates at Ban Thakuk of Vibhavadi subdistrict. (No.1 in figure 4.14). It shows the right lateral movement. Important morphotectonic feature is an offset stream at Ban Na Khoa. The trend of the Khlong Hiang segment is in the northeast-southwest direction. The total length of the segment is 22.5 km.

Tha Chang segment commences from Ban Tarn Nam Ron and terminates at Ban Mai Reab. It consists of 3 subsegment including Tha Chang-1 (10.8 km long) and Tha Chang-2 (14.7 km long) in the north and Tha Chang-3 (11.2 km long) in the south (No.2 in figure 4.15). Tha Chang-2 and Tha Chang-3 segments cut across active streams and alluviums. The trend of the Tha Chang segment varies from N30^{0}E to N45^{0}E . The total length of the segment is 23.0 km.

The Vibhavadi segment, is located in the south of and almost parallel to the Tha Chang segment-3, starts from Ban Khoe Yai and Ban Pho Thana in the north and ends at the southwest of Ban Yuan Saw in the south The segment cuts across the young alluvial deposits and the active “Khlong Yan” channel. The segment consist of 4 subsegments with the length ranging from 7.5 to 14.5 km. (No.3 Figure 4.16) The average trend is in the northeast-southwest direction. Offset streams and fault scarps are good morphotectonic features. They are found at Ban Hin Lad and Ban Sai Nam. The orientation of individual subsegments varies from the N40^{o}E to the N60^{o}E. The total length of the Vibhavadi is about 27.5 km, and the one subsegment in the north has the maximum length (16km). Geomorphologic indices, including Smf and SL, show that the segment show high SL values (2621) and low Smf values (1.56 to 1.68). This suggest that the segment is active.

The Khlong Sok segment, the newly recognized segment discovered in this study, commences from Ban Bang Pru and ends at Ban Chaew Pong along the Khlong Sok channel. (No.4 figure 4.17). The segment comprises 5 subsegments with the length varying from 3 to 16 km. the Khlong Sok segment is the outstanding segment since it orientates in the almost northnorthwest-southsoutheast (NNW-SSE) direction. This direction seems to traverse against the other fault segment and is basin-bound fault. Shutter ridges, triangular facets, pressure ridge and shutter ridges are prominent morphotectonic features, they are observed at Ban Bang Pru, Ban Ya Plong and Ban Bang Bon.

The Khao Na Dang segment starts from Ban Kuan Thong and Ban Na Tha in the north to the south of Ban Song Pea Nong in the south. It consists of 5 segments shown as No.5 in figure 4.18. There are parallel sub segments in the northern part whose length varies from 4 to 15.8 km. The middle and southern subsegments follow the Khlong Bang Song Pee Nong. There is the shortest subsegment (4 km long) in the north of Ban Song Pee Nong and acts as basin – fault. The average trend of the Khao Na Dang segment is in the northeast-southwest direction. The outstanding geomorphic features are offset stream, triangular facet and linear valley. Geomorphologic index, Smf shows that the low values (1.5 to 1.68). This suggest that the segment is active.

Almost subparallel to the Khao Na Dang segment is the Khao Wong segment (No.6 figure 4.19), to the west of Ban Ta Khun District. It has the total length of about 14.4 km and the average trend in the N30^{o}E direction. The Khao Wong segment starts from Ban Khao Wong in the north and ends at Ban Bang Lud in the south. The Khao Wong segment consists of 4 subsegments which are almost parallel to one another. Good geomorphic feature is parallel ridge and a few small ponds developed within the subsegment, they are inferred to have formed as result of releasing bend.

Next to the Khao Wong segment is the Khao Hin Paeng segment (No.7 in figure 4.20), which has the length of about 10.1km and the average trend in the N30^{o}E direction. The Khao Hin Paeng segment starts from Ban Tham Phung in the north and ends at Ban Bang Go in the south.It consists of 5 parallel subsegments, all of them cross cutting alluvial deposits.

Khao Hua Sing segment commences from Ban Thum Lay and terminates at Ban Bang Si (No.8 in figure 4.21). It is noted that this segment almost connects to the Ao Luek segment with the length of 18.2 km. But the latter has the northern segment striking in the NE direction which deviates from that of Khao Hua Sing segment. Geomorphic feature are small scarps and parallel ridges which mostly occur between Ban Bang Si and Ban Bang Hoi.

Almost nearby the Khao Hua Sing segment in the south is the Ao Luek segment (No.9 in figure 4.22), which has the total length of about 26.2 km and the average trend in the N30^{o}E direction. The Ao Luek segment starts from Ban Hin Dad in the north and ends at Ban Nai Sai in the south. It is noted that this segment almost connects to the Khao Hua Sing segment. But the latter has the southern segment striking in the NE direction which deviates from that of the average northward segment. Good geomorphic feature are small scarps and linear ridges, occurring mostly at Ban Khlong Rad to Ban Khao Yai.

Khao Phanom segment (No.10 in figure 4.23) is situated between Khao Hua Sing and The Khlong Heak segment. It commences from Ban Bang Prik in the north and terminates at Ban Kuan Sabai in the south. It has the total length of about 28.1 km and the average trend of about N30^{o}E direction. It comprises 11 subsegments and all of them almost parallel to Khao Phanom in the east. The longest subsequent is the subsegment one in middle part which is as long as 11 km. The good morphotectonic evidence includes facet spurs, parallel ridges, offset streams and linear valley. Geomorphologic indices, including Smf and SL, show that the segment show high SL values (1221) and low Smf values (1.4 to 1.5). This suggest that the segment is active.

The Khlong Heak segment (No.11 figure 4.23) starts from Ban Taling Chun in the south to Ban Bang Yuan in the north. It has the overall length of about 35.2 km and the average trend of about N40^{o}E. It consists of 9 subsegments, the main subsegments is Khlong Heak subsegment and Thap Put subsegment whose length are about 10.1 and 6.2 km, respectively. The Khlong Heak segment almost connects to the Khlong Marui in the southern portion, and in the northern portion the Khlong Heak segment converts to the Khao Wong segment. Special morphotectonic features are triangular facets, linear valleies, fault scarps and offset streams which can be observed at Ban Bang Samukkee and Ban Bang Raing Tai. Geomorphologic indices, including SL and Smf, show that the segment show high SL values (422) and low Smf values (1.32 to 1.4). This suggest that the segment is active.

The Khlong Marui segment (No.12 in figure 4.24) is the longest segment of all studies segments and its orientation almost follow the major river, viz., Khlong Marui river, which flows from southward of Khao Phanom to Phang Nga Bay at Ban Marui near Phang Nga city. The Khlong Marui segment starts from Ban San Suk, north of Phanom Town, in the north to Ban Marui in the south. It consists of more than 10 subsegments with the average trend of about N30^{o}E direction. It has the total length of about 54.8 km The shortest segment is about 3 km at Ban Khao Tam Non and the longest subsegment is about of 23 km at Ban Bang Luek. The outstanding geomorphic features are offset streams, triangular facets and linear valleys which mainly are situated at Ban Song Prak and Ban Benja. Geomorphologic indices, including Smf SL and Vf, show that the segment show high SL values (2047), low Smf values (1.32 to 1.4) and low Vf (0.29). This suggest that the segment is still active.

The Plai Phanom segment (No.13 in figure 4.25) is located in the north of Phang Nga segment with its trend in the N30^{o}E direction. The Plai Phanom segment commences from Ban Thap Vhan and ends at Ban Nai Ton. It have total subsegment with the length of about 15.1 km. The segment consists of one isolated subsegment (9.5 km long) at Ban bang Kan and the other 3 subsegments varying in length from 3.2 to 8 km.

The Phang Nga segment (No.14 figure 4.26) shows branching subsegments at the southern end. It is almost parallel to the Khlong Marui segment in the north and forms an en echelon structure with the Khlong Marui segment. Its average trend is in the N40^{o}E direction. It consists of 9 subsegments with the total length of about 31.8 km. It commences from Ban Hin Sam Khon in the north and terminates at Ban Suan Prik in the south. The maximum segment is in the north part and is as long as 17 km. Good morphotectonic features, including triangular facets, linear valleys, fault scarps and offset streams, were observed at Ban Thong Lang and Ban Bang Nu. Geomorphologic indices, including Vf and Smf, show that the segment show low Vf values (1.2 to 3.64) and low Smf (1.64) at southern part of Ban Hin Sam Khon. This suggest that the segment is active.

The Tai Maung segment consists of 4 subparallel subsegment (No.15 in figure 4.27). It is an isolated segment located onshore of Andaman Sea in the north of Tai Muang District. The segment starts from Ban Tha Kho and Ban Huay Sai in the south and ends at Ban Intanin and Ban Kanim in the north with the total length of 13.4 km.. The orientation of individual subsegments varies from the N40^{o}E to the N60^{o}E. Fault scarps and linear valleys at Ban Kanim and Ban Tha Kho, are good morphotectonic features. There are three long segment at KHo Lampi and the north of Klong Plate whose length is 7, 8 and 11 kmfrom west to east, respectively.

The Pakong segment (No.16 in figure 4.28) is an isolated segment similar to the Tai Maung segment with its trend in the N30^{o}E direction The segment is located near the Andaman Sea to the west of Kapong District. The Pakong segment commences from Ban Sapan Suae and ends at Ban Lem Khan. Well detired morphotectonic features are shutter ridges, triangular facet and sag pond. They are observed at Ban Plaiwa.

Table 4.2 Types of fault segments and criteria used for active fault segmentation in this study (McCalpin, 1996).

Type of Segment[a]	characteristics used to define the segment[a]	Likelihood of being An earthquake segment [b]
1.Earthquake	Historic rupture limits.	By definition, 100% [c]
2.Behavioral	1) Prehistoric rupture limits defined by multiple, well-dated paleoearthquakes.	High
	2) Segment bonded by changes in slip rates, recurrence intervals, elapsed times, sense of displacement, creeping versus locked behavior, fault complexity.	Mod. (26%)
3.Structural	Segment bounded by fault branches, or intersections with other faults, folds, or cross-structures.	Mod.-High (31%)
4.Geologic	1) Bounded by Quaternary basins or volcanic fields. 2) Restricted to a single basement or geologic terrain. 3) Bounded by geophysical anomalies. 4) Geomorphic indicators such as range-front morphology, crest elevation.	Variable [d] (39%)
5.Geometric	Segments defined by changes in fault orientation, stepovers, separations, or gaps in faulting.	Low-Mod. (18%)

[a] Classification following the segment boundary types of dePolo et al. (1989, 1991) and Knuepfer (1989).

[b] Percentages = percent of cases where historic ruptures have ended at this type of boundary, as opposed to rupturing through it (Knuepfer, 1989, Table 3).

[c] However, restriction of a single historic rupture to the segment does not mean that all future ruptures will be similarly restricted.

[d] Small number of observations, accuracy questionable (Knuepfer, 1989, Table 3).

Table 4.3 Fault segment lengths proposed for active fault by various authors (modified after McCalpin, 1996).

Fault name	Type[a]	Number of segments	Total fault length (km)	Mean segment length (km)	Modal segment length (km)	Criteria used for recognition[b]
1. Wasatch fault zone[c]	N	10	343	33	35	B,P,S,G,M
2. NE Basin and Range, >100 km[c]	N	10	-	25	20-35	B,P,S,G,M
3. NE Basin and Range, <100 km[c]	N	20	-	20	10-20	B,P,S,G,M
4. Idaho[d]	N	20	280	22	20-25	B,P,S,G,M
5. North-central Nevana[e]	N	70	-	10	10	M
6. San Adreas[f]	S	4	980	245	15-175?	B,P,S,G,M
6. San Adreas[g]	S	7	980	140	300?	B,P,S,G,M
6. San Adreas[h]	S	784	980	1.2	1	M
6. San Adreas[i]	S	68	980	14	12	M
7. San Jacinto[j]	S	20	250	12	10-15	M
8. Elsinore[k]	S	7	337	48	-	M,P
9. Xianshuihe[l]	S	1	220	220	-	M
10. Transverse Ranges[m]	R	-	-	20-30	-	M
11. Oued Fodda, Algeria[n]	R	3	32	11	11-12	B,P,S,M

[a]N,normal; S,strike-slip; R,reverse.

[b]B,behavioral; P,paleiseismic; S,structure; G,geological; M,geometric.

[c]Machette et al. (1992a).

[d]Crone and Haller (1991).

[e]Wallace (1989).

[f]Allen (1968).

[g]Wallace (1970).

[h]Wallace (1973).

[i]Bilham and King (1989).

[j]Sanders (1989).

[k]Rockwell (1989).

[l]Allen et al. (1989).

[m]Ziony and Yerkes (1985).

[n]King and Yielding (1983).

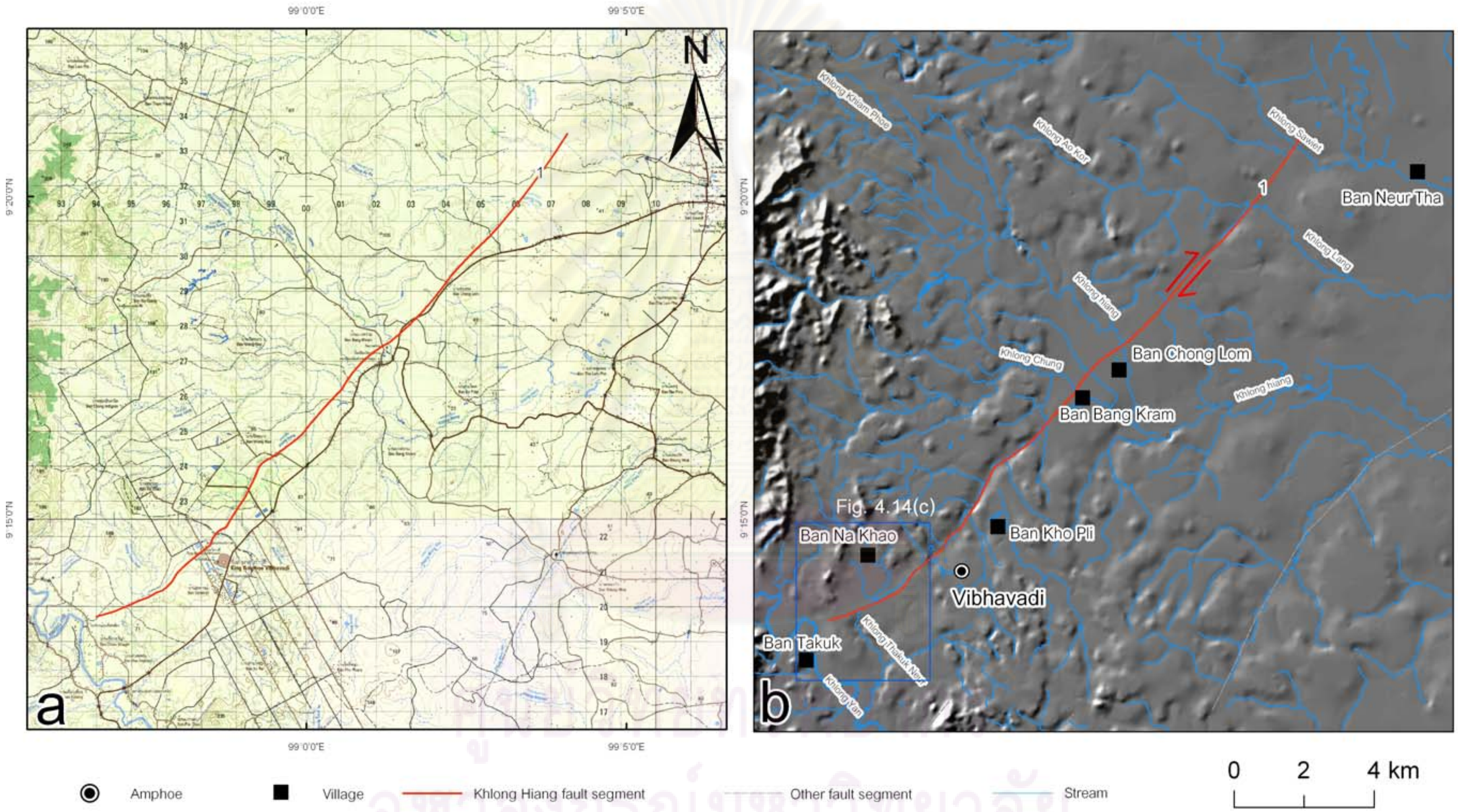

Figure 4.14 Topographic (a) and 20-m contour interval DEM (b) maps showing Khlong Hiang fault segment (no.1).

98

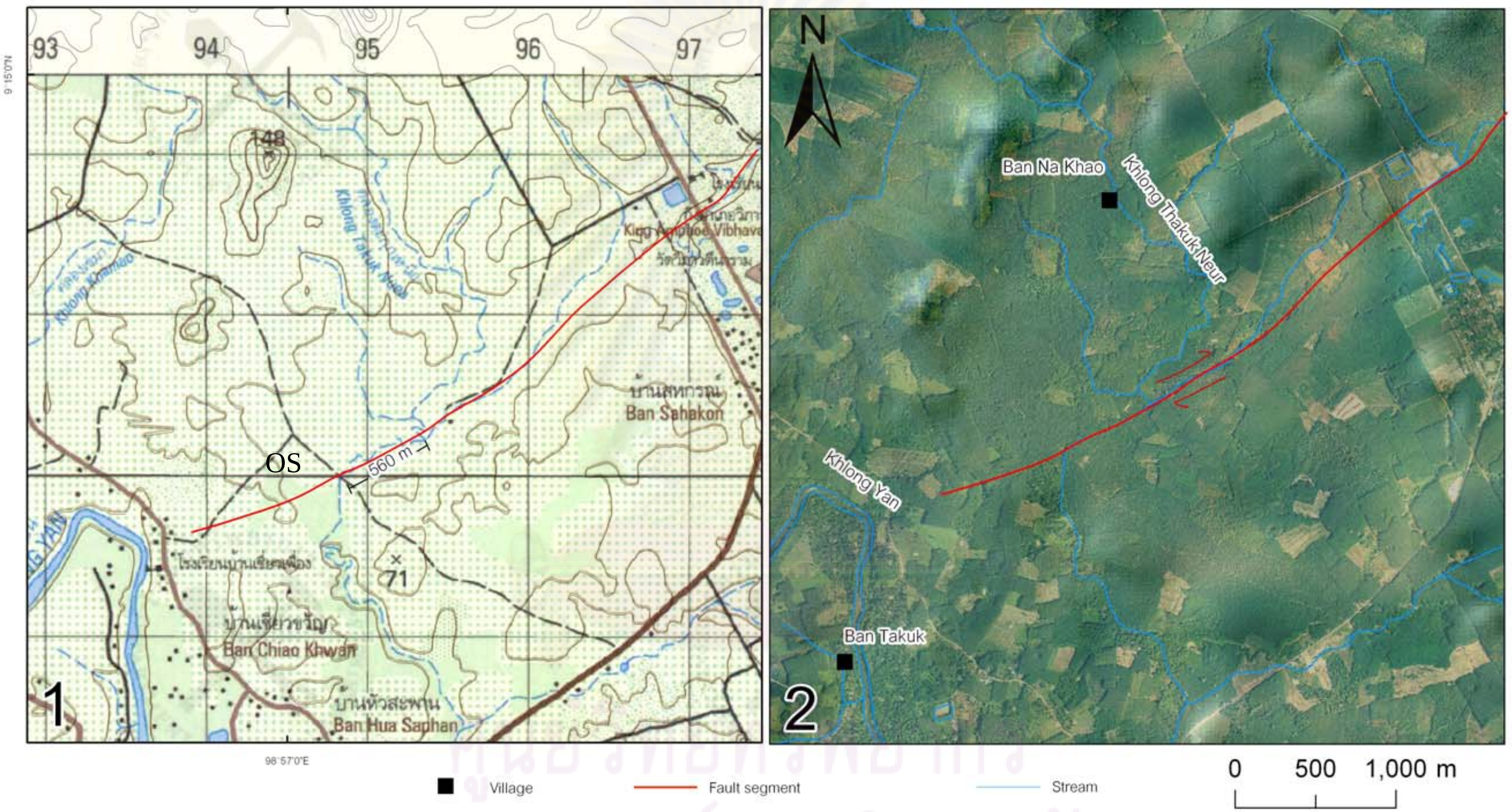

Figure 4.14 (cont.)c Active fault evidence enlarged from topographic map (1) and color-orthographic image (2) of Figure 4.14b (Khlong Haing fault segment) showing offset stream (os) with the right displacement of about 560m.

99

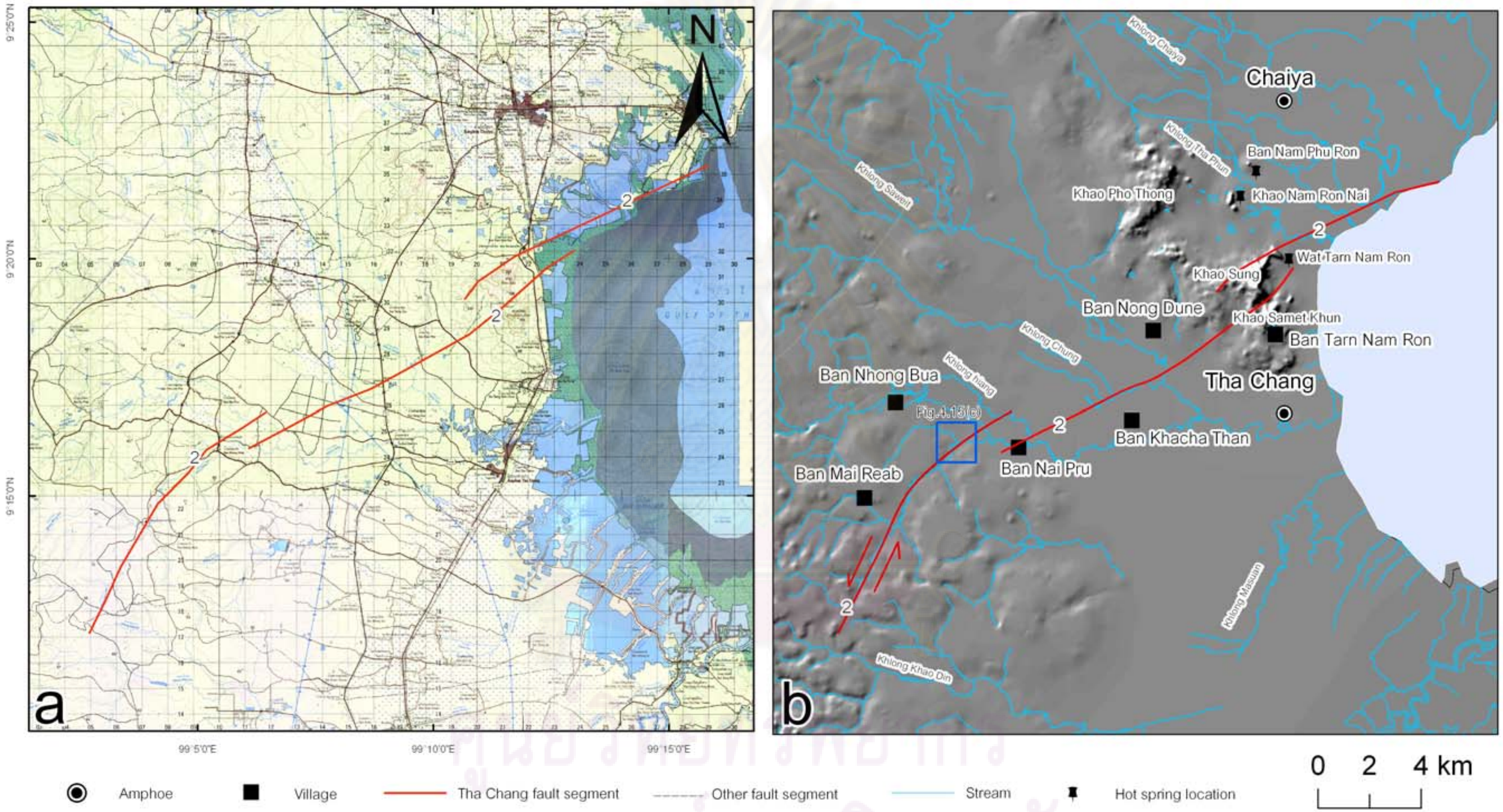

Figure 4.15 Topographic (a) and 20-m contour interval DEM (b) maps showing Tha Chang fault segment (no.2).

100

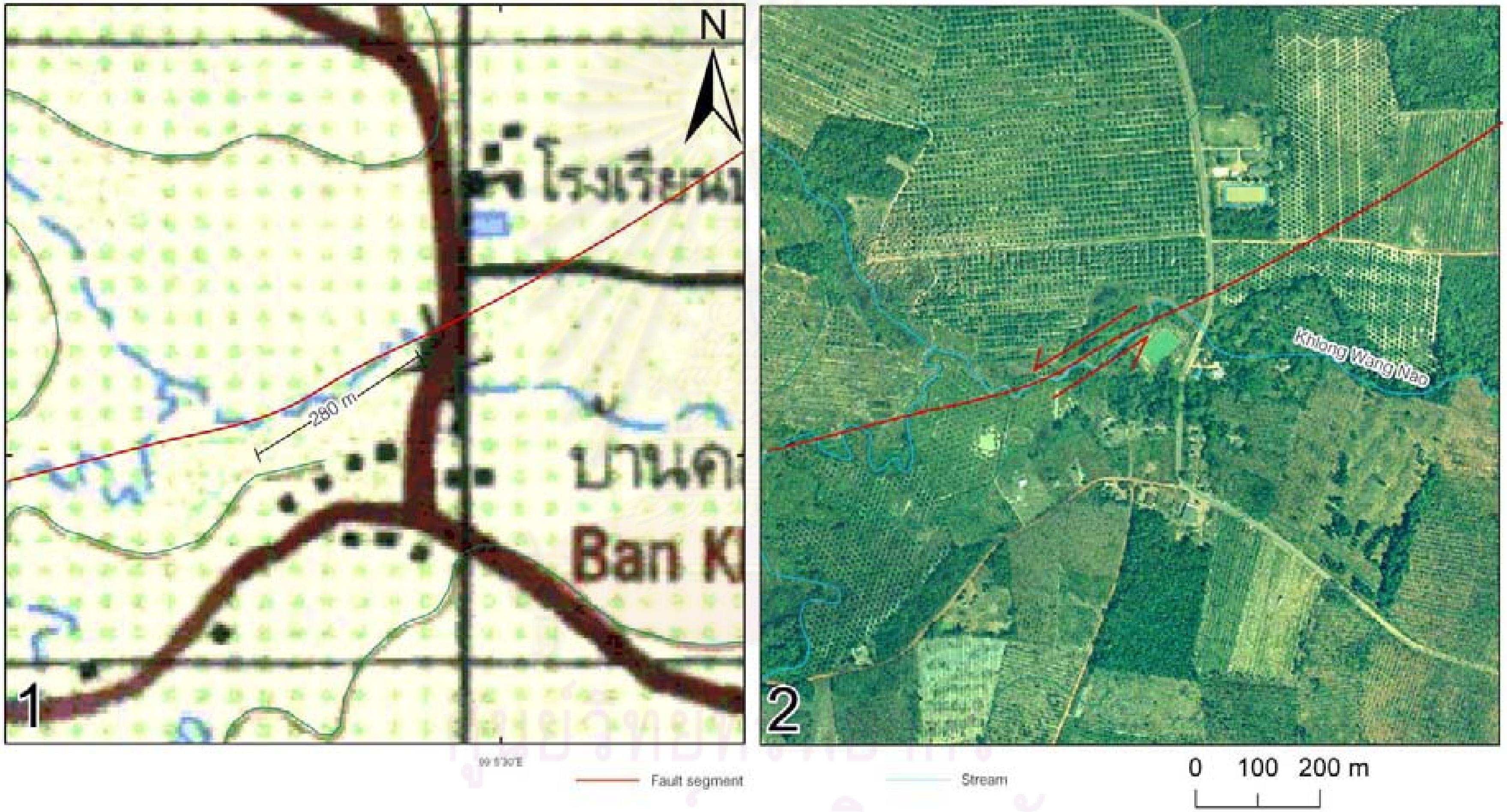

Figure 4.15 (cont.)c Active fault evidence enlarged from topographic map (1) and color-orthographic image (2) of Figure 4.15b (Tha Chang fault segment) showing offset stream (os) with the left displacement of about 280 m.

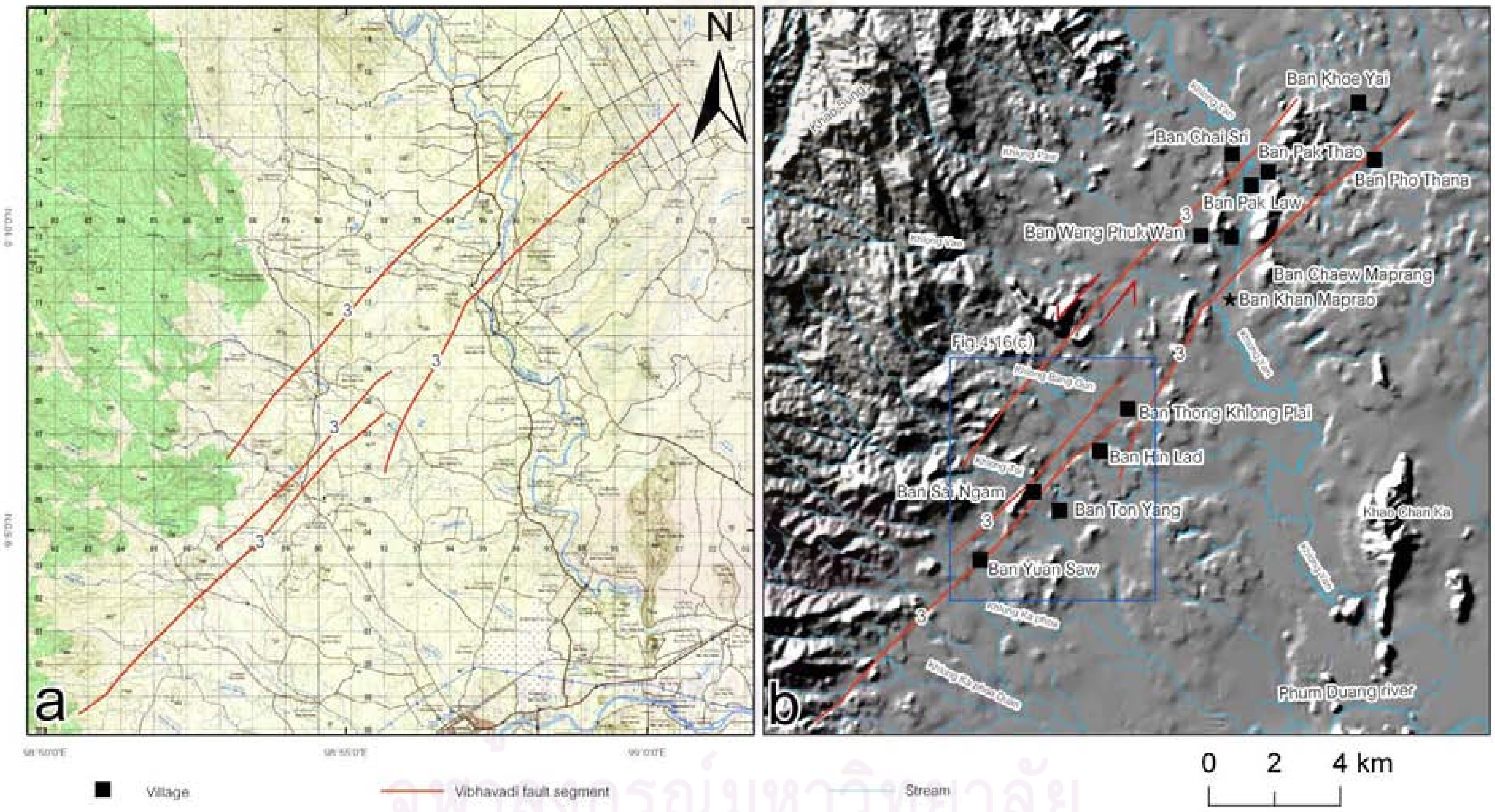

Figure 4.16 Topographic (a) and 20-m contour interval DEM (b) maps showing Vibhavadi fault segment (no.3).

102

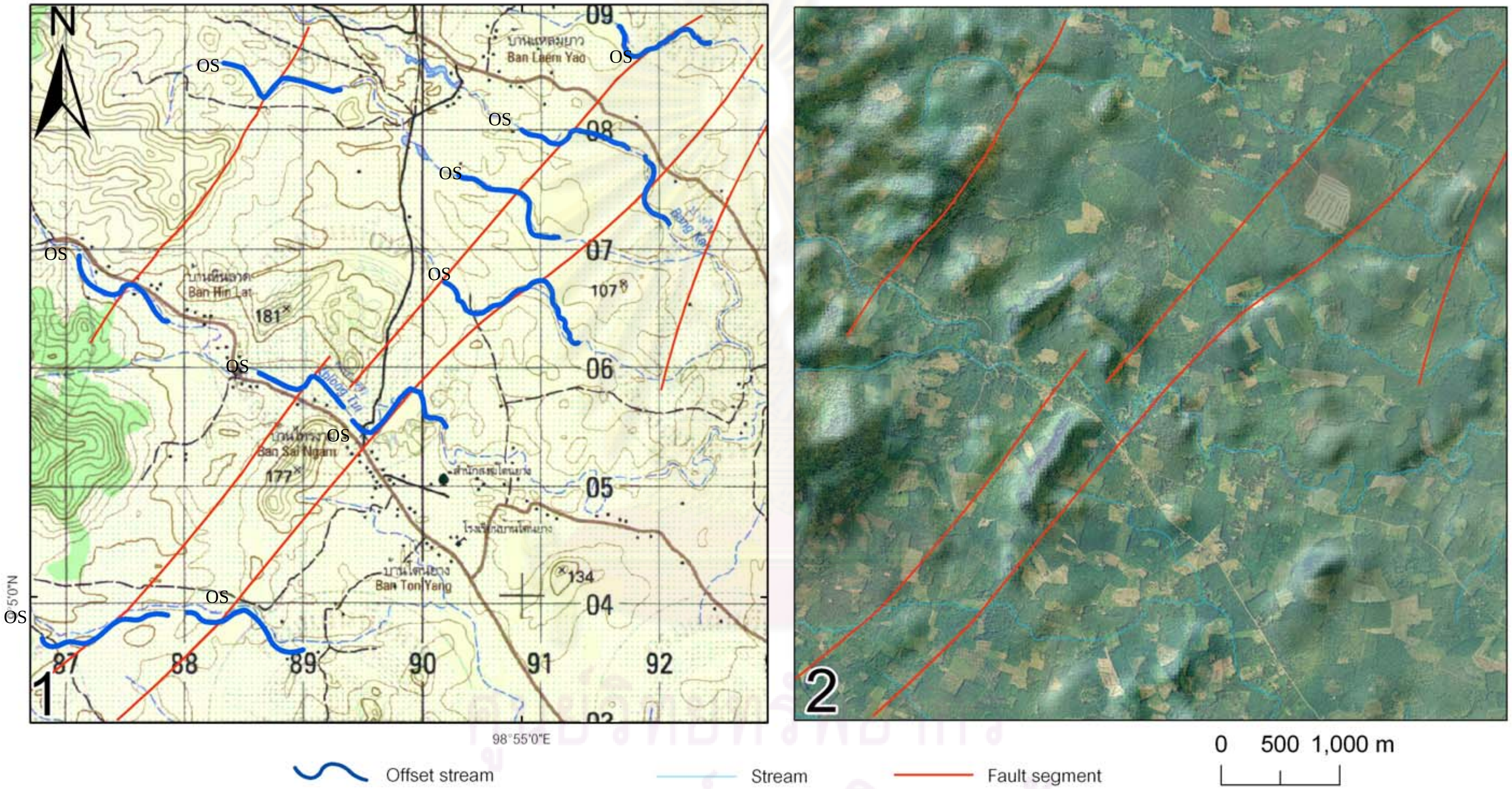

Figure 4.16 (cont.)c Active fault evidences enlarged from topographic map (1) and color-orthographic image (2) of Figure 4.16b (Vibhavadi fault segment) showing a set of offset stream (os) .

103

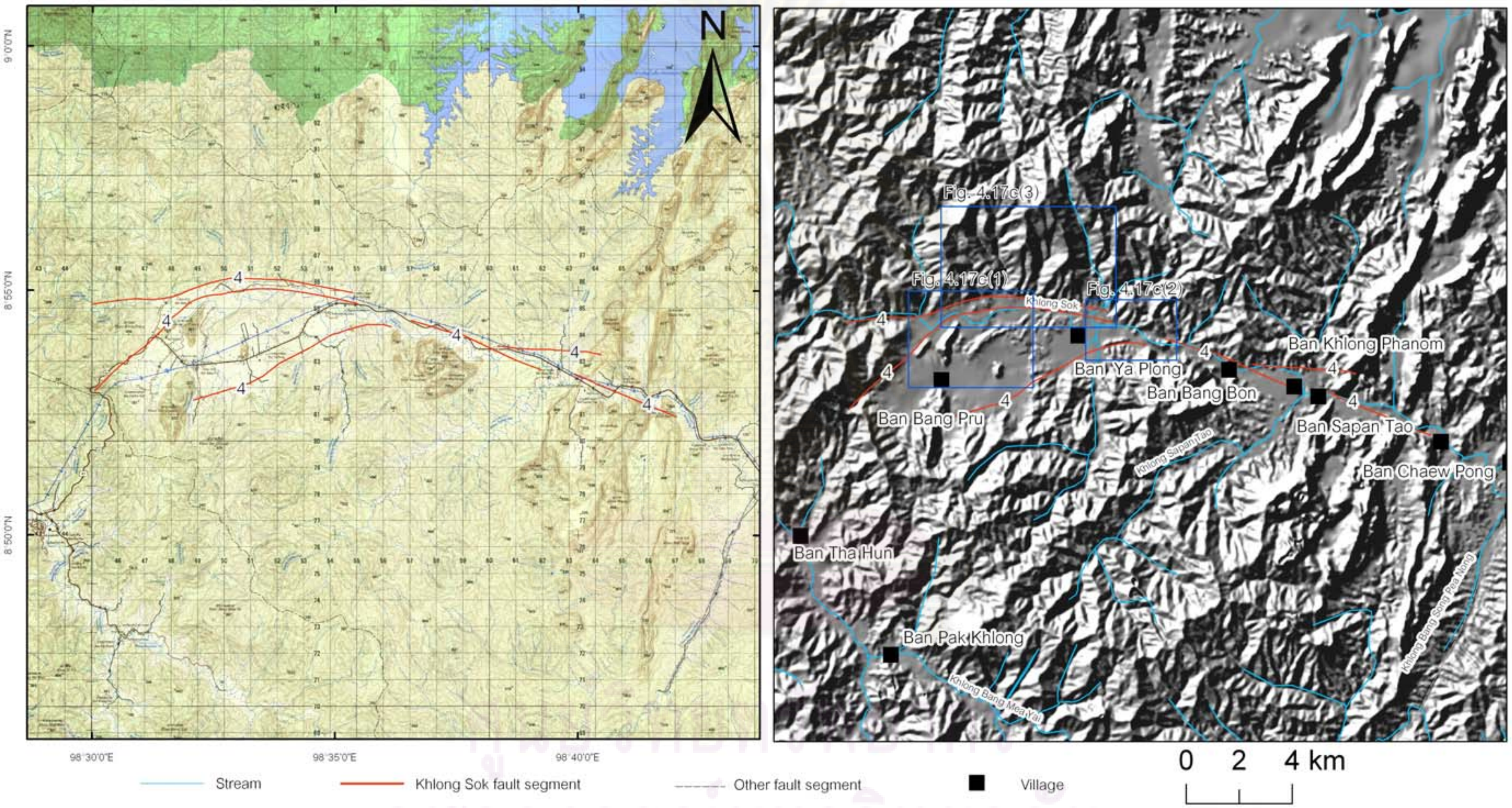

Figure 4.17 Topographic (a) and 20-m contour interval DEM (b) maps showing Khlong Sok fault segment (no.4).

104

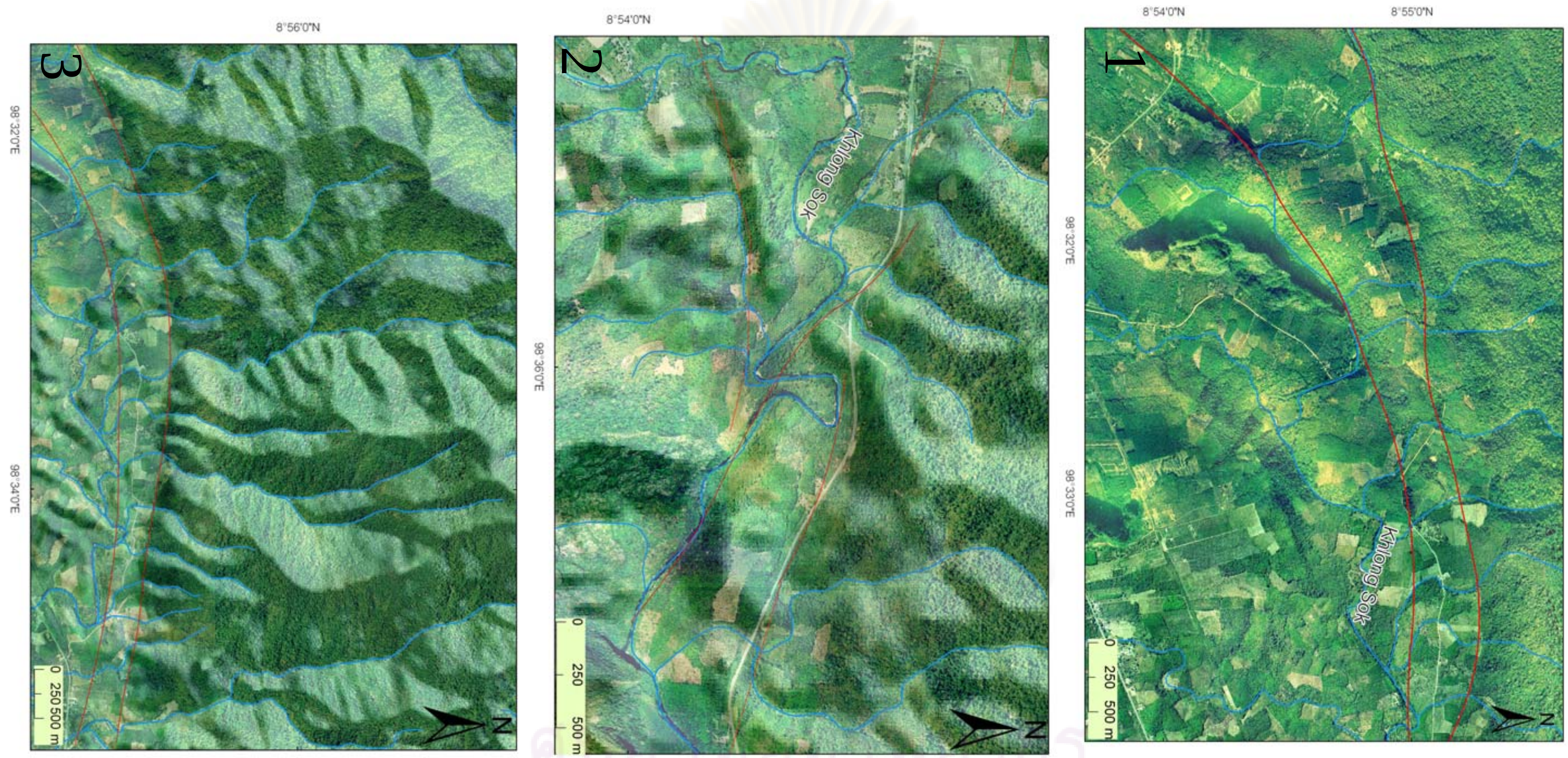

Figure 4.17(cont.)c Active fault evidences enlarged from Figure 4.17b showing (1) pressure ridges (2) shutter ridges and (3) trigular-facets.

105

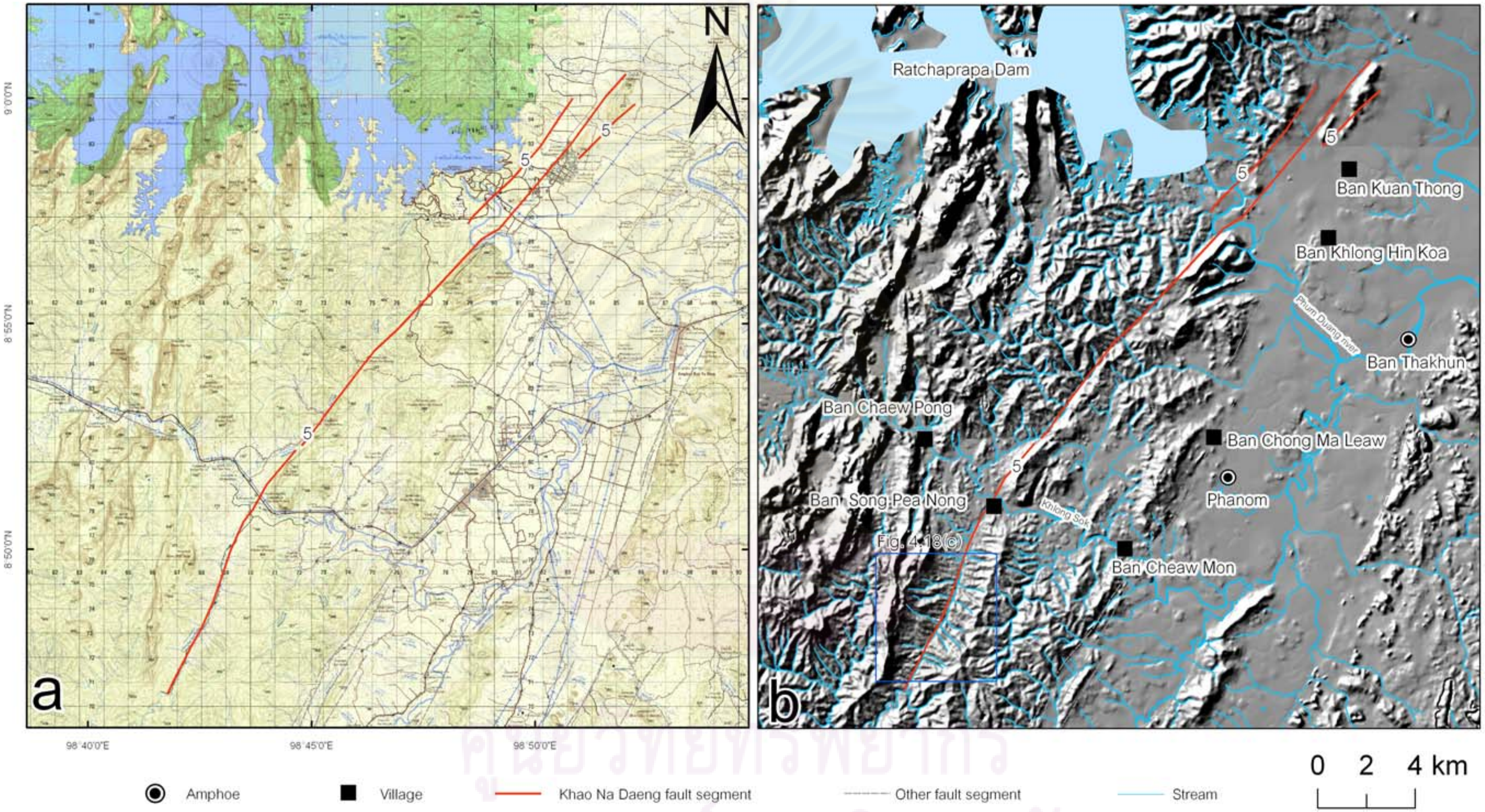

Figure 4.18 Topographic (a) and 20-m contour interval DEM (b) maps showing Khao Na Dang fault segment (no.5).

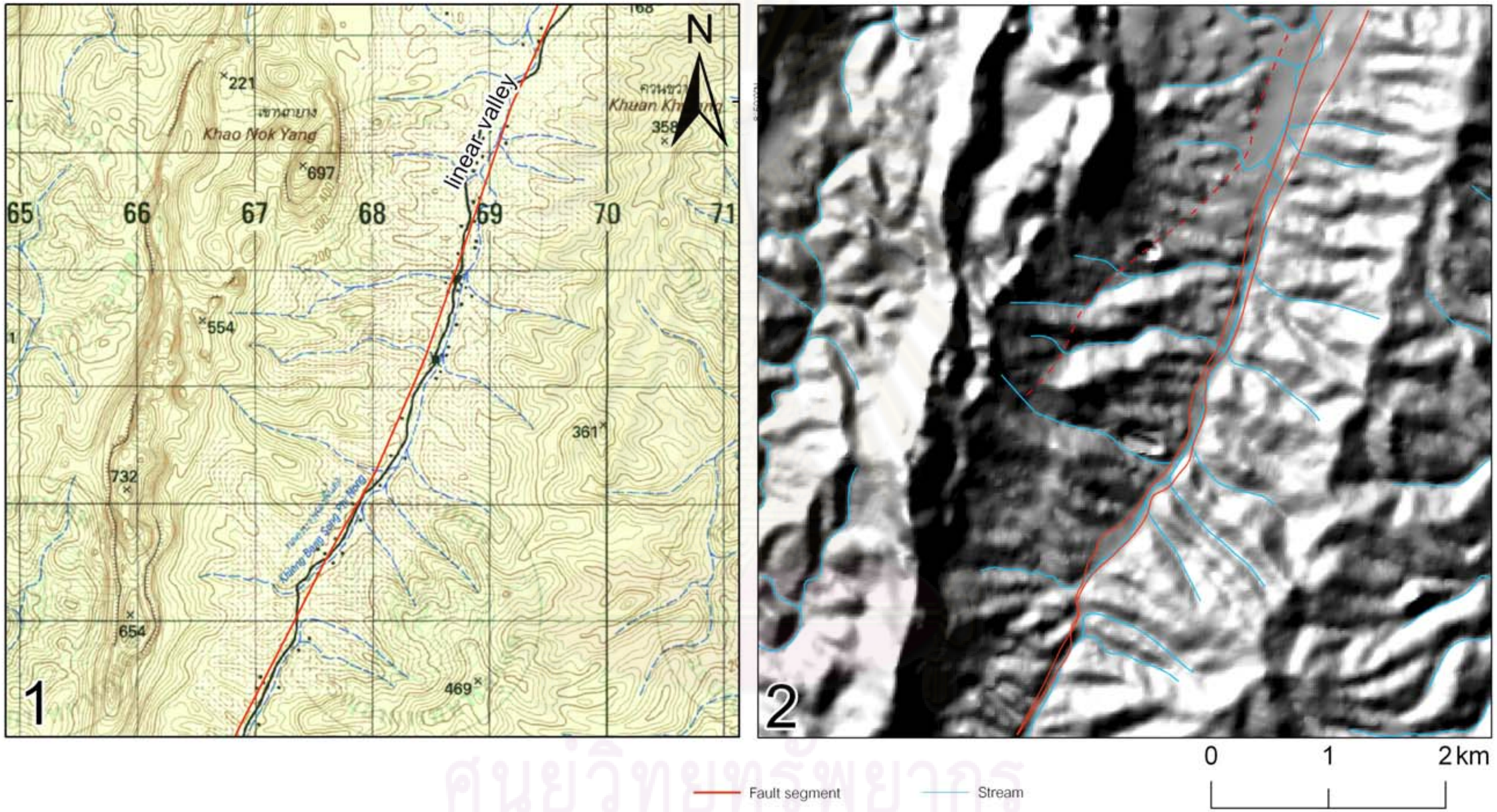

Figure 4.18 (cont.)c Active fault evidence enlarged from topographic map (1) and color-orthographic image (2) of Figure 4.18b (Khao Na Dang fault segment) showing linear valley.

107

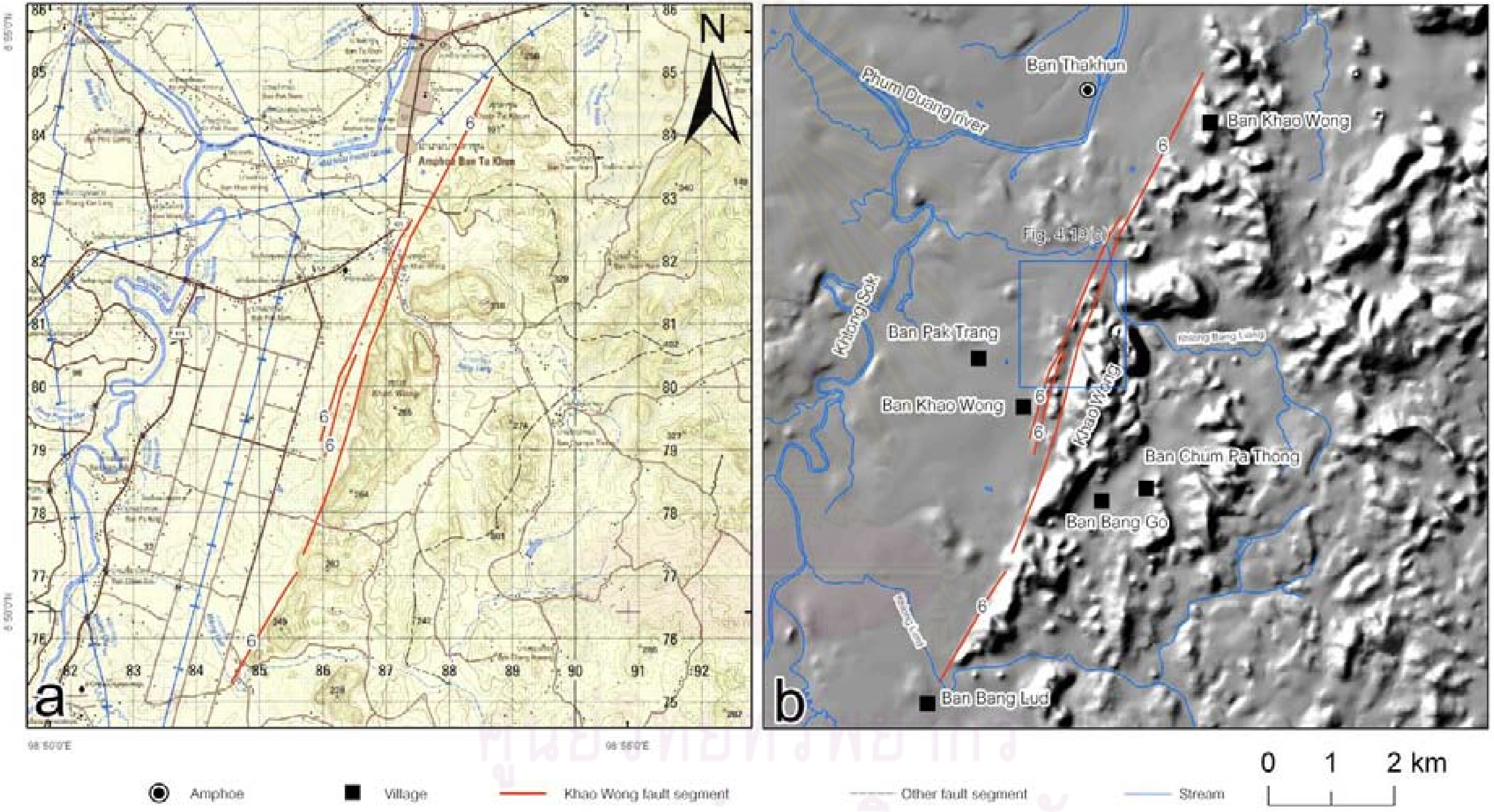

Figure 4.19 Topographic (a) and 20-m contour interval DEM (b) maps showing Khao Wong fault segment (no.6).

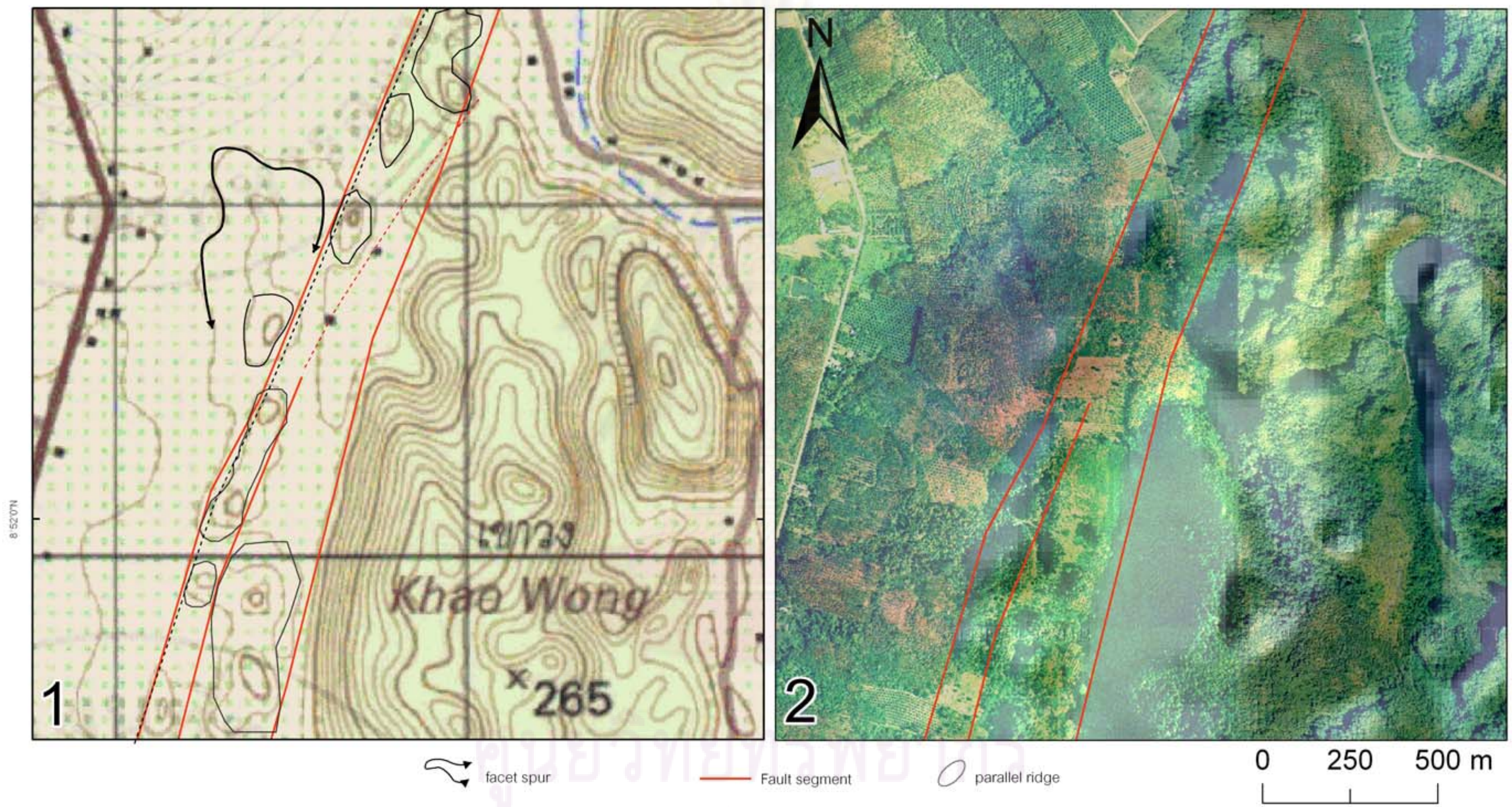

Figure 4.19 (cont.)c Active fault evidences enlarged from topographic map (1) and color-orthographic image (2) of Figure 4.19b (Khao Wong fault segment) showing a set of parallel ridges and a facet spur.

109

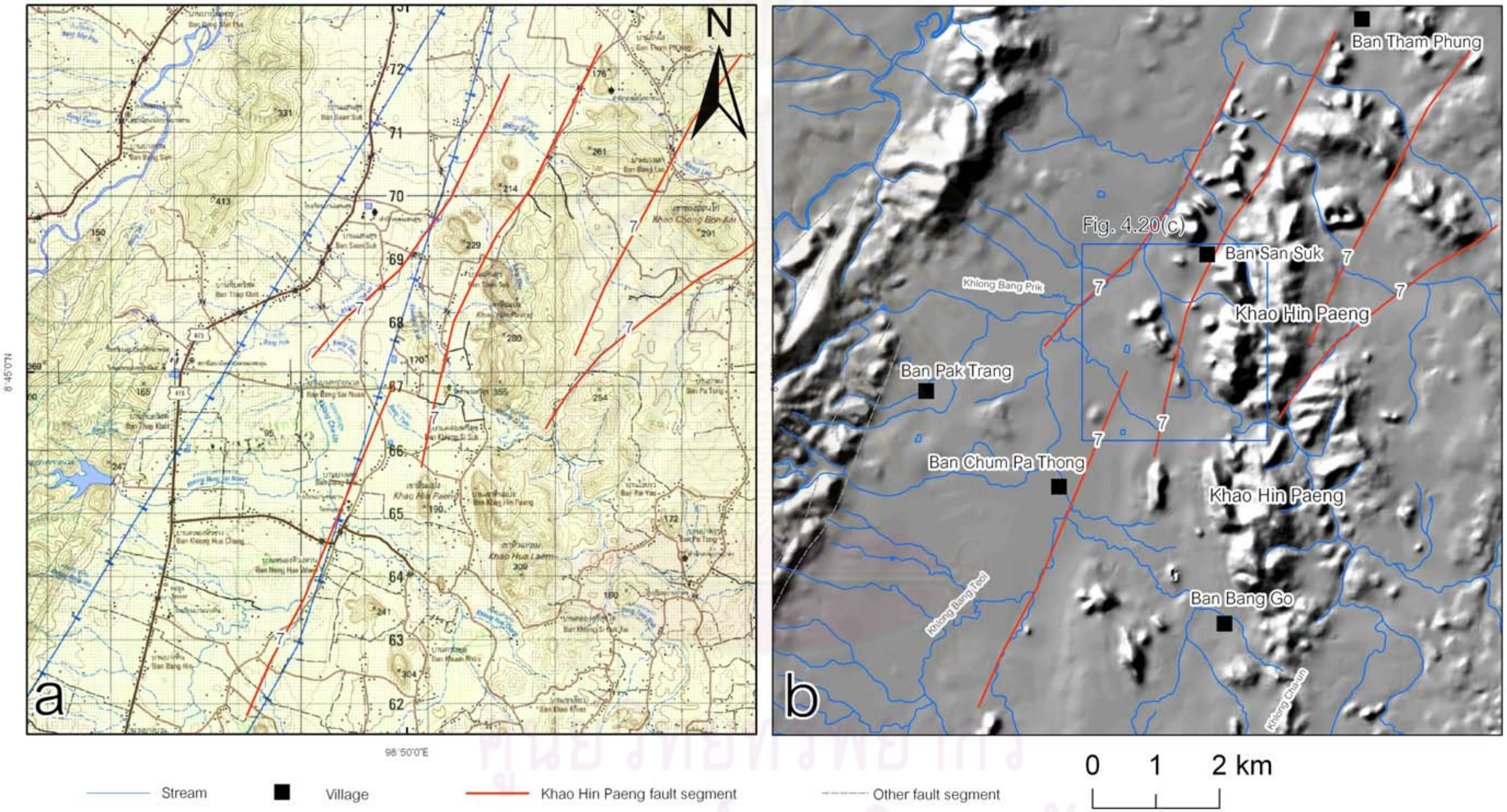

Figure 4.20 Topographic (a) and 20-m contour interval DEM (b) maps showing Khao Hin Paeng fault segment (no.7).

110

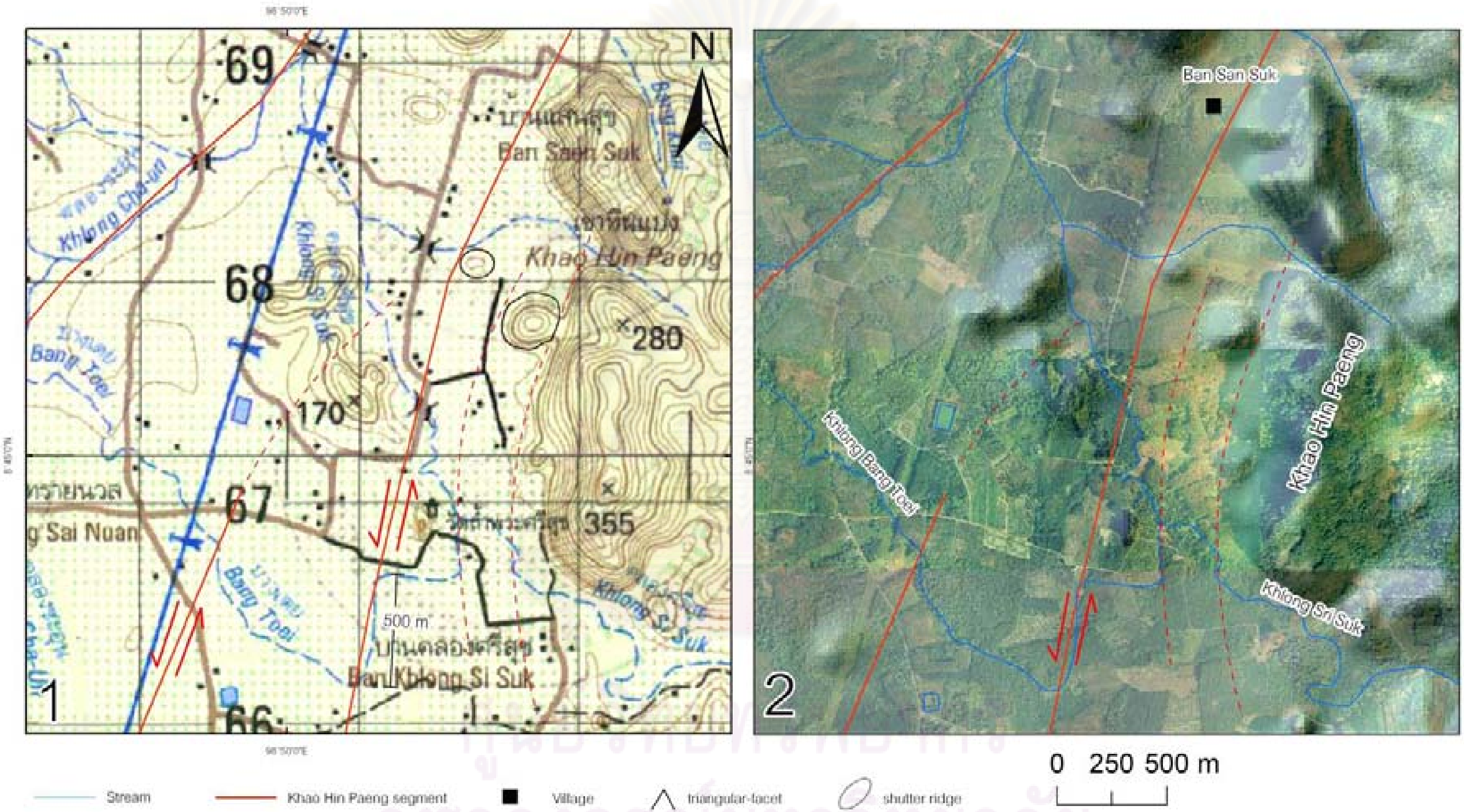

Figure 4.20 (cont.)c Active fault evidences enlarged from topographic map (1) and color-orthographic image (2) of Figure 4.20b (Khoa Hin Paeng fault segment) showing triangular facets and shutter ridges.

111

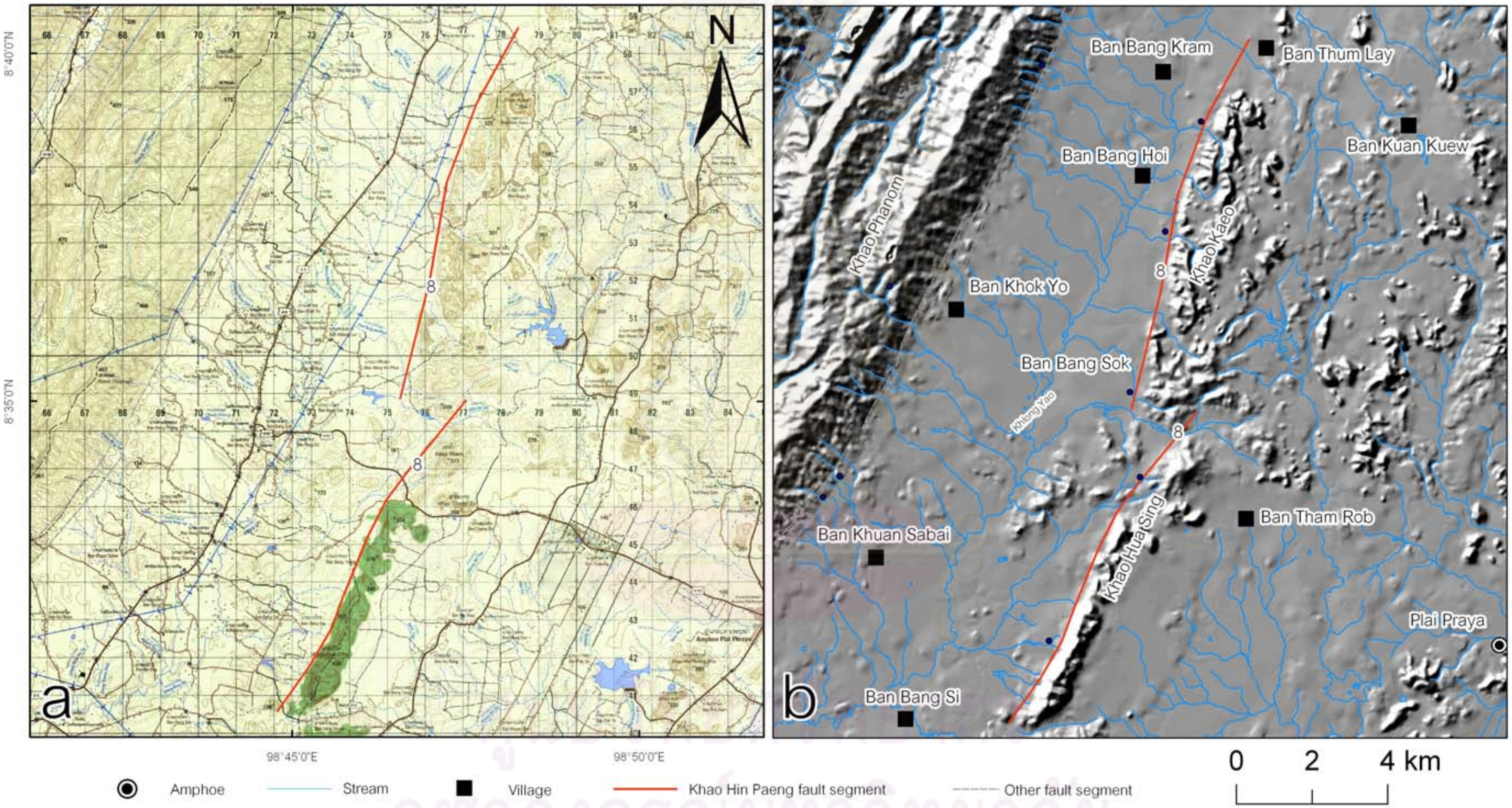

Figure 4.21 Topographic (a) and 20-m contour interval DEM (b) maps showing Khao Hua Sing fault segment (no.8).

112

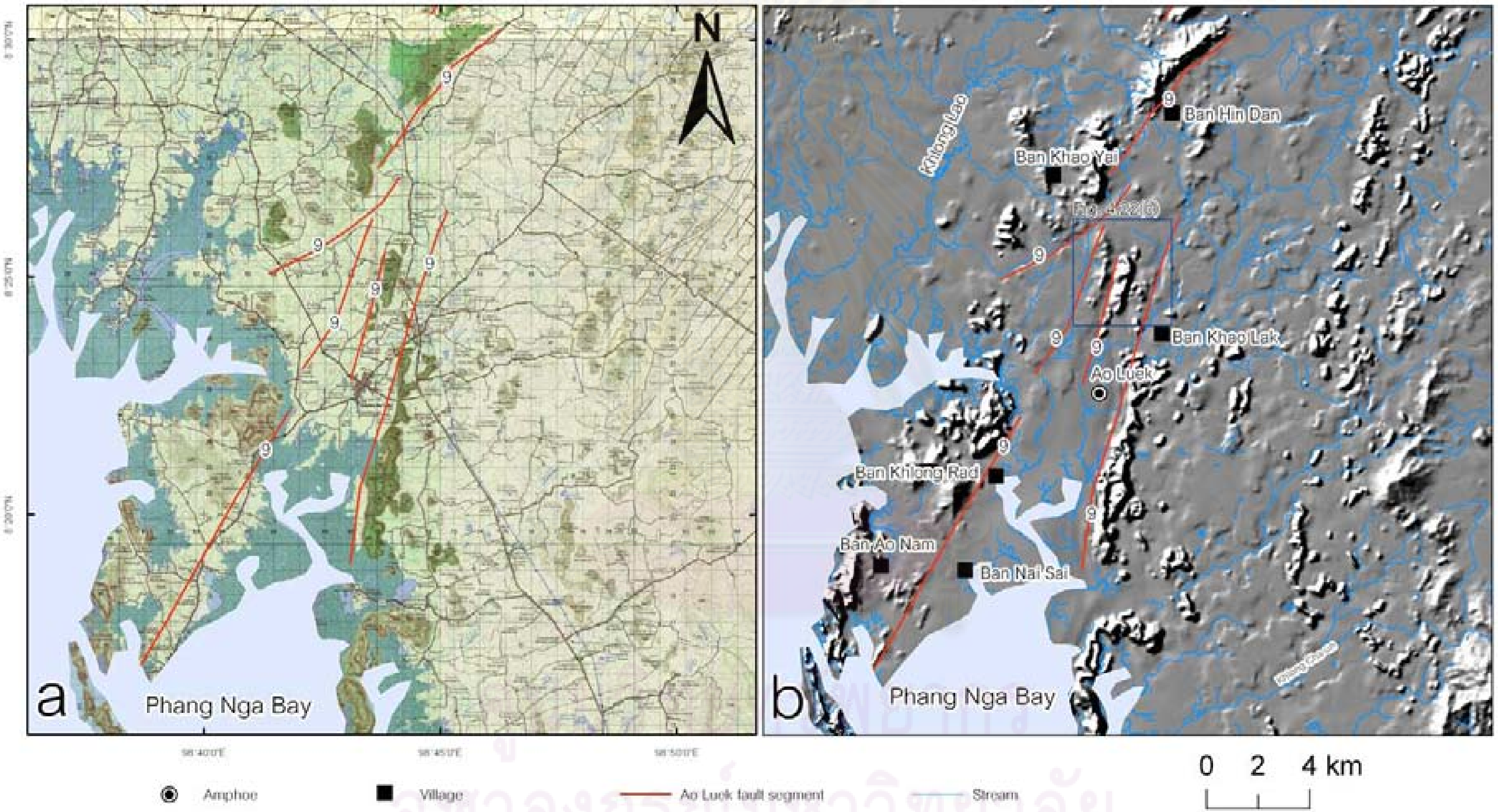

Figure 4.22 Topographic (a) and 20-m contour interval DEM (b) maps showing Ao Luek fault segment (no.9).

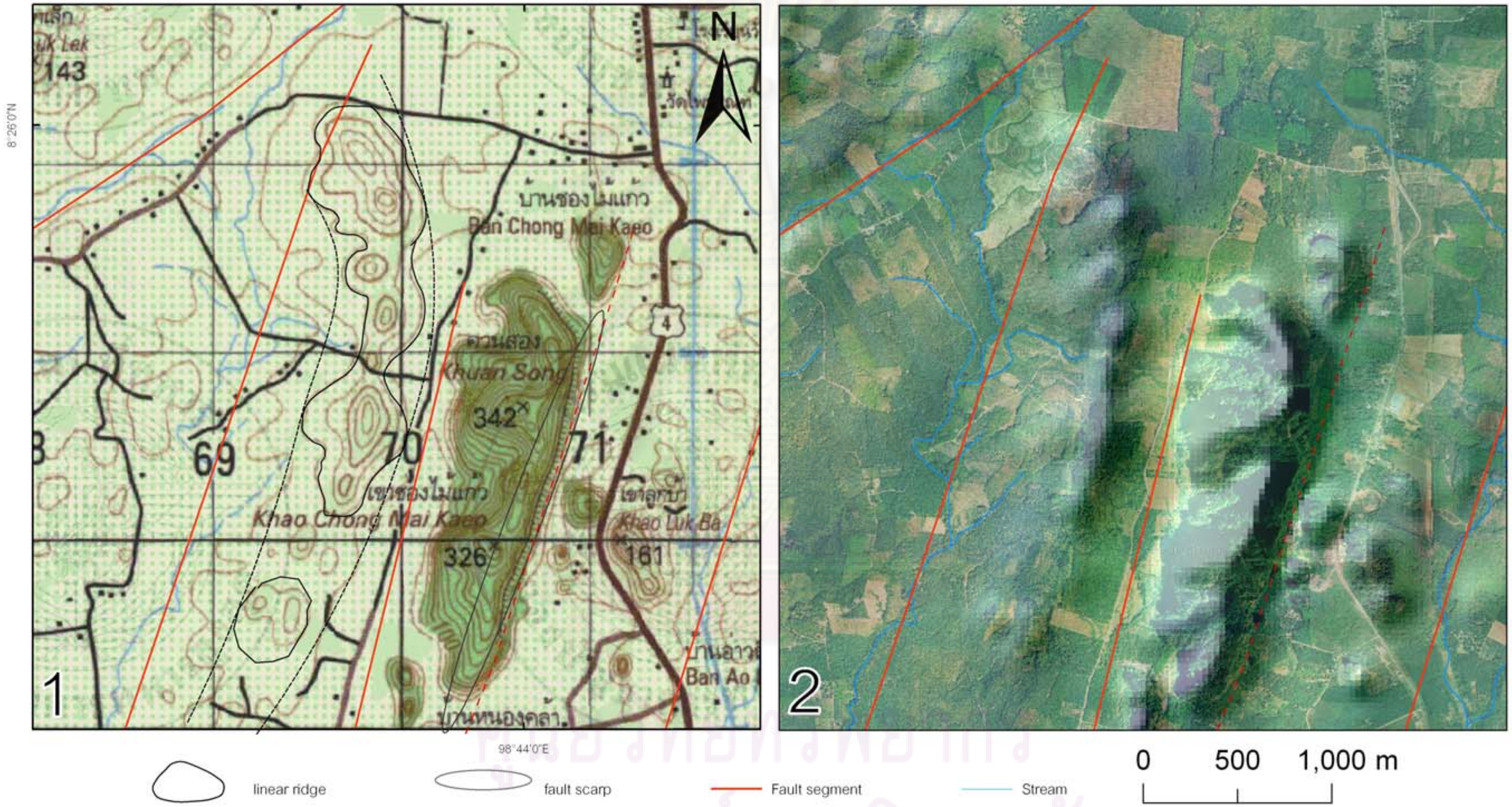

Figure 4.22 (cont.)c Active fault evidences enlarged from topographic map (1) and color-orthographic image (2) of Figure 4.22b (Ao Luek fault segment) showing a set of linear ridge and fault scarp.

114

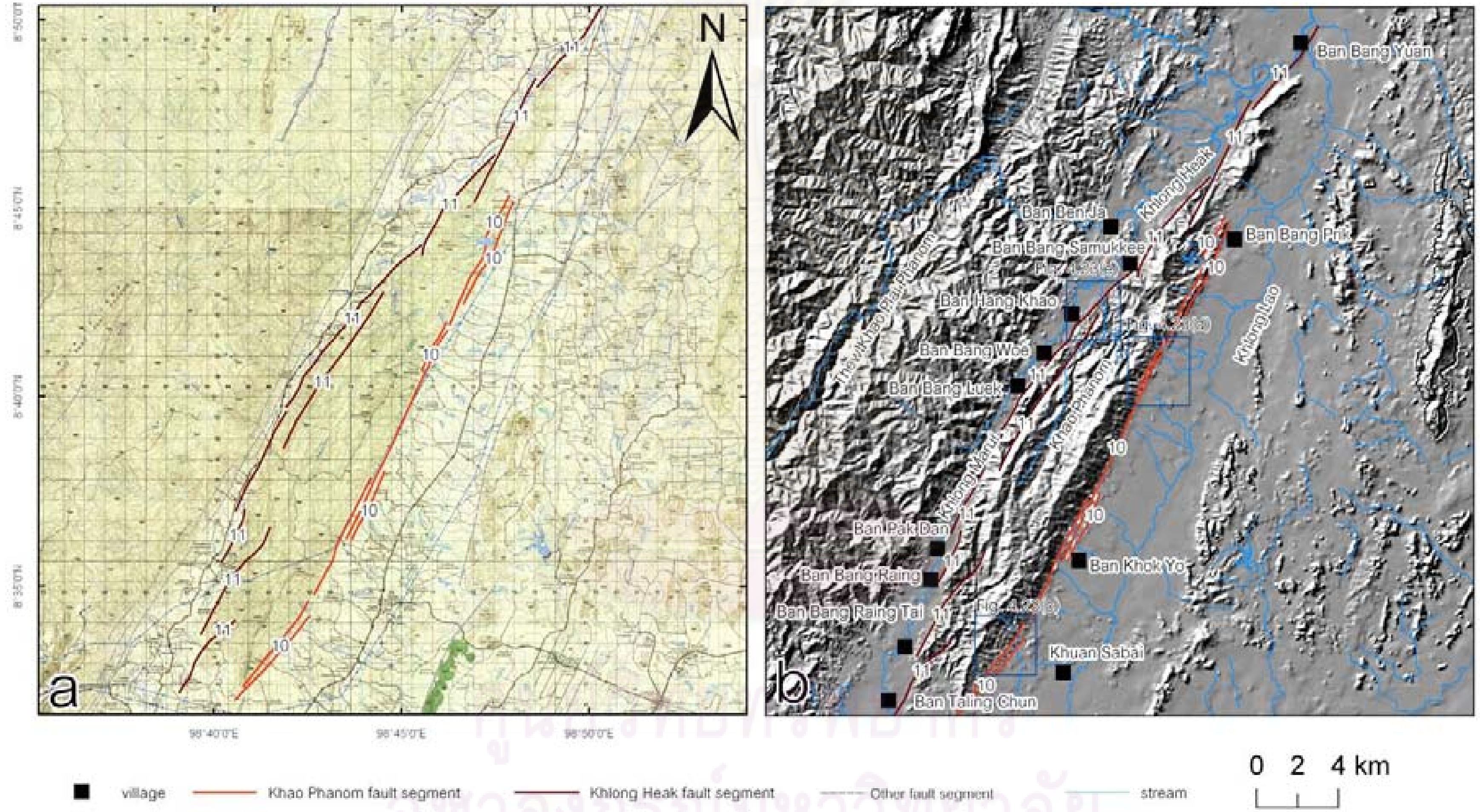

Figure 4.23 Topographic (a) and 20-m contour interval DEM (b) maps showing Khao Phanom and Khlong Haek fault segment (no.10 and no.11).

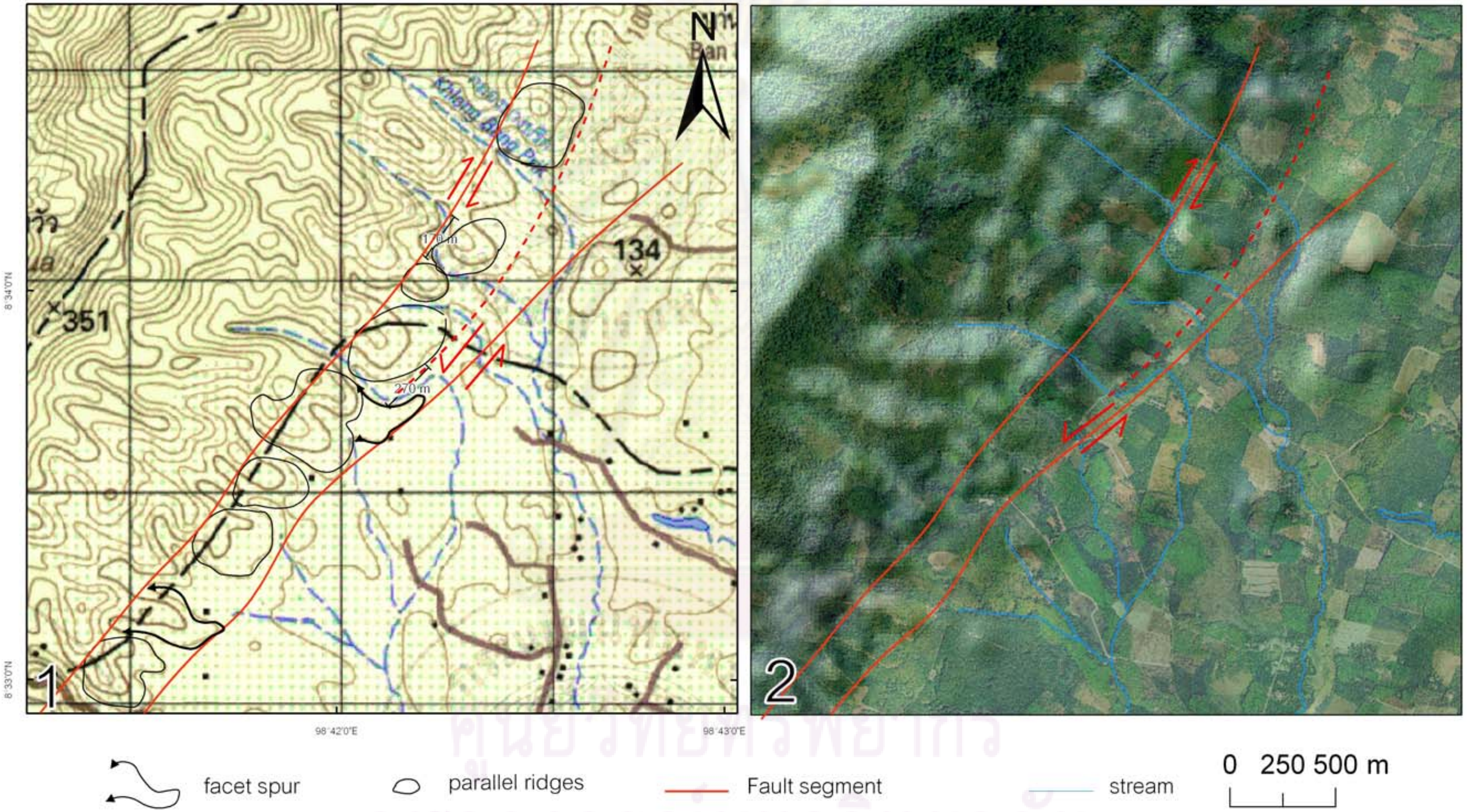

Figure 4.23 (cont.)c Active fault evidences enlarged from topographic map (1) and color-orthographic image (2) of Figure 4.23b (Khoa Phanom fault segment) showing facet spurs and parallel ridges.

116

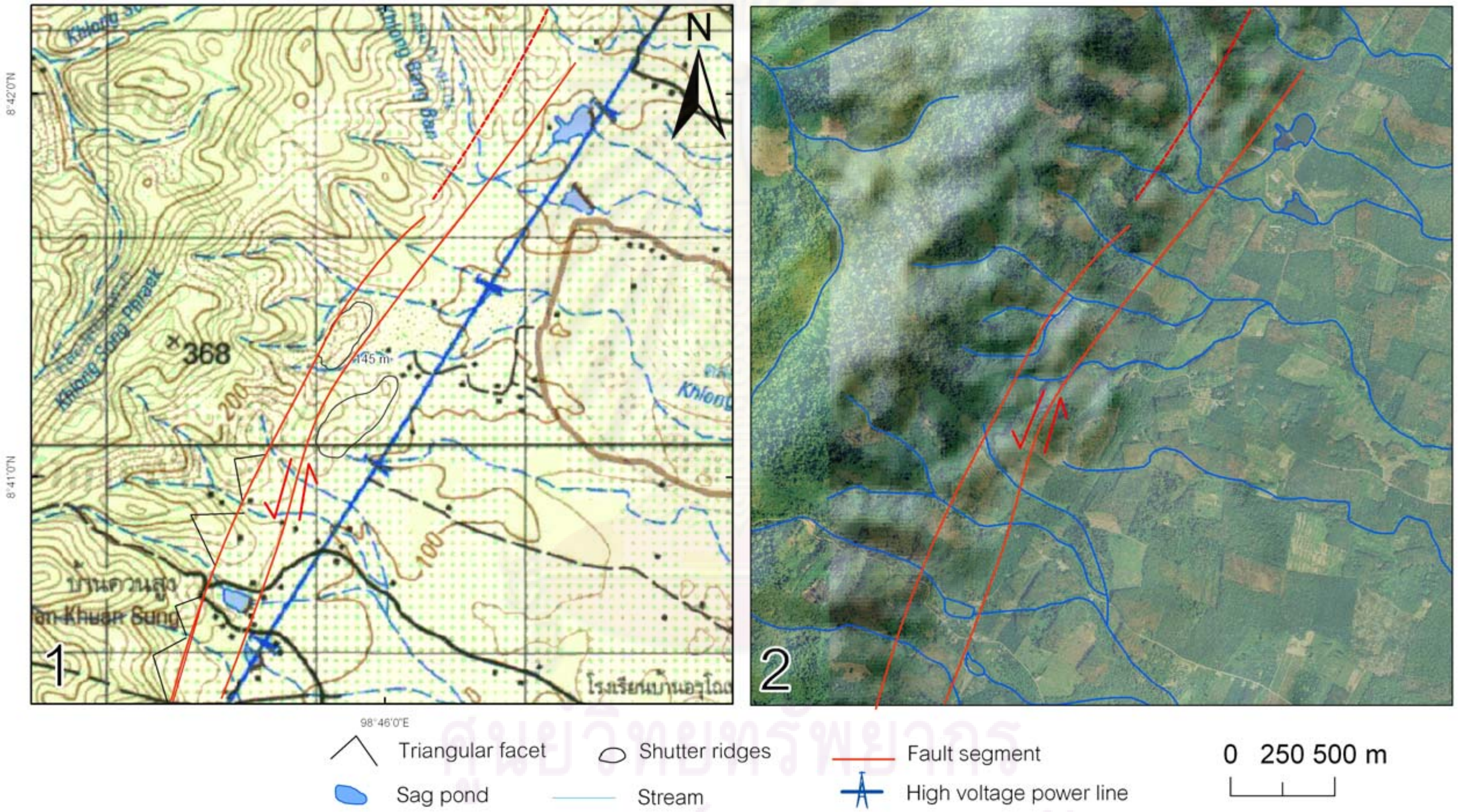

Figure 4.23 (cont.)d Active fault evidences enlarged from topographic map (1) and color-orthographic image (2) of Figure 4.22b (Khao Phanom fault segment) showing triangular facets, shutter ridges and sag ponds.

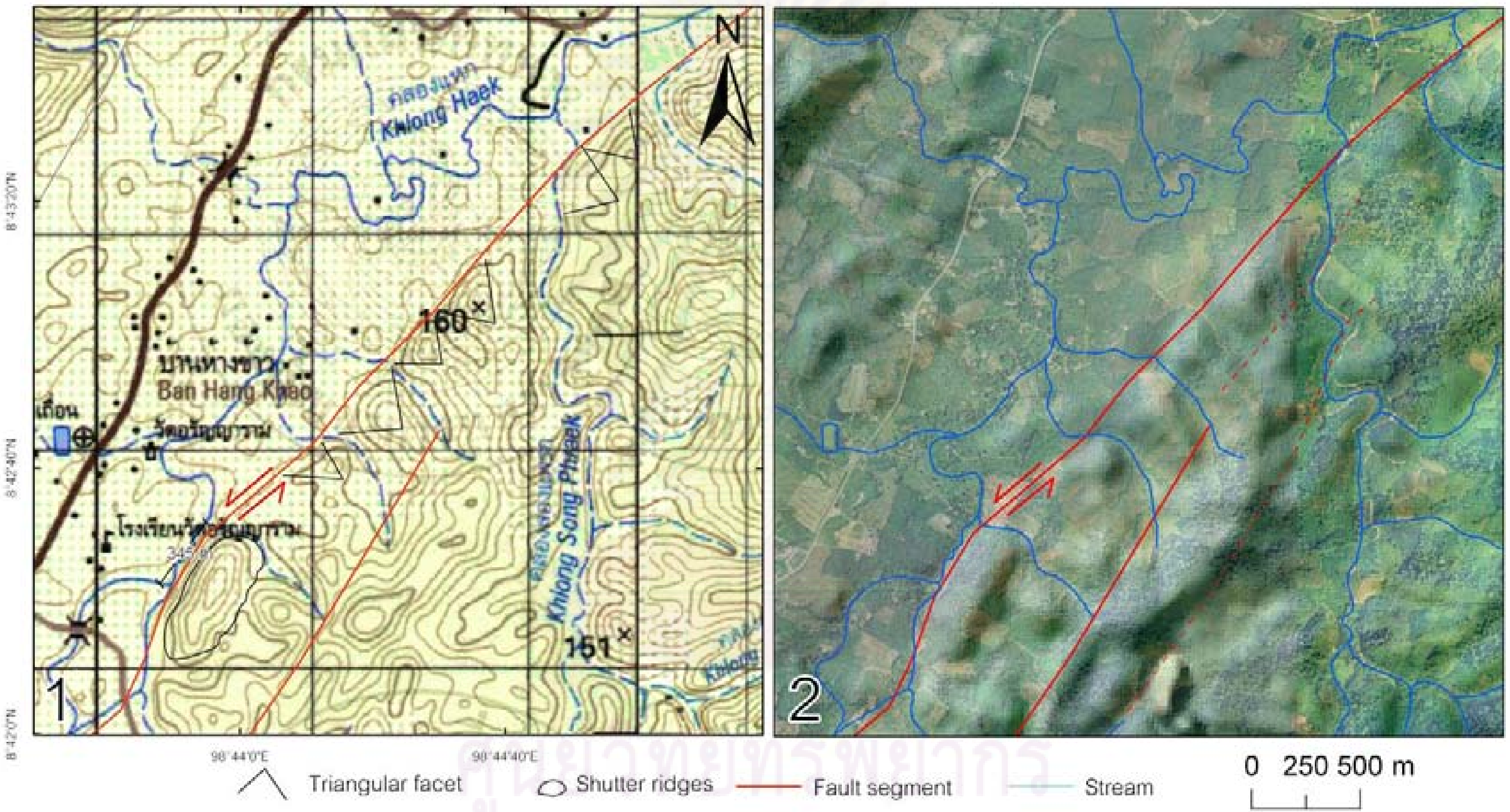

Figure 4.23 (cont.)e Active fault evidences enlarged from topographic map (1) and color-orthographic image (2) of Figure 4.22b (Khlong Haek fault segment) showing triangular facets and a shutter ridge.

118

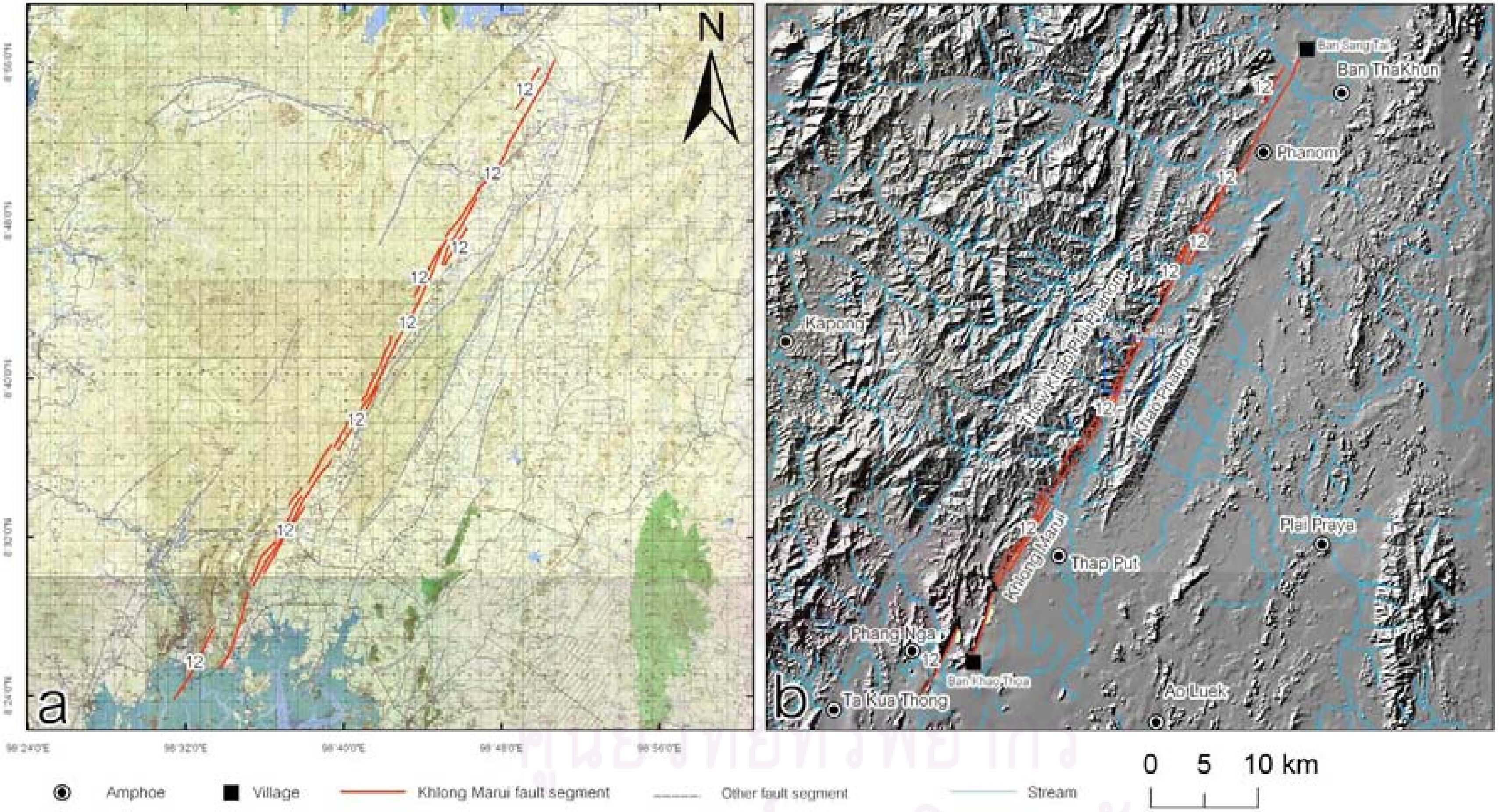

Figure 4.24 Topographic (a) and 20-m contour interval DEM (b) maps showing Khlong Marui fault segment (no.12).

119

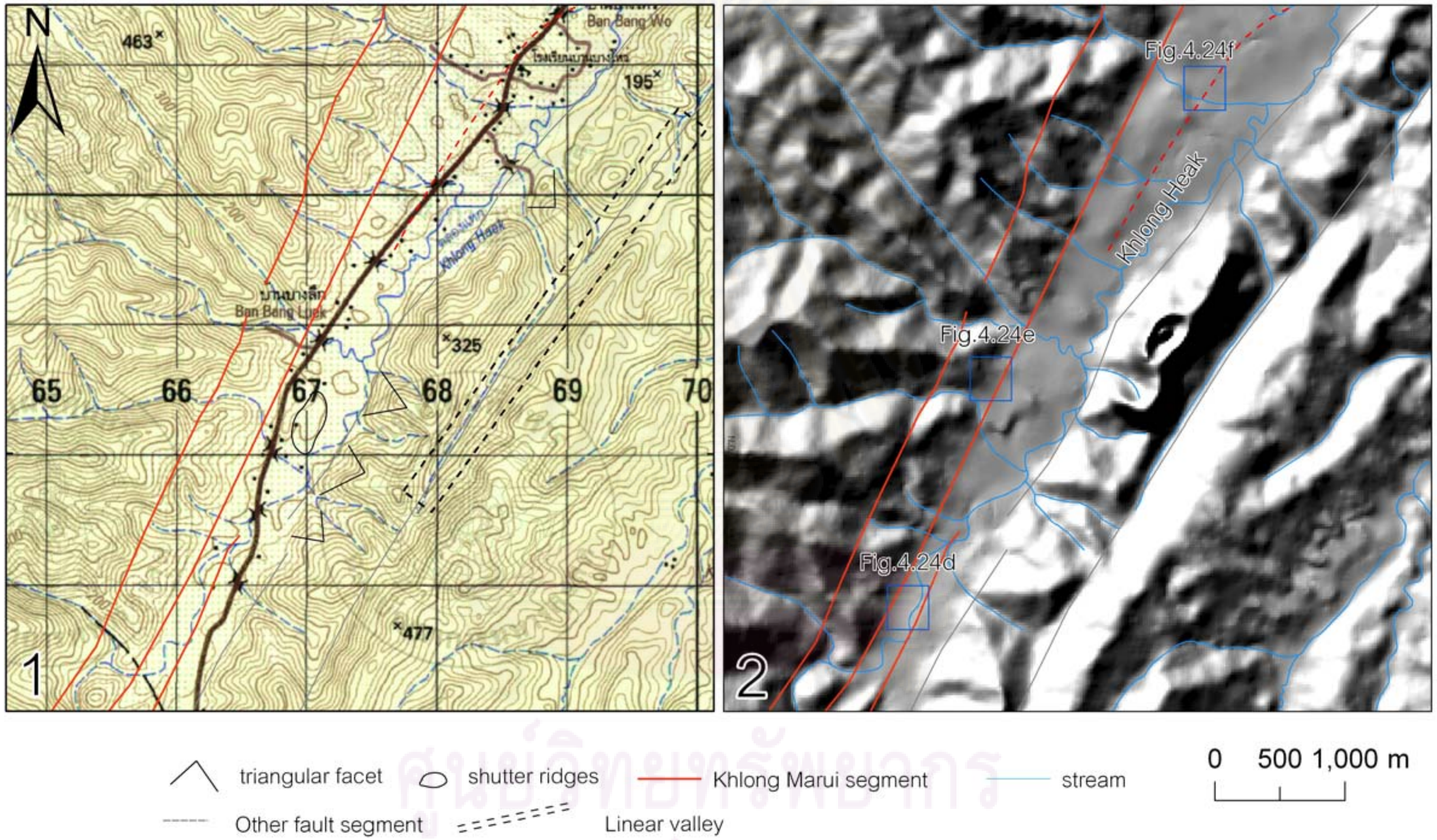

Figure 4.24 (cont.)c Active fault evidences enlarged from topographic map (1) and 20-m contour interval DEM (2) of Figure 4.24b (Khlong Marui fault segment) showing triangular facets, shutter ridges and linear valley.

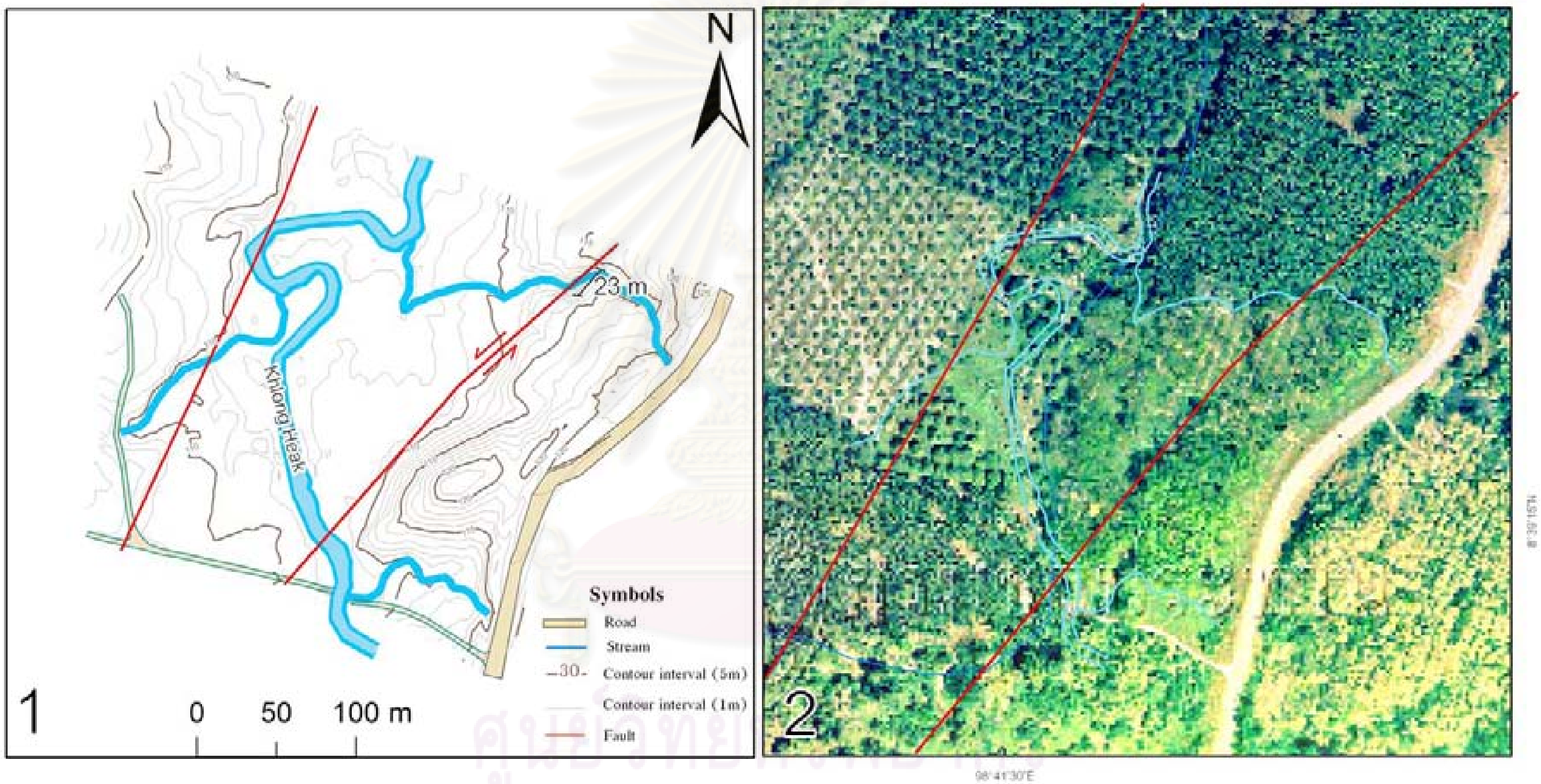

Figure 4.24(cont.)d Enlarged from Figure 4.24c(2) showing offset stream from detailed geodetic survey (1) and color-orthographic image in same area (2).

121

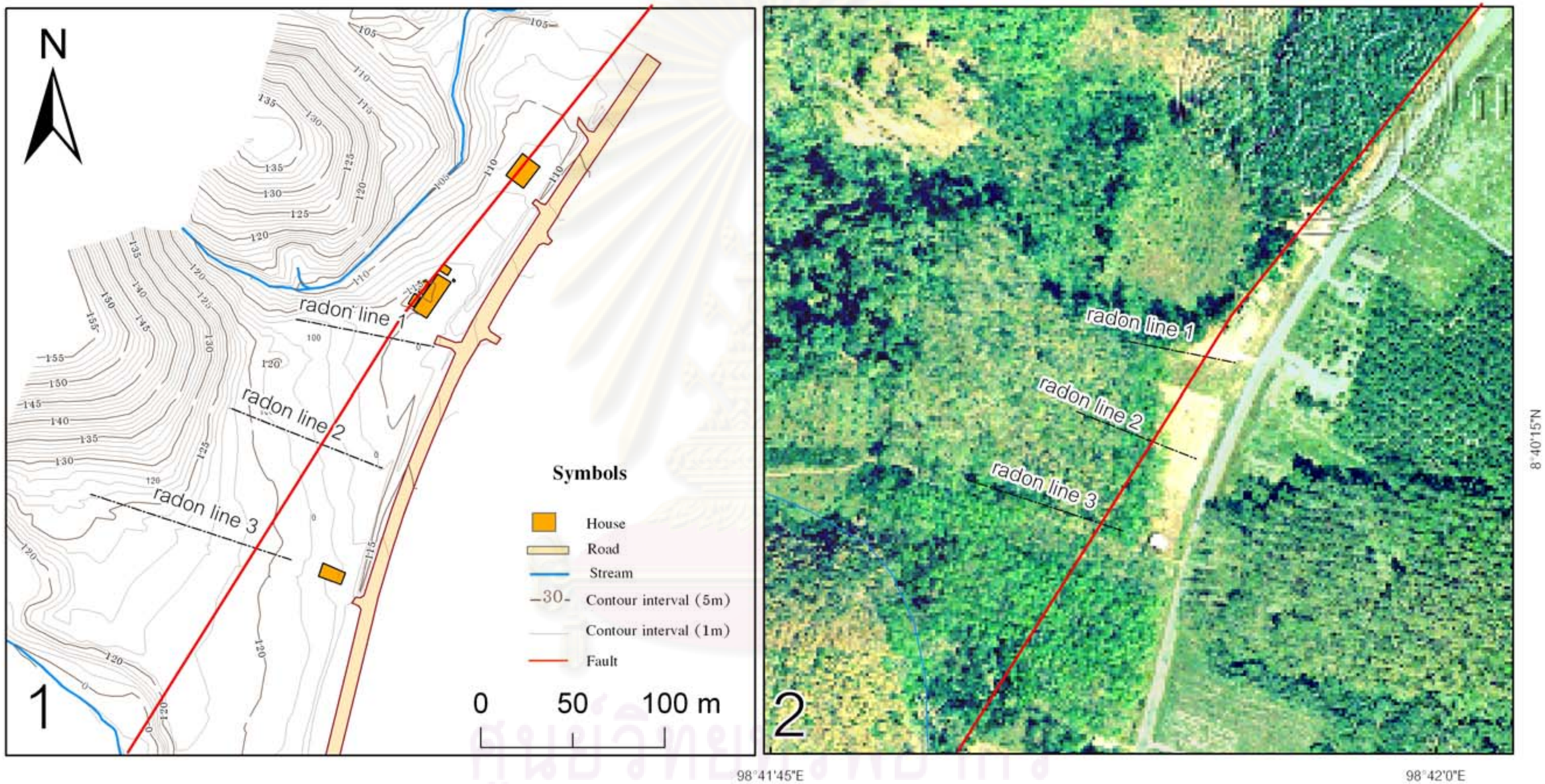

Figure 4.24(cont.)e Enlarged from Figure 4.24c(2) showing offset stream from detailed geodetic survey (1) and color-orthographic image in same area (2).

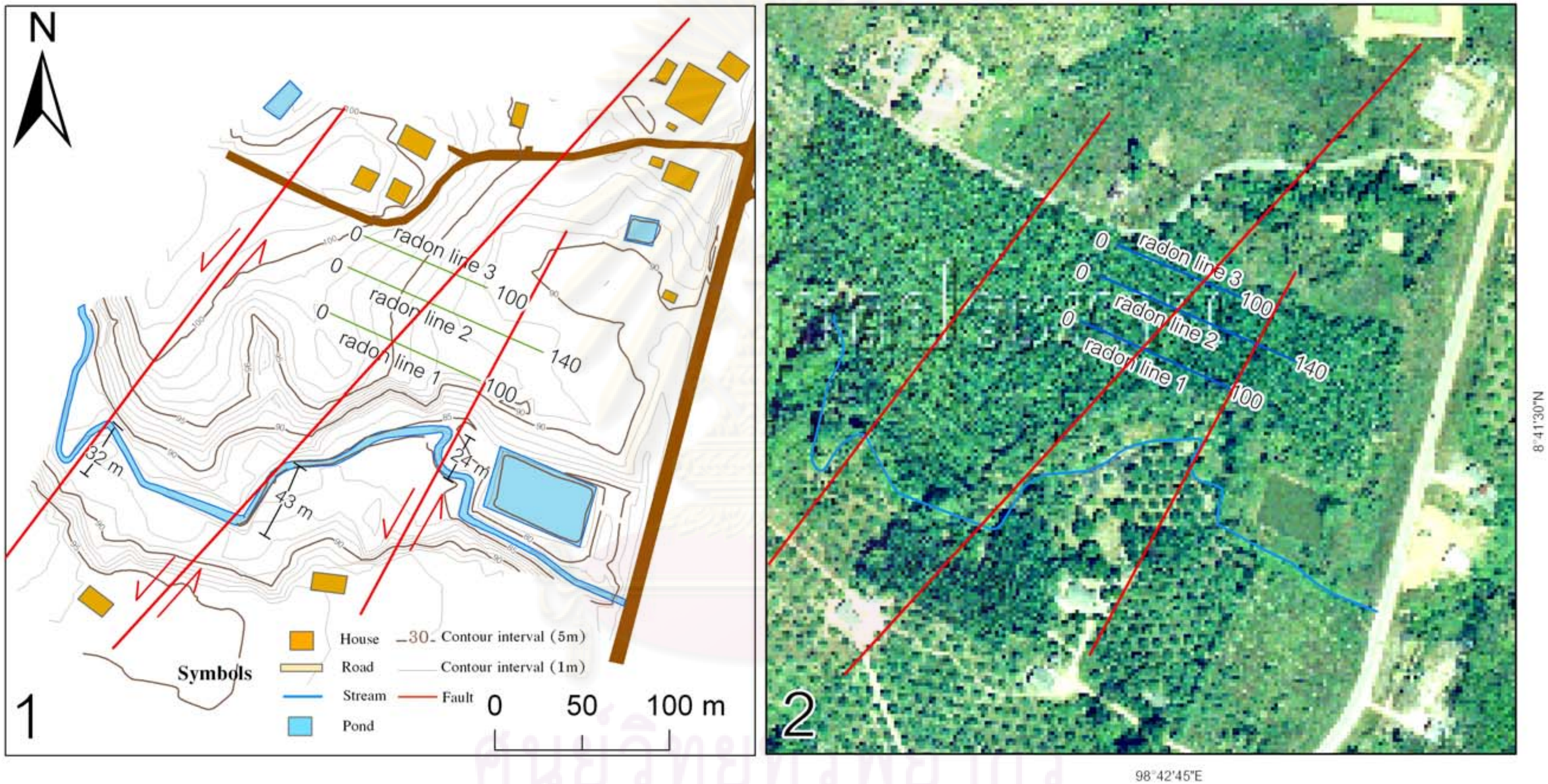

Figure 4.24(cont.)f Enlarged from Figure 4.24c(2) showing offset stream from detailed geodetic survey (1) and color-orthographic image in same area (2).

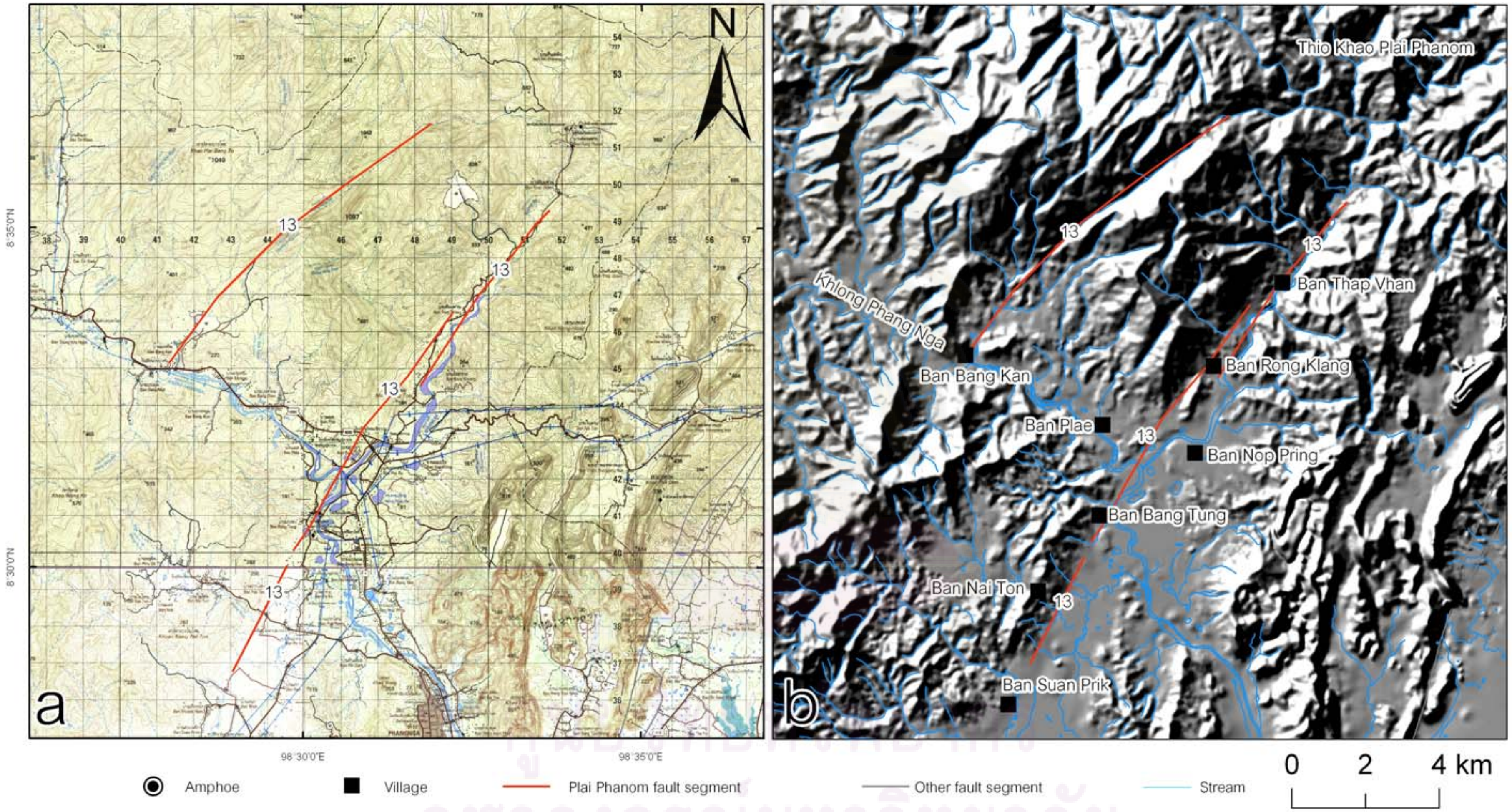

Figure 4.25 Topographic (a) and 20-m contour interval DEM (b) maps showing Plai Phanom fault segment (no.13).

124

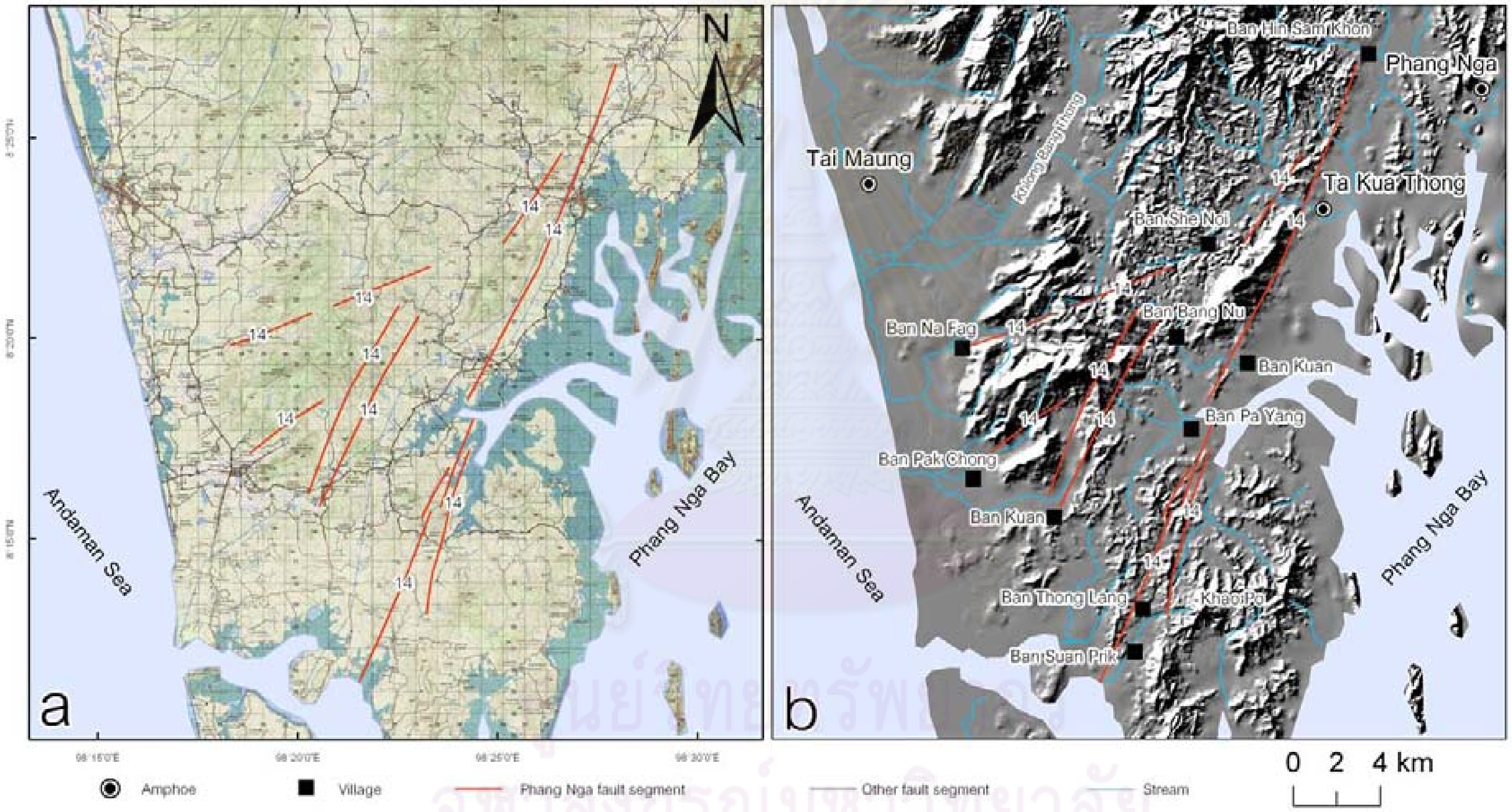

Figure 4.26 Topographic (a) and 20-m contour interval DEM (b) maps showing Phnag Nga fault segment (no.14).

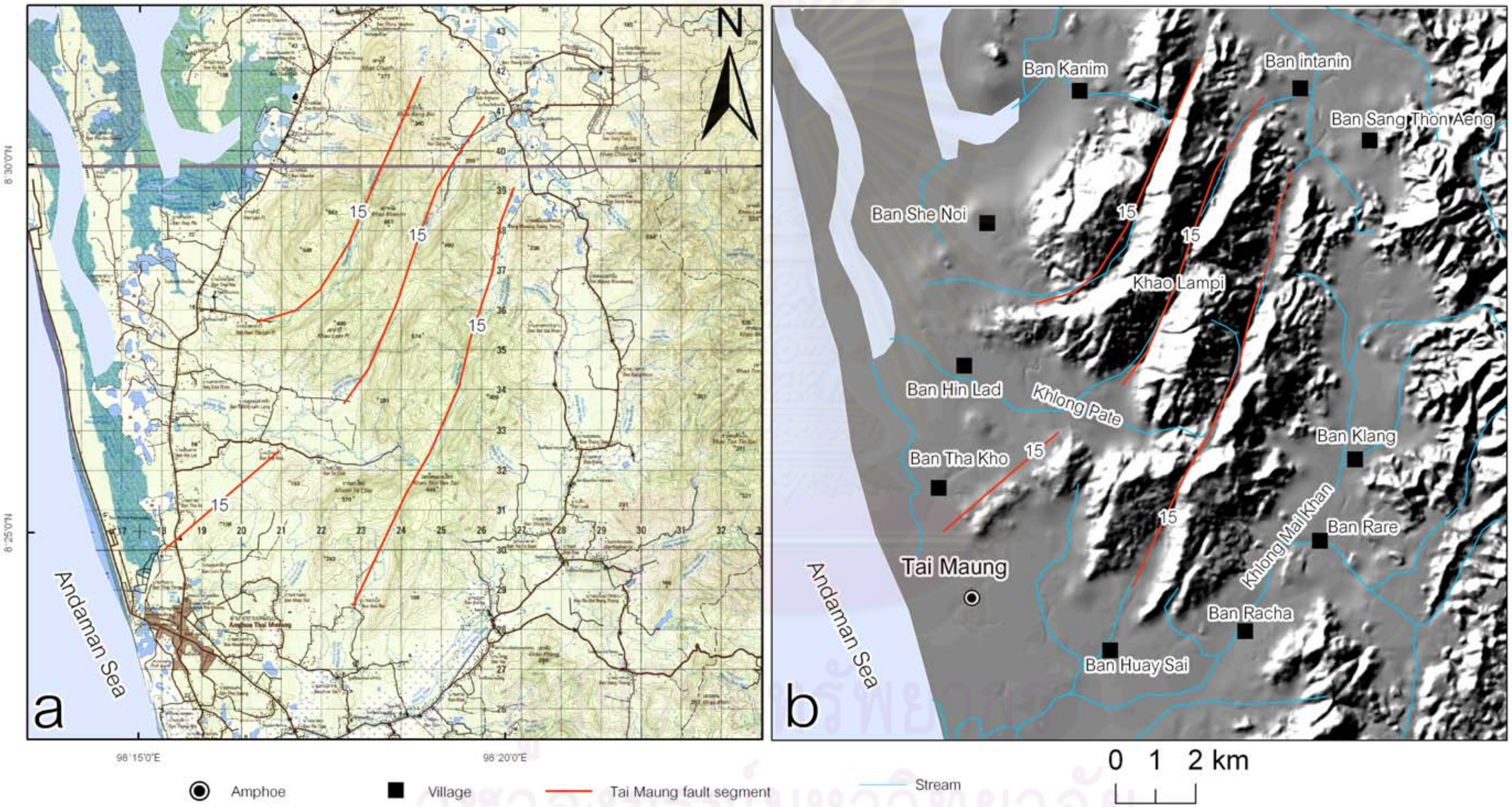

Figure 4.27 Topographic (a) and 20-m contour interval DEM (b) maps showing Tai Maung fault segment (no.15).

126

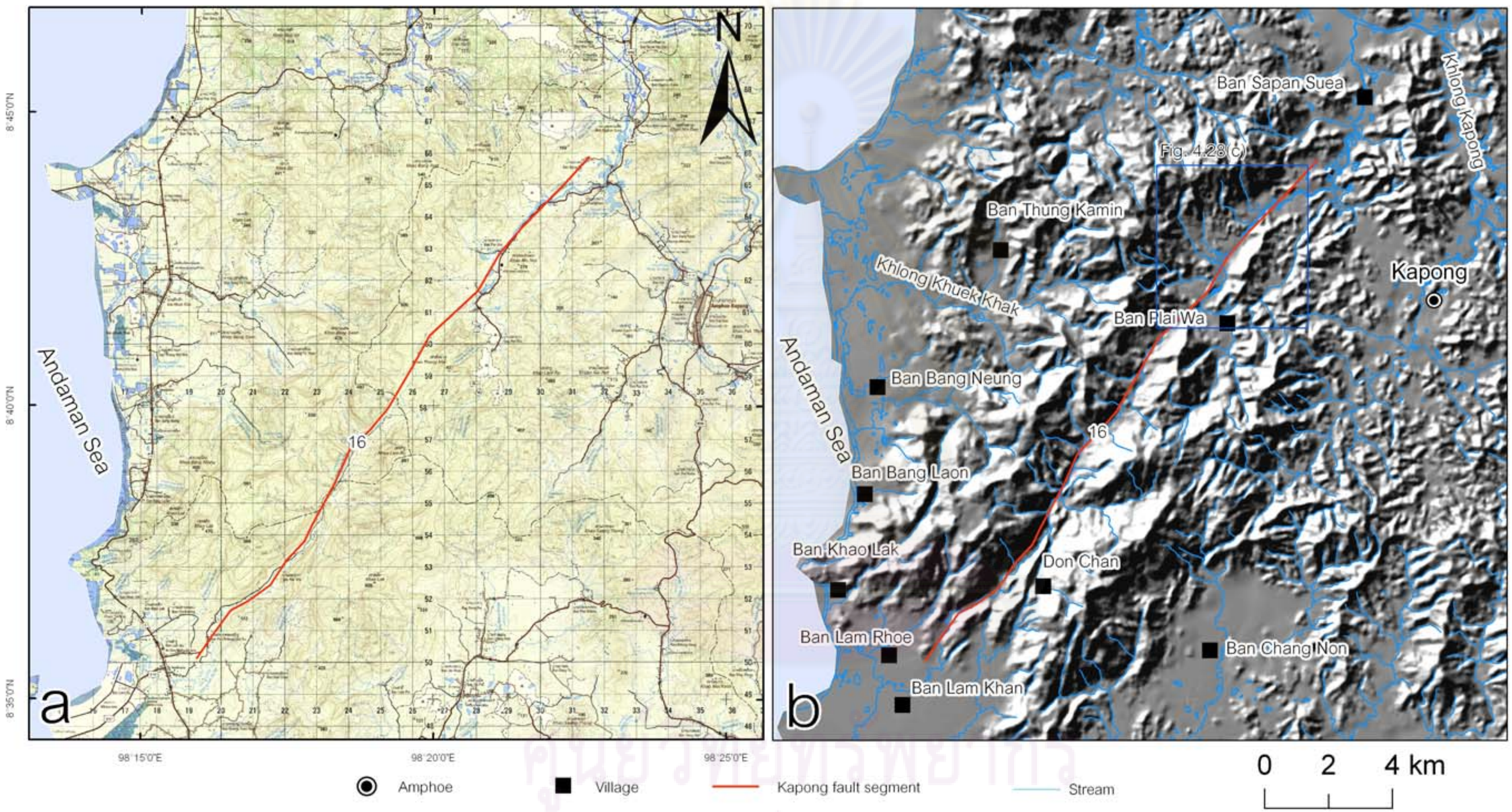

Figure 4.28 Topographic (a) and 20-m contour interval DEM (b) maps showing Pakong fault segment (no.16).

127

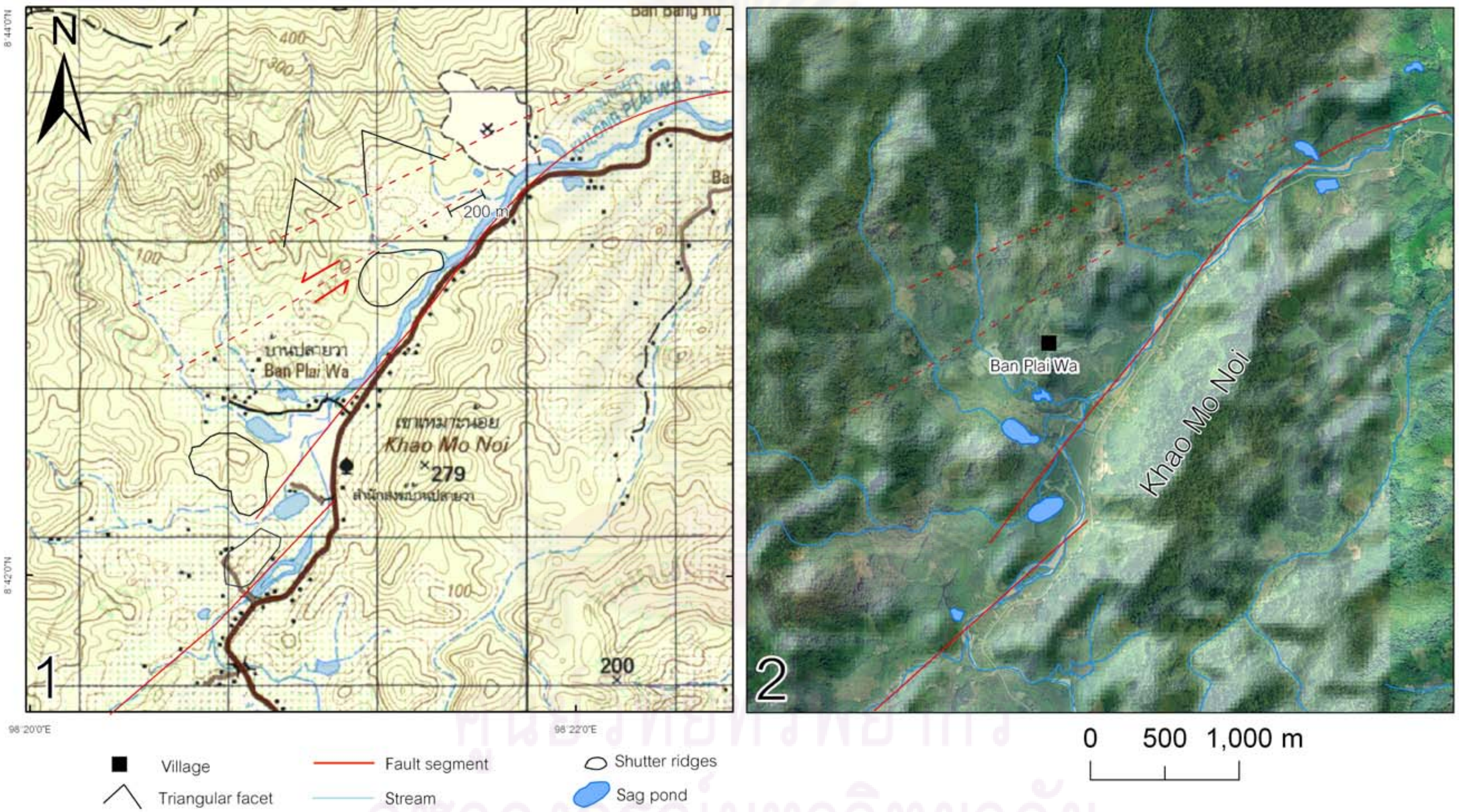

Figure 4.28 (cont.)c Active fault evidences enlarged from topographic map (1) and color-orthographic image (2) of Figure 4.28b (Pakong fault segment) showing shutter ridges, triangular facet, sag ponds and an offset stream with the left displacement of about 200m.

128

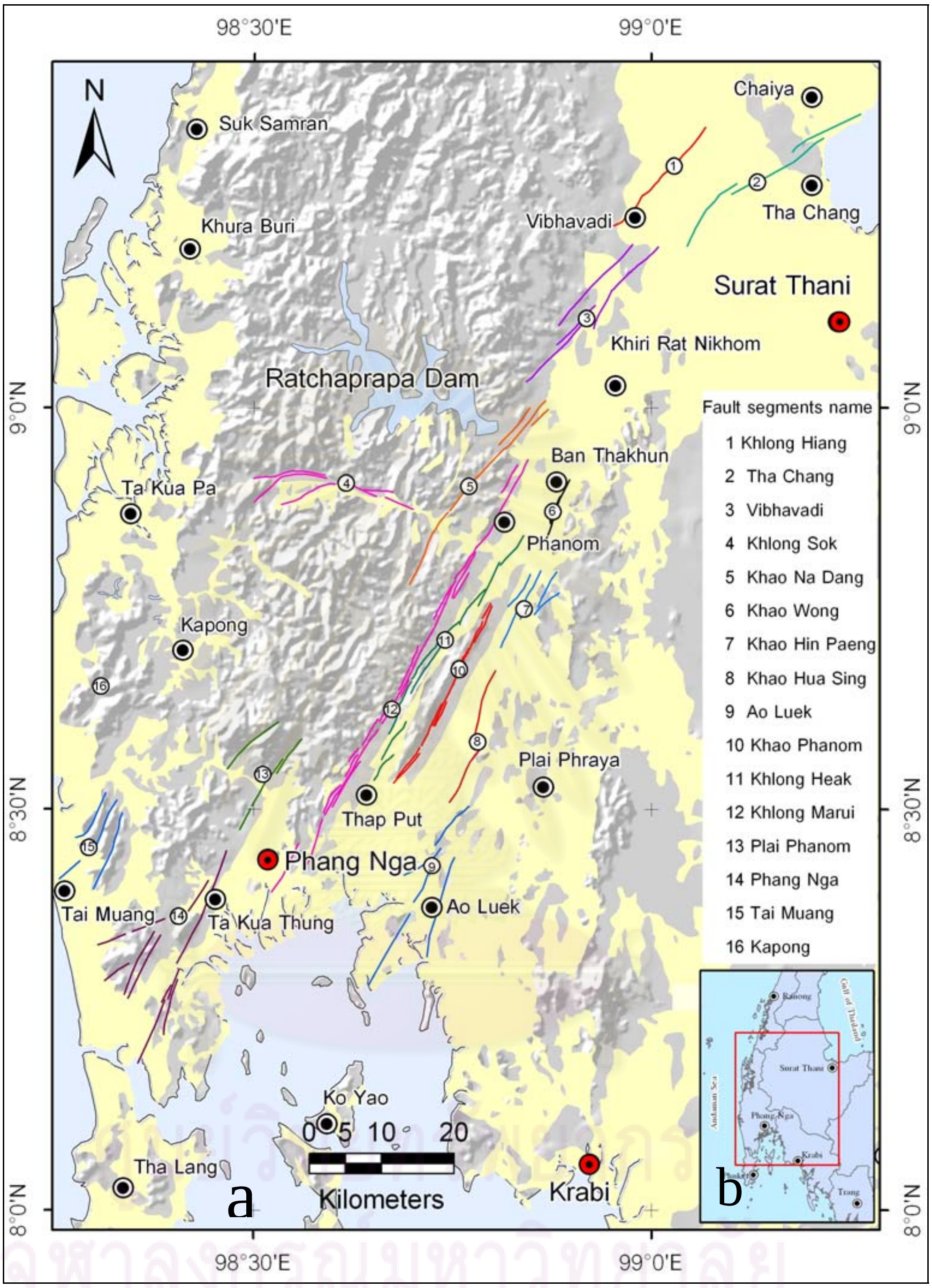

Figure 4.29 Sixteen active-faults segments (a) base on result on Remote sensing interpretation and geomorphic indices evaluation of the study area in southern peninsular Thailand (b). The inferred fault segments and epicenters of the study area is shown in (c). Noted that dashed lines are fault segments which are less important but still obvious.

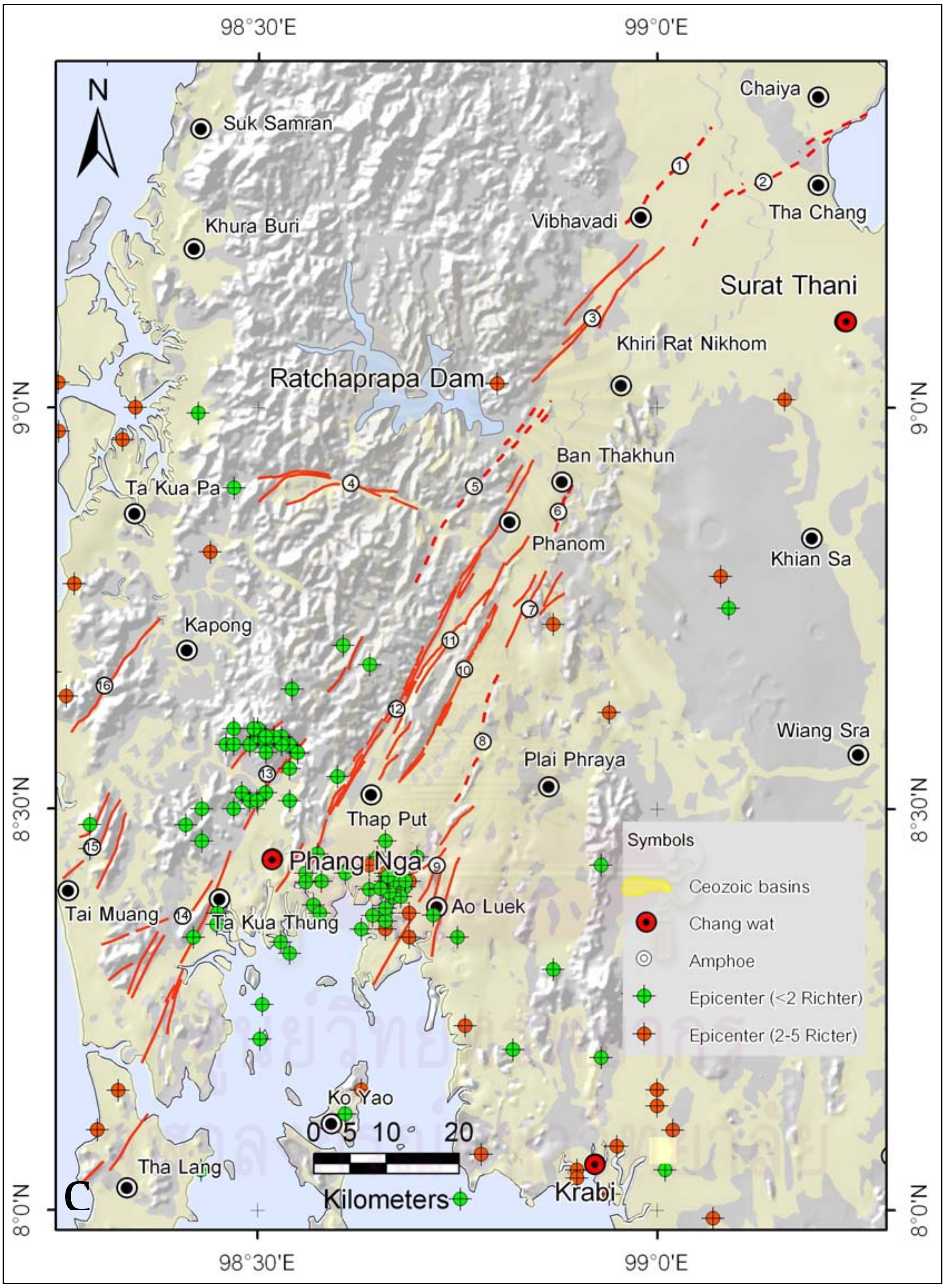

Figure 4.29(cont.)c DEM map showing epicentral distribution with small magnitude in study area (Data from Thai Meteorological Department, 2007).

Chapter V

Field Investigations

This chapter covers description mainly from the results ratated to field investigations. Firstly, it involves the reviews of privious investigations of landform evidence perhaps relatied to active tectonics, such as sinkhole and hot spring locations in this study and nearby areas. Besides, geophysic and Radon survey were also use for locating fault segments. Secondary, emphasizes were placed on field evidences as express by morphotectonic features of landsforms observed in the field along such relevant fault segments. In fact, tectonic evidence were very rarely discovered in field because dense vegetation and serve weathering process, so the 3D color othorgraphic were also helpful in this case. Lastly, the detailed field survey in the particular areas, including the detailed field observation by paleoseismic trenching traversed across the specific fault segments around Khao phanom, are were performed.

5.1 Previous Investigations

There are some field surveys along the study area, which can be the results of tectonical evidence followings are the few descriptions of field surveys.

5.1.1 Sinkholes

Sinkholes may capture surface drainages for running or standing water, but may also form in currently high and dry locations. The mechanisms of formation involve natural process of erosion or gradual removal of slightly soluble bedrocks, where the rocks beneath the land surface are limestones, carbonate rocks, salt beds, or rocks through which that can naturally be dissolved by ground water circulating. As the rock dissolves, spaces and caverns develop underground. Development of Sinkholes is dramatic because the land usually stays intact for a while until the underground spaces become too enlarged. If there is not enough support for the land above the spaces, then a sudden collapse of the land surface can occur. These collapses can be small, or they can be huge and can occur where a house or road is on surface.

Sinkholes can also form in response to a change in natural water-drainage patterns, and new water-diversion systems are developed. Some sinkholes may have formed when the land surface becomes changed, such as when industrial and man – made runoff-storage ponds are created. The water below ground is actually helping to keep the surface soil in place. Additionally, groundwater pumping for urban water supply and irrigation can produce new sinkholes, particularly in sinkhole-prone areas. If pumping results in a lowering of ground-water levels, then underground structural failure and thus, sinkholes can occure. In this study, new sinkholes in southern Thailandcan be a response due to continous seismicities and earthquakes, especially from the great Sumatra earthquake on December 26, 2004.

Department of Mineral Resources (2005) conducted the field survey and 45 sinkholes were encountered. The hole areas were entirely located in limestone mountains. After the Sumatra mega-earthquake on December 26, 2004, new sinkholes were developed in 19 areas covering 4 provinces, including Satun , Pang-nga , Krabi , and Trang. There are about 8 sinkholes which have been discovered in the study area as shown in Figure 5.1. They range in diameter from 2 m up to 30 m. Near the Phang Nga, a sinkhole (S1) is located at Khlong Marui fault segment. S2 sinkhole is found nearby the Ao Luek segment whereas S3 and S4 sinkholes which almost align in the northeast direction. S5 and S6, S7 sinkholes are located in Amphoe Plai Praya and Amphoe Pra Sang, respectively. They are in the vicinity of Kao Hua Sing Fault. S8 are situated at Amphoe Weing Sa, far from Khao Hua Sing fault. S9 and S10 sinkhole are located far east near Amphoe Khao Phanom.

5.1.2 Natural Hot Spring

The history of the hot springs distribution in Thailand was first recorded by Brown and Buravas (1978). However, not many studies have been performed so far on thenature of hot springs in Thailand, and mostly they are only preliminary work or unpublished reports by Department of Mineral Resources and Electricity Generating Authority of Thailand.

Generally three important factors control the generation of hot springs, including heat sources, ground water and reservoir rocks. The main heat source is from active magmatic activity within the crust that emplace to shallower levels from unstable areas, such as active volcanic belts, fault zones, and subduction zones, or from areas dominated by high contents of radioactive elements, such as uranium (U), thorium (Th), and potassium (K). Groundwater is the main source of water supply. The water is principally derived from rain and cool water on the surface that percolates to the subsurface along bedding planes voids, fractures, joints, or faults of rocks. Some portions may be derived from steam of magmas in a cooling stage (magmatic or juvenile water) and water-bearing pore spaces of sediments (connate water). Good properties of reservoir rocks are high porosity and good permeability produced from both primary and secondary fractured or faulted rocks. When cool water from the surface percolates to reservoir rocks and receives heat transfer from the heat sources, the water will be heated and flow up along fractures or faults of rocks to the surface and become a hot spring. There are two well-known hot spring sites are in Ranong province in southern Thailand (Figure 5.2). However, a few hot spring location in Surat Thani Krabi and Phanga were founded.

As shown in Figure 5.2, 6 hot springs are recognized in the study area, and several of them are located at the fault termination. The H1 hotspring is discovered at the southern end of the Phang Nga fault segment. The H2 and H3 hotsprings are situated at the northern end of the Pakong fault. The H4 hotspring is located nearby northern end of the Khao Wong fault segment. The hotsprings (H5 and H6) are found at the northern end of the Tha Chang fault segment. So it is quite likely that hot springs can, to some extent, help to locate the fault acitivity.

5.1.3 Radon gas survey

Radon gas was applied to surveying in a area of geothermal power resource, monitoring the explosion of a volcano, predicting earthquake events, seeking for sinkholes, and identifying active fault traces survey. Data of radon gas survey can indicate uncontinuity of tectonic or stability of geological structures because the area, dominated by active faults can show high concentrations of radon gas thanthe areas without active faults. Sometimes the anomalous values are higher than the background values for more than 20.

The radon investigation at Ban Bank Luek area (Amphoe Phanom, Changwat Surat Thani) consists of 3 line surveys in the northwest – southeast direction. Values of radon gas becomes higher than background vaule of the line survey 1 at approximately distance of 7 and 22 meters, It is so high at line survey 2 at distance 40 and 80 meters, and the last line survey at distance position 3 and 10 meters (Figure 5.3). The result show that the Ban Bang Luek area of the Khlong Marui subsegment is also active based on the high radon contents.

5.1.4 Geophysical survey in study area

5.1.4.1 Electrical resistivity method

Based on the result of electrical resistivity of Ban Bang Luek area (Department of Mineral Resources, 2007), Surat Thani, the outputs were show as the apparent resistivity format.

As shown in Figure 5.5, the result shows that no bedrock has been found beneath surface (the depth from the apparent resistivity). Sediment deposit was on foothills comprising coarse sand, gravel and pebble gravel, that consists of several values of electricity resistance (about 10 to more than 1,100 meter-ohm). From the interested line survey, it is likely that the faults or fractures are located at 26-28 meter distance position of the 1 line survey and at 50-52 meters distance position of the line survey no.3 (Figure 5.4).

5.1.4.2 Ground Penatrate Radar method

Ground Penetrate Radar (GPR), the alternate method that can be used to search for a trace fault or continuity of sediments and a stone in shallow level. The GPR survey was liberated radar frequency waves between 100-200 MHz, then measure radar waves that reflected back sediments and stones to the receiver. Data was from "Active Fault Investigation Project: Khlong Lumrhoeyai Dam, Tai Maung, Phang-Nga" (Royal Irrigation Department, 2009).

In the Ban Thung Sri Ngam area, Thap Put, Phang-Nga, the results indicated that the sediment layers have the average thickness of 1 m. Discontinuous layers suggesting bends or fold structures are located at about 0.3 – 0.5 meter depth. Besides, there exist the uncontinuity of sediment layers, which are in the 2 – 4 meters depth (Figure 5.5).

5.2 Tectonic Geomorphology

In order to clarify and visualize the evidence of morphotectonic features as deduced from the results of remote-sensing interpretation, morphotectonic investigations were conducted. The followings are the descriptions of these evidences. Results of the remote-sensing interpretation and geomorphic indices can show the interesting areas at Khao Phanom.

1) General Geology

The Khao Phanom is located between 3 provinces, i.e., Surat Thani, Krabi and Phang Nga. Generally, this hill lies in the northeast-southwest direction. Khao Phanom appeares in 1:50,000 scale of topography map series L 7018 sheet 4726 III (Amphoe Thap Put) with the northeast-southwest trendily fault segments area can be also be accessed by asphalt road number 4118 (Thap Put-Phanom) in the western side of Khao Phanom and number 415 (Phang-Nga – Thap Put) in the eastern side. Both eastern and western sides are characterize by narrow basins along the mountain. The Khlong Hak and The Khlong Marui channels are main channels, and flows northward but the branches flow in the east-west direction. The plain between the valley was supported by foothills sediment, the majority is the pebble gravel size until sand size, angular shapein poor sorted. The rocks in mountain zones are composed largely of sandstone, siltstone, claystone and quartzite, whereas some area were founded granites intrusive in limited narrow.

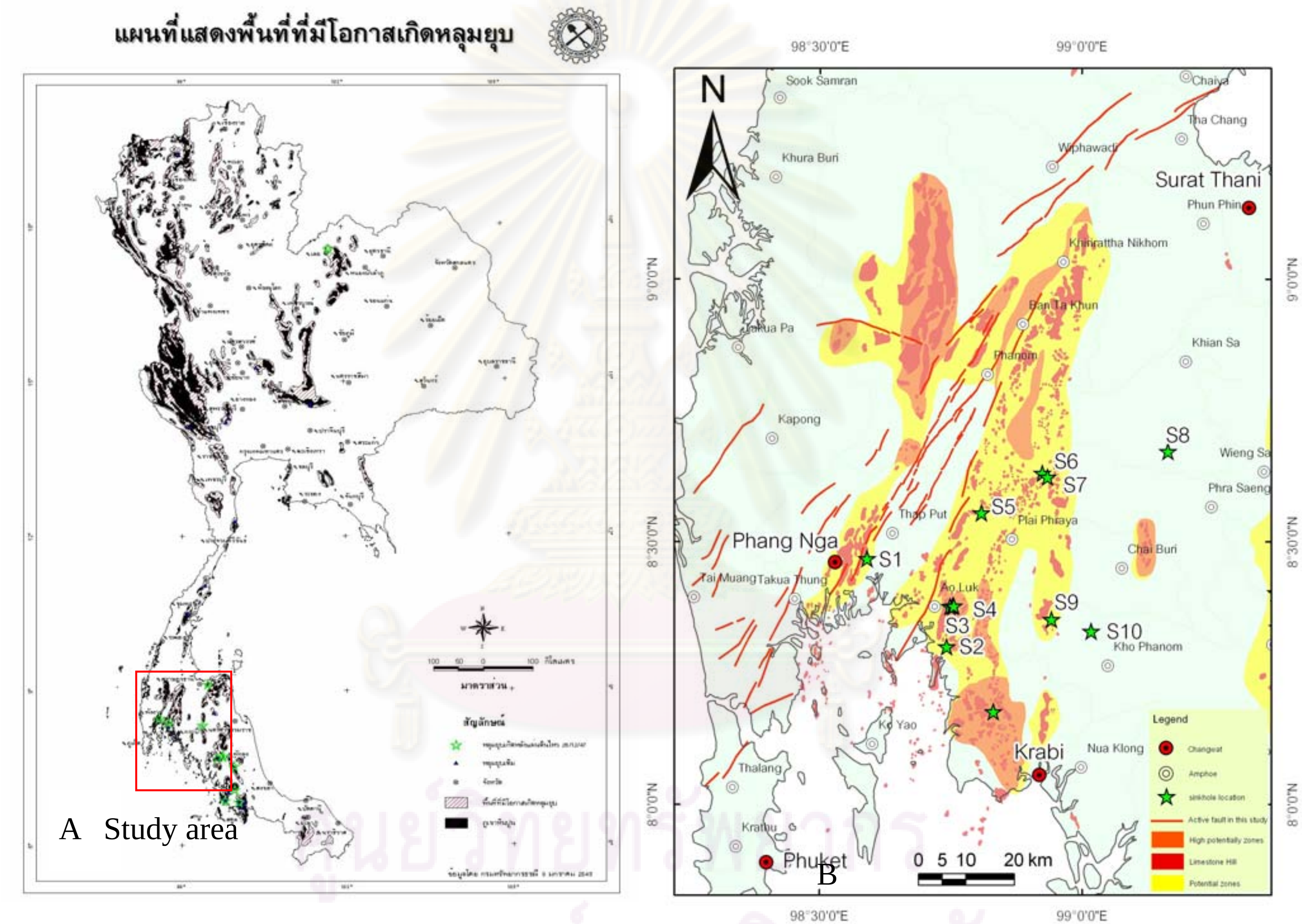

Figure 5.1 Sinkhole map of Thailand showing (A) carbonate rocks (black) and sinkhole locations and (B) relationship between sinkholes and active faults in the study area., (modified after Department of Mineral Resources, 2005).

136

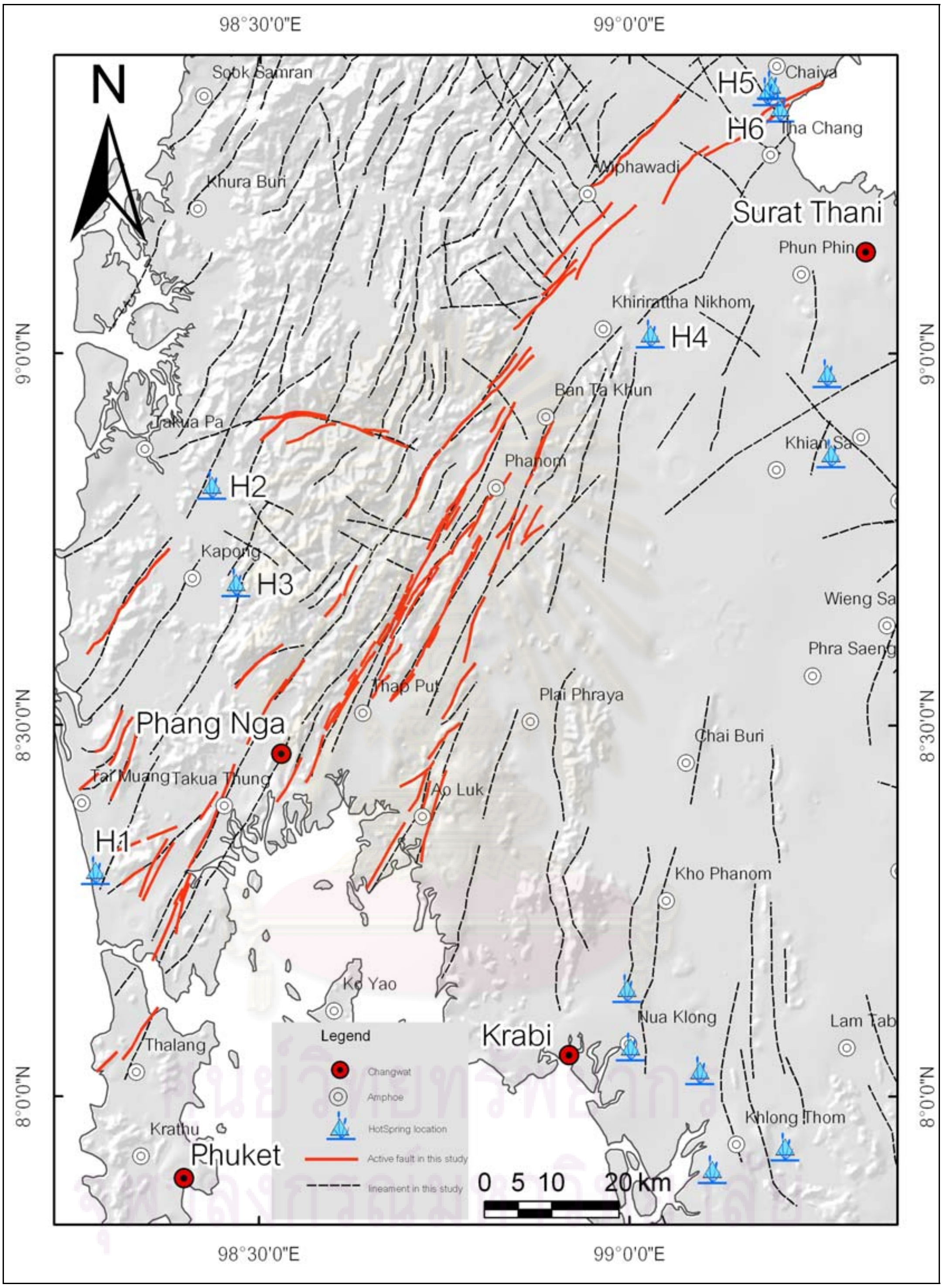

Figure 5.2 Map of southern Thailand showing relationship between hotspring locations and active fault traces (data from Department of Mineral Resources, 2004).

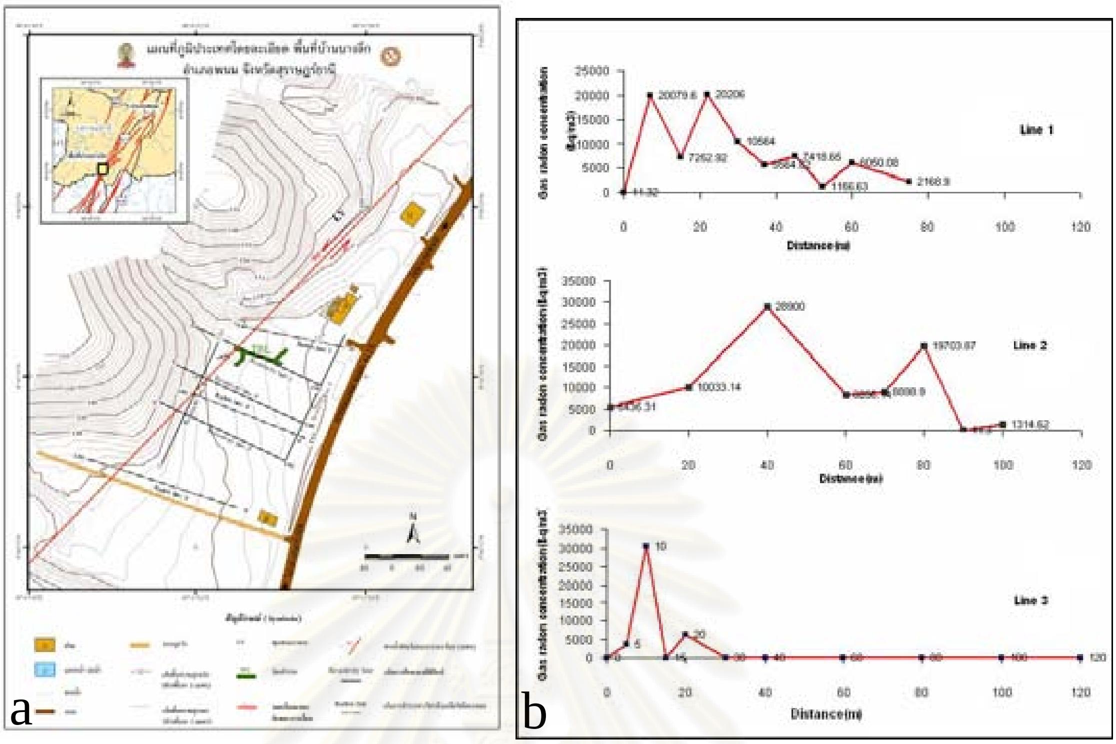

Figure 5.3 Previous radon survey in Ban Bang Luek, Surat Thani (a) detailed topographic map of Ban Bang Luek trench showing location of radon survey lines, (Department of Mineral Resources, 2006) and (b) graph of gas radon concentration and distance in radon survey lines, (Artyotha, 2007).

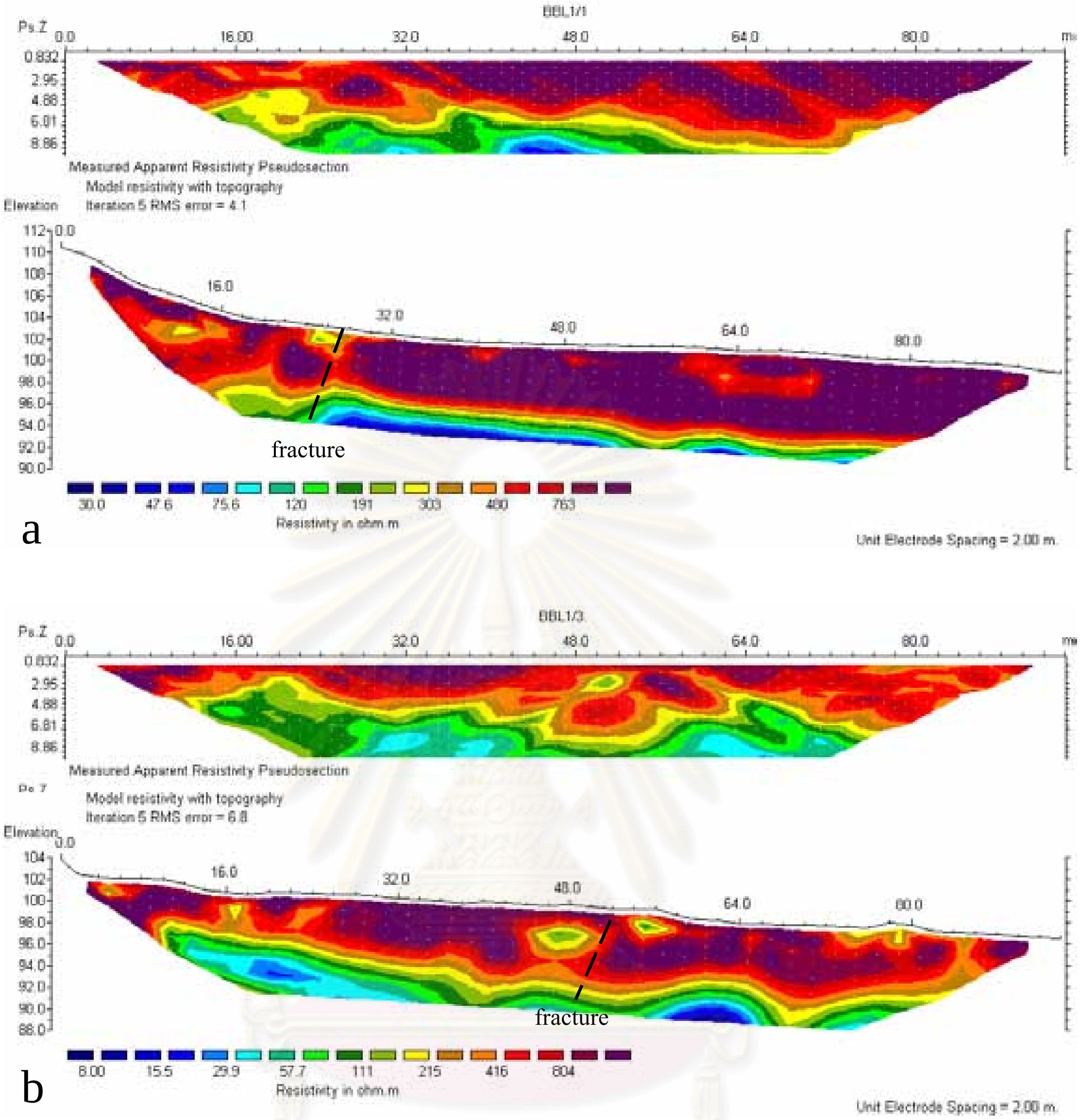

Figure 5.4 Result of Resistivity survey in Ban Bang Luek (line survey was showed in fig5.3a) (a) interpreted of survey line1 (b) interpreted of survey line 3, (modified after Department of Mineral Resources, 2006).

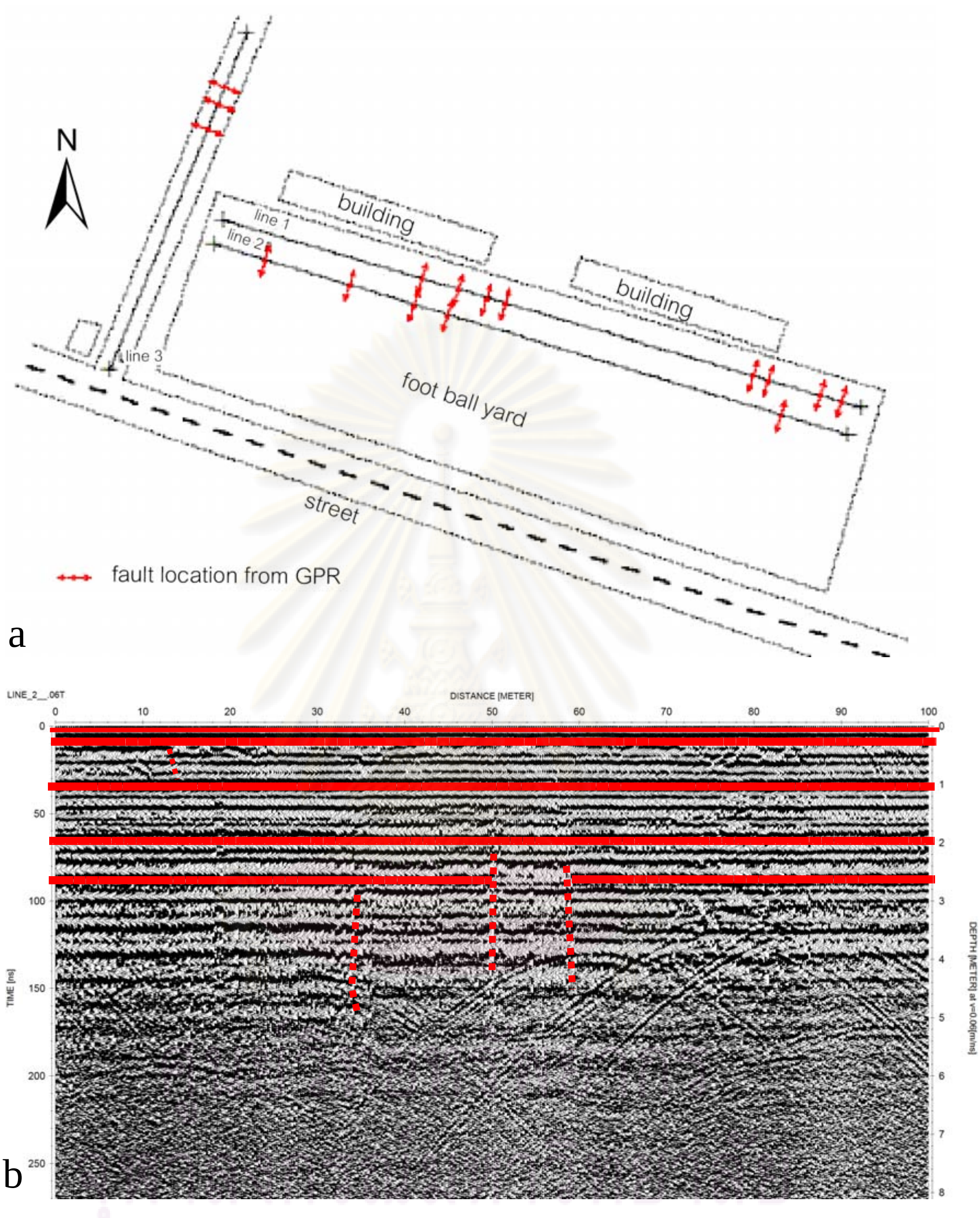

Figure 5.5 Line of Ground Penetrated Radar survey at Ban Thung Sri Ngam school showing (a) 0-100 distance of line 2 and (b) result of GPR interpretation of line 2, (Royal Irrigation Department, 2008).

2) Field investigations

In the field at western side of Khao Panom appears mountain range, namely Khao Plai Phanom, which west dipping triangular facets appear immediately at foothill. The facet set was developed in the northeast trend along the Khao Phanom and Thio Khao Plai Phanom, suggesting a fault running parallel to the mountain front (Figure 5.7). The appearance of triangular facets along the Khlong Marui segment is well developed as series of facet spurs. Perhaps this indicates that the fault shows several movements. Additionally, Khao Phanom are located within 2 fault segments, there are significant morphotectonic evidences including a stream course as linear valley feature parallel to the fault line. A small shutter ridge and a fault scarp are oriented parallel to fault trace in the northeast-southwest direction. Besides, the hill ridges and many streams were offset in same direction, i.e., northwestward. The small offset of stream in same area, such as branch of the Khong Hak stream that flow down from northwest to the southeast change its flow in the northeast then comeback in the southeast again, which, is one of the important evidence supported the left-lateral slip fault movement (Figures 5.8 – 5.12).

According to field investigation result of the Khao Phanom area, several morphotectonic evidences indicate that both sides have a potential to be the active faults and its movement is normal sense together with the left-lateral movement.

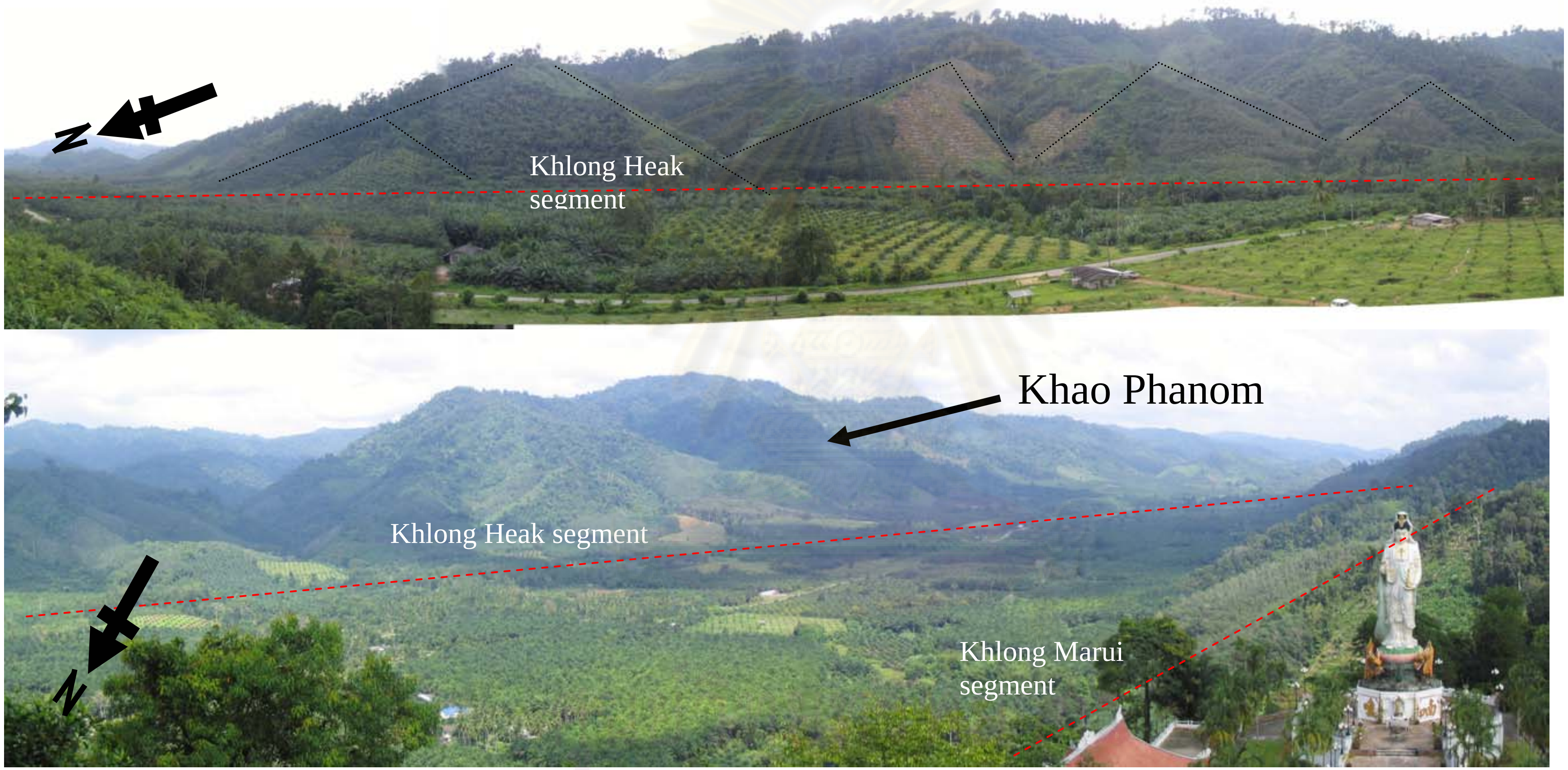

Figure 5.6 Topography view of Khao Phanom where the most sign seeing in remote-sensing visible and its triangular-facet (looking southeast).

142

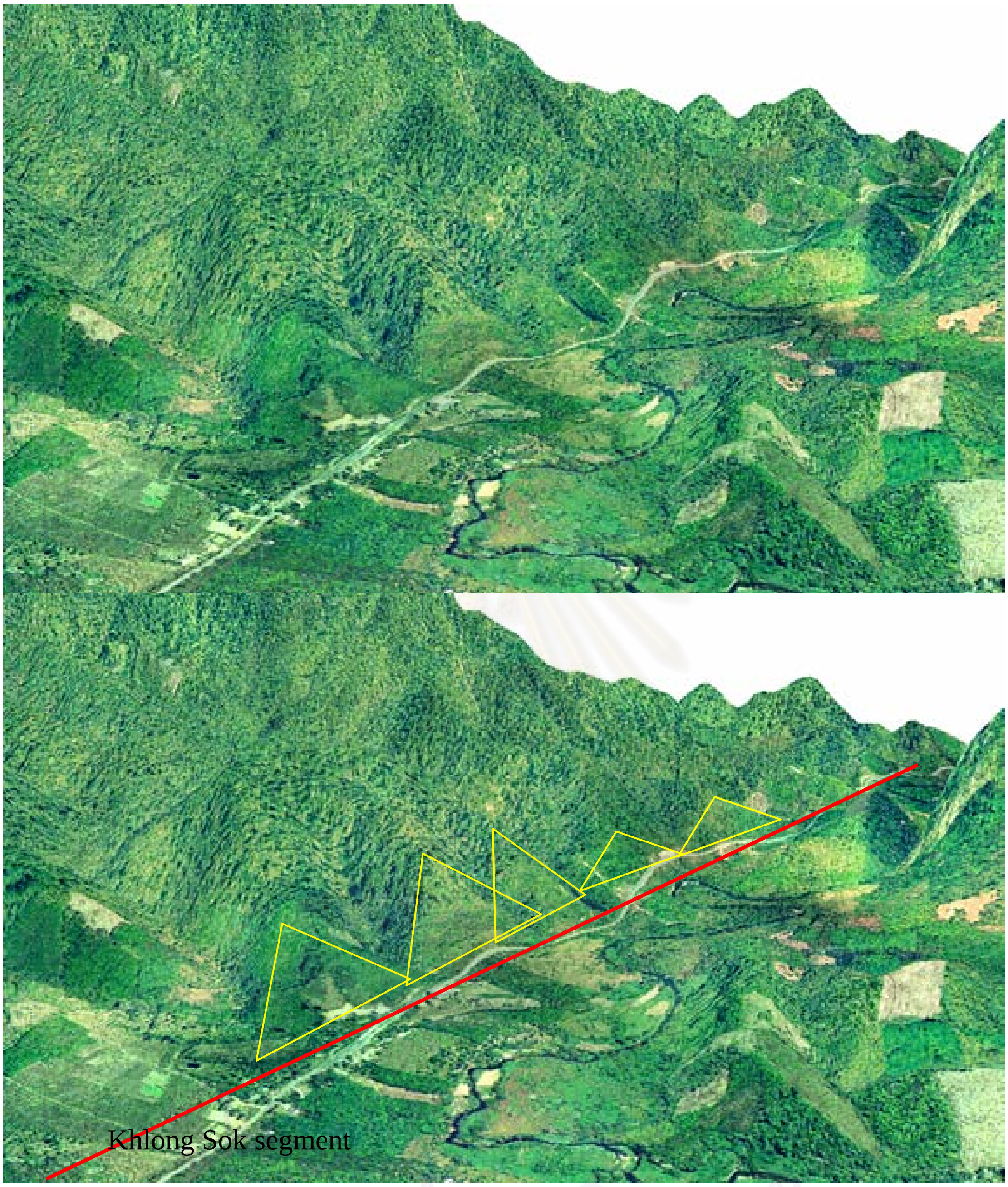

Figure 5.7 Color-orthographic image showing triangular facet at Khlong Sok segment, northwestern study area.

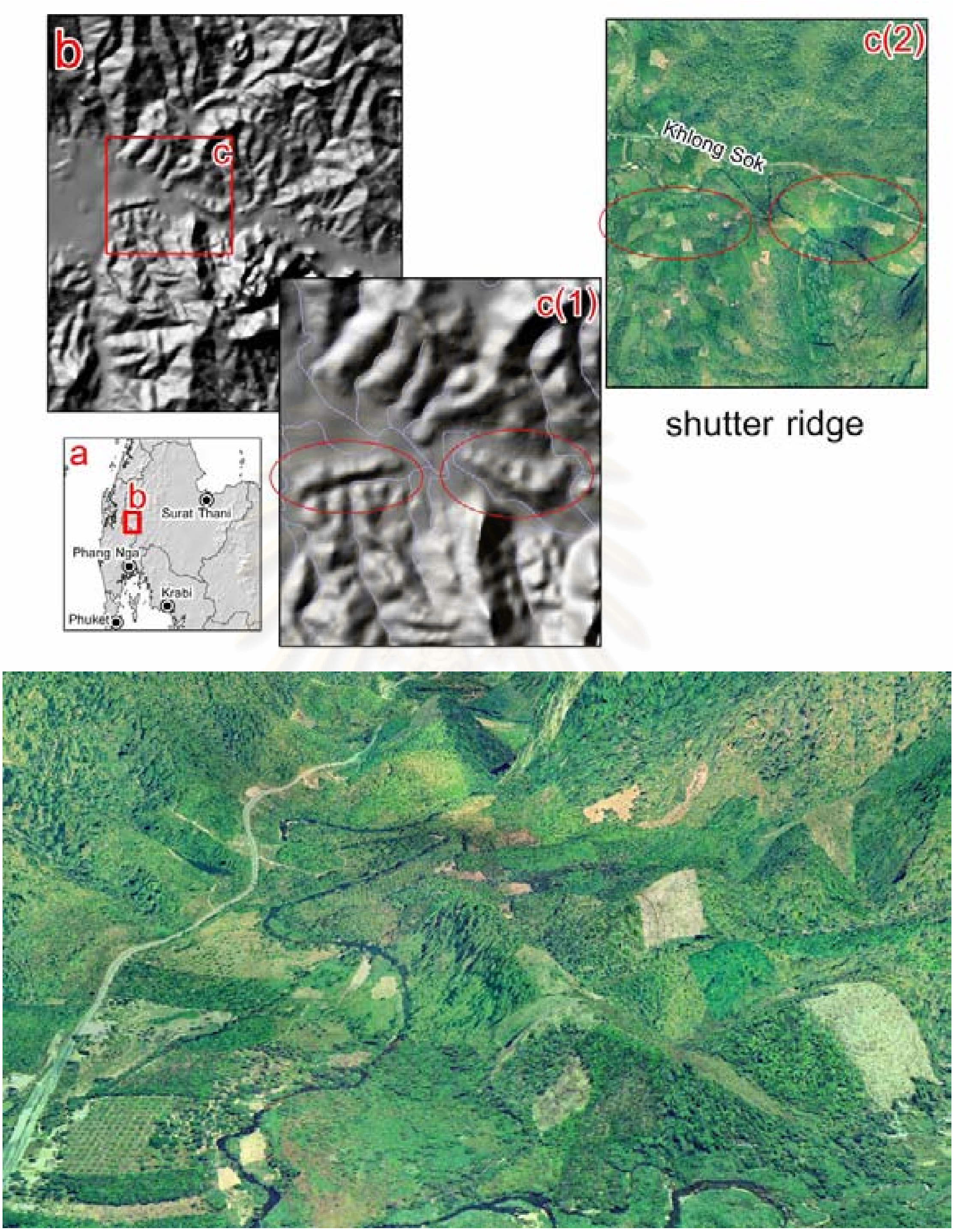

Figure 5.8 Hill shade DEM and color-orthographic maps showing some shutter ridges parallel Khlong Sok segment in west of Surat Thani.

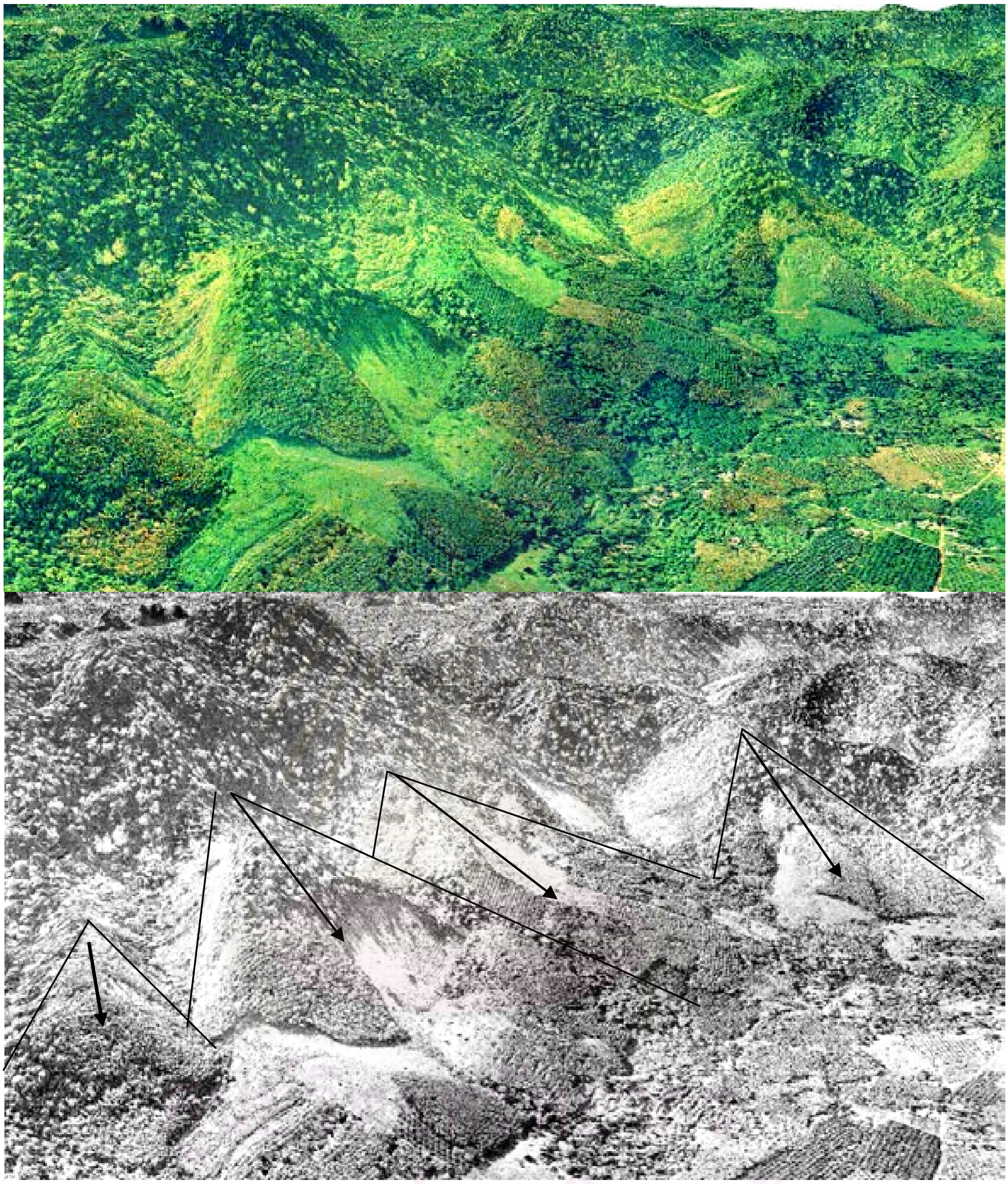

Figure 5.9 Color-orthographic image showing triangular facet and scarp at west of Khao Phanom in middle of study area.

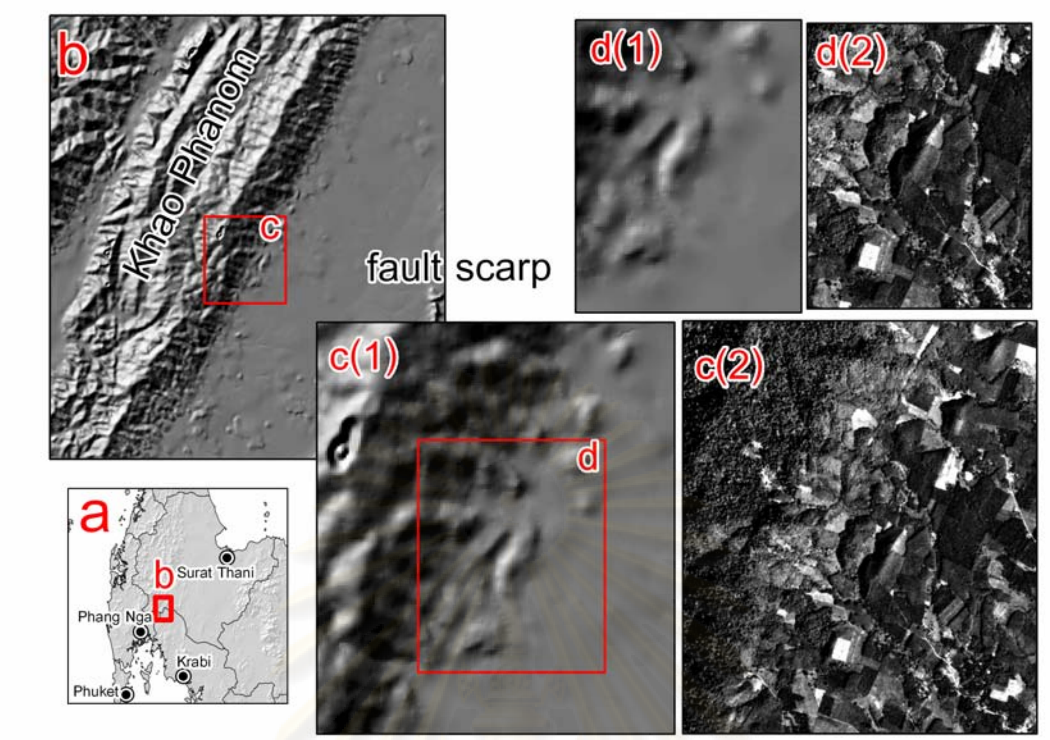

Figure 5.10 Arial photograph and DEM from topographic map showing line of fault scarp parallel west of Khao Phanom along Phanom segment.

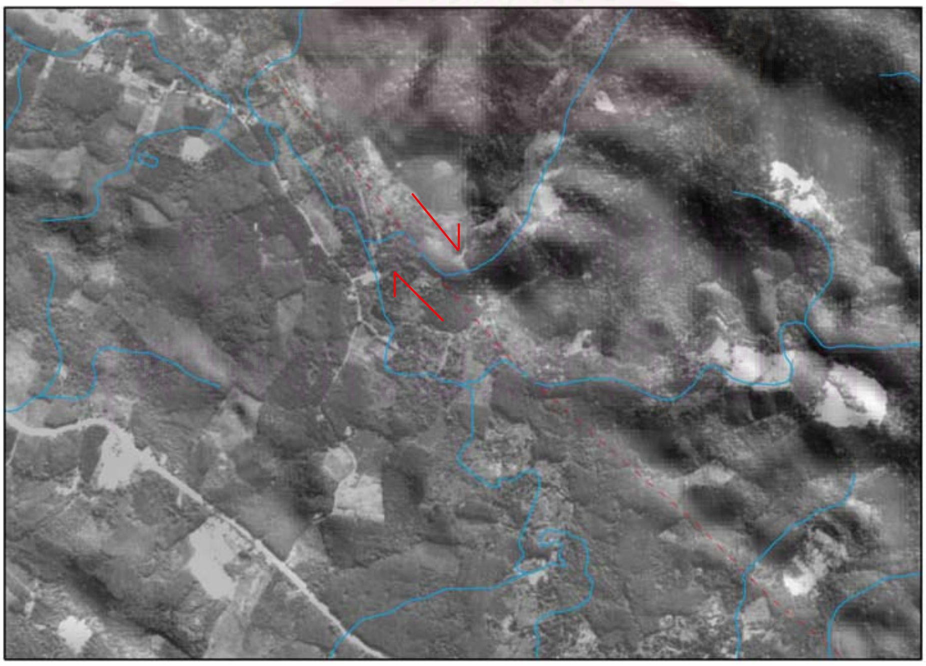

Figure 5.11 Orthographic image showing sinistral movement of offset stream nearby Ban Bang Luek and their offset distance.

Figure 5.12 Color-orthographic image showing linear ridges along the eastern side of Khao Phanom.

5.3 Paleoseismic Trench

In as much as the reliable research is the supporting field evidences relevant to the fault segments concerned, it is necessity to study all the fault segment traces. Site selection of specific areas for detailed field investigation and paleoseismic trenching require some constraints to access the specified criteria. Therefore, selection of a specific area for this paleoseismic trenching covering two areas as mentioned before was conducted by compiling relevant supporting information (Figrue 5.13). The most effective and suitable area was chosen for further detailed study and trench excavation. Nontechnically, the criteria are the accessibility since backhoe must be used for digging trench, and the ownership and authorization of the proposed area must be the second criteria.Two trend sites were selected in this study.

5.3.1 Trench 1: Ban Bang Luek

Ban Bang Luek trench is located north of Amphoe Thup Put along the main road no. 4118. Remote-sensing interpretation shows sharp lineament and geomorphology indicating offset streams, shutter ridges, linear valleys, offset ridges, and triangular facets at grid reference 466796E /958520N on topographic map scale 1:50,000, sheet 4726 III (Amphoe Thap Put). The trench site was excavated at grid reference 466758E/958431N, as shown in Figure 5.13 is situated in the steeper slope near the offset stream and triangular facets. The trench is excavated into the young sediments deposits, traverse perpendicularly across the fault trace. Trench geometry is 2 m in width, 30 m in length, and 3 m in depth.

5.3.1.1 Stratigraphic Description

As shown in Figures 5.14, 5.15, 5.16 and 5.17, it is quite clear that the Ban Bang Luek trench has relatively much more deformed stratigraphy. Trench-log stratigraphy is characterized by 9 unconsolidated sediment units. Detail of individual units is described below.

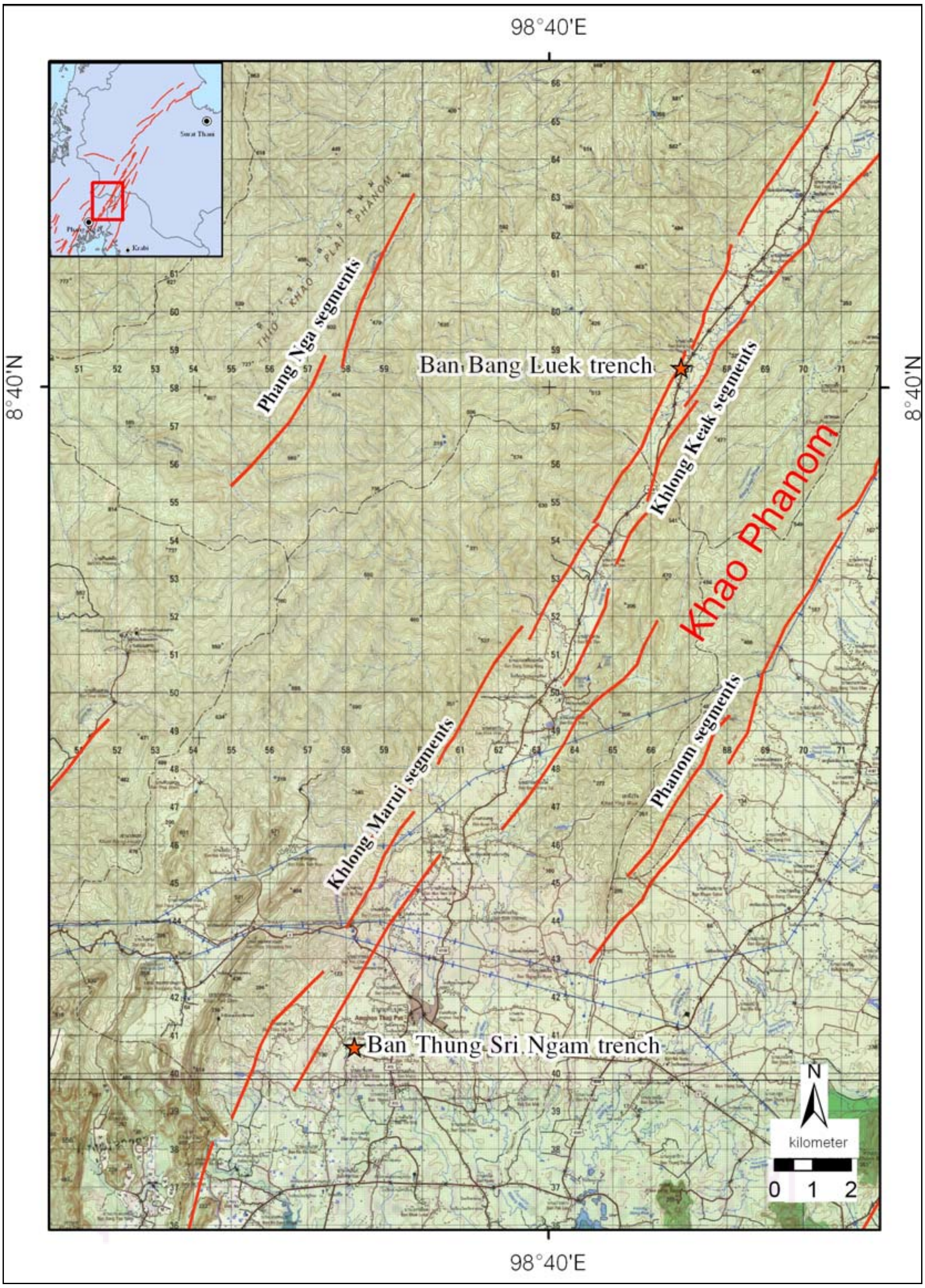

Figure 5.13 Location of paleoseismic trenching in Khlong Marui segment, west of Khoa Phanom.

Unit A is a well-defined, brown to yellowish brown colluvial deposit consisting of clay, sand, fine to coarse-pebble with angular to subangular shapes. The deposit is poorly-sorted and clay matrix. The thickness of this unit is about 0.8-2.0 meters.

Unit B is a layer of reddish brown to dark yellow clayey sand, this layer is containing iron oxide gravel (5%). The sand has the charactered by round to well round shape, high sphericity and well sorted. The thickness of this unit varies significantly from 0.20 - 0.35 meters.

Unit C is well-defined, yellowish brown to pale brown sand of alluvial deposit consisting of fine to moderate sand (85%) with clay (10%) and iron oxide (5%). The deposit is well-sorted, well roundness and mainly matrix support. Its thickness ranges from 50 to 80 cm.

Unit D is characterized by reddish brown, sandy gravel layer. The general gravel was sandstone with subangular shape. The unit is well-sorted and thickness of it is about 0.40 meter.

Unit E is light brown to dark brown colluvial deposit sandy clay. This layer consisting of clay (70%), fine-sand (25%) and rock fragment (5%). The thickness of this unit is about 0.80 -1.20 meter and the middle of this layer have the lense interbeded of sandy gravel with thickness abouth 10 centimeter (unit H).

Unit F is orange to dark yellow clayey sand of alluvial deposit and morethan 75% is sands. The sand has the characterized by well roundness, high sphericity and moderate. The thickness of this unit is about 0.20 - 0.30 meter.

Unit G is the topmost unit and consists chiefly of light grey sandy clay with well sorting and contaminated by human activity. The upper part of the unit is the organic-rich top soil and plant debris. Thickness of the unit varies from 0.50 – 0.80 meter.

5.3.1.2 Evidence of faulting

In the excavated trench, there are several pieces of evidence regarding faulting based on trench-log stratigraphy. One fault system was recognized (F1) which cut through the sedimentary units B, C, D and F. The important fault evidence includes the discontinuity of clayey and of unit B, sand of unit C and throughout gravel of unit C as shown in Figures 5.16. The F2 was cut through unit like to F1 fault andThe units A and the offset of those unit refered type both F1 and F2 were reverse fault. The other evidence is some gravels of unit A near the fault F3 change their orientation following the west-dipping fault plane and appear shape contact between unit A and unit E.

5.3.1.3 Structural geology

According to the fault evidence mentioned above and together with the current morphotectonic investigation, the sense of fault movement in the area is mainly reverse with some left-lateral slip. At the northeast wall, the fault F1-F3) cuts through layers with a steep dip to the east, like to southwest wall, which the Faults (F1-F5) were dipping to the east, too (Figure 5.17). The true displacement of F1 be not sure to observe because the hanging wall of units B, C and D are different thinkness from each side of fault but at least, we can estimate the fault offset by assuming the top of layer D exposed at the bottom of E. So its offset is approximately at least 1.7 m.

5.3.2 Trench 2: Ban Thung Sri Ngam

Ban Thung Sri Ngam trench is located at Ban Thung Sri Ngam school, southwest of Amphoe Thap Put, Phang Nga at grid reference 458158E / 940695N. This trench is an open wall next to football yard of that scholl with height of about 2.0 -2.5 meters and length more than 30 meters. The school located on Phap Put- Phang Nga road (no.418) nearby Ban Khao Tao Nox. The open wall was fortuitous found and a sharp dishorizontal of the sediment layer seems to suggest a stress compress by tectonism. Sedimentary layers on the open wall were then sketched and logged for structural geology and sample collection for TL dating and OSL dating.

5.3.2.1 Stratigraphic Description

Trench-log stratigraphy of the Ban Thung Sri Ngam trench is characterized by 4 unconsolidated sediment units. As shown in Figures 5.18, it is quite clear that the Ban Thung Sri Ngam trench has relatively much more deformed stratigraphy. Details of individual units (units A to D) are described below.

Unit A is characterized by semi-consolidated sandy clay with some sub-angular sandstone, quartz pebbles and Fe- oxide interbedded with light brown alluvial deposit consisting largely of pebble, modurate-sorted. Its thickness ranges from 0.30 to 0.50 meter. It is noted that the can be 'paleosol' this unit have gravel lense intervene at lower part and uncontinuous from overlain layer.

Unit B is well-defined, reddish brown gravel layer (somewhat can be laterite) consisting of pebble to cobble of sandstone, metasandstone and Fe-oxide. Its thickness ranges from 0.20 to 0.30 m.

Unit C is defined as reddish brown to yellow sitly clay, which composed of clay, silt, very fine sand, well-sorted. Thickness of the unit is about 0.50 meter. The bottom part of unit C contains larger fragments than upper part.

Unit D is consists of dark grey sandy clay with poorly sorted, possibly by human activity. The upper part of the unit is the organic-rich top soil and plant debris. Thickness of the unit varies from 20 to 30 cm.

5.3.2.2 Evidence of folding and faulting

Based on the lithostratigraphy data, Unit B is a folded layer and underlain unconformably by unit A. Both of units A and D have a sharp contact with unit B and all of them overlain by unit D. The folding of unit B and unit C (Figure 5.19) implies that the fault was moved nearby and effect to unit B and C. As introduced above, the sharp contact of units A and C with unit B is similar to a reverse fault style from compression stress in this region. It is considered that the unit B is possible to be effedted of restraining bend of strik-slip fault.

5.3.2.3 Structural geology

The evidence of faulting is found in unit B and unit C, which are the alignment of pebbles as a result of compressive folding. The structure observed in the trench is a fault cutting through units A, B and lower part of unit C with dip to the south and then an open fracture was formed due to younger fault movement and enlarged so as to develop a laterite layer. Then the sediment of unit C was deposited in fracture zone and covered by top soil of unit D. Based on topographic loation, this area is zone of Khlong Marui segment and found some offset streams and fault scarp and stratigraphy data from trenching, the fault in this area is the reverse fault with left-lateral movement.

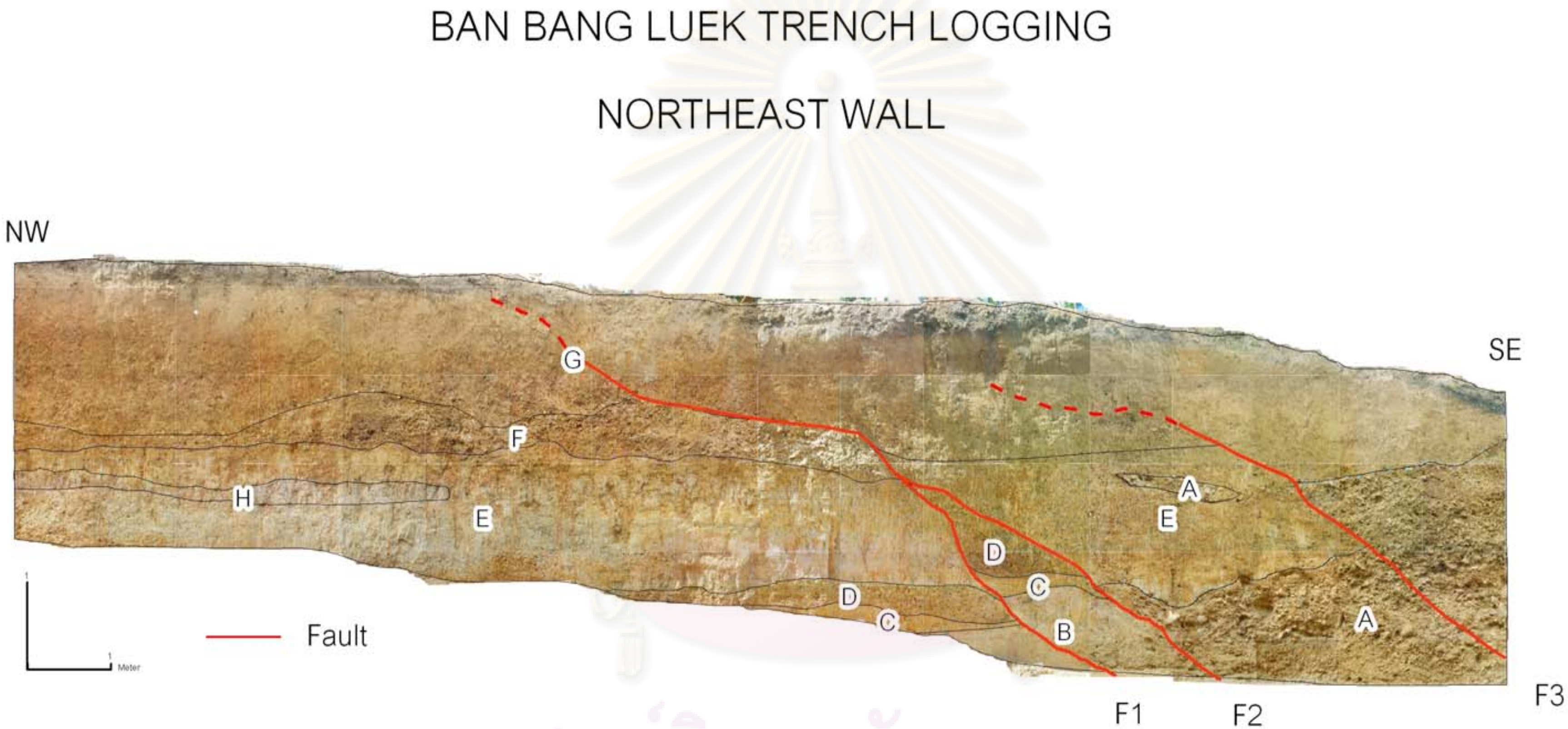

Figure 5.14 View of paleoseismic trench section on the north-east wall, Ban Bang Luek, Surat Thani showing sediment stratigraphy and faults oreintation.

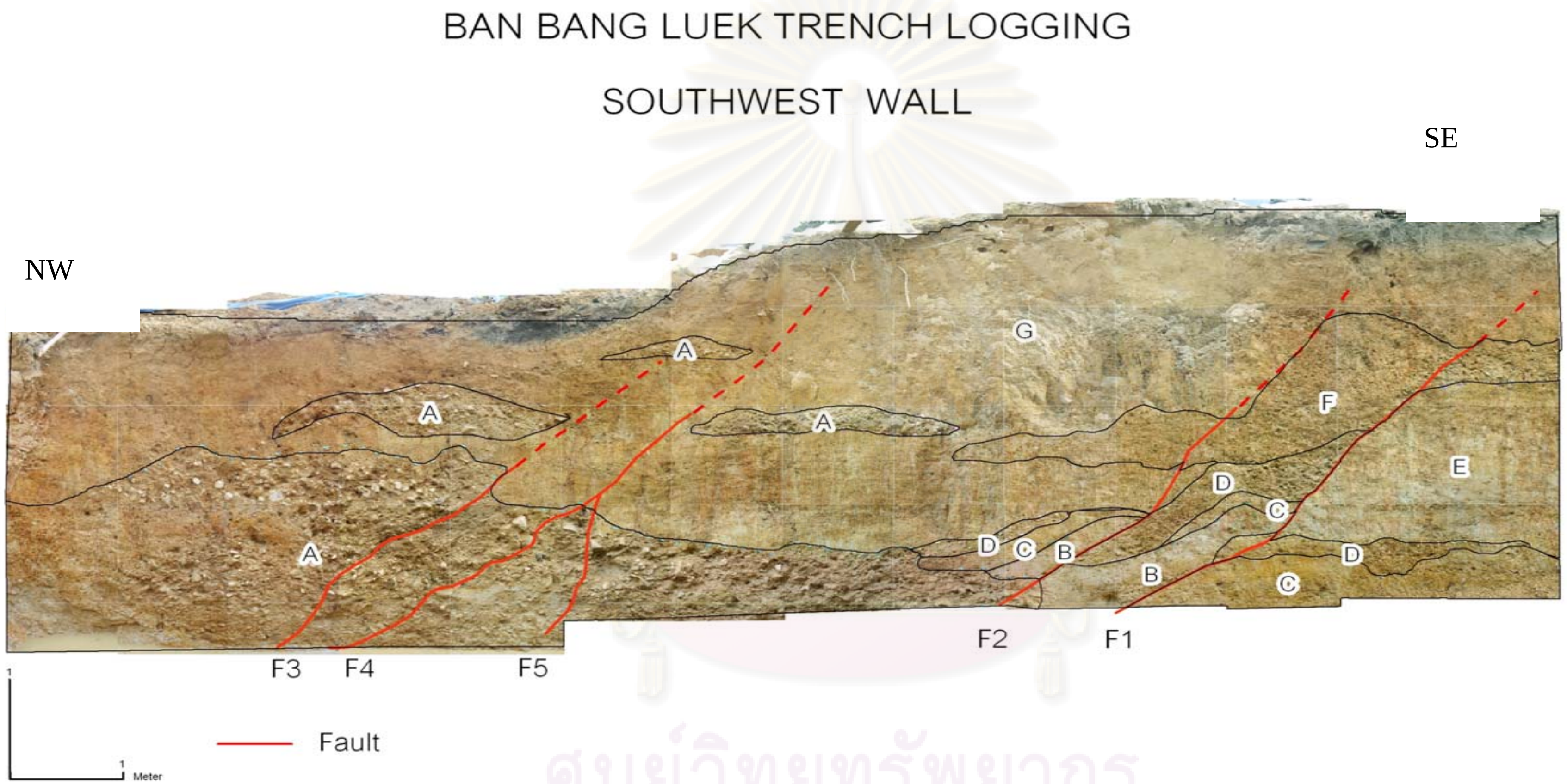

Figure 5.15 View of paleoseismic trench section on the south-west wall, Ban Bang Luek, Surat Thani showing sediment stratigraphy and faults oreintation.

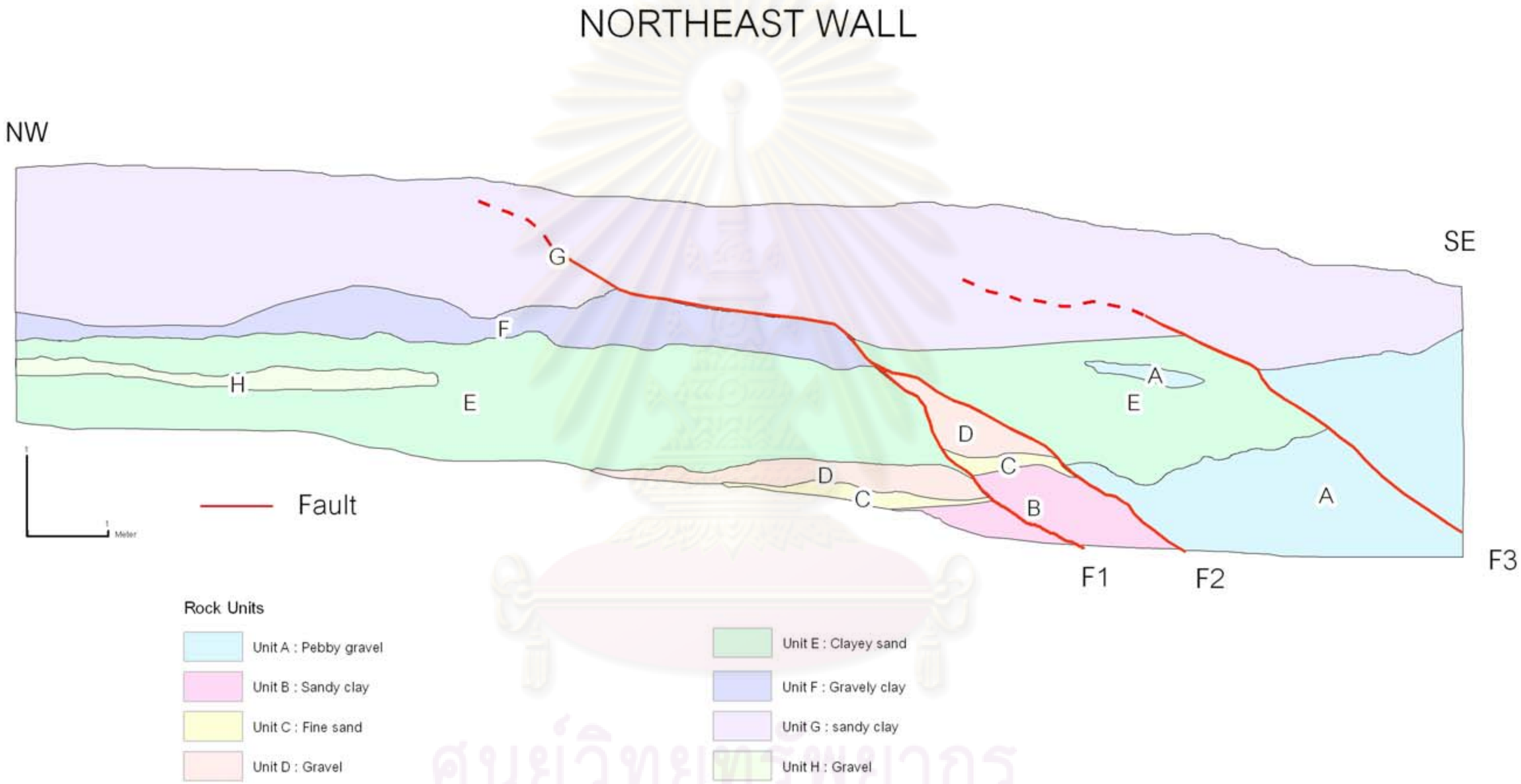

Figure 5.16 Trench log section of the north-west wall, Ban Bang Luek, Surat Thani showing preliminary sediment stratigraphy, major faults orientation.

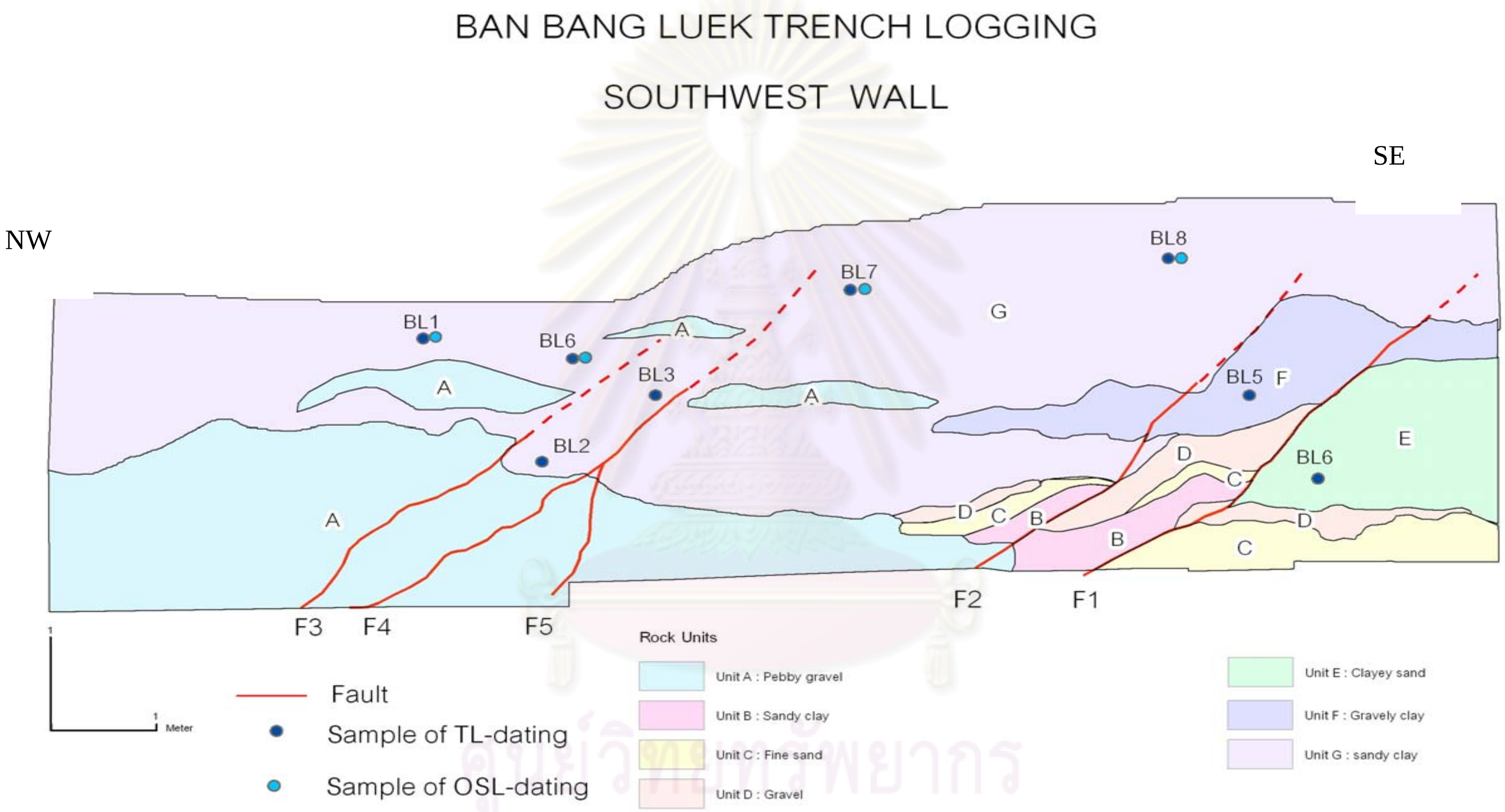

Figure 5.17 Trench log section of the south-east wall, Ban Bang Luek, Surat Thani showing preliminary sediment stratigraphy, major faults orientation and sample location for dating.

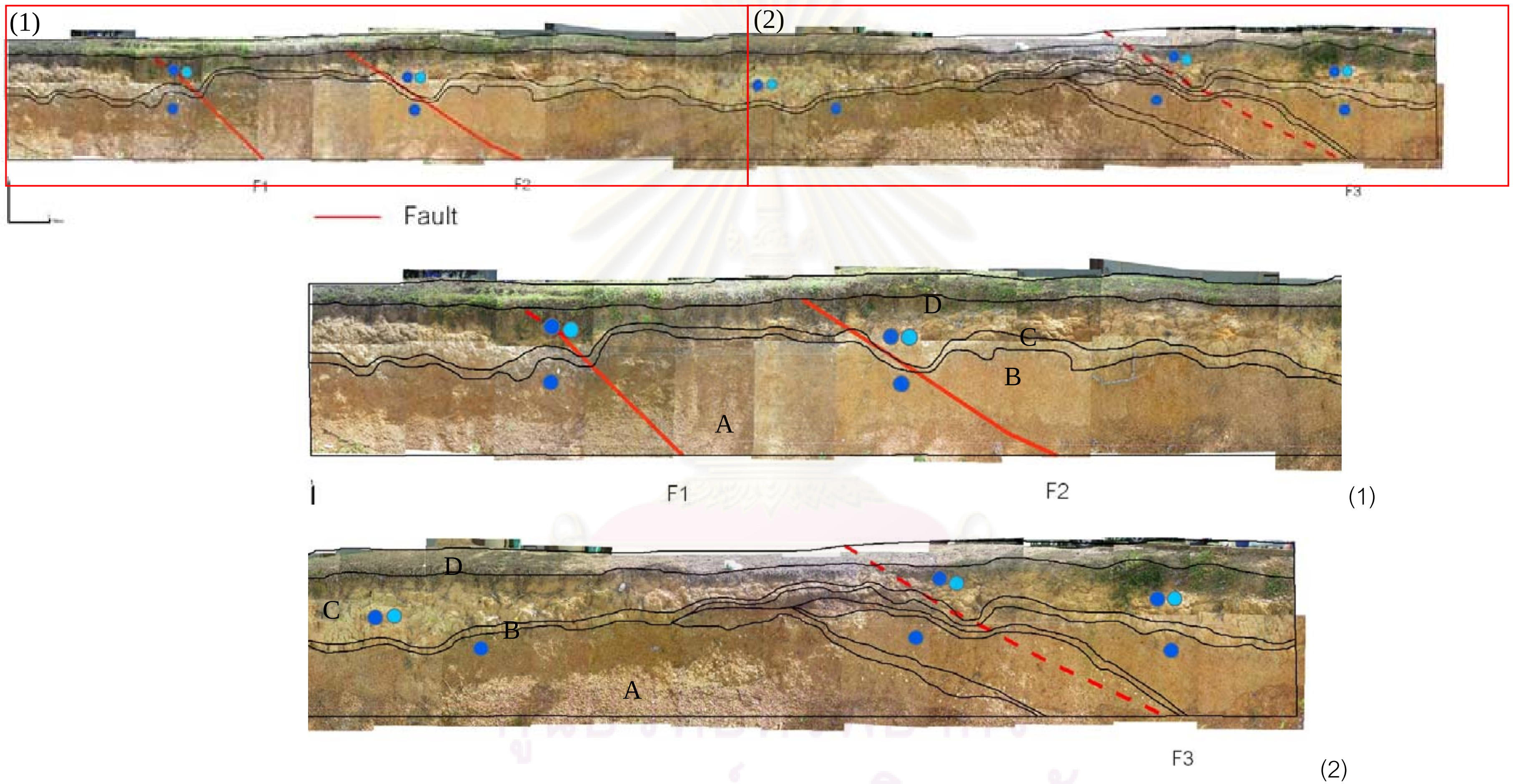

Figure 5.18 View of paleoseismic trench section on the north-west open wall, Ban Thong Sri Ngam school, Phang Nga showing sediment stratigraphy, compress stress orientation and faults.

158

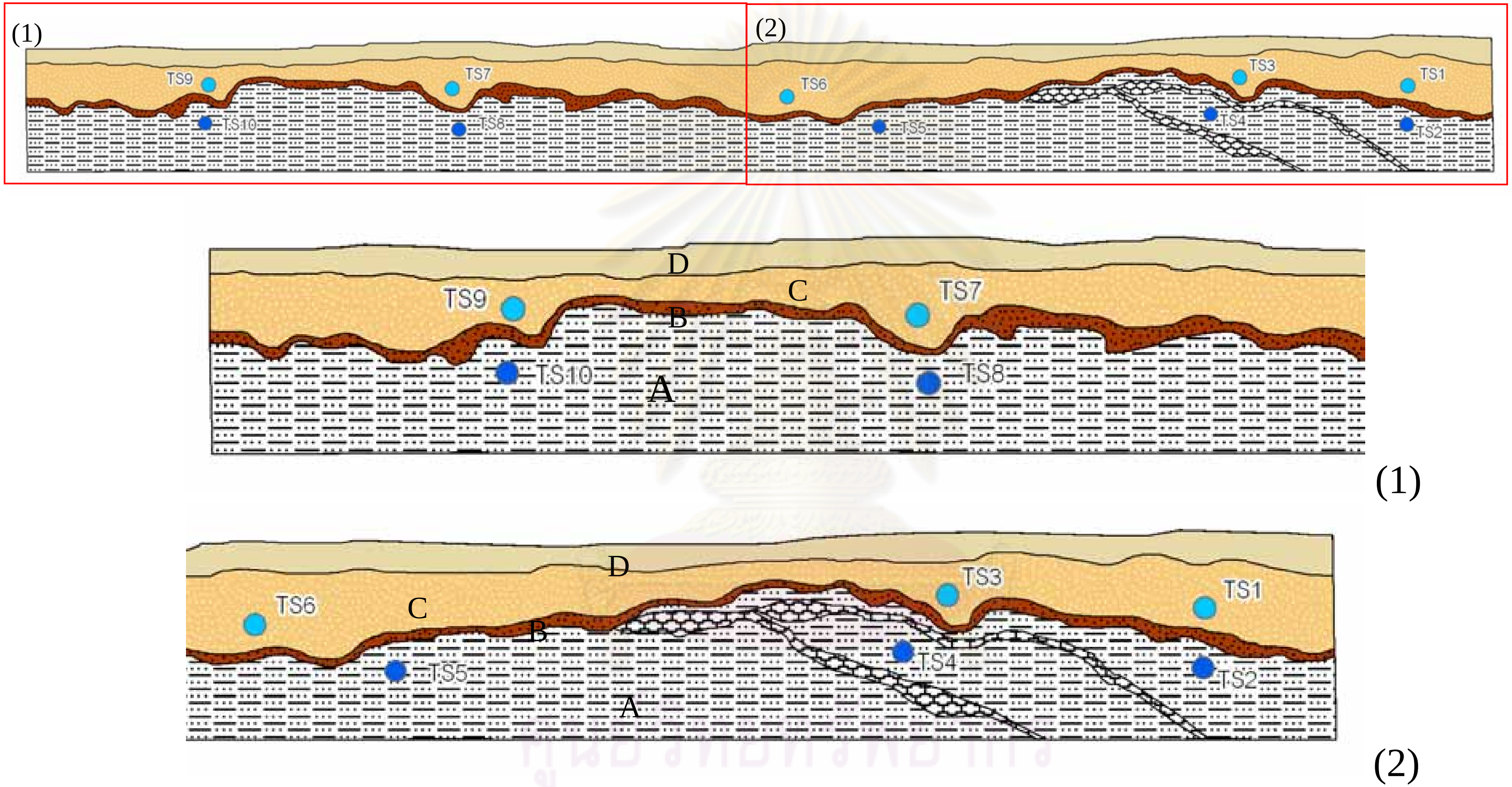

Figure 5.19 Wall log section of north-west open wall, Ban Thong Sri Ngam school, Phang Nga showing preliminary sediment stratigraphy, major faults orientation and sample location for dating.

Chapter VI
Luminescence Dating

In this section, we reported the thermoluminescence (TL) and Opitcal Stimulated Luminescence (OSL) dating procedures and results. The (TL & OSL) procedures are proposed by Takashima and Honda (1989). The methodology of analysis is composed of 2 main procedures, including equivalent dose evaluation and annual dose evaluation

6.1 Basic Concept

Thermoluminesence (TL) and Optically Stimulated Luminesence (OSL) are related techniques which measure when objects were last heated (TL) or when buried deposits were last exposed to light (OSL).

TL and OSL are known as 'electron trap' techniques. Some natural materials such as various stones and soils (and also things made from them, such as pottery and stone tools) absorb or 'trap' naturally occurring electrons from their surroundings. This happens at a known and regular rate until the material becomes saturated with electrons after about 50,000 years. Since the world is much older than this, most objects are already saturated. However, if these substances are heated (such as when pottery is fired in a kiln or stones are dropped in a fire) this releases these trapped electrons and resets the 'clock' to zero. The object will then begin to trap electrons again. These electrons can be released and counted in a laboratory to give a date since the object was fired (TL). Some soils can have their electron 'clocks' reset simply by being exposed to sunlight. If they are then buried beneath later deposits, they begin to trap electrons again and can be dated by similar methods (OSL). This produces a date for the burial of the deposit.

The object to be dated is heated in a laboratory until it glows. Part of this is the ordinary glow of burning, the remainder is due to escape of these trapped electrons and this is measured. These techniques can date objects up to 50,000 years old, although both are more accurate within the past 10,000 years. Even so, for the past 5000 years

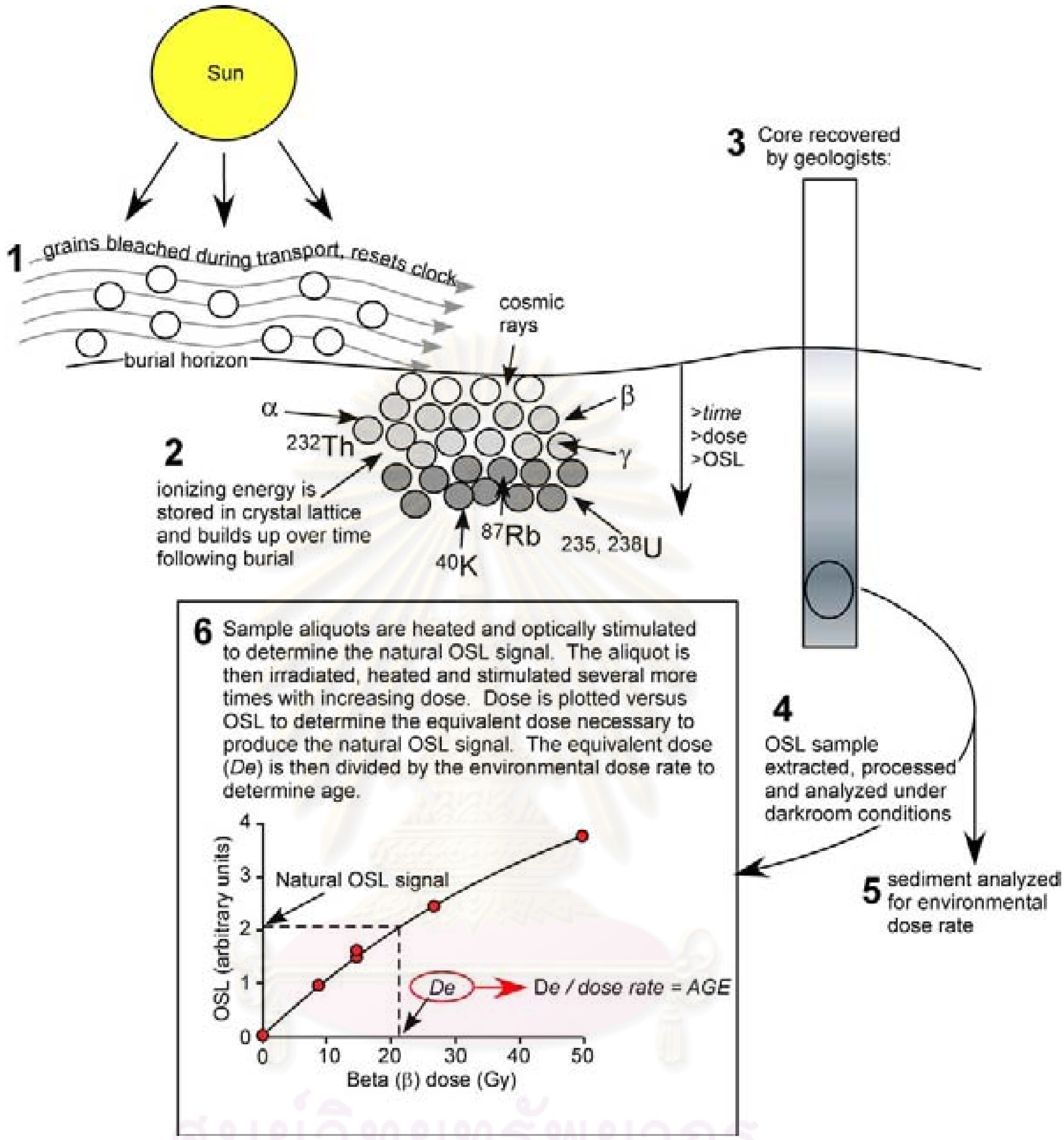

Figure 6.1 Generalized processes that produce the luminescence signal (steps 1 and 2), and the sampling and analytical procedure to determine the age of deposition (steps 3 through 6), (Mallinson, 2008).

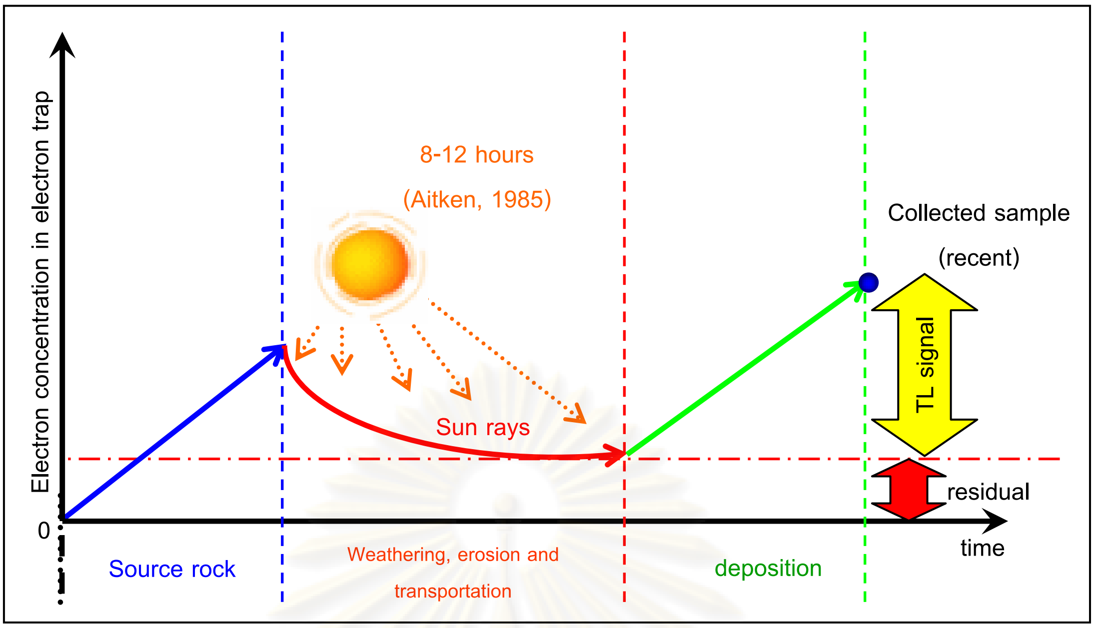

Figure 6.2 Applied thermoluminescence method for dating by showing relationship between amount electron in electron trap and time, (modified after Won-in, 2002).

they are less accurate than other dating methods like radiocarbon. They can be useful for dating early sites and those that don't contain material suitable for radiocarbon or other dating methods (Figure 6.1 and Figure 6.2).

Generally, insulators such as covalence solids and glasses can generate thermoluminescence (TL-dating) signal, but metals cannot. As a result, TL-dating method can be only applied with an insulator crystal. A simple model to review on general background of TL-dating method is based on ionic crystal model, which is simplified as shown in Figure 6.3

Ionic crystals, for example calcium carbonate and sodium chloride, are composed of lattice of positive and negative ions. In this lattice, it can be defected due to at least three reasons; an impurity atom, a rapid cooling from the molten stage, and damage by nuclear radiation. The defected lattice is presented by lacking of electron from its proper place or electron vacancy, called "electron trap", leads ionized electrons from vicinity to fill up in this trap hole. In addition, ionized electron is the result of nuclear radiation from earth materials or solar radiation. However, both nuclear radiation and solar radiation have caused much less damages to the lattice structure.

Electrons have been trapped in trap holes lasted until shaken out due to the vibration of crystal lattice. A rapid increase of temperature to high in narrow range leads this vibration to be stronger. In addition, high temperature usually upward of 400^{o}C can evict electrons from deep electron traps to be diffused around the crystal. Note that, because of different crystals, there are different types of traps, and then optimum temperatures to evict electrons in different crystal traps are unique. However, diffused electrons can be directed into two different ways; firstly to be retrapped at different types of defect which is deeper trap, and secondly to be recombined with an ion in lattice which electrons once have previously been evicted.

There are electron traps (T) and center of luminescence (L) located as intermediate between the valence band and the conduction band. The energy (E) is required in an optimum level to shaken out electrons from its deepest hole. In general, when electrons have already shaken out by heating, and recombination is done at the centers of luminescence, light is emitted. However, in some case which recombination has done at non-luminescence center or killer center, there is no emission of light and the energy is represented in the form of heat.

In summary, the luminescence process can be concluded in four steps (Figure 6.4). Firstly, ionization of electrons is caused by nuclear radiation. Secondly, some of these electrons are trapped in continuous and constant rates lasted until temperature has increased. Thirdly, some of electrons are heated at the optimized temperature level to evict electrons from deep trap hole. Fourthly, some of these electrons are then reach luminescence centers and in case of recombination process has done, light emission from luminescence centers is generated. The amount of emitted light or the number of photon in this stage is depended on the number of trapped electrons, which in turn is the amount of nuclear radiative proportion or paleodose. In addition, dose rate of nuclear radiative applied to environment is called annual dose.

Ultimately, based on TL or OSL process mentioned above, age of quartz-bearing sediments (such as those of this study) can be determined by simple equation 6.1 below;

$$\text{Age} = \frac{\text{Paleodose}}{\text{Annual dose}} \quad \text{..} \quad (6.1)$$

6.2 Laboratory Precesses

The laboratory procedure in this study is mainly followed that of Takashima and Honda (1989). The methodology of analysis is composed of 2 main procedures, including paleodose or equivalent dose evaluation and annual dose evaluation (Figure 6.5).

6.2.1 Crushing and Sieving

Upon arrival in the laboratory, TL samples normally were dried by 40-50°C baked in the dark room. Water content is also measured for all samples being dated because it is the one significant parameter for annual dose determination. The formula of water

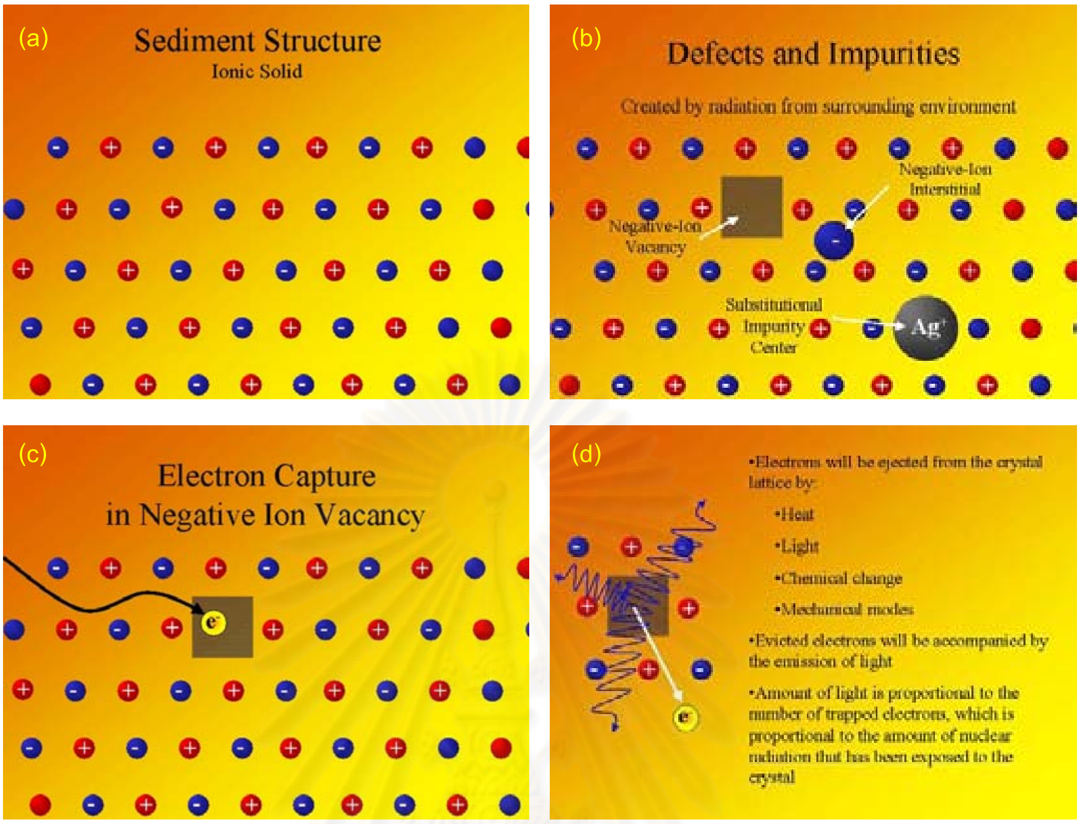

Figure 6.3 Simplified diagram of lattice structure and ionic crystal showing (a) ideal model of completely lattice (b) negative-ion vacancy occurred in ionic crystal cause negative-ion interstitial and substitution impurity center (c) electron capture by electron trap in negative ion vacancy and (d) electron escape from electron trap by heat or Light, (http://www.rses.anu.edu.au).

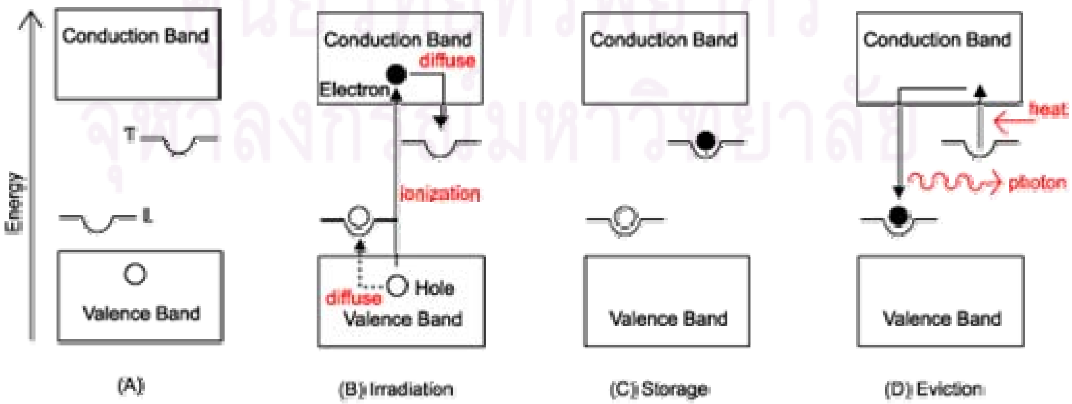

Figure 6.4 Simplified model showing energy states in Thermoluminescense processes, (Aitken, 1985).

content calculation is shown in equation 6.2.

$$\text{Water content} = \frac{(\text{weight of a wet sample-weight of a dried sample})\text{x } 100}{\text{weight of a dried sample}} \ldots\ldots (6.2)$$

After getting dried sample, each sediment sample was shattered by using a rubber-hammer and the material passed through sieves to isolate the grain size fraction in 2 parts. Sediments which grain size pass through 20 mesh (<841μm) were collected about 300 g and was separated to keep in plastic containers for annual dose determination. Remnant part from annual dose collection is carefully re-sieved and the material passed through sieves to isolate the grain size fraction between 60-200 mesh. Both of these portions were kept in beakers for purifying quartz grain and equivalent dose determination, respectively. In the annual dose, a sample portion is ready and skips to the measurement step but in both of two portions for equivalent dose determination is necessary to participate in chemical treatment.

6.2.2 Annual Dose Evaluation

Generally, sediments are exposed continuously to ionizing radiation, which originates from their radioactive contents, plus a small fraction from cosmic rays (Aitken, 1985). There are essentially 3 radioactive elements which contribute to the natural dose rate (annual dose) i.e. uranium (U), thorium (Th) and potassium (K). The decay of uranium and thorium results in α, β and γ radiation whereas potassium emits β and γ normally, the natural dose rates in most sediment are of the order of mGy/year.

For age determination it is necessary to evaluate the natural dose rate accurately. Several components are needed for an accurate annual dose is:

a. Measurement of U, Th and K contents;

b. Calculation of environmental water content in field at time of sample and

c. Cosmic ray component evaluation

The annual dose to the sample is computed from the concentrations of K, U and Th by the method described by Bell (1979) and Aitken (1985), as shown in equation 6.3.

Annual dose = (AD) = Dα+Dβ+Dγ+Dc ………….………. (6.3)

Where α = Alpha irradiation content,

β = Beta irradiation content,

γ = Gamma irradiation content, and

C = Cosmic ray irradiation content.

A) Measurement of Uranium, Thorium, and Potassium Contents

shows the schematic preparation and procedure for measurement of U, Th, and K contents by neutron activation analysis (NAA). The estimated standard errors were less than 10% for U and Th, and less than 3% for K using the fixed count error calculation method (Takashima and Watanabe, 1994).

B) Annual Dose Calculation

Annual dose is calculated from chemical data of U, Th, and K contents with the equations proposed by Bell (1979) and Aitken (1985), as shown

$$\begin{aligned} AD = & [0.15(2.783U + 0.783Th)/(1+1.50(W/100))] \\ & +[(0.1148BU + 0.0514BTh +0.2492BK)/(1+1.14(W/100))] \\ & + [(0.1462U + 0.0286Th + 0.8303K)K/(1+1.25(W/100))] \\ & + 0.15 \quad \ldots\ldots\ldots\ldots (6.4) \end{aligned}$$

Where ; AD = Annual dose (mGy/year),

U = Concentration of uranium in ppm,

Th = Concentration of thorium in ppm,

K = Concentration of potassium oxide (%),

B = Beta coefficient in quartz grains, and

W = Water content (%).

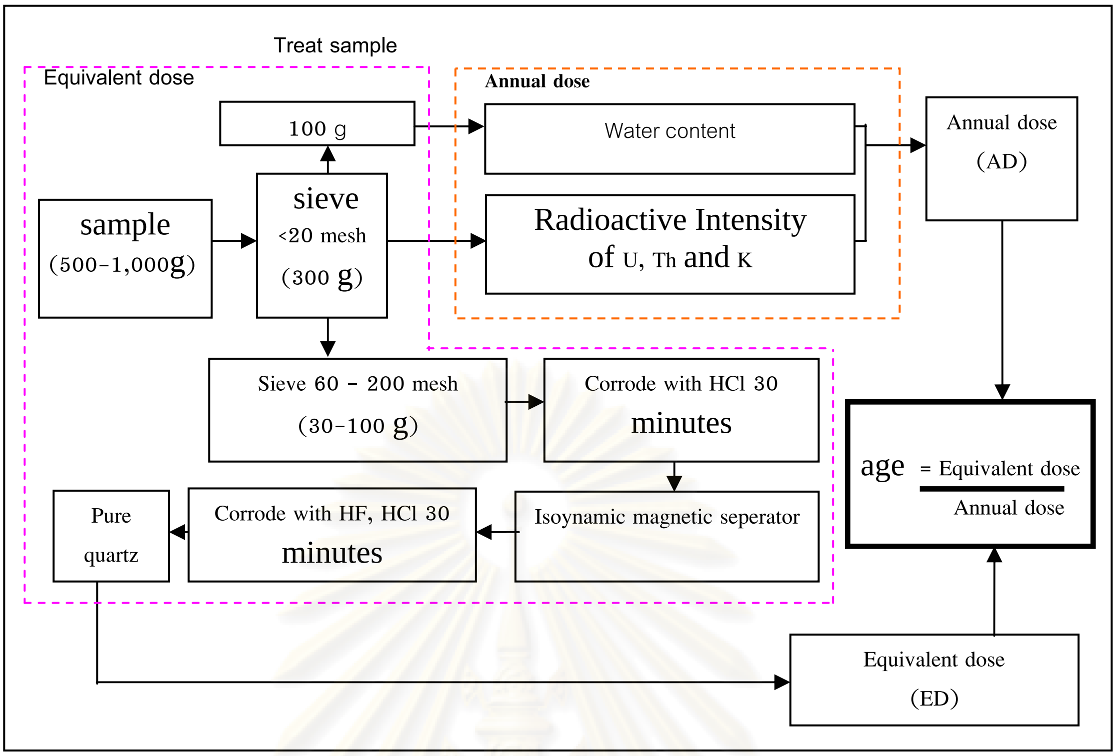

Fig 6.5 Chart of calculate annual dose and equivalent dose for TL and OSL dating, (modified after Takashima and Honda, 1989).

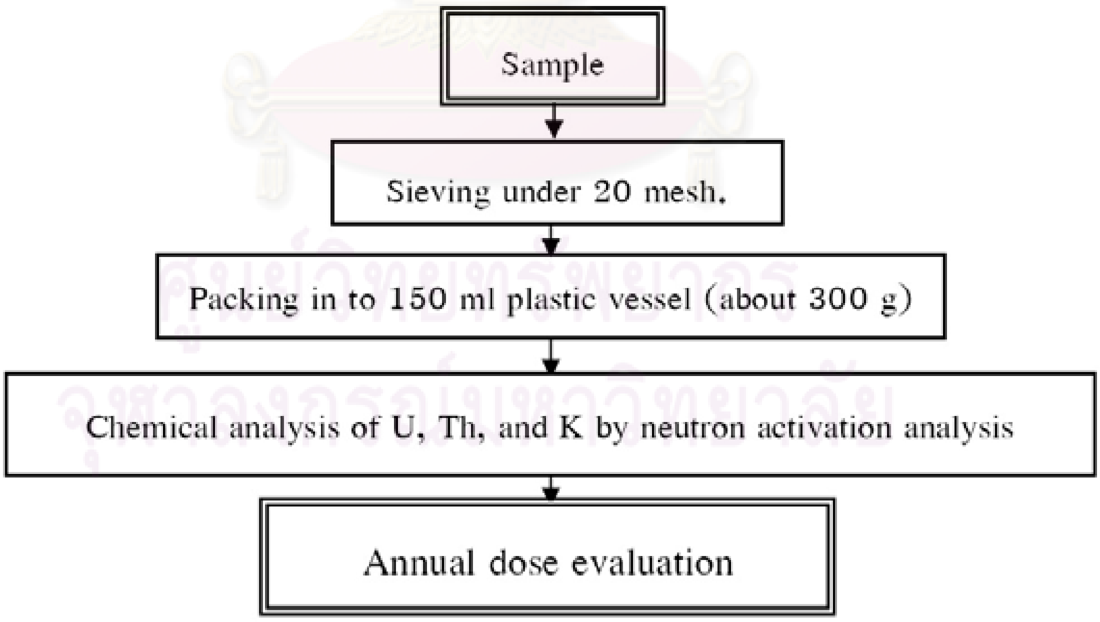

Figure 6.6 Summary of neutron activation analysis (NAA) procedures with sample preparation and annual dose determination.

6.2.3 Paleodose or Equivalent Dose Evaluation

I) Chemical Treatment

The main objective of chemical treatment is purification of quartz mineral in TL samples from the method in order to keep off destroying the signal of sample. The detail of chemical treatment is shown below:

a) Washing the sample by distilled water 10 times for removing some organic materials and clay particles;

b) Chemically cleansed the sample in dilute 35% HCl at 50^{o}-$60^{o}C$ in a period of 15-30 minutes and re-washed several times with distilled water for eliminating carbonates and deep-rooted organic material;

c) Etching the sample in 24% HF at 50^{o}-$60^{o}C$ for 15-30 minutes and rewashed it several times with distilled water. HF was used to dissolve the plagioclase and outer layer of quartz grains to a depth sufficient for the core remaining to have a negligible component of alpha particle dosage; and

d) After washing with water and drying in the dark room, the dried sample was then separated to remove out the dark minerals (e.g. zircon, garnet, and metallic minerals) by using an isodynamic separator (Frant'z isodynamic magnetometer)

After finishing sample treatment, it is necessary to check purity of quartz sample by XRD analysis. If the quartz-rich samples contain less than 10% of the other minerals, the samples were supposed to contain pure quartz concentrates.Then the sample was ready for determine equivalent dose in the next step.

II) Sample Preparation for Equivalent Dose Measurement

The pure quartz sample after chemical treatment is subdivided into 3 parts:

Part 1: Natural quartz sample was used for evaluated natural sensitivities of previously acquired TL signal;

Part 2: Sample was exposed directly with natural sunlight for 12 hours (Aitken, 1985) to effectively remove all of the previously acquired TL leaving only what is termed as the unbleachable TL/OSL signal. This part used for determining residual levels; and

Part 3: Sample used to find out the characteristic of quartz effective with artificial irradiation that amount of radioactive irradiation (in unit Grey) is known. The gamma ray source for artificial irradiation is a Co 60 from Office of Atomic Energy for Peace (OAEP), Bangkok.

III) Equivalent Dose Measurement

This study used the Thermoluminescence Detector (TLD) at geology department, facuty of science, chulalongkorn university (Figure 6.7) for evaluation of equivalent dose commences with measurement of TL intensities on 3 sample portions: 1) natural sample portion, 2) artificial irradiation sample portion and, 3) residual sample portion (in sediment sample). About 20 mg of sample was filled in aluminum planchettes and placed on a molybdenum heater. The graph shows a relationship between TL intensity and temperature which is called “glow curve” (Aitken, 1985). The term glow curve is given to plot intensities of emitted light versus temperature (Figure 6.4a). Calculation of equivalent dose can be done by extrapolating natural signal intensity and residual signal intensity with a growth curve from artificial irradiated signal intensity. The result is assumed to be proportional to the equivalent dose of equation 6.1.

Although the glow curve shown in Figure 6.4b is smooth continuum, it is really composed of stable and unstable signals. This procedure makes by comparing the shape of the natural glow-curve (i.e. the glow-curve observed from a sample which has not received any artificial irradiation in the laboratory) with the artificial glow-curve observed as a result of artificial irradiation. Thus a constant ratio between natural and artificial glow curves gives an indication that, throughout this plateau region, there has been negligible leakage of electrons over the centuries that have elapsed since all traps were emptied in the course of the stimulation by ancient environment.

The next step is for the construction of growth curve. This can be done by the increases of TL/OSL output with known amounts of additional radiation that 160 induced the sample. The graph showing this relationship is called “growth curve”.

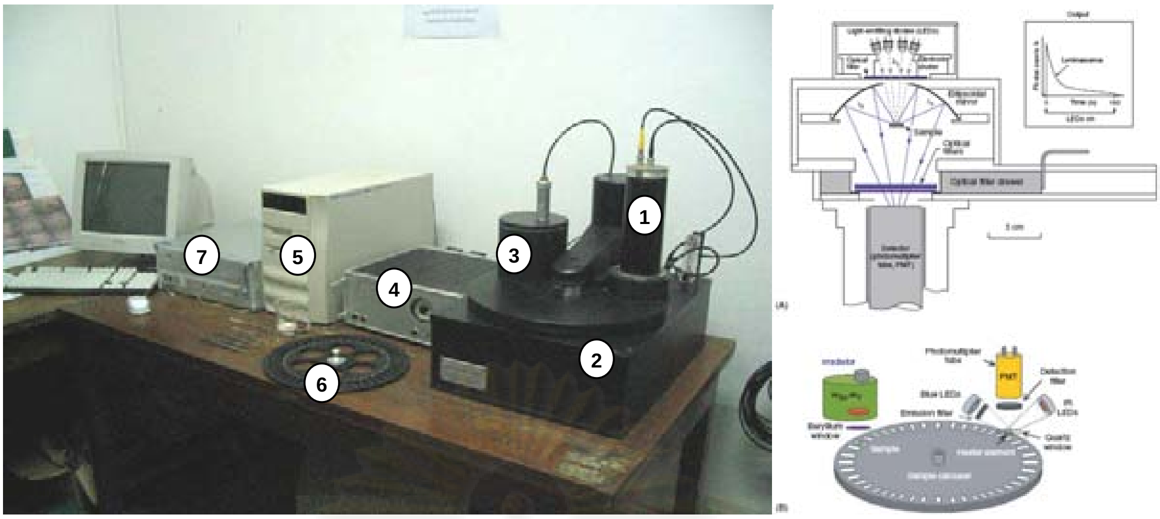

1. Photo detector and Photo multipliers
2. Heater system
3. Radioactive Irradiation system
4. Hardware control system
5. Software control system
6. Sample dish
7. Output storage system

Figure 6.7 TL and OSL equipment component.(a) Thermoluminescence Detector (TLD) at geology department, facuty of science, chulalongkorn university (b) Main equipment that comprises the “reader”, which is necessary for measuring the paleodose, irradiating the sample, heating the sample, and deriving a “growth” curve, (Lian, 2007).

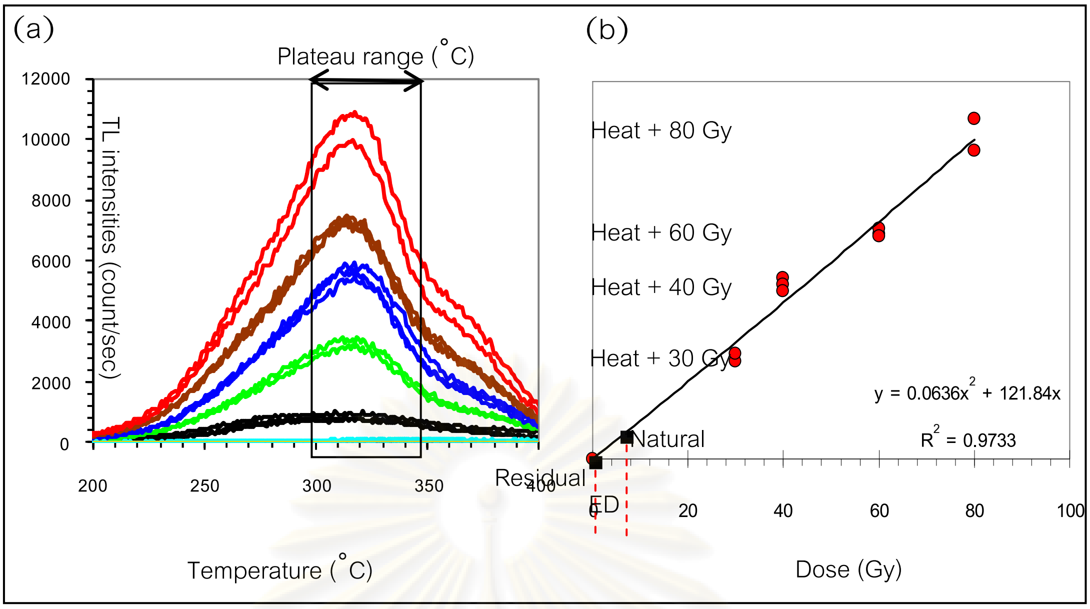

Figure 6.8 example result of BL1 after run with Thermoluminescence Detector for calculated equivalent dose (a) growth curve (b) grow curve.

IV) Regeneration Technique

In this technique, the simplest approach to the evaluation of equivalent dose is by the straight-forward procedure of measuring the natural TL intensity from a natural sample (N) and comparing it with the artificial TL intensity from the same sample that know certain dosage (artificial irradiate sample). In this study, after heating the quartz-extracted at 320^{o}C for 5 hrs, individual samples were liquated for 5 sub-samples (Takashima et al., 1989). For each sub-sample, artificial irradiation was added with the doses of 44, 103, 303, 723, and 1,440 Gy. The values of TL intensity (N/H+γ) (as shown in Figure 5.6) versus temperature ranges were plotted for each sample and they are shown in Appendix.

The growth curve plot is a graph of TL ratio or TL intensity (as shown in Appendix). It should be noted herein that most graphs of the natural intensity values close to the artificially irradiated liquated (i.e., H+1,440 Gy). Therefore their paleodose can be read after curve fitting for each aliquot. (Figure 6.9).

V) Residual Test

In case of sediment sample, evaluation of equivalent dose is complicated by the need to allow for the fact that the equivalent dose is composed of two components: the natural TL signal acquired since deposition and the residual signal that the sample had when it was deposited in the last time. Many scientists (e.g. Wintle and Huntley, 1980; Tanaka et. al., 1997) proposed several methods to simulate the light source exposures. Samples were exposed to some kinds of light sources. Natural sunlight, UV-ray lamp (365 nm) and xenon lamp were the important illumination sources for bleaching experiments (Won-in, 2003).

In this research study, the naturally bleaching experiment by sunlight requires and depends significantly upon a long sunny day. For the artificial bleaching experiment, it is important to check the minimum of time that can completely bleach samples to the residual level and how much residual level in each sediment sample. The methodology of residual testing starts with bleaching sample and check TL intensity of sample in every 1 hour. Plotting graph showing a relationship between TL intensity and time used for bleaching reveal the minimum time that residual signal begin stable (unbleachable).

VI) Plateau Test

According to glow-curve, there are overlapping peaks that may be raised to make misinterpretation of the peak, which is the result of electron emission from deep traps not other shallow traps. Glow-curve peak, which has located in the stable region, is that of interest. The stable region is usually at 300oC or higher where electrons from deep traps are evicted near zero. The method to recognize the stable region is a plateau test as shown in Figure 5.8. There are two glow-curves of natural sample (N) and natural + artificial sample (N+γ) that had been plotted as solid lines in the same graph. Ratio between N and N+γ is shown as dots. The plateau of dots is the stable region red-colour zone or band. In addition, peaks of both samples have been generated at the same temperature, and N+γ peak is higher than N peak, it means that deep traps are deep enough to contain other electrons.

6.2.4 Error Determination

Error in TL-dating result derives mainly from sample preparation and TL measuring apparatus (av. 10%), as well as standard deviation (SD) from measured values of ratio H+γ / N on growth curve. So equation for dating errors is described as

Error = Absolute $[(SD^2_{ED}) + (SD^2_{AD})]$ x age ……………………….. (6.5)

Where SD_{ED} = Absolute $[(x-\bar{x})^2/N]$

SD_{AD} = 10 %

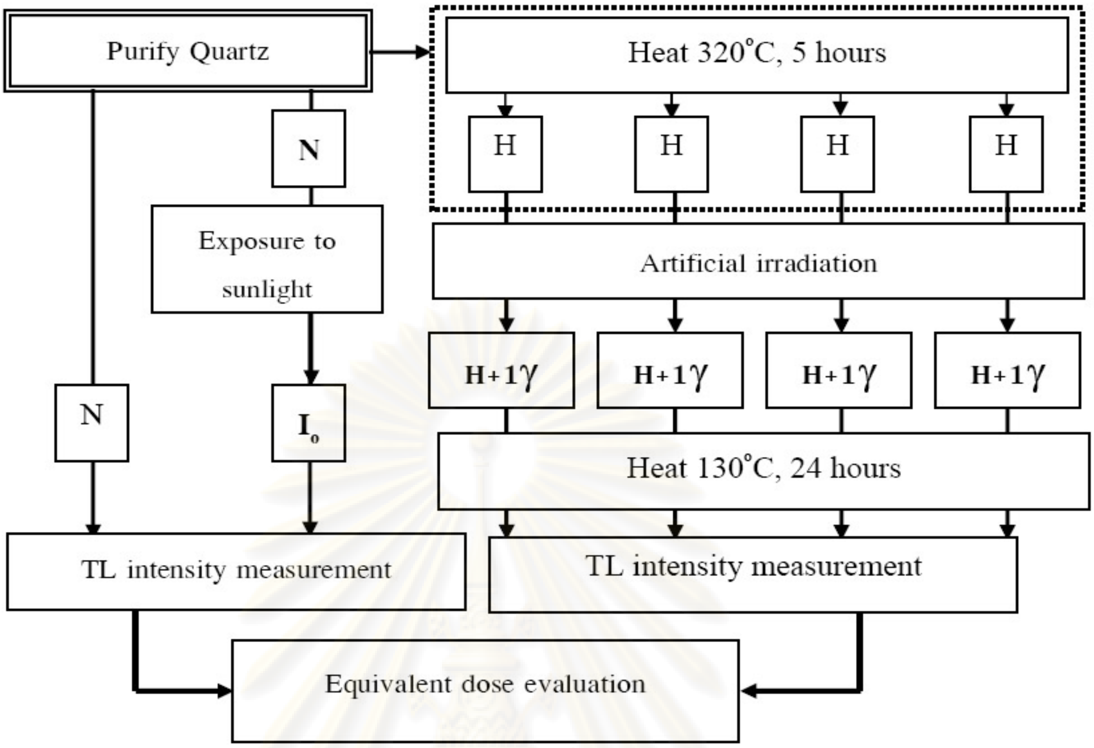

Figure 6.9 (a) Schematic charts of regeneration technique (Takashima et. al., 1989). Note that several portions are used for measurement of the TL intensity; N is natural sample; Io is residual intensity from sample; H is 350°C heated sample; and γ is known dosage that irradiated sample.

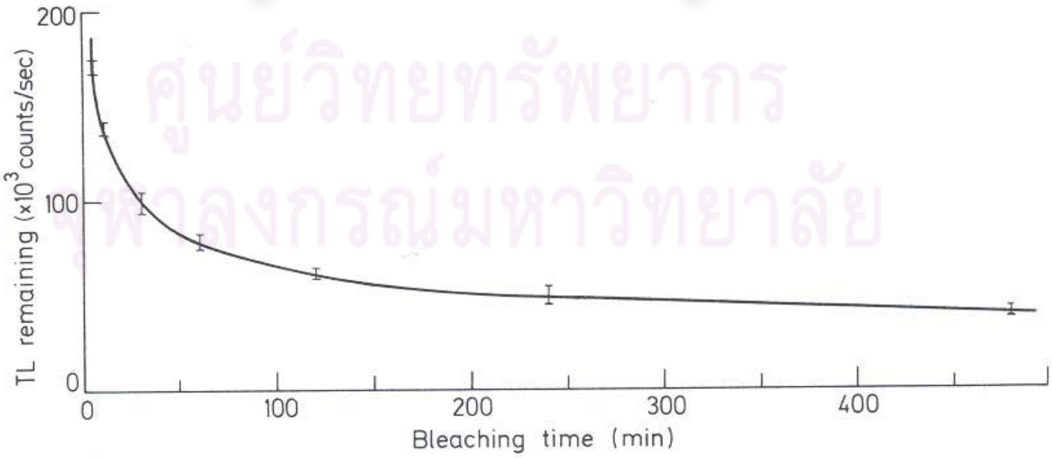

Figure 6.9 (b) Thermoluminescence remaining after bleaching by exposes to sunlight For various time (Aitken, 1985)

6.3 Dating result from this study

A total of Quaternary sediment samples were selected from paleoseismic trench at Ban Bang Luek and Ban Thung Sri Ngam (as shown in Figure 5.17 and 5.19). About 18 samples were selected for TL dating and 3 samples for OSL dating and their results are shown in Table 6.1 and Table 6.2, respectively. For annual dose analysis, the dated samples contain U contents varying from 1.08 to 20.4 ppm, Th contents from 5.89 to 32.34 ppm, and K contents from 0.41 to 2.43 %. In general, water contents of the dated samples are between 0.66 and 13.11. The annual dose of the dated samples vary from 1.99 to 7.03 mGy/Y, and the paleodose (or equivalent) dose range from 11.48 to 907.31 Gy. As shown in Table 5.1 and Table 5.2 ratios of paleodose to annual dose of individual dated samples give rise to the TL and OSL dates between 4,000 to 231,000 years. It is inferred from this study that the dating and geological results show more than one paleoseismic event. The oldest age of the fault movement is about 88,900±1,3000 years are the latest movement took place at about 4,400±1,900 years ago.

Table 6.1 TL dating results of quartz concentrates sediments for sample collected from the study area, Surat Thani and Phang Nga, Southern Thailand.

No.	Sample	U (ppm)	Th (ppm)	K (%)	Water Content (%)	Annualdose (mGy/yr.)	Paleo Dose(Gy)	Age (yrs)
1	TS1	1.66	14.20	0.41	8.47	1.99	22.07	11,100 ± 3,400
2	TS2	20.4	23.35	0.47	9.56	7.03	103.90	14,000 ±2,500
3	TS3	1.90	19.78	0.59	10.07	2.60	87.97	33,800 ±11,400
4	TS4	2.02	22.57	0.66	10.45	2.89	185.36	64,200±20,700
5	TS5	2.63	32.34	1.18	13.11	4.18	255.17	61,000±27,800
6	TS6	2.31	15.99	0.68	4.56	2.59	11.48	4,400±1,900
7	TS7	2.53	21.62	0.91	6.00	3.26	42.94	13,100 ±5,200
8	TS8	2.03	26.27	1.66	12.90	4.12	262.00	63,600 ±20,700
9	TS9	1.77	15.31	0.66	5.22	2.38	17.91	7,500 ±2,600
10	TS10	2.02	25.79	1.23	10.96	3.68	96.09	26,100 ±7,700
11	BL1	2.01	7.91	2.43	3.07	3.74	131.61	35,100 ±4,800
12	BL2	1.75	5.97	2.03	0.66	3.15	280.63	88,900 ±9,100
13	BL3	1.08	5.89	2.08	1.46	3.03	143.34	47,300 ±5,300
14	BL4	1.61	7.27	1.96	6.00	3.09	197.23	63,900 ±6,200
15	BL5	2.76	9.80	2.33	5.64	3.92	907.31	231,300 ±29,400
16	BL6	2.24	10.03	2.10	5.50	3.58	322.04	89,900 ±13,000
17	BL7	2.39	9.74	2.27	8.26	3.73	414.56	111,000±14,200
18	BL8	2.99	7.53	2.20	2.94	3.72	120.03	32,300±6,000

TS = Thung Sri Ngam   BL = Ban Bang Luek

Table 6.2 OSL dating results of quartz concentrates sediments for sample collected from the study area, Surat Thani, Southern Thailand.

No.	Sample	Annual dose (mGr/yr.)	Paleodose (Gy)	Age (yrs)
1	BL6	3.58	16.47	4,600±1,400
2	BL7	3.73	18.27	4,900±1,200
3	BL8	3.72	17.85	4,800±1,100

BL = Ban Bang Luek

BAN BANG LUEK TRENCH LOGGING

SOUTHWEST WALL

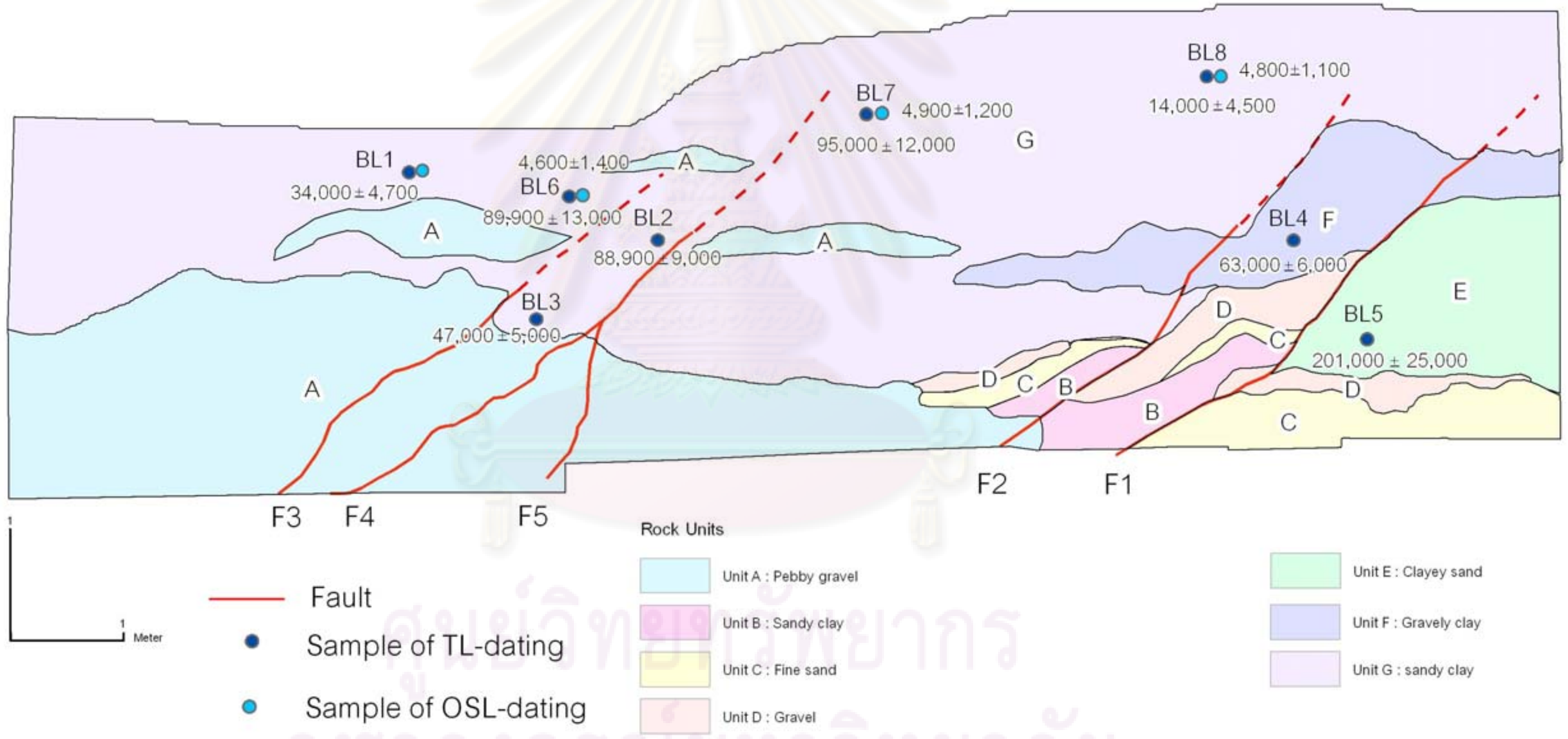

Figure 6.10 Trench-log stratigraphy showing faults orientation ,TL and OSL ages of sedimentary layers, on southwest wall, Ban Bang Luek trench.

179

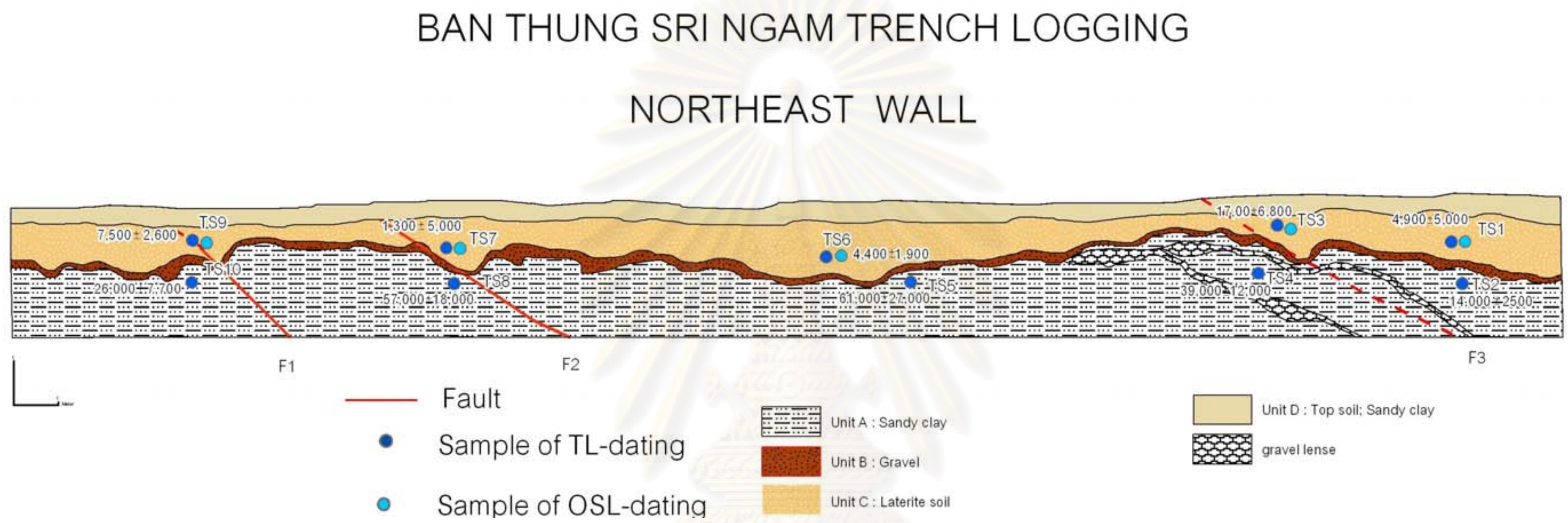

Figure 6.11 Trench-log stratigraphy showing faults orientation ,TL and OSL ages of sedimentary layers, on northeast wall, Ban Thung Sri Ngam trench.

.

Chapter VII
Discussion

In this chapter, a main point is made on the discussion related to the the results from current paleoseismic investigations along with the existing previous works. The discussion compose of characteristic of the Khlong Marui Fault zone, geomorphic features, maximum paleoearthquake magnitudes, their ages and slip rate, recurrence interval and evolution of active fault.

7.1 Characteristics of the KMF

Garson et al. (1970) stated that the sinistral displacement is due to transform faults related to the development of the Andaman/Nicobar and Sumatra/Java island arc, and the mega movement took place in late Jurassic to early Cretaceous times. These are the major northeast-trending faults (the Klong Marui-KMF and the Ranong Fault-RF) cut across Thai Peninsula. These two faults are located to the south of the other two major faults which are the Three Pagoda (TPF) and Mae Ping Faults in western Thailand. Both RF and KMF faults orientates about 100^0 to the TPF and MPF and act as the conjugate fault set (Lacassin et al., 1997; Tapponnier et al., 1986). Due to the remote-sensing and paleoseismic trenching informations from this study it reveals that the KMF is the strike-slip fault with the high dip angle (>50^o), corresponding to those reported by Watkinson et al. (2008) and Kanchanapayon (2009) is It consists of twelve fault segments. The studied fault and shows sinistral sense of movement. The left lateral movement is well observed at Khao Phanom, Phang –Nga and Surat Thani of Khlong Marui segment, Phang Nga segment and Phanom segments are located. The results indicate that the KMF also show its near vertical movement in both normal and reverse senses. It is likely that in the trenches, the reverse fault are much more common.

Smith and Arabasz (1991) also considered that seismic sources may have been occurred along the faults. However, as shown in Figure 7.1, base upon the epicentral distribution (Thailand Meteorological Department, 2008 and USGS) in the study as well

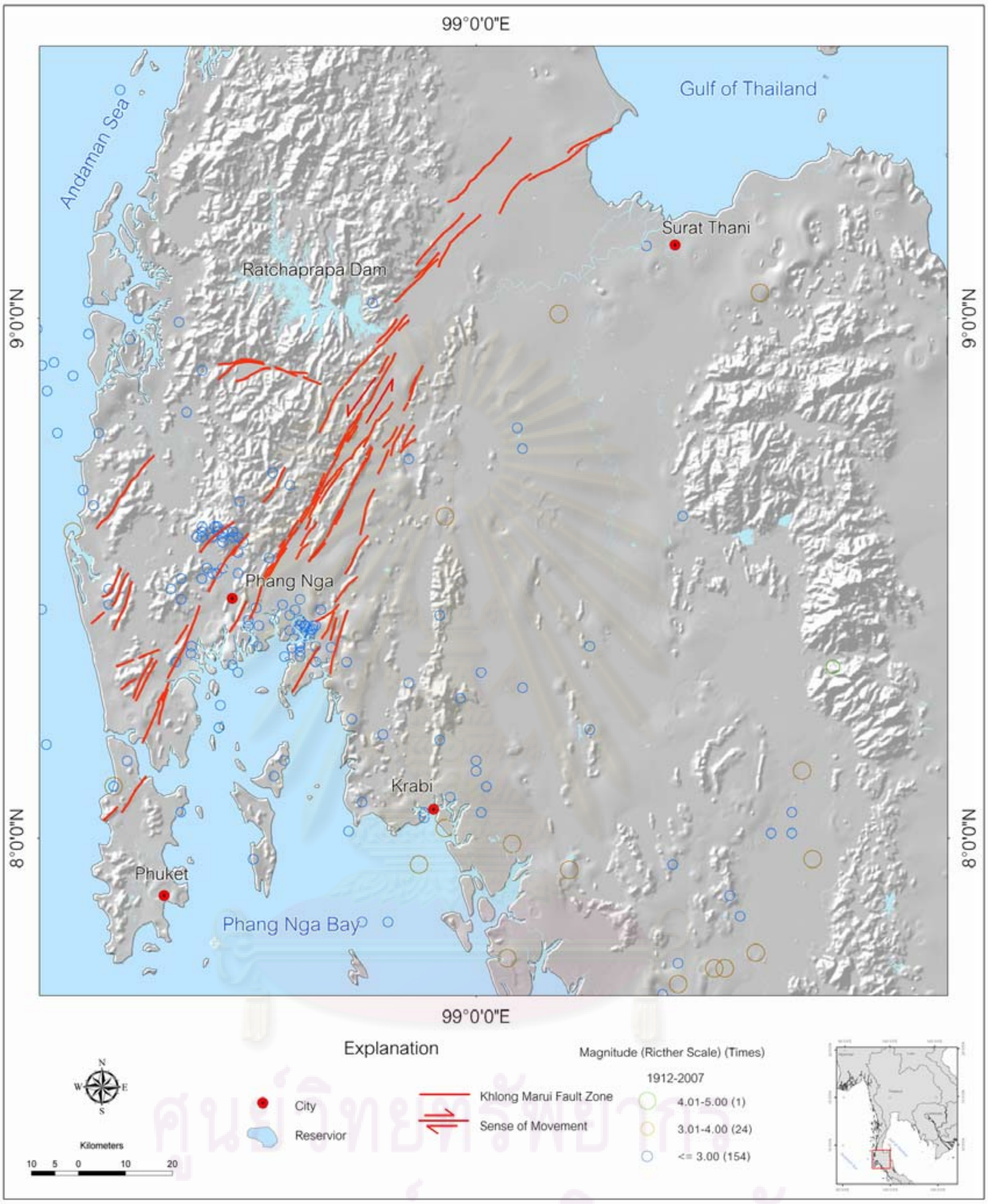

Figure 7.1 Hill shade map of study area and adjacent area showing epicentral distribution from 1912 to 2007, (Data from Thai Meteorological Department, 2007 and http//neic.usgs.gov/neis/epic/epic_global.html, 2007).

as the nearby areas, around the Khlong Marui Fault, only of about 179 earthquake events are detected instrumentally and they are mainly present in the Andaman Sea. It is also interesting that there is no large earthquake occurring in the study area and that if the epicenters shown in Fig. 7.1 are accurate, then the Khlong Marui Faults can be traced into the sea. Therefore, it is also anticipated herein that in-coming, intermediate earthquakes may happen in the future.

7.2 Geomophic Features and Paleoearthquake Magnitudes

Department of Mineral Resource (2007) used the tectonic geomorphology in the RF and KMF and showed that then 2 fault are active faults. They found that the trend of all fault segments were in northeast direction. However no northwest or another direction been reported for the fault segment.

In this study, not only the detailed morphotectonic evidence was reported for active fault investigation, but also evidence deduced from geomorphic indices are provided. This study shows that the 150 km-long active fault has been found on land. Moreover, as shown in Figure 7.2, there are 12 fault segments observed in the current study. Almost segments are confirmed by several places of morphotectonic evidences in the northeast-southwest trend. Although there are a number of faults trending approximately northwest-southeast, along only one of these, the Khlong Sok fault segment, is an evidence of the appreciable movement.

Well and Coppersmith (1994) reported the relationship between surface rupture length (SRL) along the active faults and the paleoearthquake magnitudes. They also found that the vertical slips are related to the earthquake magnitude. The SRL can be used to calculate the maximum credible earthquake (MCA). These relationships lead them to propose the empirical equations (7.1, 7.2, 7.3 and 7.4) as shown below.

M = 5.08 + 1.16 log (SRL) ………………………………(7.1)*

M = 5.16 + 1.12 log (SRL) ………………………………(7.2)**

M = 6.93 + 0.82 log (AD) ……………………………… (7.3)***

M = 6.61 + 0.71 log (MD) …………… …………….. (7.4)****

Whereas:

M = moment magnitude;

SRL = surface rupture length;

MD = maximum displacement;

AD = average displacement

* Equation for all fault type;

** Equation for strike-slip fault; and

*** Equation for normal fault.

**** Equation for normal fault

The surface rupture lengths are deduced from measurement base upon both field and remote-sensing data. The average displacements (AD) are from the average of the stream offset and are estimated from geodetic surveys and remote-sensing interpretation. As stated in chapter IV, there are about 16 fault segments in the study area. In order to receive reliable results, the present study preferably applied only the equation using surface rupture length (SRL). Following are the the paleoearthquake magnitude calculated fromIequation (7.1) and as shown as a graph in Figure 7.3.

1) Khlonf Haing fault segment has surface rupture length (SRL) of about 22.5 km, it reveals estimated magnitudes of 6.67 on the Richter scale.

2) Tha Chang fault segment has surface rupture length (SRL) of about 23 km, it reveals estimated magnitudes of 6.68 on the Richter scale.

3) Vibhavadi fault segment has surface rupture length (SRL) of about 27.5 km, it reveals estimated magnitudes of 6.77 on the Richter scale.

4) Khlong sok fault segment has surface rupture length (SRL) of about 23.3 km, it reveals estimated magnitudes of 6.69 on the Richter scale.

5) Khao Na Dang fault segment has surface rupture length (SRL) of about 15.8 km, it reveals estimated magnitudes of 6.50 on the Richter scale.

6) Khao Wong fault segment has surface rupture length (SRL) of about 14.4 km, it reveals estimated magnitudes of 6.45 on the Richter scale.

7) Khao Paeng fault segment has surface rupture length (SRL) of about 10.1 km, it reveals estimated magnitudes of 6.28 on the Richter scale.

8) Khao Hua Sing fault segment has surface rupture length (SRL) of about 18.2 km, it reveals estimated magnitudes of 6.57 on the Richter scale.

9) Ao Luek fault segment has surface rupture length (SRL) of about 26.2 km, it reveals estimated magnitudes of 6.74 on the Richter scale.

10) Khao Phanom fault segment has surface rupture length (SRL) of about 28.1 km, it reveals estimated magnitudes of 6.78 on the Richter scale.

11) Khlong Haek fault segment has surface rupture length (SRL) of about 35.2 km, it reveals estimated magnitudes of 6.89 on the Richter scale.

12) The longest surface rupture length (SRL) is the Khlong Marui fault segment which is about 54.8 km long. So the SRL of Khlong Marui segment gives the paleomagnitude equivalent to 7.10 M.

13) Plai Phanom fault segment has surface rupture length (SRL) of about 15.1 km, it reveals estimated magnitudes of 6.48 on the Richter scale.

14) Phang Nga fault segment has surface rupture length (SRL) of about 31.8 km, it reveals estimated magnitudes of 6.84 on the Richter scale.

15) Tai Maung fault segment has surface rupture length (SRL) of about 13.4 km, it reveals estimated magnitudes of 6.42 on the Richter scale.

16) Pakong fault segment has surface rupture length (SRL) of about 24 km, it reveals estimated magnitudes of 6.70 on the Richter scale.

Table 7.1and Figure 7.2 summarize the individual paleoearthquake magnitudes that are considered to have occurred for each fault segment.

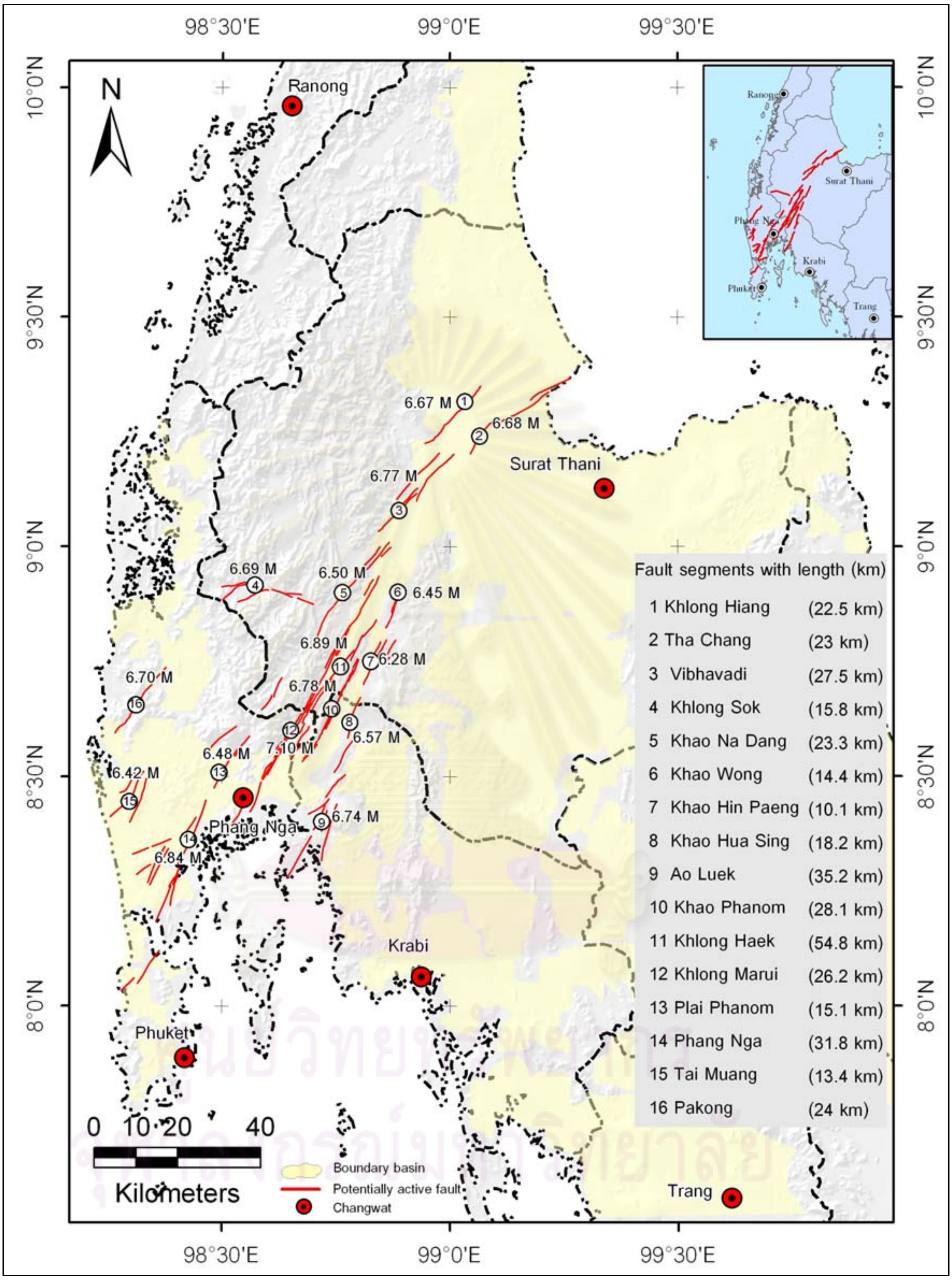

Figure 7.2 Map showing active fault segments, their length and estimated maximum cridible earthquakes of paleomagnitudes of The Khlong Marui Fault Zone.

Table 7.1 Paleoearthquake magnitudes of the KMF in southern Thailand, estimation from Well & Coppersmith (1994).

No.	Fault segment	Surface rupture length (SRL,km)	Moment magnitude (Mw)
1	Khlong Haing	22.5	6.67
2	Tha Chang	23.0	6.68
3	Vibhavadi	27.5	6.77
4	Khlong Sok	23.3	6.69
5	Khao Na Dang	15.8	6.50
6	Khao Wong	14.4	6.8
7	Khao Hin Paeng	10.1	6.57
8	Khao Hua Sing	18.2	6.74
9	Ao Luek	26.2	6.74
10	Khao Phanom	28.1	6.78
11	Khlong Haek	35.2	6.89
12	Khlong marui	54.8	7.10
13	Plai Phanom	15.1	6.48
14	Phang Nga	31.8	6.84
15	Tai Maung	13.4	6.42
16	Pakong	24.0	6.70

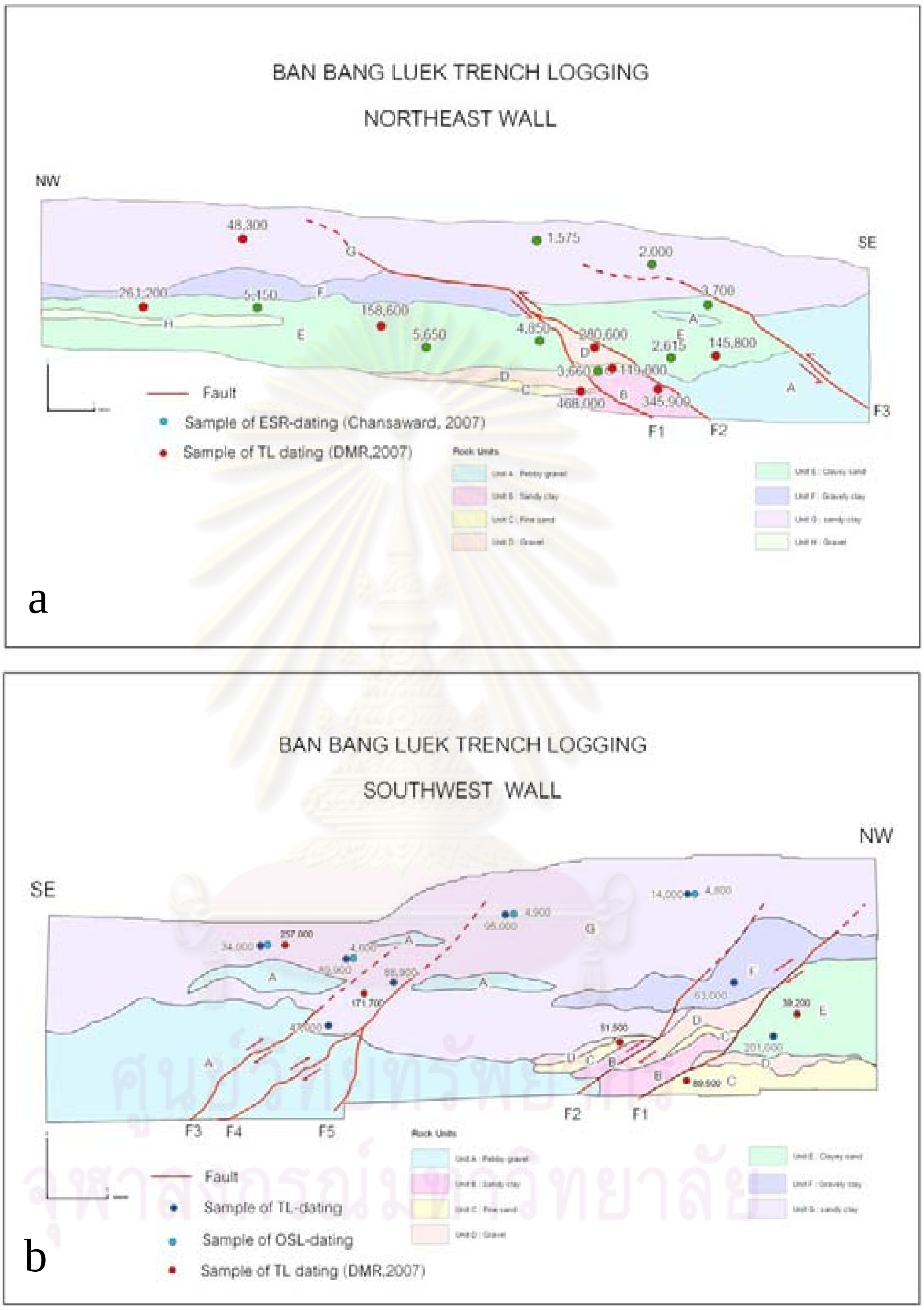

Figure 7.3 Trench log section at the (a) northeast and (b) southwest wall of Ban Bang Luek, Surat Thani showing principle stratigraphy and TL & OSL ages of this study, TL ages of Department of Mineral Resource (2007) and ESR ages of Chansaward (2007).

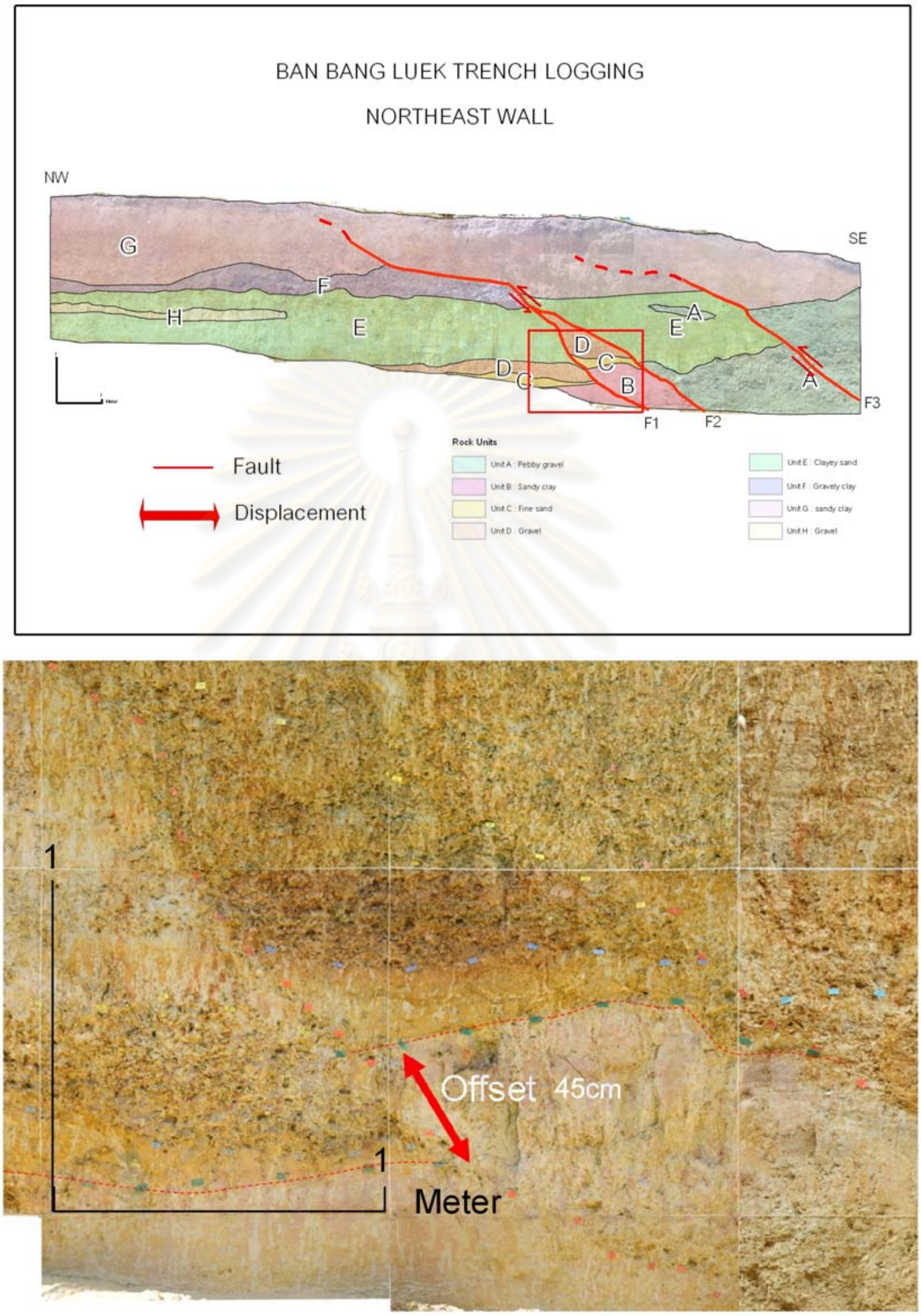

Figure 7.4 Trench log section at the northeast wall of Ban Bang Luek showing structure of reverse-fault and clearly offset of Unit b which displacement approximately 40 cm.

7.3 Age, Slip Rates and Recurrence Interval

Detailed discussion of individual faulting events are discussed below.

The earliest faulting of the Khlong Marui Fault Zones may have taken place at about 12,700 years age based on the offset sedimentary layers and the TL dating methods from Ban Nong Tao area, (Royal Irrigation Department, 2008) which placed on Ao Luek segment of Khlong Marui Fault Zone.

The next faulting occurred at about 9,400 to 10,000 yrs based on the results of exploratory trench at Ban Bang Woe area by TL dating. (Department of mineral resource, 2007) Because they suggest that the fault also cut across and partly disturbed the unit C, which underlain by the 9,000 yrs of unit D in the southeastern wall.

The third faulting of the Khlong Marui Fault Zones took place at about 8,300 years age based on the trench log and the TL dating methods from Ban Don Chan area, (Royal Irrigation Department, 2008) which placed on Pakong segment of Khlong Marui Fault Zone.

The forth faulting occurred at about 7,500 yrs base of the result of open wall at Ban Thung Sri Ngam school, Phang Nga. The Faults F1 cut through and disturbed the layer bottom of unit C. However, the fault did not cut the upper of unit C and bottom of unit C was dated by TL method to be about 7,500 yrs that represent of the approximately fault ages.

The fifth faulting along the Khlong Marui Fault Zone took place at about 5,000 yrs based on exploratory trench at Ban Bang Luek (this study), Vibhavadi trend (Department of Mineral Resources, 2007), Ban Nong Tao and Ban Don Chan trench area (Royal Irrigation Department, 2008). Because these four areas are nearby to each other, so the faulting is considered to be the same event. Beside the above trenching area was located into Khlong Marui, Vibhavadi, Ao Luek and Pa Kong segments, respectively. For Ban Bang Luek the fault cut through unit F and lower part of unit G. However the fault did not cut the upper part of unit G which was dated by OSL method to be about 4,900 yrs. For another trenches, the Fault age were considered based on TL method to be about 4,700, 4,600, and 4,400 years.

The early faulting of The Khlong Marui Fault Zones took place at about 2,700 – 3,000 yrs ago. Faulting of this event by C-14 AMS dating occurred at least 2 places, namely the Khlong Marui segment at Ban Bang Luek and Ban Bang Luek2. At Ban Bang Luek at least 3 faults was recognized, one fault (F1 and F3 in Fig. 7.3) cut through the gravel of Unit A. The overlying unit (Unit E) was also truncated, the ESR age of this unit is about 2,600 yrs. The unit underlying the Unit A which was also cut through by the fault was dated by ESR to be about 3,600 years. So the date of this faulting event is estimated to be possibly at 3,000 yrs. Such faulting may have offset reversely the gravel layer of Unit B to be about 0.45 m vertically. Therefore we can estimate the slip rate to be about 0.43 mm/yr. At Ban Bang Luek2, the similar fault cut through the gravel layer of Unit B but not through the upper part of the Unit C silty clay sediment. Because the C-14 AMS dating date yield the age of the Unit C layer to be as young as 2,700 yrs.

The very early faulting of the Khlong Marui Fault Zones happened at between about 3,000 yrs to about 2,300 yrs ago. Active faults belonging to the Phanom segment have passed the trench site at Ban Kuan Sabai (Department of Mineral Resources, 2007). This top layer was dated using the C-14 AMS to be at 2,300 yrs.

The last faulting occurred at about 1,300 yrs base of the result of open wall at Ban Thung Sri Ngam school, Phang Nga. The Faults F3 cut through and disturbed the layer bottom of unit C. However, the fault did not cut the upper of unit C and bottom of unit C was dated by TL method to be about 1,300 yrs that represent of the approximately fault ages.

From the above discussion, a summary of earthquake events is shown in Table 7.2 and Figure 7.5. Based upon the above result of discussion with earlier dating data and this study, it can preliminary deduced that the recurrence interval for 7 Mw of the Khlong Marui Fault Zone is 2,000 yrs.

7.4 Neotectonic Evolution of The KMF

Our integrated result reveal that the northeast-southwest-trending KMF indicates its major sense of movement along its strikes with the sinistral displacement of about 30 km. However one can argue when such left-lateral movement occurred.

Based on the work of Watkinson et al. (2008) in the KMF and Ranong Fault using structural field and petrographic relations and geochronological synthesis, it is quite likely that during the Tertiary Period and shortly after the Indian-Asian collision at 52 Ma, The Ranong and KMF served as the major and deep fault (see Figure 7.6 and Figure 2.3). They showed a sense of movement with the right lateral 250 km long, ductile displacement during 87 - 56 Ma. They also showed the such movement in the NNE to NE trends , which may have occurred at least 4 times. Sense of movement became reversed in Quaternary to late Tertiary Period after 52 Ma. Their field and petrographic evidence strongly indicate that the brittle deformation may have occurred during 23 Ma.

Our TL and OSL age-dating data also indicate that the strike slip movement with the sinistral offset may have occurred before 231,000 yrs. Such lateral movement occurred simultaneous with a vertical movement as shown by a slip in the paleoseismic trench at Ban Bang Luek. Our age dating data from the trenches were also confirmed by the work of Department of Mineral Resources (2007) and Royal Irrigation Department (2008).

Our result also illustrate that there are many times of displacement during Quaternary as shown in Table 7.1. Locations of hot springs and sinkhole also provide the good supporting evidence for such neotectonic processes. Such the neotectonic activity, the epicentral distribution, as well as the present-day movement along the KMF by GPS measurement (Tingay ,2010), all point to the fact that the KMF is still active till present with the major component of motive in the sinistral sense. However as quoted by Watkinson et al. (2008), the sense of movement may have been largely higher in the Tertiary Period than the present.

Table7.2 Earthquake Events in study area

Event	Khlong Marui segment (Phap Put, DMR)	Vibhavadi segment (Keim Poe, DMR)	Phanom segment (Song Prak, DMR)	Ao Luek segment (Khlong Suk, RID)	Pa Kong segment (Lum Rhoe, RID)
	1,300 yr[8]				
1	3,000 yr[6]		2,300 yr[7]		
2	4,900 yr[5]	4,700 yr[5]		4,600 yr[5]	4,400 yr[5]
3	7,500 yr[4]				8,300 yr[3]
4	9,400 yr[2]			12,700 yr[1]	

This study

DMR, 2007

RID, 2008

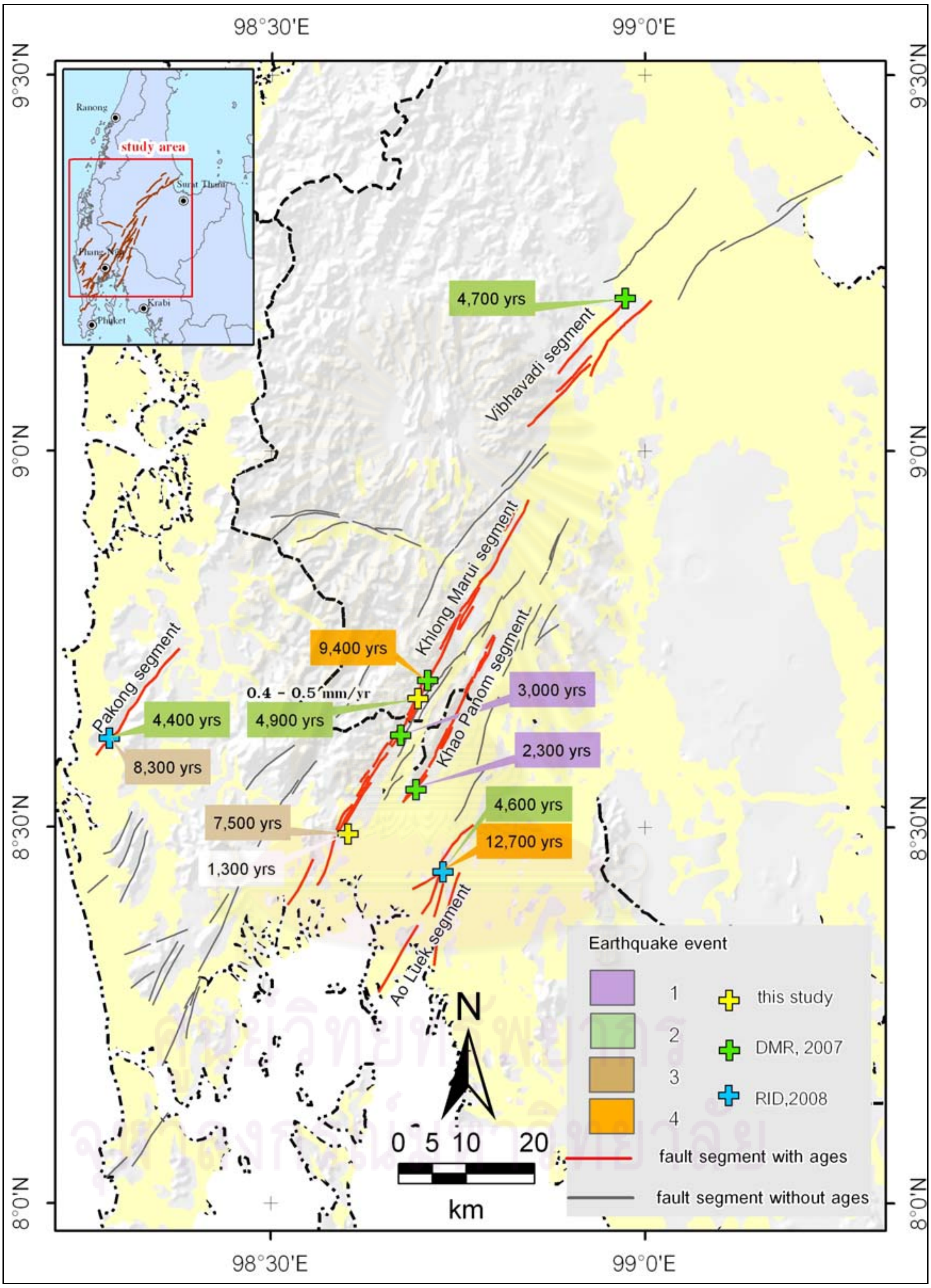

Figrure 7.5 Acitve fault map of the KMF showing the major period of paleoearthquakes and the slip rate of Khlong Marui fault segment. Noted that the red line indicates the segments with trenching data support.

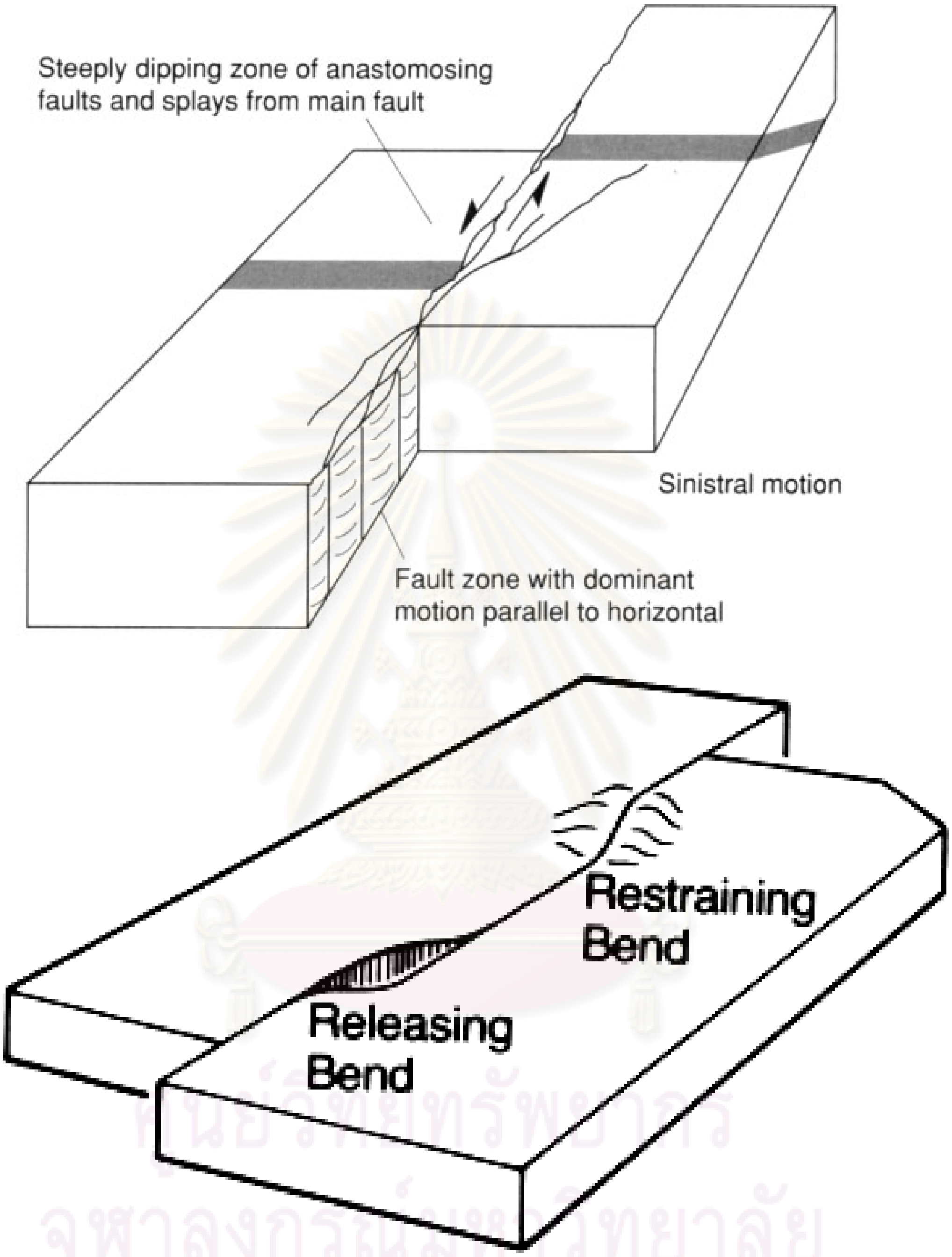

Figure 7.6 Geometry and anatomy of strike-slip fault showing releasing bend and restraining bend, which help in explaining evolution of Sinistral movement of the Khlong Marui Fault Zone (Crowell, 1974).

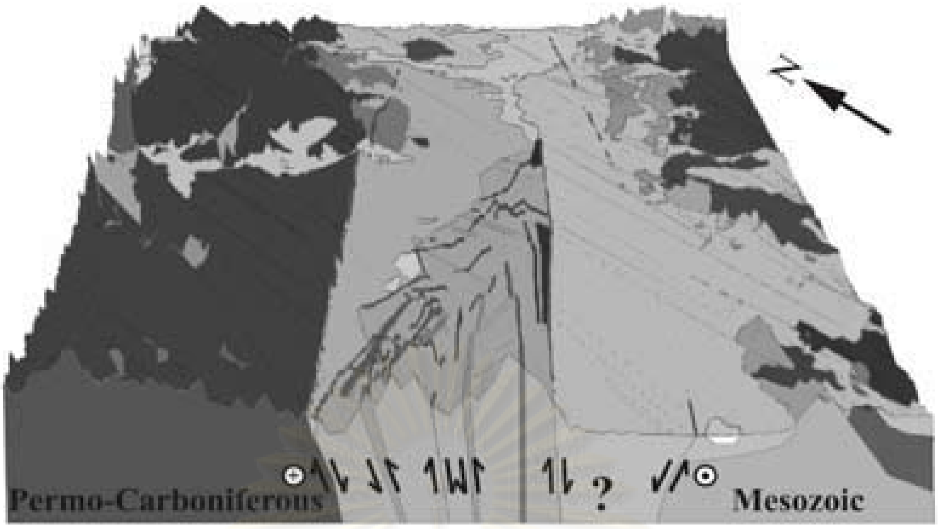

(a)

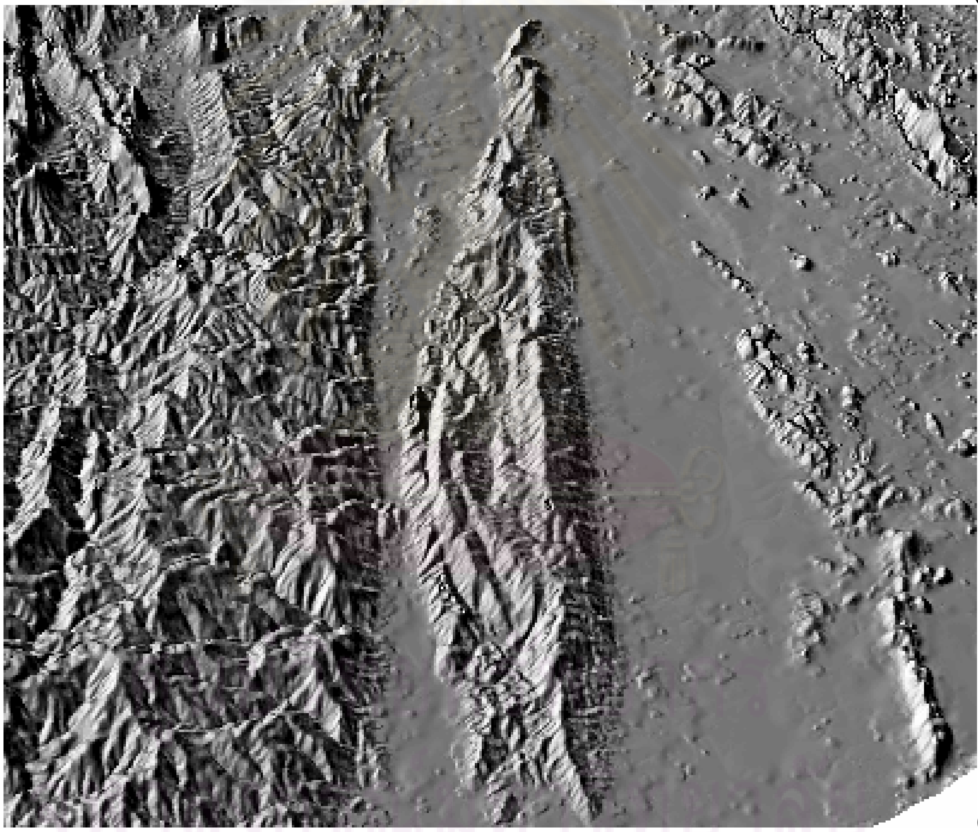

(b)

Figure 7.7 Hypothetical structure showing (a) schematic positive flower structure of Klong Marui shear zone in between Permo-Carbon iferous and Mesozoic sedimentary units.(Kanyanapayon et al., 2008) and (b) 3D model of DEM from topographic map in same area.

CHAPTER VIII
CONCLUSIONS

Based on the results of remote-sensing interpretation (Landsat 7 ETM^{+}, SRTM DEM and aerial photograph) integrated with ground-truth investigation, detailed topographic survey as well as those of TL-dating of fault related sediments, and fault evolution of KMF, southern Thailand, the conclusions can be drawn as the followings;

1) Khlong Marui Fault Zone is the northeast to north-northeast trending, 180 km-long fault extending from Phuket to Surat Thai, and perhaps extended both side to the Gulf of Thailand and Andaman Sea.

2) Lineaments belong to the Khlong Marui Fault Zone orientated in the northeast – southwest and northwest – southeast directions. The major trends of lineaments are the northeast – southwest directions and are regarded as a major fault zone.

3) The Khlong Marui Fault Zone can be divided, based on discontinuity criteria, from north to south and east to west in to sixteen fault segments, viz, Khlong Hiang (22.5 km), Tha Chang (23.0 km), Vibhavadi (27.5 km), Khlong Sok (23.3), Khao Na Dang (15.8 km), Khao Wong (14.4 km), Khao Hin Paeng (10.1 km), Khao Hua Sing (18.2 km), Ao Luek (26.2 km), Khao Phanom (28.1 km), Khlong Haek (35.2 km), Khlong Marui (54.8 km), Plai Phanom (15.1 km), Phnag Nga (15.1 km), Tai Maung (13.4 km) and Pakong (24 km).

4) Significant and well-defined types of morphotectonic evidences are triangular facets, fault scarp, offset streams, shutter ridges, and linear valleys. They are well recognized along the Khlong Marui Fault zone, particularly where bed rock connects with the Cenozoic basins boundary.

5) Estimation from the surface rupture length of about 54.8 km, the Khlong Marui segment indicates that an earthquake may have occurred in this area with the maximum magnitude of 7.10 M. If calculate moment magnitude using vertical displacement (1.2 m) would be about 6.67 M. The fault show the left – lateral sense of movement at present with the slip rate of this fault segment is about 0.43 mm/yr.

6) Four major earthquakes with the paleoearthquake of about 6-7 M and they roughly occurred of about 10,000, 8,000, 5,000, and 3,000 years ago which the recurrence interval is around 2,000 years for The Khlong Marui Fault zone.

7) Based on classification of active fault as proposed by Charusiri et al., (2001), the Khlong Marui zone are classified as active following the definition. Additional data of historical and instrumentally earthquake records in southern Thailand and adjacent area also indicated that this area is tectonically active.

8) Based on kinematic hostory of KMF as suggested by Watkinson et al., (2008), ductile dextral strike-slip shear have develop during 87 – 56 Ma and became sinistral reverse oblique strike-slip shear after 52 Ma. In the contrast, they found that brittle dextral strike-slip shear at about 23 Ma.

9) However, at present-day sinistral movement along the studied fault is responsible for the development of the opening of Andaman sea, GPS spot reference data, displacement granite belts in south of Thailand and also seismic beach ball of the Ranong Fault Zone (perhaps the same mechanism as their of KMF).

Reference

Aitken, A. J. 1985. Thermoluminescence Dating. New York: Academic Press.

Aki, K. 1984. Asperities of Barrier on an Earthquake Fault and Strong Motion Prediction. Jour. Geophys. Res., 98: 681-698.

Albee. A. L. and Smith, J. L. 1966. Earthquake Characteristics and Fault Activity in Southern California. Engineering Geology in Southern California. Association of Engineering Geologists. Glendale, California. Los. Angeles Section Special Publication: 9-34.

Allen, C. R. 1986. Seismological and Paleoseismological Techniques of Research in Active Tectonics. In: Wallace, R. E. ed. In: Active Tectonics: Studies in Geophysics. Natl. Washington: DC Acad. Press.

Allen, C. R. Armand, F. Richter, C. F. and Nordquist, J. M. 1965. Relationship between Seismicity and Geologic Structure in the Southern California Region. Bulletin of the Seismological Society of America; 55, 4: 753-797.

Artyotha, W. 2007. Radon Gas Investigation along the Ranong and Khlong Mauri Faults, southern Thailand. Master's thesis, Department of nucleartecnology Faculty of Engineer Chulalongkorn University.

Barr, S. M. and Macdonal, A. S., 1979, Paleomagnetism age and geochemistry of the Denchai basalts, Northern Thailand, Earth Planet Science Letters, 46: 113-124.

Biddle, K. T. and Christie-Blick, N. 1985. Glossary-Strike-Slip Deformation, Basin Formation, and Sedimentation. In Biddle, K. T., and Christie-Blick, N. eds., Strike-Slip Deformation, Basin Formation and Sedimentation, pp.375–385. Tulsa :Spec. Pub. Soc. Econ. Paleont. Miner.

Bott, J. Wong, I. Prachuab, S. Wechbunthung, B. Hinthong, C. and S. Sarapirome. 1997. Contemporary seismicity in Northern Thailand and its tectonic implications, in Proceedings of the International Conference on Stratigraphy and Tectonic Evolution of Southeast Asia and the South Pacific, 453-464. Bangkok, Thailand.

Botter-Jenson, L.; McKeever, S.W.S. ; and Wintle, A.G. 2003. Optically Stimulated Luminescence Dosimetry. 1st ed. Netherland : ELSEVIER SCIENCE B.V.

Bull, W.B., and L.D. McFadden, 1977, Tectonic geomorphology north and south of the Garlock fault, California, in Geomorphology in arid regions, D.O. Doehring, editor, Proceeding 8th Annual Geomorphology Symposium, pp.115-137. Binghamton: State University New York.

Bunopas, S., 1981, Paleogeographic history of Western Thailand and adjacent parts of Southeast Asia - A plate tectonics interpretation, Doctoral dissertation, Victoria University of Wellington, New Zealand.

Capetta, H., Buffetaut, E. and Suteethorn, V., 1990, A new hypodont shark from the Lower Cretaceous of Thailand, Neues Jahrbuch for Geologie und Paleontologie, Monatshefte, 11: 659-666.

Carver, G. A. and McCalpin, J. P. 1996. Paleoseismology of Compression Tectonic Environment. In McCalpin, J. P. (ed.), Paleoseismology, New York: Academic Press.

Chansawad, P., 2007. ESR-dating Investigations of Sediments by Using Soil Along the Southern Part of Khlong Marui fault, Phang Nga Province, Southern Thailand, Department of Geology Faculty of Science Chulalongkorn University.

Charusiri, P. Daorerk, V. and Supajanya, T. 1996. Applications of Remote-Sensing Techniques to Geological Structures Related to Earthquakes and Earthquake-Prone Areas in Thailand and Neighbouring Areas. A Preliminary Study. Journal of Scientific Research. Chulalongkorn University, 21, 1: 14-38.

Charusiri, P. Daorerk, V. Kosuwan, K. Choowoing, M. 2004. Active Fault and Determination of Seismic Parameters Hutgyi Hydropower Project. Department of Geology, Faculty of Science, Chulalongkorn University submitted to Electricity Generating Authority of Thailand.

Charusiri, P. Kosuwan, S. Fenton, C. H. Tahashima, T. Won-in, K. and Udchachon, M. 2001. Thailand Active Fault Zones and Earthquake Analysis: A Preliminary Synthesis. Jour. Asia Earth Sci. (submitted for publication).

Charusiri, P., Kosuwan, K., Daorerk, V., Vajbunthoeng. B., and Khutaranon, S. 2000. Final Report on Earthquake in Thailand and Southeast Asia. Final Report Submitted to The Thailand Research Fund (TRF.) (in Thai).

Charusiri, P., Kosuwan, S., Imsamut, S. 1997. Tectonic Evolution of Thaialnd: From Bunopas (1981)'s to a new scenario. The International Conference on Stratigraphy and Tectonic Evolution of Southeast Asia and the South Pacific, pp. 436-452. 19-24 August, Bangkok: Department of Mineral Resources.

Charusiri, P. Takashima, I. Kosuwan, S. Won-in, Saithong, P. Saensrichan, W Khaowiset, K. Pailoplee, S. and Meetuwong, R. 2006. The Study of Mae Yom Active Fault, Keang Sua Ten, Amphoe Song, Changwat Phare. Department of Geology, Faculty of Science, Chulalongkorn University submitted to Department of Royal Irrigation. Ministry of Natural Resources and Environment. Bangkok.

Charusiri, P.; Daorerk, V.; and Supajanya, T. Applications of Remote-Sensing Techniques to Geological Structures Related to Earthquakes and Earthquake-Prone Areas in Thailand and Neighbouring Areas: A Preliminary Study. Journal of Scientific Research, 21, 1(1996) : 23-43.

Charusiri, P.; Kosuwan, S.; Lumjuan, A.; and Wechbunthung, B. Review of active faults and seismicity in Thailand. 1998. Proceedings of the Ninth Congress on Geology, Mineral, and Energy Resourses of Southeast Asia-GEOSEA'98 and IGCP 383, Malaysia:symposium, pp.653-665. 17-19 August 1998, Kuala Lumpur : Geological Society of Malaysia.

Christie-Blick, N. and Biddle, K. T. 1985. Deformation and Basin Deformation along Strike-Slip Fault. In: Biddle, K. T., and Christie-Blick, N. eds. Strike-SlipDeformation, Basin Formation, and Sedimentation, Society of Economic Paleontologists and Mineralogists, Spec. Pub. 37: 1-34.

Chuaviroj, S. 1991. Geotectonic of Thailand. Bangkok: Geological Survey Division, Department of Mineral Resources.

Cluff, L. S. and Bolt, B. A. 1969. Risk from Earthquake in the Modern Urban Environment with Special Emphasis on the San Francisco Bay Area, Urban Environmental Geology in the San Francisco Bay Region. In Association Engineering Geologist Sacramento, California: San Francisco Section Special Public: 25-64.

Daly, M. C. Cooper, M. A. Wilson, I. Smith, D. G. and Hooper, B. G. D. 1991. Cenozoic Plate Tectonics and Basin Evolution in Indonesia. Marine and Petroleum Geology. 8: 2-21.

Department of Mineral Resources. 1999. Geologic Map of Thailand 1: 1,000,000. Department of Mineral Resources. Bangkok (with English explanation).

Fenton, C. H. Charusiri, P. and Wood, S. H. 2003. Recent Paleoseismic Investigations in Northern and Western Thailand, Annals of Geophysics2003: 957-981.

Fenton, C. H. Charusiri, P. Hinthong, C. Lumjuan, A. and Mangkonkarn, B. 1997. Late Quaternary faulting in northern Thailand. Proceedings of the International Conference on Stratigraphy and Tectonic Evolution of Southeast Asia and the South Pacific, pp.436-452. August 1997, Department of Mineral Resources, Bangkok, Thailand.

Garson, M.S., Mitchell, A.H.G., 1970. Transform faulting in the Thai Peninsula. Nature 22, 45-47.

Garson, M.S., Young, B., Mitchell, A.H.G., and Tait, B.A.R., 1975. The geology of the tin belt in peninsular Thailand around Phuket, Phangnga and Takua Pa. London: Overseas Mem. Inst. Geol. Sci.

Gutenberg, B. andRichter, C. F., 1954, Seismic of the Earth and Associated Phenimena. New Jersey: Priceton University Press.

Hall, R. 1996. Reconstructing Cenozoic SE Asia. In: Hall, R. and Blundell, D. eds., Tectonic Evolution of Southeast Asia. Geological Society of London Special Publication 106: 153-184.

Hamblin, W.K. 1976. Patterns of displacement along the Wasatch Fault, Geology, 4: 619-622.

Hinthong, C. 1991. Role of tectonic setting in earthquake event in Thailand. In ASEAM-EC Workshop on Geology and Geophysics, pp.1-37. Jakarta, Indonesia.

Hinthong, C. 1995. The Study of Active Faults in Thailand. Proceedings of the Technical Conference on the Progression and Vision of Mineral Resources Development, pp.129-140. Department of Mineral Resources, Bangkok, Thailand.

Hinthong, C. 1997. The Study of Active Faults in Thailand. Report of EANHMP. An Approach to Natural Hazards in the Eastern Asia: 17-22.

Hobbs, W. H. 1972. Earth Features and Their Meaning. New York: Macmillan.

Hoke, L. and Campbell, H. J. 1995. Active mantle melting beneath Thailand?. Proceedings of the International Conference on Geology, Geotechnology, and Mineral Resources of Indochina, pp.13-22. Department of Geotechnology, Khon Kaen University, Khon Kaen, Thailand.

Huchon, P. LePichon, X. and Rangin, C. 1994. Indochina Peninsula and the collision of India and Eurasia. Geology, 22: 27-30.

International Atomic Energy Agency. 1988. Code on the Safety of Nuclear Power Plants: Siting, Code 50-C-S. IAEA. Vienna.

International Atomic Energy Agency. 1992. Code on the Safety of Nuclear Research Reactors: Design, Safety Series 35-S1. IAEA. Vienna.

Kanjanapayont, P., Grasemann, B., and Edwards, M.A., 2008. Deformation microstructures within the Klong Marui shear zone, southern Thailand. Proceeding of the International Symposium on Geoscience Resources and Environments of Asian Terranes (GREAT 2008), 4th IGCP 516, 5th APSEG, pp.116-121. November 24-26, 2008, Bangkok, Thailand,

Keawmaungmoon, S., Thipyopass, S. and Charusiri, P. 2009. Preliminary Geomorphic Indices Associated to Active Faults in Khao Phanom area, Surat Thani Province. Journal of Remote Sensing and GIS Association of Thailand, Vol.10 No.2 May-August 2009: 54 -62.

Keller, E. A. and Pinter, N. 1996. Active tectonics: Earthquake, uplift, and landscape, New Jersey: Prentice-Hall.

Knuepfer, P. L. K. 1989. Implications of the Characteristics of End-Points of HistoricalSurface Fault Ruptures for the Nature of Fault Segmentation. In Schwartz, D. P. and Sibson, R. H. (ed.), Fault Segmentation and Controls of Rupture Initiation and Termination, pp.89-315, 193-228. U.S.: Geological Surv.

Kosuwan, S. Saithong, P. Lumjuan. A. Takashima, I. and Charusiri, P. 1999. Preliminary Results of Studies on the Mae Ai Segment of the Mae Chan Fault Zone, Chiang Mai Northern Thailand. The CCOP Meeting on Exodynamic Geohazards in East and Southeast Asia, pp.1-8. July 14-16, Pattaya, Thailand.

Lacassin, R. Maluski. P. Leloup, P. H. Tapponnier, P. Hinthong, C. Siribhakdi, K. Chuavithit, S. and Charoenpravat, S. 1997. Tertiary Diachronic Extrusion and Deformation of western Indochina: Structural and 40Ar/39Ar evidence from NW Thailand. Journal of Geophysical Research, 102: 10013 -10037.

Lee, T. Y. and Lawver, L. A. 1995. Cenozoic plate reconstructions of Southeast Asia. Tectonophysics, 251: 85–138.

Loboonlert, P. 2007. Crustal Displacement after Earthquake in September 12th 2007, from August 1st to October 31th 2007, Using GPS Data at Phuket, Thailand. Department of Geology Chulalongkorn University.

Lorenzetti, E.A. Brennan, P.A. and Hook, S.C. 1994. Structural styles in rift basins: interpretation methodology and examples from Southeast Asia, Bull. Am. Assoc. Pet. Geol., 78, 1,152.

MaCalpin, J. P. 1996. Paleoseismology. California: Academic press.

Macdonald, A.S., Barr, S.M. Dunning, G.R. and Yaowanoiyothin, W. 1993. The Doi Inthanon metamorphic core complex in NW Thailand: age and tectonic significance, J. Southeast Asian Earth Sci., 8 (1-4), 117-125.

Matthews, S. J. Fraser, A. J. Lowe, S. Todd, S. P. and Peel, F. J. 1997. Structure, Stratigraphy and Petroleum Geology of the SE Nam Con Son Basin, Offshore Vietnam. In: Fraser, A. Matthews, S. Murphy, R. eds., Petroleum Geology of Southeast Asia. Geol. Soc. London, Spec. Publ., 126: 89–106.

Mccabe, R. Celaya, M. Cole, J. Han, H.C. OHNSTAD, T. PAIJITPRAPAPON, V. and Thitipawarn, V. 1988. Extension tectonics: the Neogene opening of the north-south trending basins of Central Thailand, J. Geophys. Res., 93, 11,899-11,910.

Mccabe, R. Harder, S. Cole, J.T. and Lumadyo, E. 1993. The use of paleomagnetic studies in understanding the complex Tertiary tectonic history of east and southeast Asia, J. Southeast Asian Earth Sci., 8 (1-4), 257-268.

Meesook, A., 2000, Cretaceous environments of Northeastern Thailand, in H. Okada and N.J. Mateer, eds. Cretaceous environment of Asia, Elesevier Science B.V.: 207-223

Ministry of Natural Resuorces and Environment, Department of Mineral Resources. 2007. Investigation on Recrrence Interval in Areas Showing Trace of Movement along the Faults in Prachuap Khiri Khan, Chumporn, Ranong, Surat Thani, Krabi, Phang Nga and Phuket Provinces (Ranong and Khlong Marui Faults). Bangkok: Environmetal Geology Division.

Molnar, P. and Deng, Q. 1984. Faulting Associated with Large Earthquake and the Average Rate of Deformation in Central and Eastern Asia. Journal of Geophysical Research, 89: 6,203-6,227.

Molnar, P. and Tapponnier, P. 1975. Cenozoic tectonics of Asia: effects of a continental collision. Science, 280: 419–426.

Ni, J. and York, J. E. 1978. Late Cenozoic Tectonics of the Tibetan Plateau. J. Geophys. Res., 83: 5,377-5,384.

Nutalaya, P. Sodsri, S. and Arnold, E. P. 1985. Series on Seismology-Volume II-Thailand. In Arnold, E. P (ed.), Southeast Asia Association of Seismology and Earthquake Engineering.

O' Leary, D. W. and Simson, S. L. 1977. Remote Sensing Application to Tectonism and Seismicity in the Northern Part of the Mississippi Embayment. J. Geophysics, 42, 3: 542-548.

O' Leary, D. W. Fridman, J. D. and Pohn, H. A. 1976. Lineament, Linear, Lineation: Some Proposed New Standards for Old Terms. Bull. Geol.soc.Am, 87: 1463-1469.

O'LEARY, J. and HILL, G. S. (1989): Tertiary basin development in the Southern Central Plains, Thailand. Proceedings of the International Symposium on Intermontaine Basins: Geology and Resources, pp. 254-264. Chiang Mai University, Chiang Mai, Thailand.

Packham, G. 1996. Cenozoic SE Asia: reconstructing its aggregation and reorganization. In: Hall R., and Blundell, D. J. eds., Tectonic Evolution of Southeast Asia, pp. 123-152. London: Geol. Soc.

Park, R. G. and Jaroszewski, W. 1994. Craton Tectonics, Stress and Seismicity. In: Hancock, P. L. ed., Continental Deformation, pp. 200-222. Oxford: Pergomon Press.

Peltzer, G. and Tapponnier, P. 1988. Formation and evolution of strike-slip faults, rifts, and basins during the India-Asia collision: an experimental approach, J. Geophys. Res., 93: 15,085-15,117.

Phillip, H. Pogozhin, E. Cisternas, A. Bousquet, J. C. Borison, B. and Karakhanian, A. 1992. The Armenian Earthquake of 1988 December7; Faulting and Folding, Neotectonics and Paleoseismicity. Geophys. Jour. Int, 110: 141-158.

Polachan, S. 1988. The Geological Evolution of the Mergui Basin, SE Andaman Sea, Thailand. Doctoral dissertation. Royal Holloway and Bedford New College, Univesity of London.

Polachan, S. and Satayarak, N. 1989. Strike-Slip Tectonics and the Development of Tertiary Basins in Thailand. Proceedings of the International Symposium on Intermountain Basin, Geology and Resources, pp.243-253. 30 Jan-2 Feb 1989, Chiang Mai, Thailand.

Polachan, S. Prадidtan, S. Tongtaow, C. Janmaha, S. Intrawijitr, K. and Sangsuwan, C. 1991. Development of Cenozoic basins in Thailand, Mar. Pet. Geol., 8: 84-97.

Rangin, C. Jolivet, L. and Pubellier, M. 1990. A Simple Model for the Tectonic Evolution of Southeast Asia and Indonesia Region for the past 43 m.y. Bulletin de la Société géologique de France, 8 VI: 889-905.

Remus, D. Webster, M. and Keawkan, K. 1993. Rift architecture and sedimentology of the Phetchabun intermontaine basin, Central Thailand, J. Southeast Asian Earth Sci., 8 (1-4): 421-432.

Rhodes, B. P. Perez, R. Lamjuan, A. and Kosuwan, S. 2002. Kinematics of the Mae Kuang Fault, Northern Thailand Basin and Range Province. The Symposium on Geology of Thailand, pp. 298-308. August 2002, Bangkok, Thailand.

Saithong, P. 2006. Characteristics of the Moei-Mae Ping Fault Zone, Changwat Tak, Northwestern, Thailand. Master's Thesis. Department of Geology Faculty of Science Chulalongkorn University.

Schwart, D. P. 1998. Geological Characterization of Seismic Sources: Moving into the 1990's. In J.L. von Thun (ed.), Earthquake Engineering & Soil Dynamics II Proceedings; 2, Recent Advances in Group Motion Evaluation, pp.1-42. Spec. Publ. Am. Soc. Civil Engineers Geotech 20.

Segall, D. and Pollard, D. D. 1980. Mechanics of Discontinuous Faults. J, Geophys, Res., 85: 4,337-4,350.

Siribhakdi, K. 1986. Seismicity of Thailand and Periphery. Geological Survey Division, Department of Mineral Resources Bangkok. In: Panitan Lukleunaprasit et al. Proceedings of the 1 st Workshop on Earthquake Engineering and Hazard Mitigation, pp.151-158. November 1986, Bangkok, Chulaongkorn University.

Smith, R.B. and Aabasz, W.J. 1991. Seismicity of the Intermountain Seismic Belt, in Neotectonics of North America, Geological Society of America Decade Map, vol. 1: 185-228.

Strandberg, C. H. 1967. Aerial Discovery Manual. New York: John Wiley & Son.

Sylvester, A. G. 1988. Strike-Slip Faults. Geol. Soc. Am. Bull., 100: 1666-1703.

Takashima, I. and Walanabe, K. 1994. Thermoluminescence Age Determination of Lava Flows/Domes and Collapsed Materials at Unzen Volcano, SW Japan. Bulletin of the Volcanological Society of Japan, 39: 1-12.

Tanaka, K. Hataya, R. Spooner, N. A. Questiaux, D. G. Saito, Y. and Hashimoto, T. 1997. Dating of Marine Terrace Sediments by ESR, TL and OSL Methods and their Applicabilities. Quaternary Science Reviews, 16: 257-264.

Tapponnier, P. Peltzer, G. and Armijo, R. 1986. On the Mechanics of Collision between India and Asia. In: Coward, M. P., and Ries, A. C. eds., Collision Tectonics. Journal of the Geological Society of London. Special Publication, 19: 115-157.

Tapponnier, P. Peltzer, G. Armijo, R. Le Dain, A. and Coobbold, P. 1982. Propagating Extrusion Tectonics in Asia: New insights from simple experiments with plasticine. Geology, 10: 611-616.

Thailand Meteorological Department. 2008. Earthquake Information Catalogue. Report of Thailand Meteorological Department. Bangkok (digital files and unpublished Maunscript).

U.S. Nuclear Regulatory Commission. 1982. Appendix A: Seismic and geologic sitting criteria for nuclear power plants. Code of Fed. Rogul. 10. Chap. 1, Part 100. 1 September, 1982: 549-559.

Weldon, R. J. McCalpin, J. P. and Rockwell, T. K. 1996. Paleoseismology of Strike-Slip Tectonic Environments. In: McCalpin, J. P. ed. Paleoseismology, pp.271-329. New York: Acad. Press.

Wells, D. L. and Coppersmith, K. J. 1994. New Empirical Relationships among Magnitude, Rupture Width, Rupture Area, and Surface Displacement. Bulletin of the Seismological Society of America, 84: 974-1002.

Wheeler, R. L. 1989. Persistent Segment Boundaries on Basin-Range Normal Faults. In: Stewartz D. P. and Sibson, R. H. eds., Fault Segmentation and Controls of Rupture Initiation and Termination, pp.432-444. U.S.: Geol. Surv.

Won-in, K. 1999. Neotectonic evidences along the Three Pagoda Fault Zone, Changwat Kanchanaburi. Master’s Thesis. Department of Geology Faculty of Science Chulalongkorn University.

Wood, H. O. 1915. California Earthquake, A Synthetic Study of Recorded Shocks. Bulletin of the Seismilogical Society of America, 6: 54-196.

Appendix

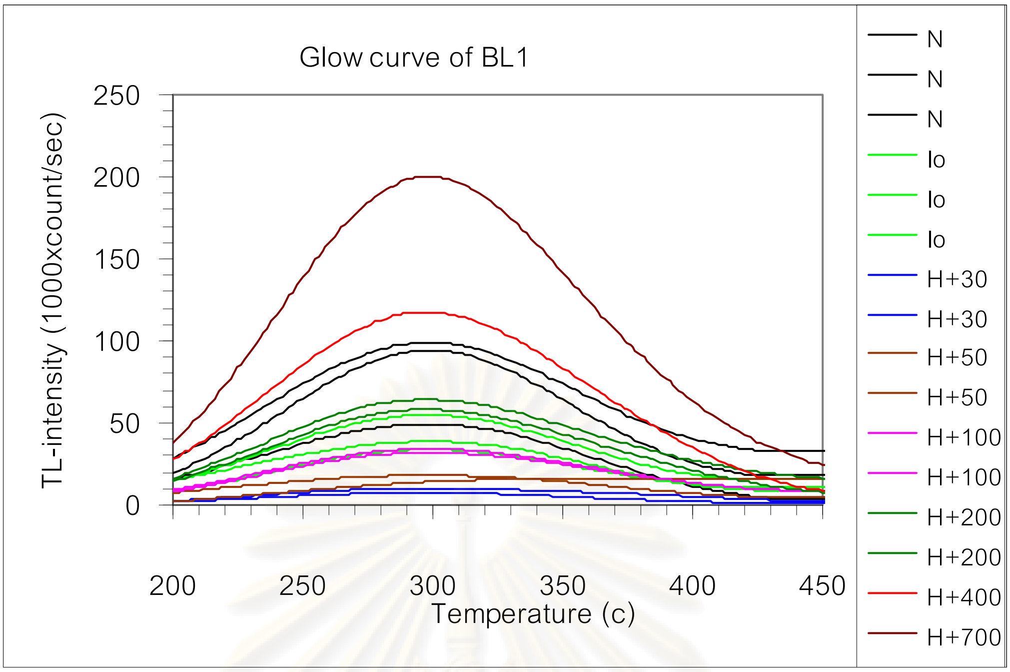

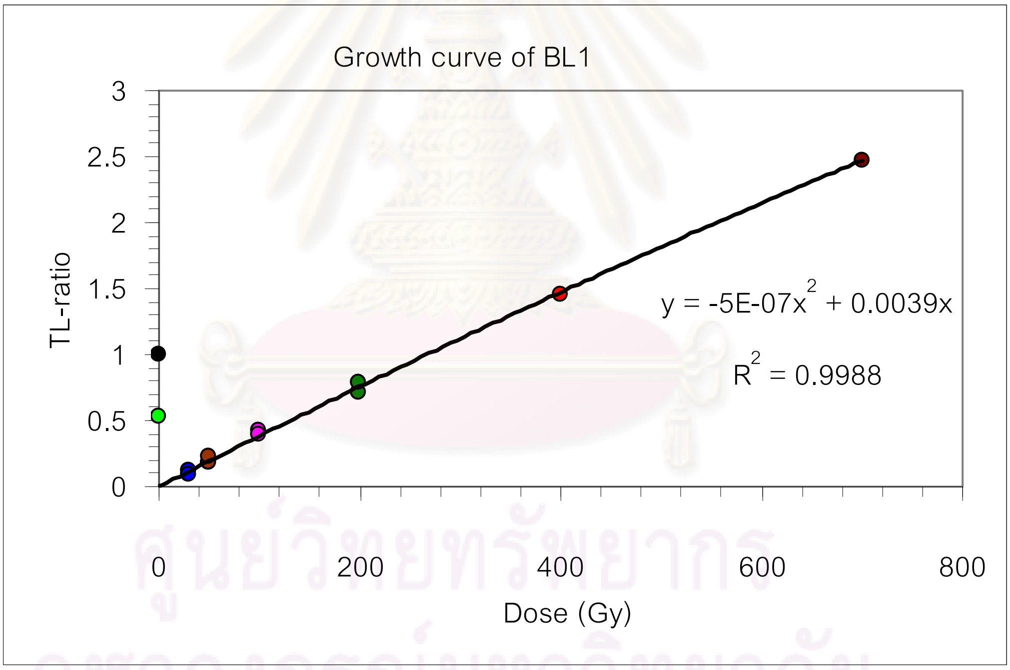

Sample No. BL 1

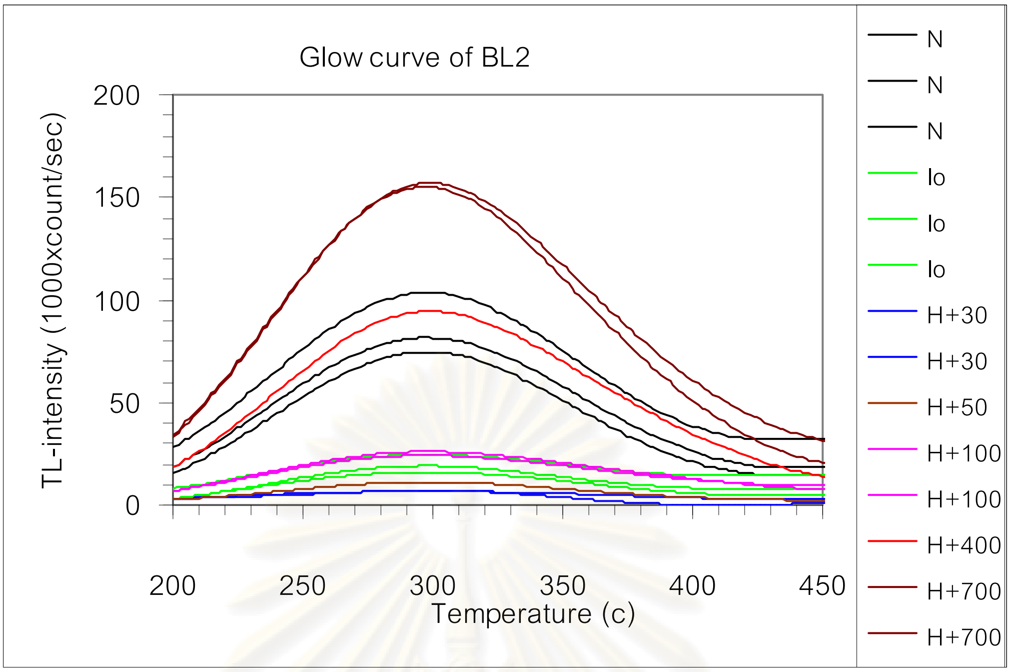

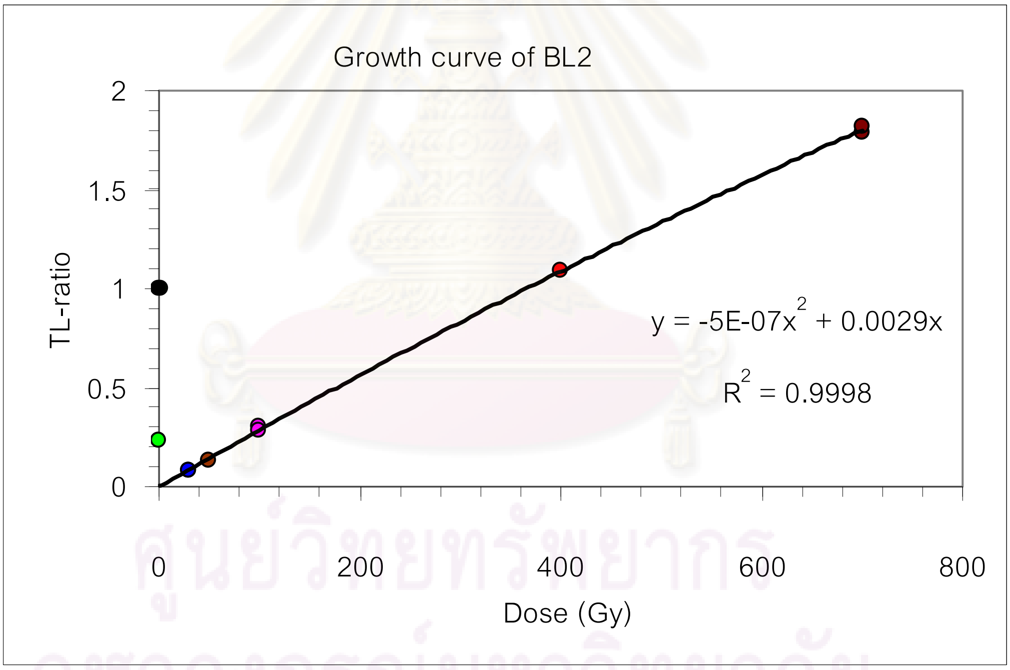

Sample No. BL 2

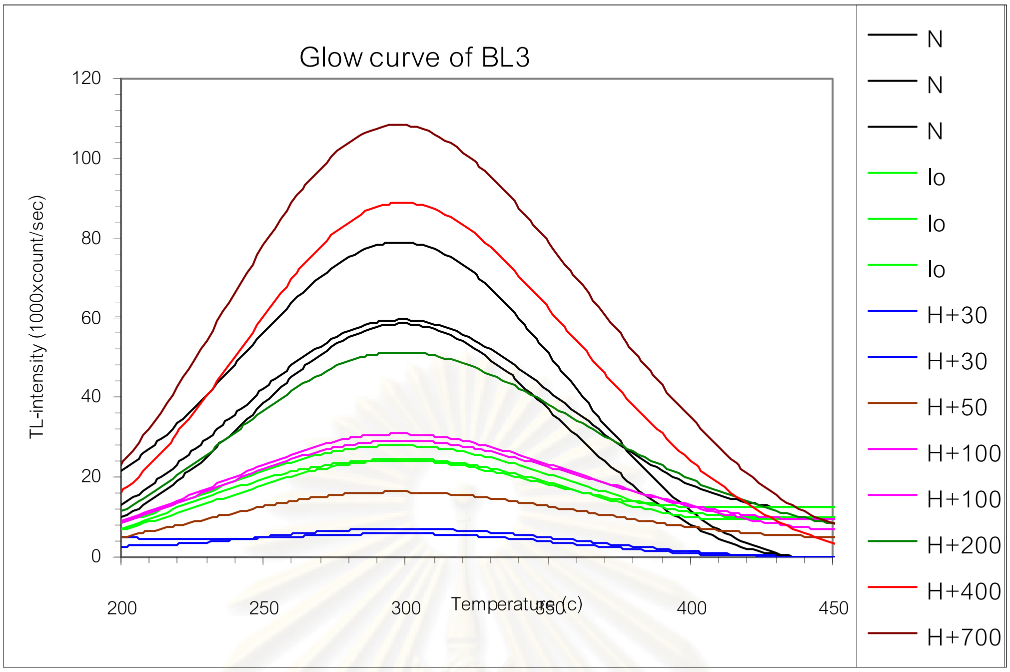

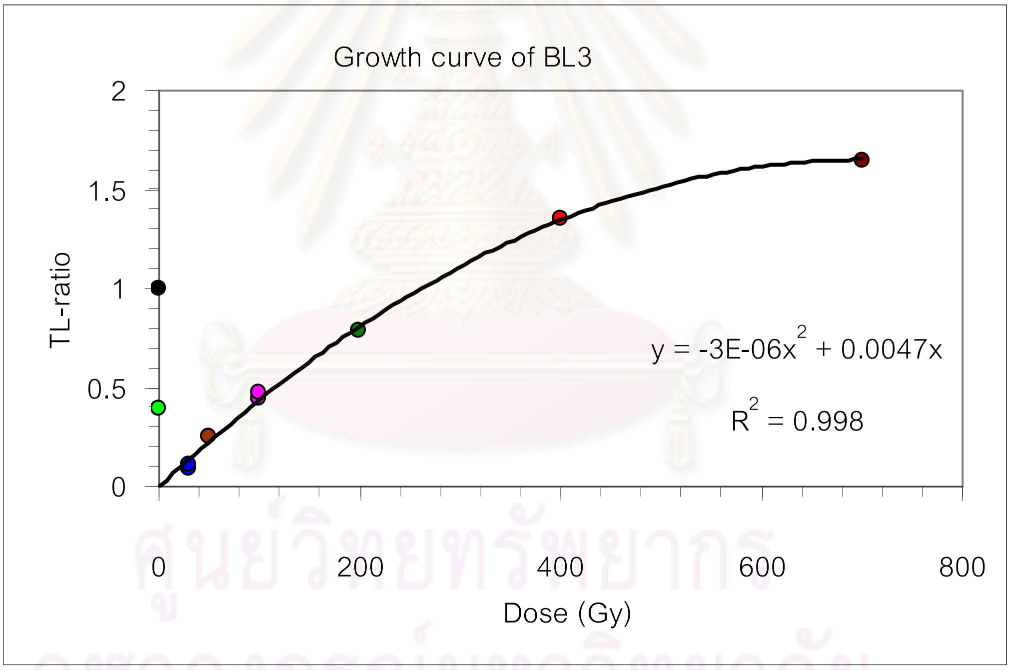

Sample No. BL 3

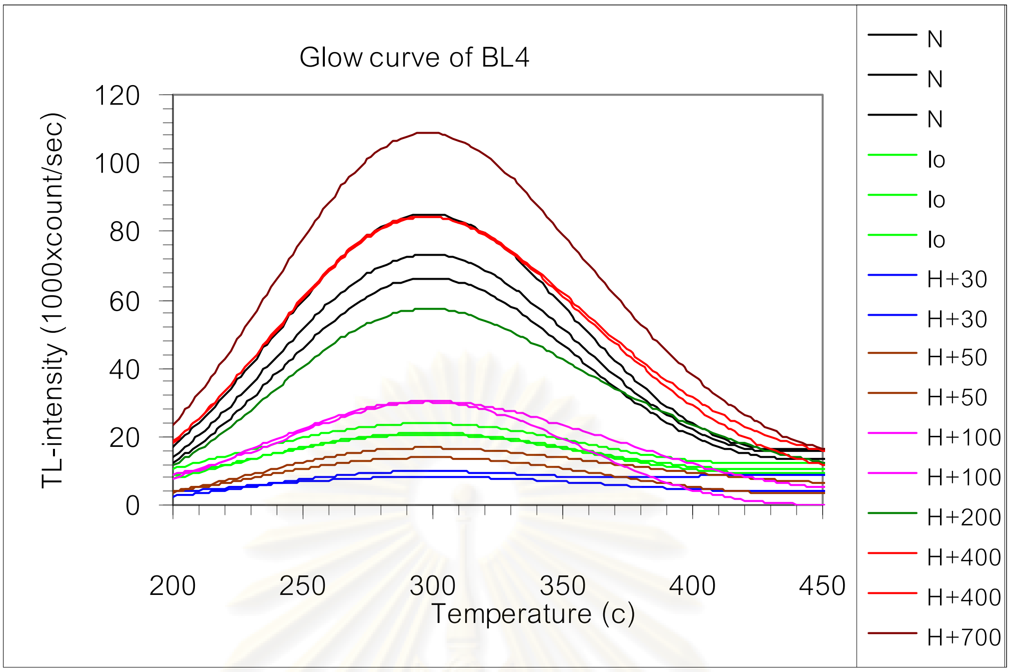

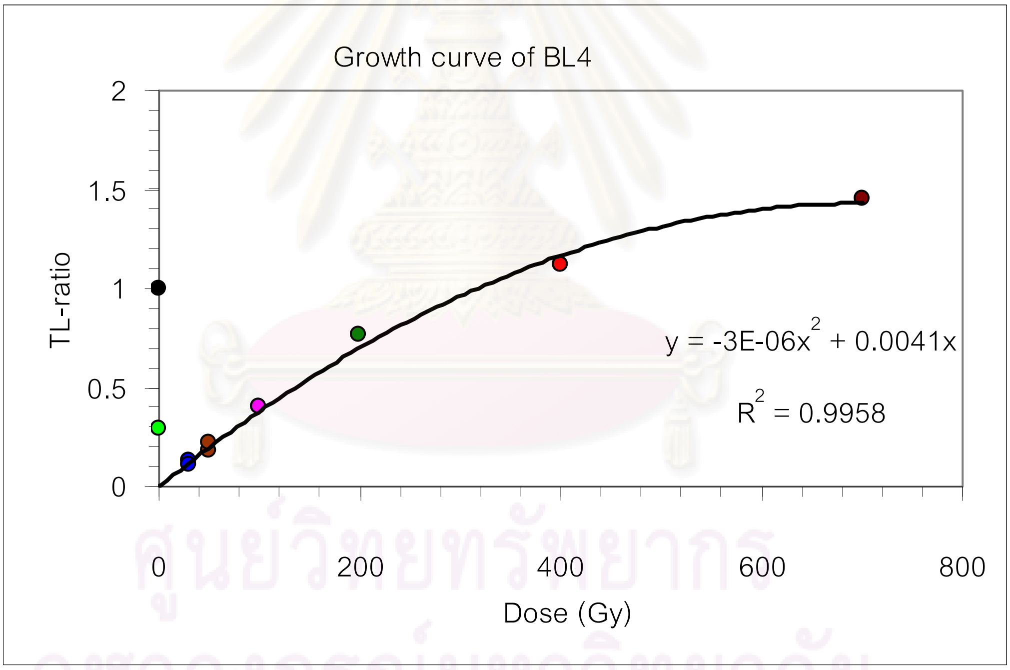

Sample No. BL 4

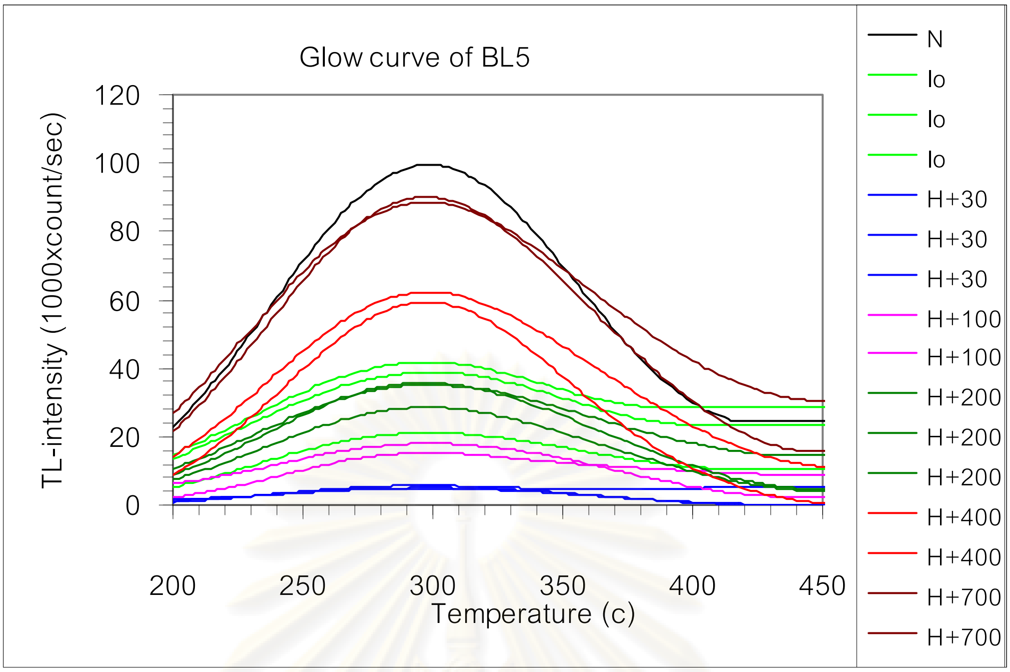

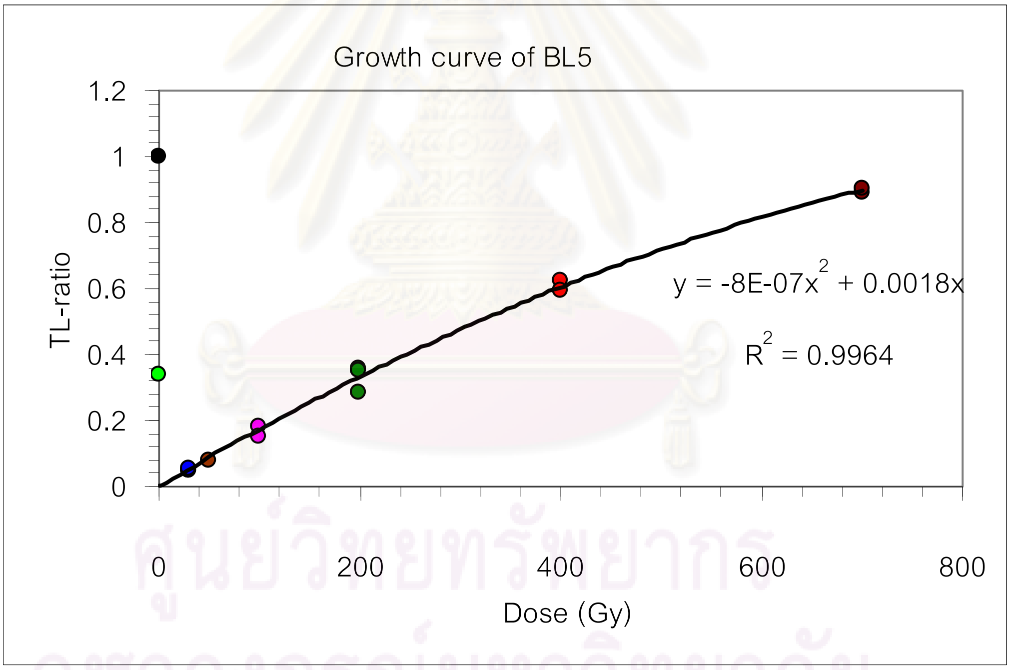

Sample No. BL 5

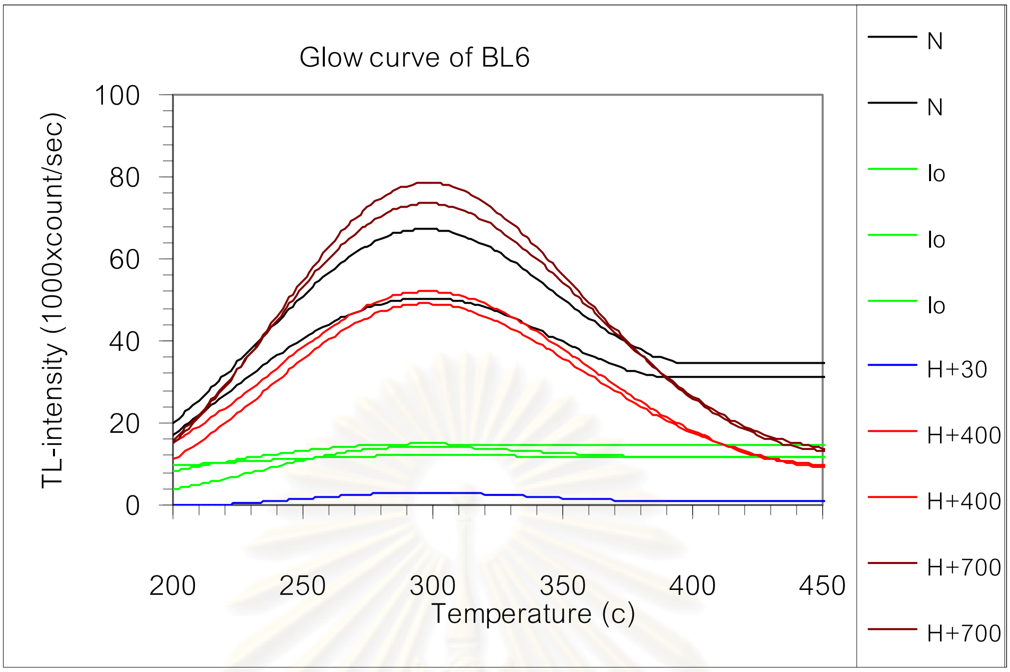

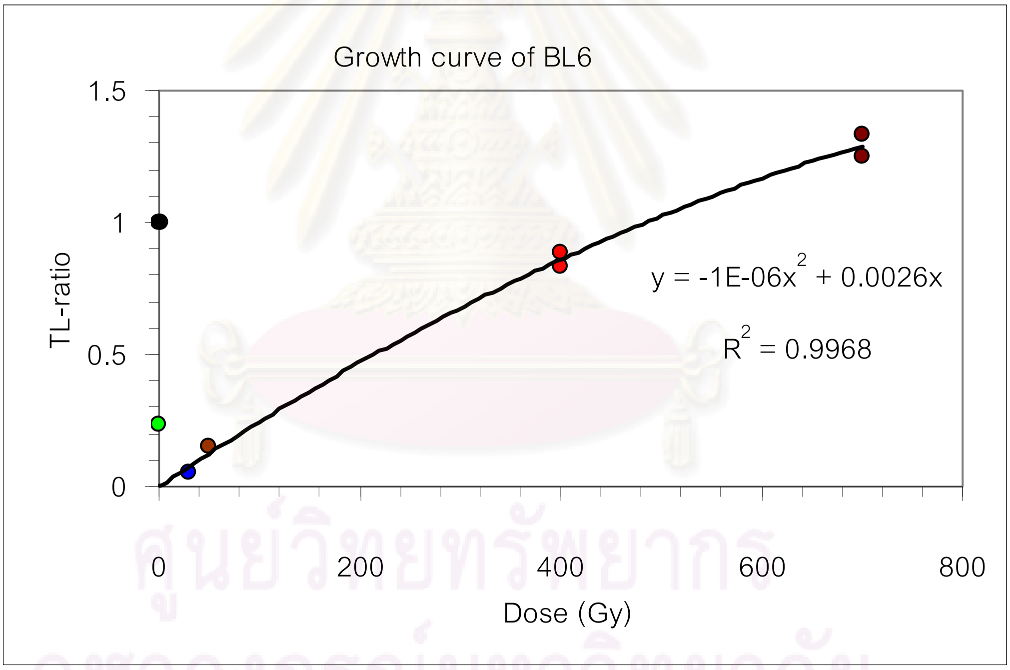

Sample No. BL 6

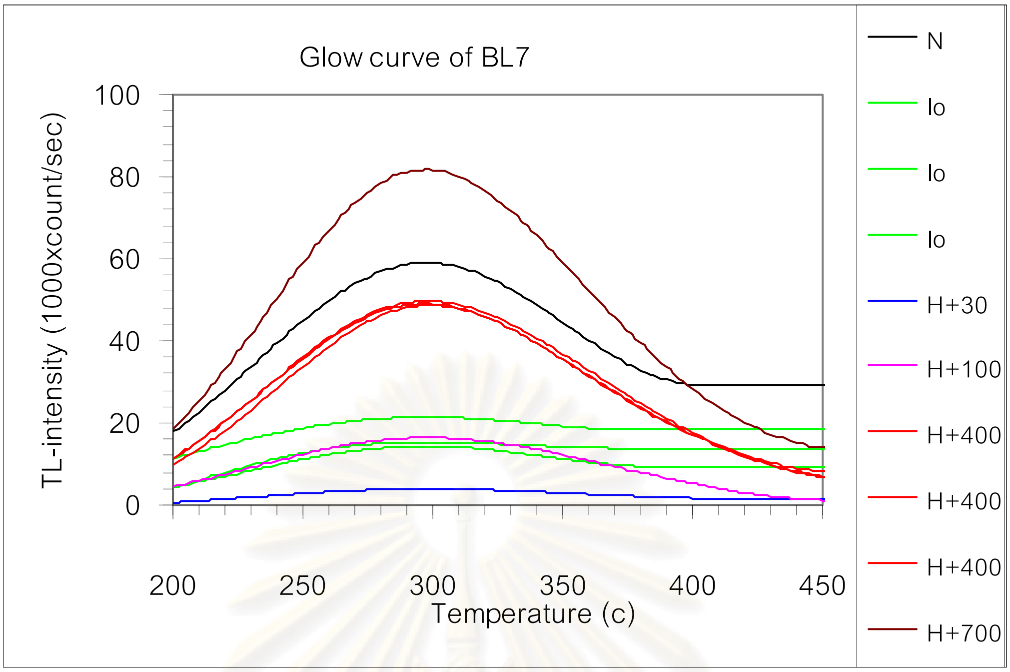

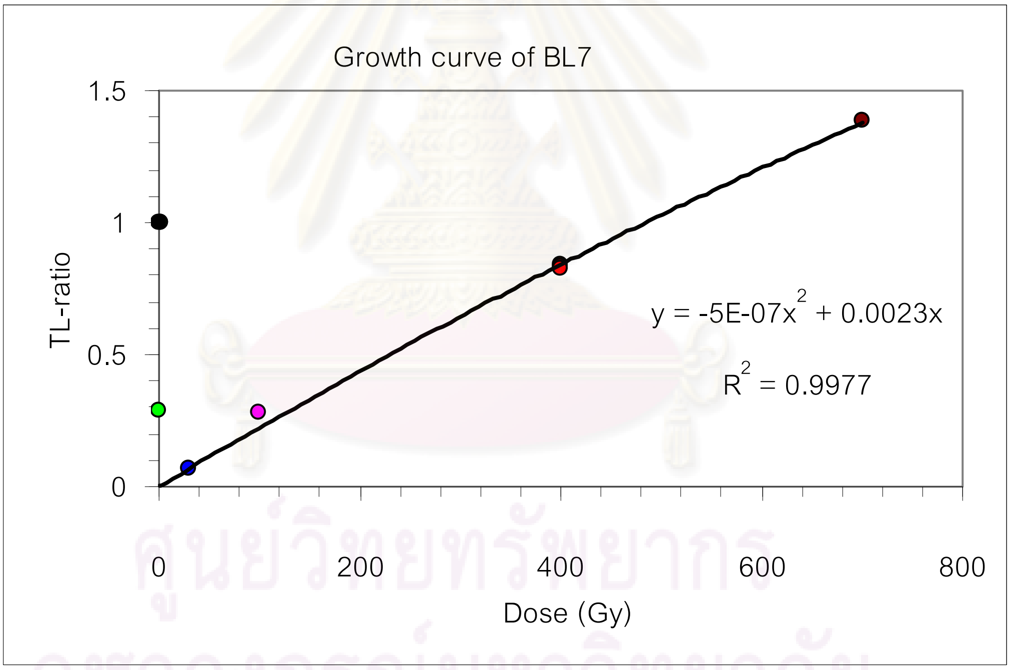

Sample No. BL 7

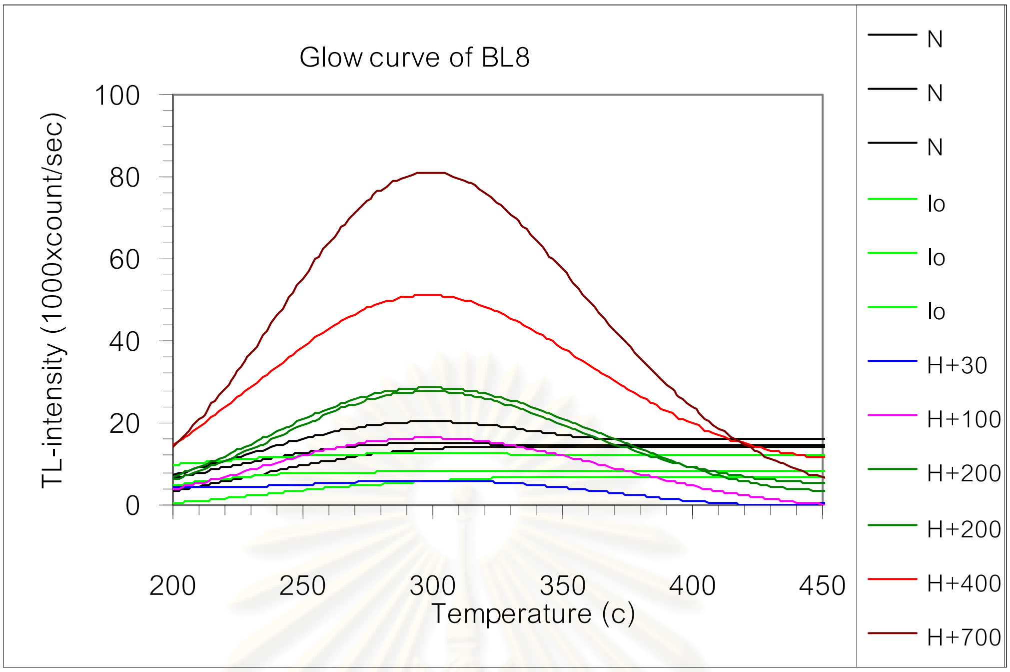

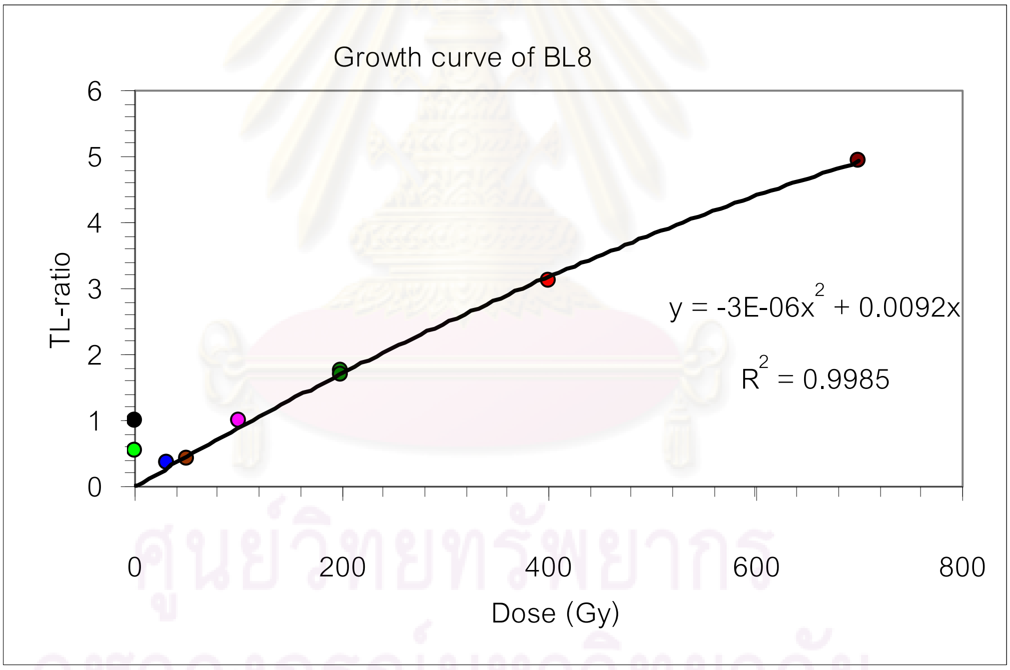

Sample No. BL 8

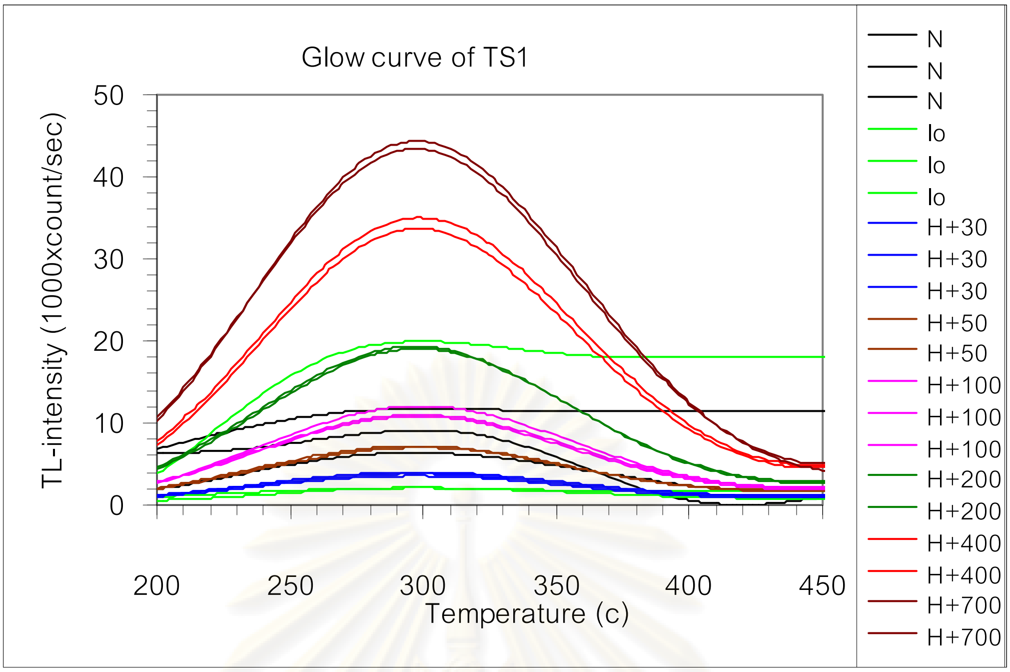

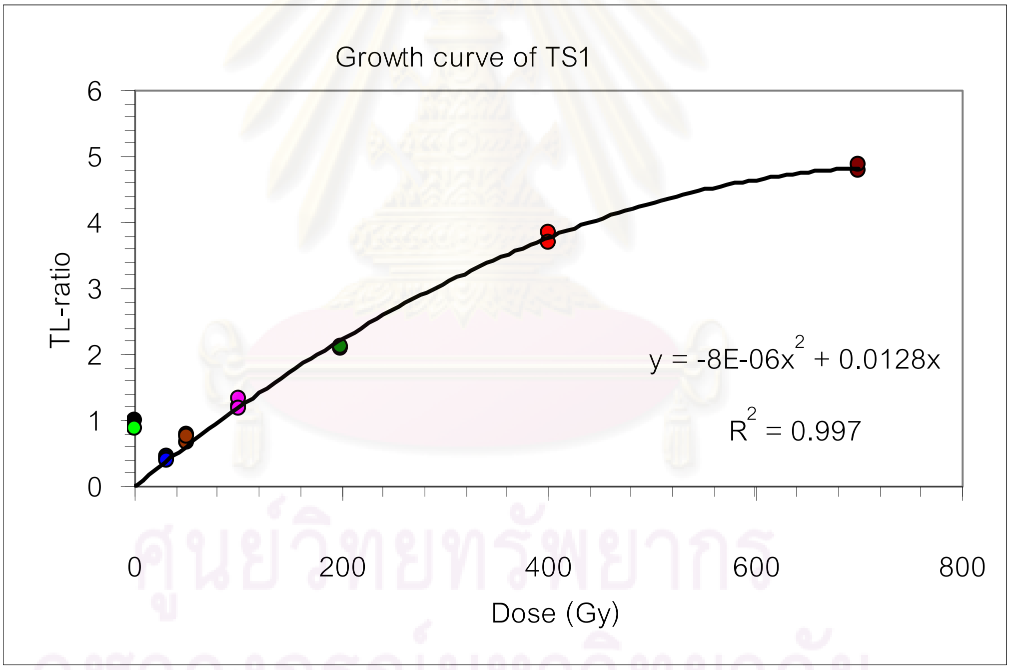

Sample No. TS 1

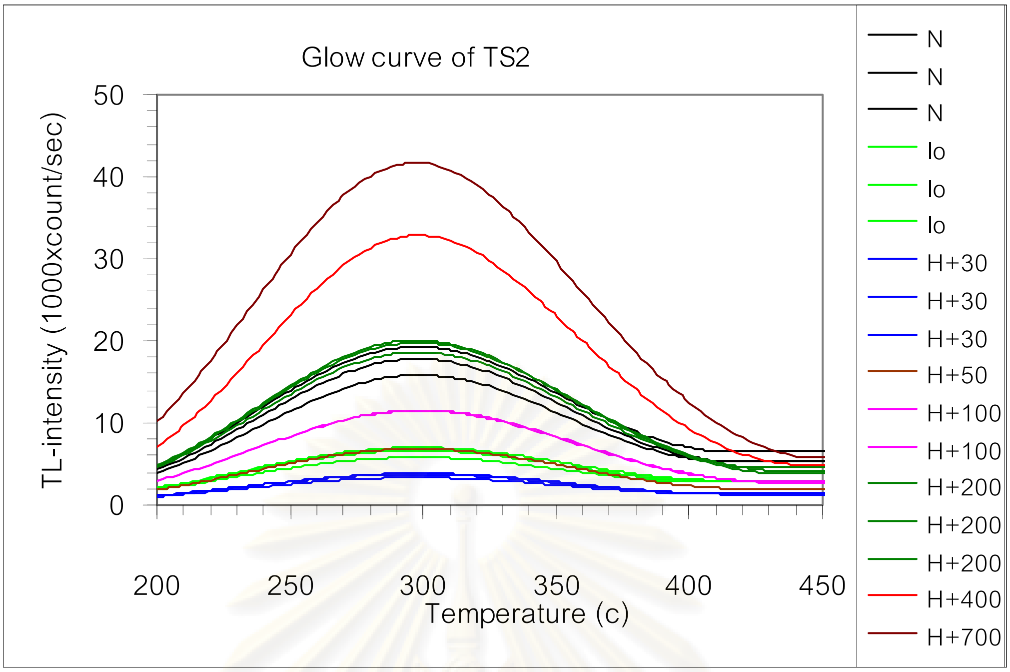

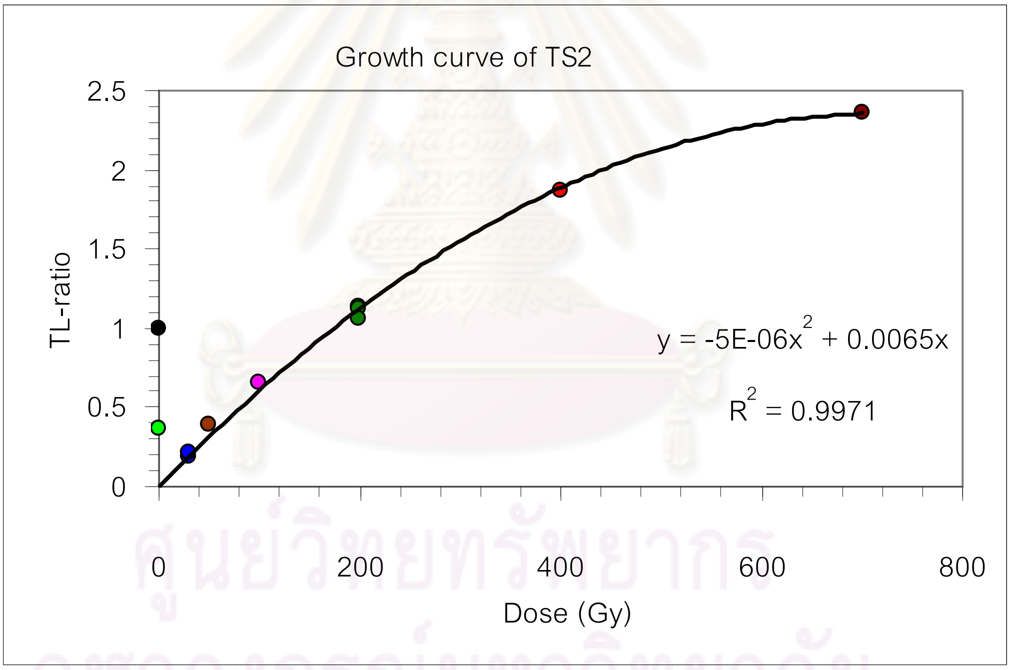

Sample No. TS 2

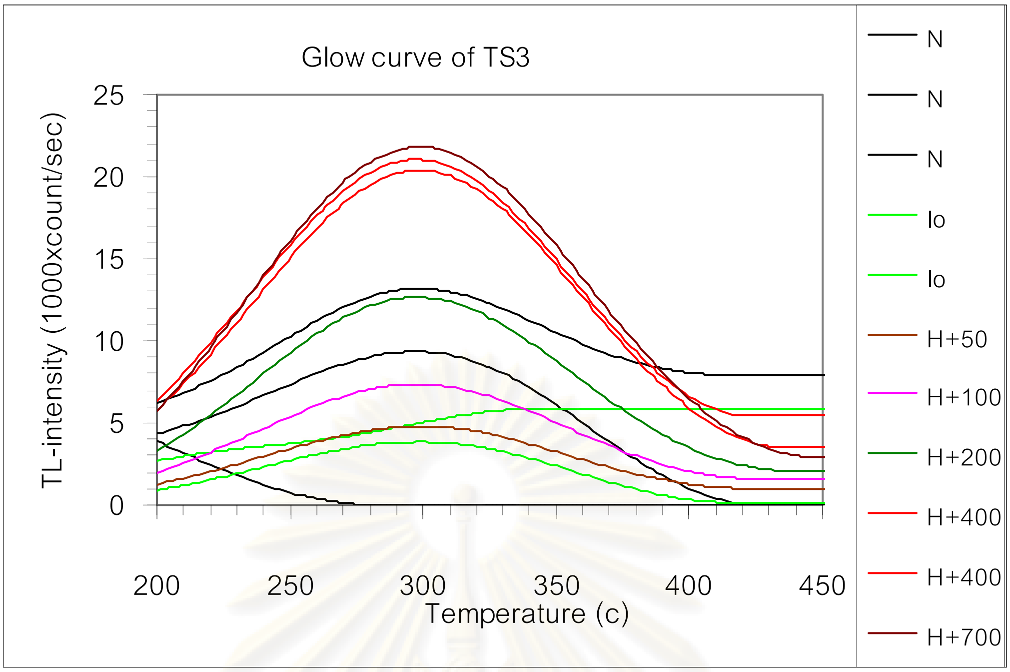

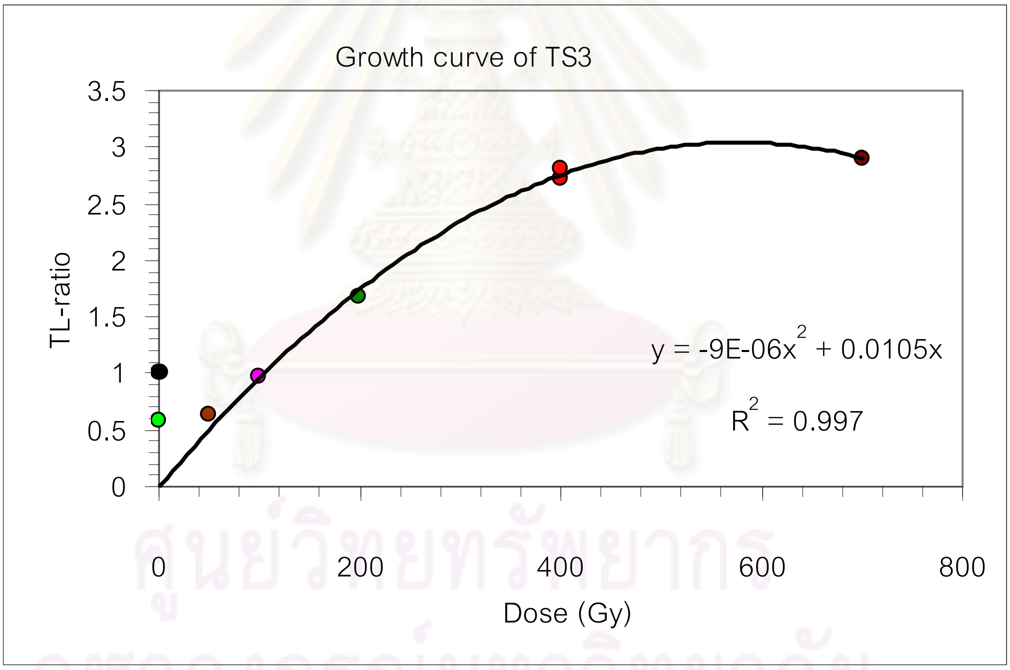

Sample No. TS 3

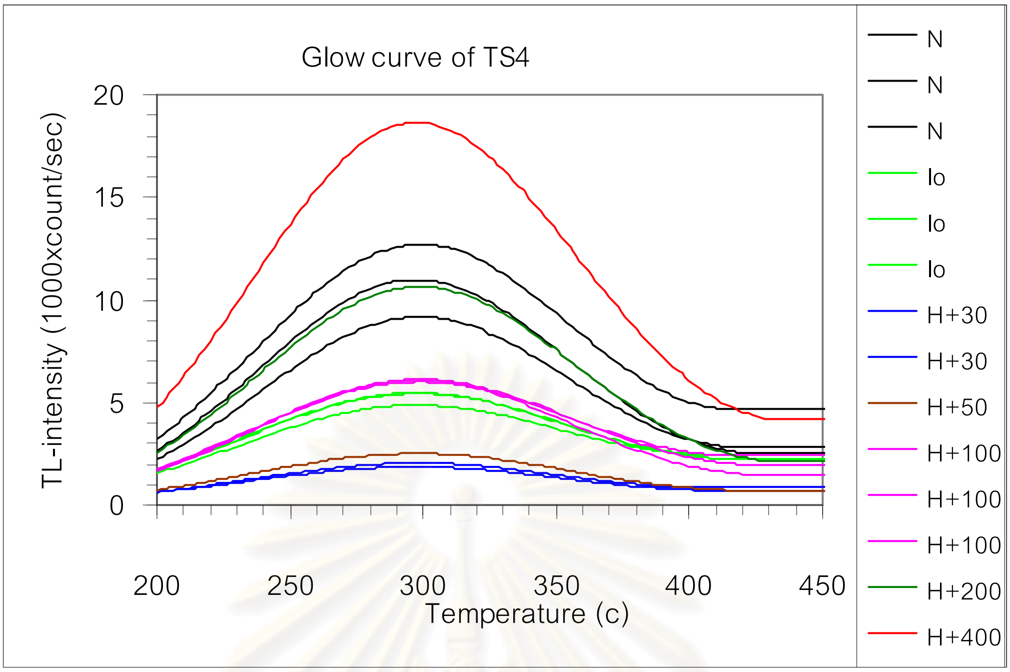

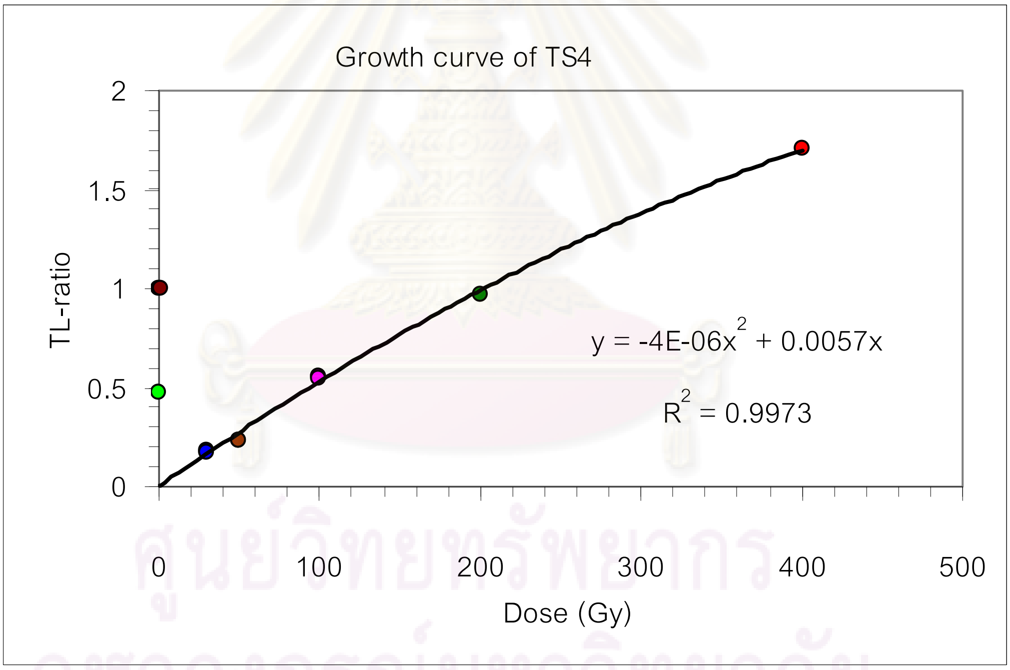

Sample No. TS 4

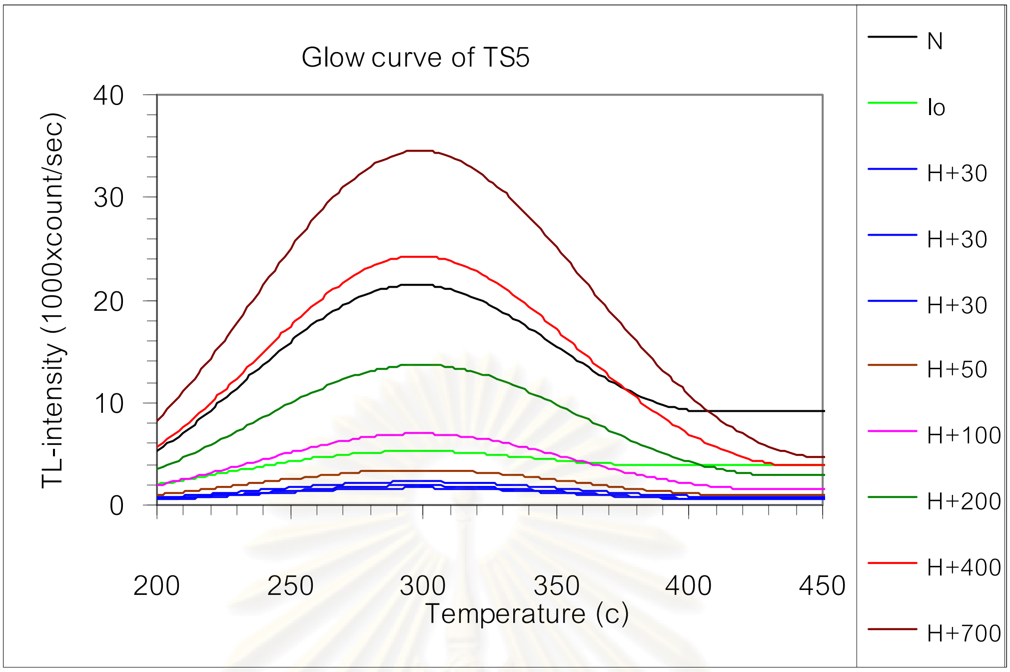

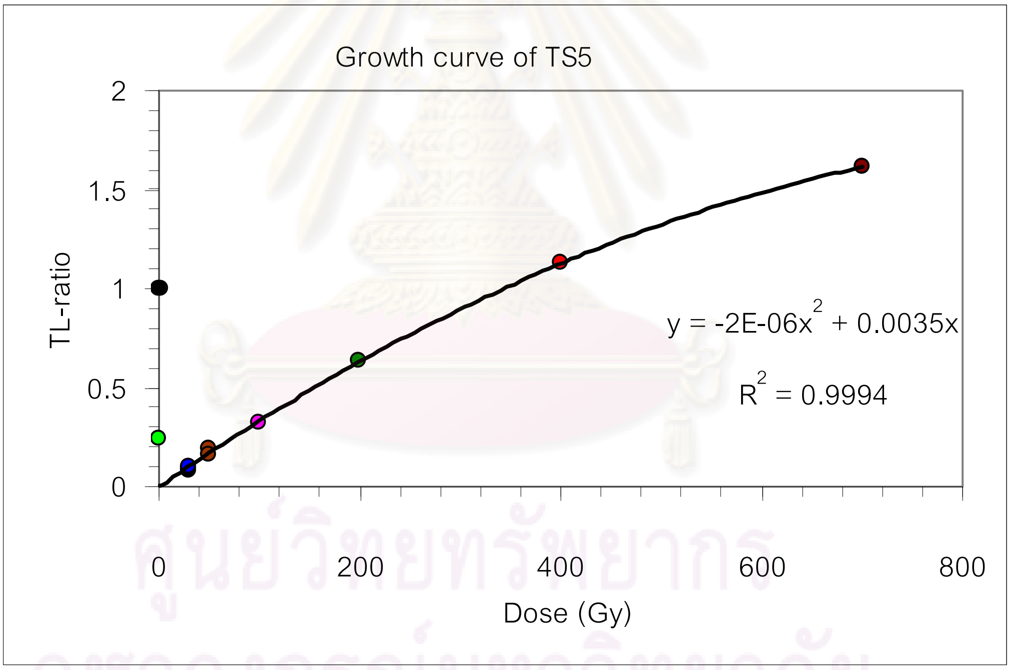

Sample No. TS 5

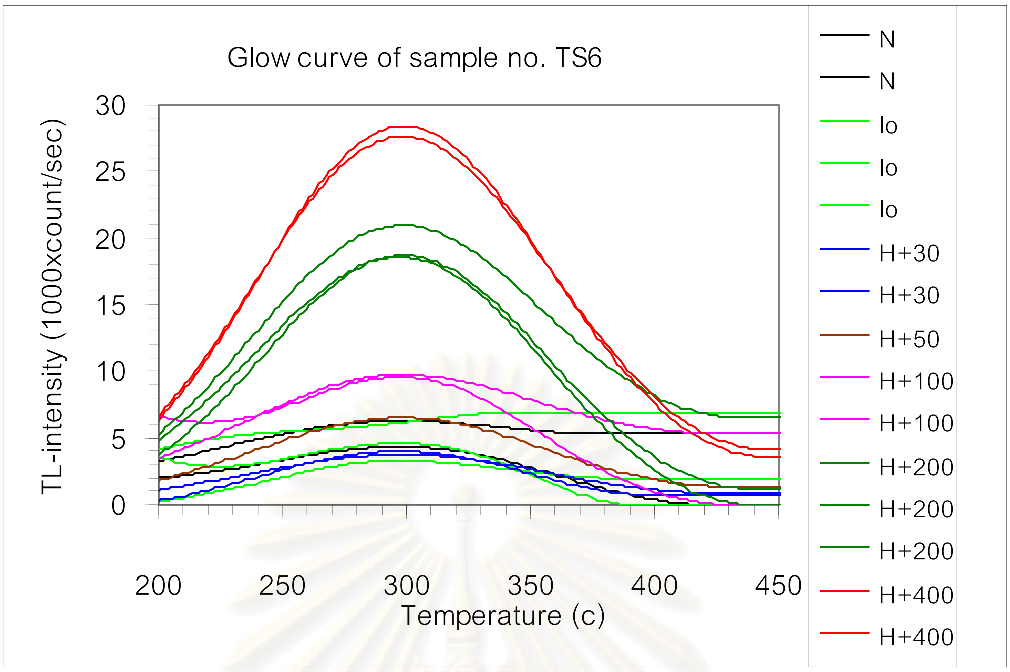

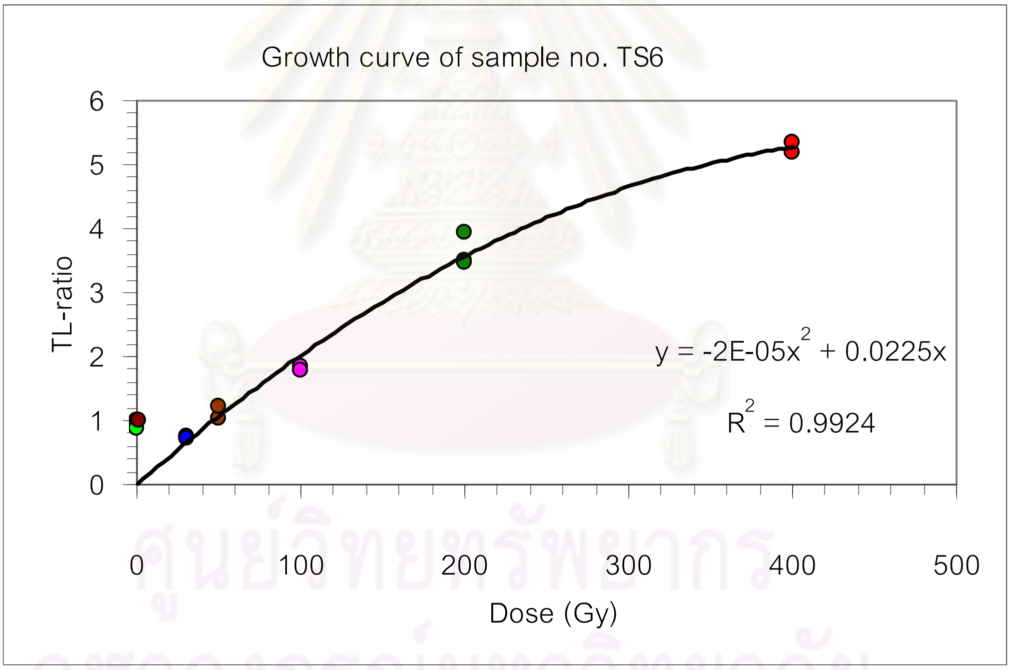

Sample No. TS 6

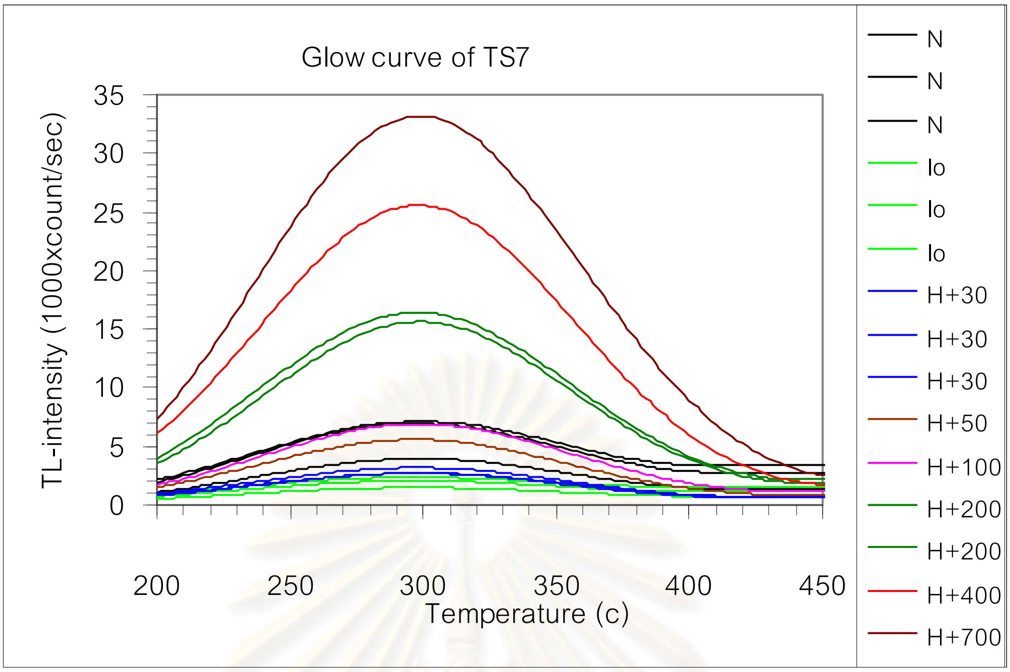

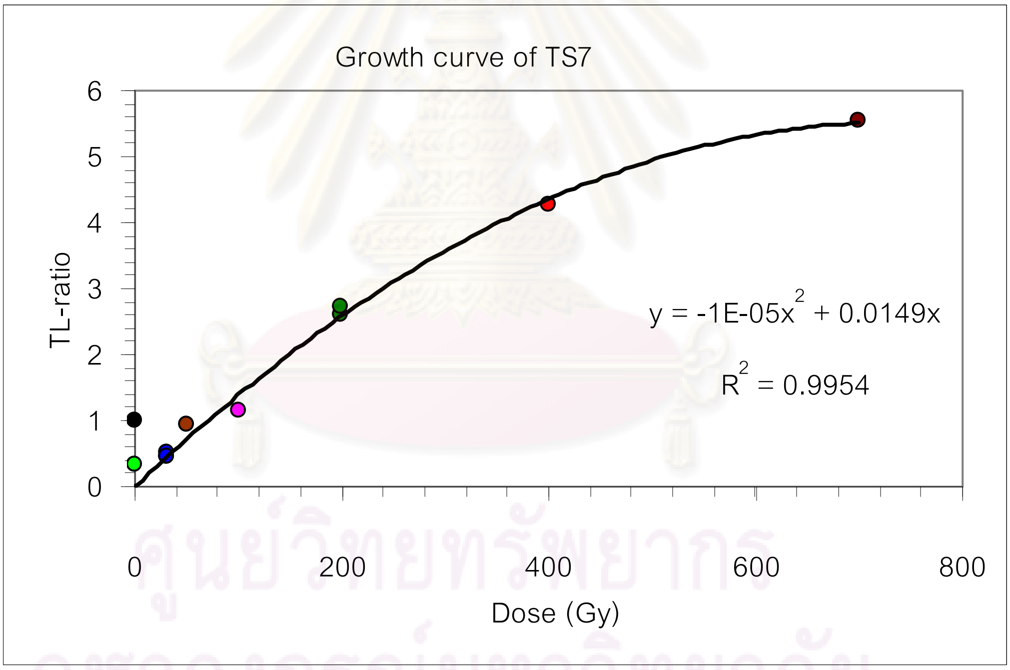

Sample No. TS 7

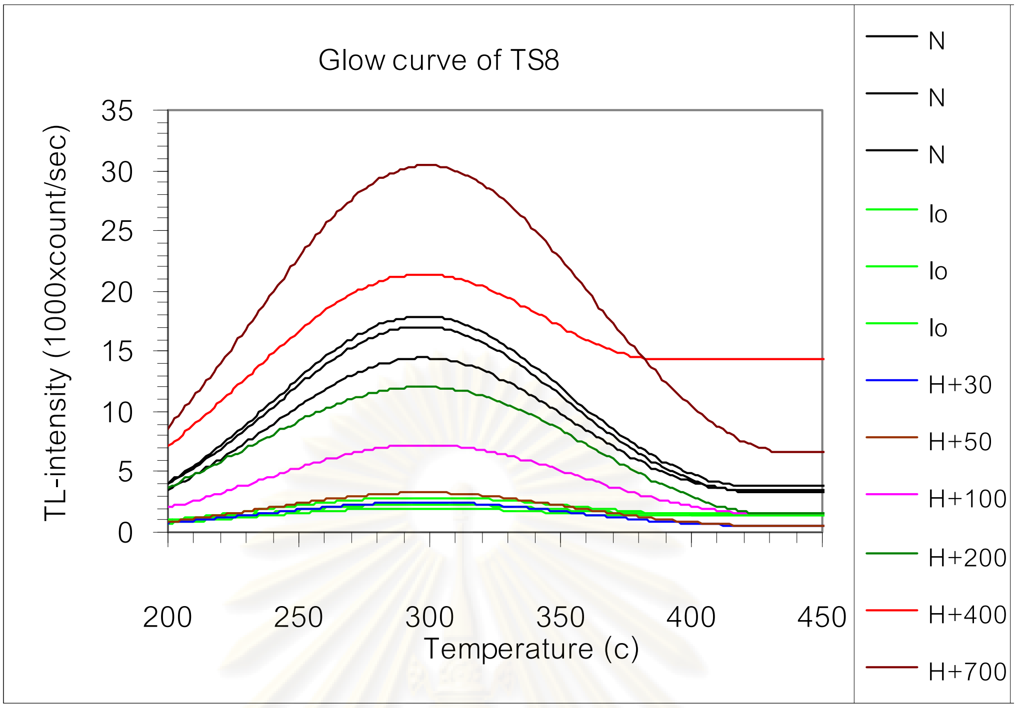

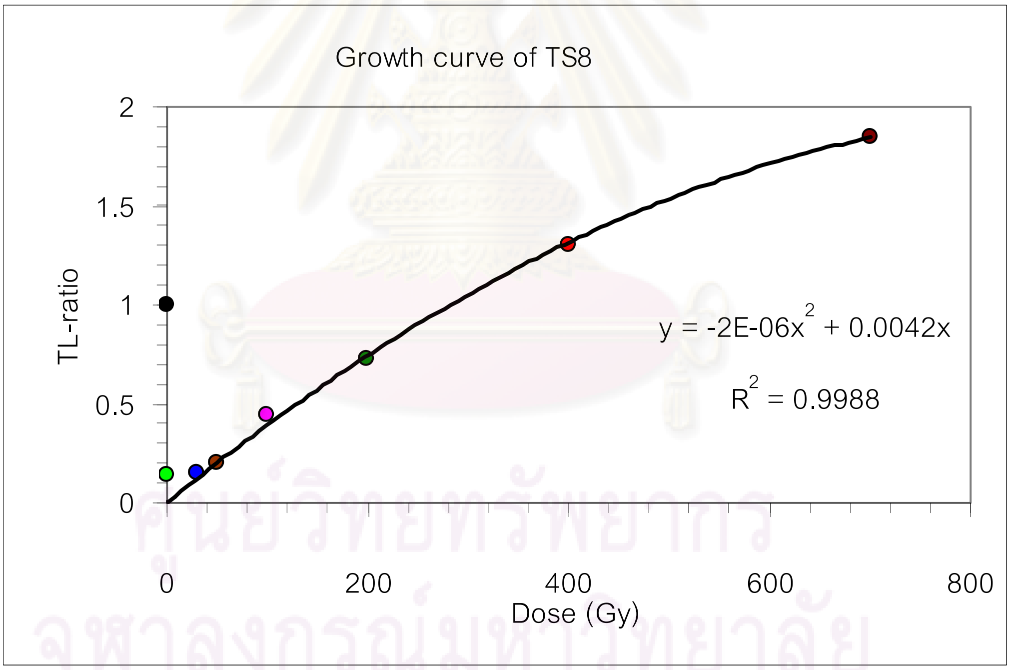

Sample No. TS 8

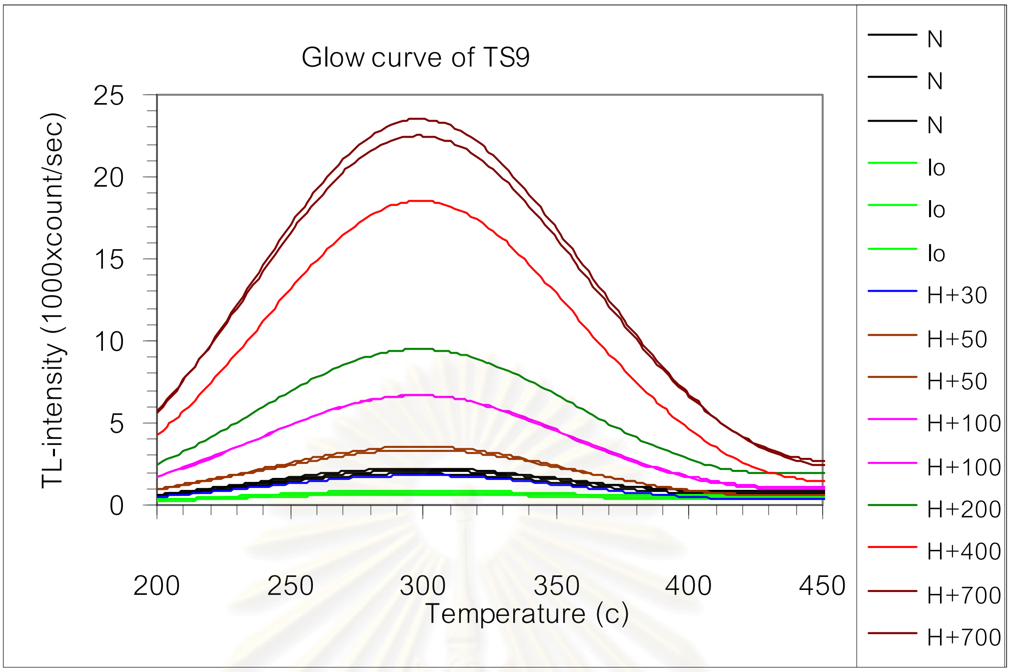

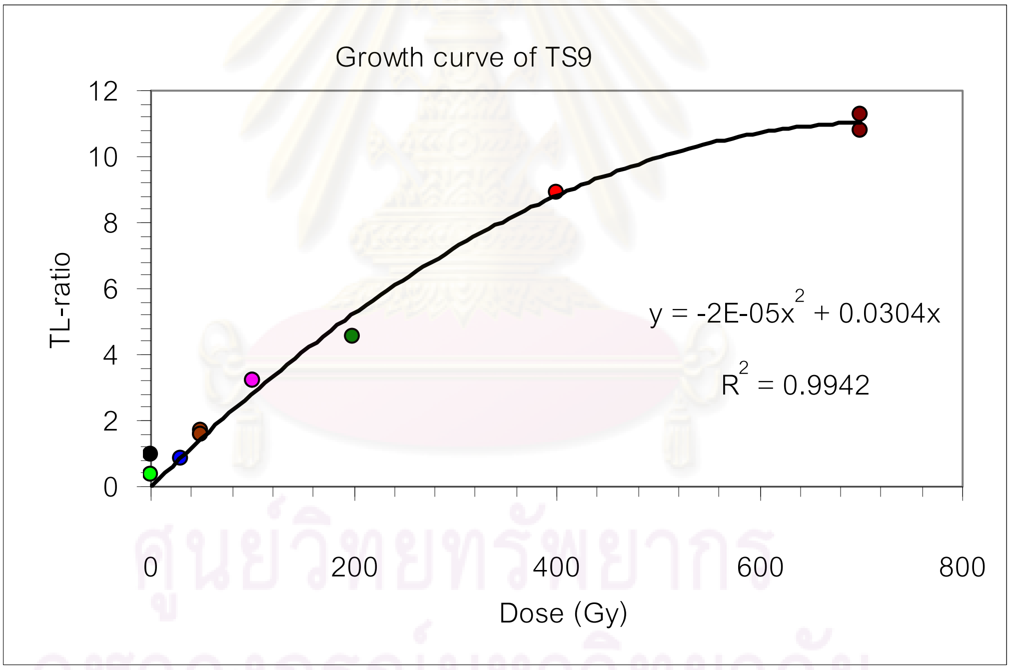

Sample No. TS 9

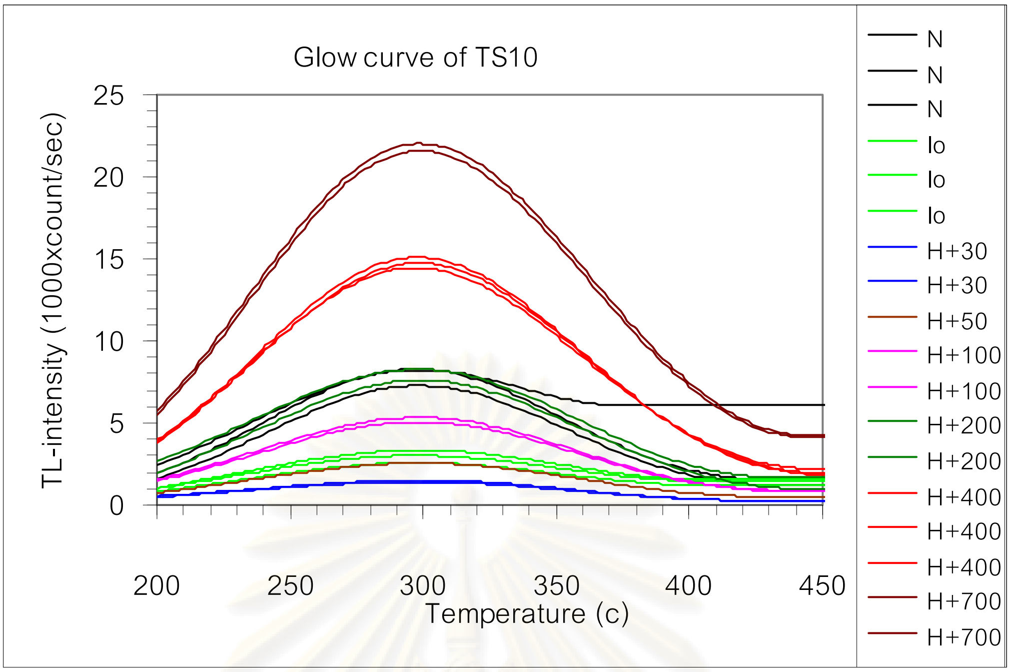

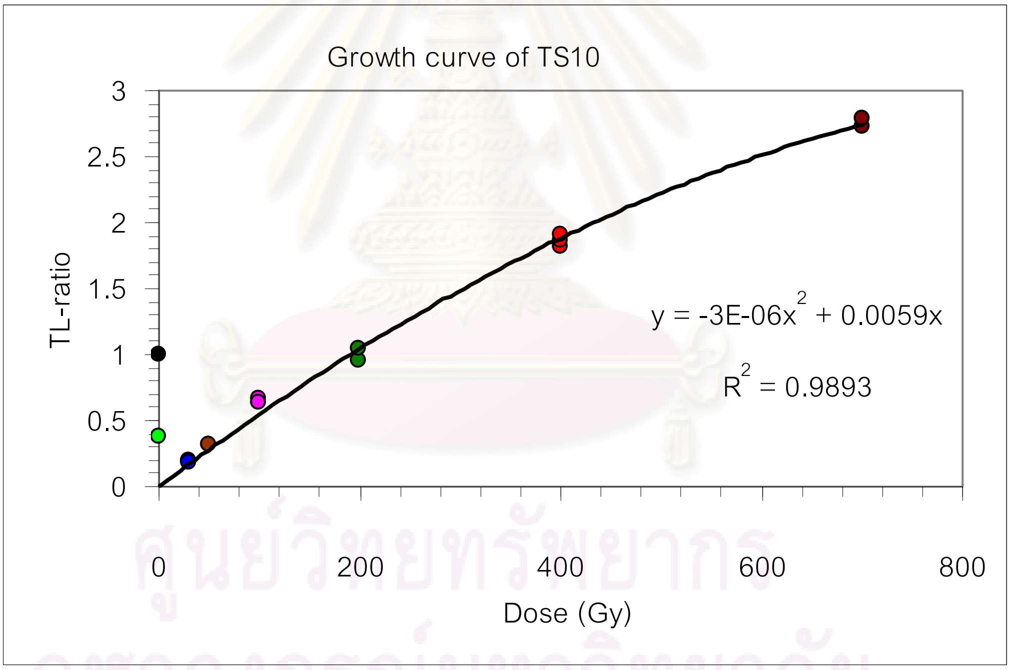

Sample No. TS 10

BIOGRAPHY

Mr. Sarun Keawmaungmoon was born on February 11, 1983 in Lamphun, northern Thailand. He graduated at high school level from Yupparaj Wittayalai School, Chiang Mai, in 2002. In 2006, he received a B.Sc. degree in Geology from the Department of Geology, Faculty of Science, Chaing Mai University, Thailand. In 2007 he enrolled as a graduate student for the M.Sc. program of Geology programme at Graduate School, Chulalongkorn University, Bangkok, Thailand. He published a geoscientific paper on “Investigations on Tectonic Geomorphology along the Khlong Marui Fault, Khao Phanom area, Southern Thailand: Application of ArcGIS Approach” which appeared on Proceeding of International Syposia on Geoscience Resources and Environments of Asian Terranes, GREAT 2008/4th IGCP 516/ 5th APSEG, Bangkok, Thailand and published other one on “Preliminary Geomorphic Indices Associated to Active Faults in Khao Phanom area, Surat Thani Province” in Journal of Remote Sensing and GIS Association of Thailand in 2009.